



HAL
open science

Subcellular mechanisms governing the spatiotemporal regulation of simultaneous morphogenetic processes

Nicolas Roby

► **To cite this version:**

Nicolas Roby. Subcellular mechanisms governing the spatiotemporal regulation of simultaneous morphogenetic processes. Molecular biology. Université Côte d'Azur, 2024. English. NNT : 2024COAZ6012 . tel-04848553

HAL Id: tel-04848553

<https://theses.hal.science/tel-04848553v1>

Submitted on 19 Dec 2024

HAL is a multi-disciplinary open access archive for the deposit and dissemination of scientific research documents, whether they are published or not. The documents may come from teaching and research institutions in France or abroad, or from public or private research centers.

L'archive ouverte pluridisciplinaire **HAL**, est destinée au dépôt et à la diffusion de documents scientifiques de niveau recherche, publiés ou non, émanant des établissements d'enseignement et de recherche français ou étrangers, des laboratoires publics ou privés.



THÈSE DE DOCTORAT

Mécanismes subcellulaires gouvernant la régulation spatiotemporelle d'événements morphogénétiques simultanés

Nicolas ROBY

Institut de Biologie Valrose

Equipe « Morphogénèse et mécanique des tissus épithéliaux »

Présentée en vue de l'obtention

du grade de docteur en Sciences de la Vie
et de la Santé, Interactions moléculaires et cellulaires
d'Université Côte d'Azur

Dirigée par : Matteo RAUZI, Ph.D.

Soutenue le : 13/09/2024

Devant le jury, composé de :

Edwin MUNRO, Prof., University of Chicago, États-Unis
Nicolas MINC, Ph.D., Institut Jacques Monod, Paris, France
Darren GILMOUR, Prof., Universität Zürich, Suisse
Thomas LECUIT, Prof., Collège de France, France
Stéphane NOSELLI, Ph.D., iBV, Nice, France



Mécanismes subcellulaires gouvernant la régulation spatiotemporelle d'événements morphogénétiques simultanés

Jury :

Président du Jury :

Stéphane NOSELLI, Ph.D., iBV, Nice, France

Rapporteurs :

Edwin MUNRO, Prof., University of Chicago, États-Unis

Nicolas MINC, Ph.D., Institut Jacques Monod, Paris, France

Examineurs :

Darren GILMOUR, Prof., Universität Zürich, Suisse

Thomas LECUIT, Prof., Collège de France, France

Invités :

Matteo RAUZI, Ph.D., iBV, Nice, France

Mécanismes subcellulaires gouvernant la régulation spatiotemporelle d'événements morphogénétiques simultanés

La morphogénèse est le processus fondamental par lequel un organisme acquiert sa forme, établissant les fondations structurelles et fonctionnelles nécessaires à son développement correct. Pendant l'embryogenèse, la morphogénèse tissulaire découle du contrôle génétique des forces locales et globales pour façonner les feuilletts épithéliaux en structures matures. Nous avons désormais une compréhension de la régulation génétique impliquée dans le remodelage du cytosquelette pour générer ces forces et réaliser des processus morphogénétiques simples. Cependant, ces événements ont été étudiés individuellement, alors qu'ils surviennent simultanément durant le développement. Pour explorer comment un même tissu subit plusieurs changements de forme simultanés, nous utilisons l'embryon de *Drosophile* comme modèle, en nous concentrant sur le repliement et l'extension simultanés du mésoderme présomptif. Cette transformation tissulaire complexe repose sur la réorganisation du réseau cortical d'actomyosine en deux niveaux subcellulaires. Le premier niveau, situé à l'apex des cellules mésodermiques, médie la constriction apicale pour le repliement du mésoderme, tandis que le second niveau, situé au cortex latéral, entraîne l'intercalation cellulaire polarisée pour la convergence-extension du tissu. Nous étudions maintenant comment les cellules mésodermiques parviennent à contrôler spatio-temporellement la distribution d'actomyosine en niveaux subcellulaires distincts pour réaliser des changements simultanés de forme et de topologie. Des travaux antérieurs ont mis en évidence le déplacement basal des noyaux pendant le repliement du mésoderme, un phénomène conservé durant l'embryogenèse de nombreuses espèces. Bien que de nombreuses recherches aient pu élucider la régulation du positionnement nucléaire, l'effet de la position du noyau sur la morphogénèse tissulaire reste inconnu. Dans cette étude, je démontre que le noyau contrôle la distribution subcellulaire du réseau d'actomyosine. En raison des contraintes géométriques imposées par la forme colonnaire des cellules épithéliales du mésoderme, le noyau agit comme une barrière, protégeant le cortex latéral du réseau de microtubules et régulant la distribution de la molécule de signalisation RhoGEF2. Le repositionnement basal du noyau, entraîné par la contraction du premier niveau d'actomyosine et le flux cytoplasmique résultant, permet de libérer le cortex latéral pour que RhoGEF2 s'y accumule, dirigeant ainsi la formation stéréotypée du second niveau d'actomyosine. Ce travail identifie donc un nouveau rôle du noyau permettant la compartimentation spatio-temporelle du cytosquelette, générant ainsi une structure modulaire qui alimente plusieurs processus morphogénétiques simultanés.

Mots-clés : Embryogenèse, Morphogénèse concomitante, Contractilité d'Actomyosine, Dynamiques du Cytosquelette, Positionnement nucléaire

Subcellular mechanisms governing the spatiotemporal regulation of simultaneous morphogenetic processes

Morphogenesis is the fundamental process by which an organism acquires its shape, establishing the structural and functional foundations for proper development. During embryogenesis, tissue morphogenesis arises from genetic patterning that drives both local and organismal forces to shape epithelial sheets into mature structures. We now broadly understand the genetic regulation involved in the remodelling of cytoskeletal elements to generate these forces and drive simple morphogenetic processes. However, these events have typically been studied individually, despite occurring simultaneously during development. To explore how a single tissue undergoes multiple simultaneous shape changes, we use the *Drosophila* embryo as a model system, focusing on the simultaneous folding and extension of the presumptive mesoderm tissue. This complex tissue transformation relies on the timely reorganization of the cortical actomyosin network in two subcellular tiers. The first tier, at the apex of mesoderm cells, mediates apical constriction for tissue folding, while the second tier, at the lateral cortex, drives polarized cell intercalation for tissue convergence-extension. We now investigate how mesoderm cells segregate actomyosin into distinct subcellular tiers to achieve simultaneous shape and topology changes. Previous work highlighted the basal displacement of nuclei during mesoderm folding, a feature conserved across species. While much research has focused on nuclear positioning regulation, the effect of nuclear position on tissue morphogenesis remains unclear. In this study, I demonstrate that the nucleus controls the establishment of the two-tier actomyosin network. Within the geometric constraints of mesoderm columnar epithelial cells, the nucleus acts as a barrier, shielding the lateral cortex from the microtubule network and regulating the distribution of the signalling molecule RhoGEF2. The relocation of the nucleus, driven by the contraction of the first actomyosin tier and the resulting cytoplasmic flow, unshields the lateral cortex for RhoGEF2 delivery to direct the stereotypic formation of the second actomyosin tier. This work identifies a new role for the nucleus as a spatiotemporal cytoskeleton compartmentalizer, establishing a modular scaffold that powers multiple simultaneous morphogenetic processes.

Keywords: Embryogenesis, Composite morphogenesis, Actomyosin contractility, Cytoskeletal dynamics, Nuclear positioning

« *Down the Rabbit Hole* »

Table of Contents

Acknowledgements	iv
List of figures.....	vii
List of abbreviations	viii
Chapter I-Introduction.....	2
1. Embryogenesis	3
1.1 <i>Drosophila</i> as a model system	4
1.2 An introduction to <i>Drosophila</i> early development	5
1.2.1 Cellularization	6
1.2.2 <i>Drosophila</i> axis specification	8
1.2.3 Gastrulation	11
2. Shape and topology changes of epithelia during gastrulation	17
2.1 Epithelial sheets: the ideal substrate for tissue morphogenesis	17
2.1.1 Adhesion and apico-basal polarity in epithelial sheets	18
2.1.2 Planar cell polarity in epithelial sheets	21
2.1.3 Epithelia-Matrix interactions	23
2.2 Cell shape and topology changes driving gastrulation movements	23
2.2.1 Cell behaviours driving tissue bending.....	24
2.2.2 Cell behaviours driving tissue elongation.....	27
2.3 A brief perspective on biophysical approaches of tissue morphogenesis	34
3. Force generation and transmission: cytoskeleton and organelles at play	34
3.1 The cell cytoskeleton	34
3.1.1 Microtubules	35
3.1.2 Intermediate filaments	37
3.1.3 Actin filaments	37
3.2 Force generation by the cell cytoskeleton.....	39
3.2.1 Actomyosin contractile machinery	39
3.2.2 Microtubules as force generators	43
3.3 Force transmission between epithelial cells	44
3.3.1 Adhesive contacts	44
3.3.3 Indirect methods of force transmission through membrane and organelles	47
4. Composite morphogenesis	50
4.1 Concomitant morphogenetic processes during development	50

4.2 <i>Drosophila</i> mesoderm invagination as a new paradigm for concomitant folding and extension	51
Chapter II-Results	54
Summary of research findings.....	55
Chapter III-Discussion	110
1. How is RhoGEF2 planar cell polarity established?	112
2. What are the molecular requirements to generate MyoII lateral clusters?	113
3. How do microtubules control actomyosin contractility?.....	115
4. Experimental limitations to address the impact of nucleus positioning on microtubule dynamics	116
5. What is the role of the apicobasal microtubule arrays surrounding the nucleus?	116
6. Why do mesoderm cells rely on nuclear positioning to coordinate morphogenesis?.....	117
7. Contraction or coalescence: a dive into the differential behaviour of subcellular actomyosin networks	118
References.....	119

Acknowledgements

I would like to begin by expressing my sincere gratitude to the members of the jury for taking the time to review my work and discuss my research findings.

I would like to thank my supervisor **Matteo** for giving me the opportunity to carry this work in his team, his guidance and feedback throughout this project, and the great scientific synergy. Additionally, I am deeply appreciative of the autonomy he granted me, allowing me to pursue my own ideas and develop confidence as an independent researcher.

I would like to thank the rest of the team, both past and current members for their scientific feedbacks and our joyful discussions throughout the years. Special thanks to: **Alphy**, who taught me a lot when I first entered this field and whose PhD work laid the foundations for my own research. **Barthélémy**, for his help with coding and data analysis and the many discussions, **Anna** for the microscopy and genetic advices, and her kindness. **Abdul** for the cool hikes and the many tools he setup within the lab. **Sami**, for his support with fly stocks and his constant good mood. S/O to all the Master students that passed by the lab, especially **Fatima, Herica, Tanguy** and **Adrien** for the poker evenings, laughs and tasty recipes.

Many thanks to my TAC committee who followed my work and whose feedback was extremely valuable: **Yohanns BELLAICHE, Manuel THERY, Stéphane NOSELLI**.

Many thanks to the great **Fly community** of the iBV and the Fly Media Platform!

More generally, many thanks to the iBV community, students, researchers and staff who made this place feel like a second home. Une attention particulière à **Mouna, Dominique, Santhi** et **Laurence** pour leur bonne humeur et bienveillance.

S/O to the **PhD/PostDoc Club** Committee, my early co-founder **Zeinab** and the new team **Emily, Margot, Mathilde, Niels & Paolo**. Fantastic job that created a caring and supporting student community! Way too many names to cite within the PhD/PostDoc attendees, just know I am thankful that I got to know many of you, through shared passions or scientific discussions. I enjoyed every single moment and have constantly been impressed by the scientific/personal qualities of all !

S/O to the **JEDN Team, Alex & Alex, Océane, Raph, Marion, Nathan** et **Adri** pour les soirées d'organisation et les souvenirs.

S/O to the **Nucleate France UniCA Team, Sophie, Gaelle**, and all the others members, for what we accomplished and the fulfilling mission !

Une pensée à tous les membres du **Ethics Research Committee**, particulièrement **Yves** pour sa bienveillance et nos échanges toutes ces années.

So much appreciation to the **DUB Therapeutics** Team. Special mention to **Tere** for the opportunity to take part in this venture, her support and great mentorship.

Un grand merci à ma première équipe de recherche au sein de l'iBV, **Florence, Caro, Fabienne** pour leur soutien depuis la licence jusqu'à cette étape. Une mention spéciale à ma première mentore, **Nadia**, qui m'a motivé à poursuivre dans la recherche scientifique.

Un grand merci à l'équipe voisine du 8^{ème} Hubstenberger, pour l'ambiance à l'étage et tous les moments passés ensemble : **Alia, Flo, Amira, Chloé**. Mention spéciale à **Andrés** pour les tutos Illustrator, R et Python.

Un grand merci à l'équipe du 4^{ème}, **Olivier, Raph, Franck, Hélène, Bernard et Michel**, pour le soutien et les bons moments !

Adri et Nathan, merci du fond du cœur les amis. Les longues soirées, la Faille, les déj' au Garpo et toute nos aventures sont mémorables. Vous êtes inspirants, sincèrement. (S/O le serveur de la Générosité évidemment)

Niels, partenaire d'escalade et ami de longue date désormais. Ça fait plaisir d'avoir passé toutes ces étapes ensemble, de voir que l'émulation a toujours été positive et qu'on se tire systématiquement vers le haut mutuellement. Je te remercie pour ça et tous les moments passés ensemble !

My bros **Lulu & Coco** : Les bonne réfs et nos escapades musicales à travers les années, les soirées à la maison, la bonne humeur contagieuse et tous les moments passés et à venir !

S/O le Nooduitgang: **Paul, Nils, Nico, Amira**: partenaires de Padel et voyageurs musicaux, merci pour les souvenirs !

Of course, team 4^{ème}, **Marion, Ana Sofia, Mailys** et mon lapin **Arnaud** pour tous les souvenirs.

Une pensée toute particulière à **Benoît et Emilie**, et l'adorable **Maël**. Vous êtes incroyablement gentils. On vient bientôt en Corse, promis !

Omar, pour les discussions, Portal et les séances de 6h de puzzles d'échecs en fuseau horaire New York-Nice.

Amandine & Bryan, Marylou, Smaranda, Marion et tous les amis de la Principauté, pour tous les moments et le soutien !

Caroline, Valérie, Philippe, Théo et Paul, ainsi que tous les autres membres de votre grande famille.

Je dédie cette thèse à **Madre, Padre, Clem et Vicky, et Lana** qui m'ont soutenu sur ces 4 années, et qui j'espère sont fiers des efforts réalisés et du travail accompli.

Une pensée à tous les autres membres de ma famille, notamment au cousin **Maxence, Grand-Mère et Marie-Jo.**

Last but not least, à ma **Cam**, pour ton amour, soutien, aide et conseils. Mention spéciale aux 1000+h que tu as passées à m'écouter parler du projet ou de manips, du changement de police sur la version 16 de telle figure ou tel paragraphe du papier. Sache que je t'admire. Gorfou.

List of figures

Figure 1. From zygote to gastrula

Figure 2. *Drosophila* early division cycles and cellularization

Figure 3. Anterior-Posterior axis specification in *Drosophila melanogaster*

Figure 4. Dorso-Ventral axis specification in *Drosophila melanogaster*

Figure 5. Mesoderm invagination: from morphogens to morphogenesis

Figure 6. Terminal gene patterning drives posterior midgut invagination through Fog signalling

Figure 7. Germband Extension : A-P signalling patterns drive the convergence-extension of the ectoderm

Figure 8. Adhesion proteins and cell domains in columnar epithelial tissues

Figure 9. Activity of polarity protein complexes in epithelial polarization in *Drosophila melanogaster* and vertebrates

Figure 10. Planar cell polarity pathways drive tissue-wide cell orientation

Figure 11. Actomyosin-dependent apical constrictions drive tissue bending

Figure 12. Cellular behaviours promoting epithelial folding

Figure 13. Mechanisms driving junction shrinkage during cell intercalation

Figure 14. Junction lengthening and rosette formation during cell intercalation

Figure 15. Collective cell migration via cytoskeleton remodelling, cell-cell adhesion and ECM signalling

Figure 16. Cell oriented divisions drive tissue elongation

Figure 17. Microtubule assembly and dynamic instability

Figure 18. Actin structure, assembly and regulation by partner proteins

Figure 19. Force generation via the coupling of non-muscle Myosin II and F-actin

Figure 20. Signalling pathways regulating actomyosin contractility

Figure 21. Adherens junction organization and role in force transmission

Figure 22. Nuclear envelope and LINC complex as subcellular force transducers

Figure 23. Concomitant folding and extension of the *Drosophila* presumptive mesoderm

List of abbreviations

A-P: Anterior-Posterior

D-B: Dorsal-Ventral

MT: Microtubule

GPCR: G-Protein Coupled Receptor

EMT: Epithelial-to-Mesenchymal Transition

GBE: Germband Extension

PMG: Posterior Midgut

JAM: Junctional Adhesion Molecule

ZO: Zonula Occludens

ECM: Extracellular Matrix

PSB: Parasegmental Boundary

MTOC: Microtubule Organizing Center

MAP: Microtubule-associated Protein

γ -TuRC: Gamma-Tubulin Ring complex

G(D)TP: Guanine (Di)Triphosphate

PTM: Post-Translational Modification

IF: Intermediate Filament

ATP: Adenosine Triphosphate

MyoII: Non-muscle Myosin II

AJ: Adherens Junction

FA: Focal Adhesion

+TIP: Plus-end Tracking Protein

Chapter I-Introduction

1. Embryogenesis

The animal kingdom displays an outstanding diversity of shapes. These morphological differences are established early in the life of organisms, during a process termed embryonic development or embryogenesis (Figure 1). Embryogenesis describes a series of successive steps that define the shape and function of living organisms. It begins with fertilization, during which the male gamete (sperm cell) merges with the female gamete (egg cell) to form a diploid zygote, thus restoring the total number of chromosomes in the newly-formed organism (Hertwig, 1875). Following fertilization, the zygote undergoes multiple cleavage steps, initially driven by mitotic divisions of the blastomeres (the resulting daughter cells). This process transforms the zygote into a multicellular structure known as the morula. Subsequently, a fluid-filled cavity called the blastocoel forms within the morula, leading to the creation of a hollow sphere called the blastula (Rossant and Tam, 2022). The following stages include gastrulation, neurulation and organogenesis during which the interplay between gene regulatory networks and cell mechanics dictates division cycles, cell shape and topology changes, and cell fate specification. Altogether, these processes help transitioning a simple cell mass into a multi-layered organism with functioning organs. Gastrulation reshapes the blastula, forming the primary germ layers : endoderm, ectoderm, and mesoderm. These germ layers will give rise to specialized cell types and define the organs and tissues of the organism (Kiecker et al., 2015). Neurulation follows gastrulation and is a two-step process during which the ectoderm layer will develop into the central nervous system (Gasser, 1878). Finally, organogenesis occurs, where cells from the three germ layers will diversify to generate tissues and organs. This process relies on the coordination of several developmental mechanisms, such as pattern formation, morphogenesis, cell proliferation, and differentiation. As a result, organs are generated, allowing the organism to perform specialized functions.

Despite the robustness of embryogenesis, which can often correct for perturbations of both intrinsic and extrinsic cues (Zhu and Zernicka-Goetz, 2020), developmental disorders can still occur. For example, defects in neurulation can lead to conditions such as spina bifida and anencephaly (Avagliano et al., 2019). In severe cases, developmental disorders can even be fatal, as illustrated among individuals with respiratory and heart defects or chromosomal aberrations (Lipinski and Krauss, 2023). Research efforts are thus being made to unravel the mechanisms of embryogenesis to prevent such defects, and to deepen our understanding of the processes that govern the formation of life. Interestingly, despite the variety of shapes and functions observed among metazoans, the underlying mechanisms of embryogenesis still show a significant amount of conservation (Kalinka and Tomancak, 2012; Gerri et al., 2020). This allows researchers to leverage animal models to decipher the mechanisms at play, dive into comparative analyses to evaluate their possible conservation or highlight the need for other processes, ultimately speeding up our understanding of embryogenesis and identifying the key principles that govern organismal

development. My work uses the *Drosophila* embryo as a model system to tackle some of these research interrogations.

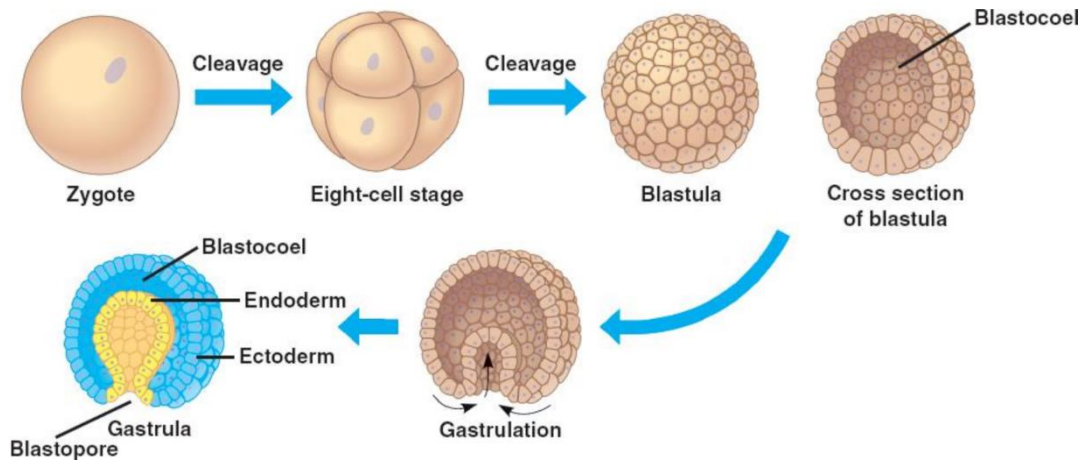


Figure 1. From zygote to gastrula

Representation of the successive steps of early embryogenesis leading to the formation of the blastula and primary germ layers (later becoming the various tissues and organs). Image adapted from (Campbell et al., 2000).

1.1 *Drosophila* as a model system

Drosophila melanogaster, most commonly known as the fruit fly, has been used for more than a hundred years in scientific research and proved to be suitable for the discovery of fundamental conserved processes. Its contribution was notably rewarded by six Nobel Prizes in Physiology and Medicine, including the early discovery of the role of chromosomes in heredity (Morgan, 1910), the description of the genetic control of embryonic development (Nüsslein-Volhard and Wieschaus, 1980), or the discovery of the molecular mechanisms controlling circadian rhythms (Zehring et al., 1984). *Drosophila melanogaster* is highly popular in developmental biology for several key reasons, I'll outline a few now:

(a) It has a short generation time (10 days at 25°C) and high fecundity, allowing for rapid studies and providing a large experimental sample size. Phenotypic changes are easily observable and simplify the study of gene function (Tolwinski, 2017).

(b) It is cheap and easy to maintain in the lab. *Drosophila melanogaster* possesses balancer chromosomes: they are multiply inverted and rearranged chromosomes that prevent genetic recombination. These balancer chromosomes are of great help during genetic crosses or to maintain stable lines carrying genetic mutations (Miller et al., 2019).

(c) Many genetic tools have been engineered to allow precise and fast manipulations, such as gene knockout with RNA interference, transgenic approaches, inducible gene expression using the GAL4-UAS system, and endogenous manipulations using CRISPR-Cas9 methods (del Valle Rodríguez et al., 2012). Several behavioural studies

have also been developed in *Drosophila melanogaster* (McKellar and Wyttenbach, 2017).

(d) It has a fully-sequenced and well-annotated genome. Curated databases and resources to share and order fly stocks are well implemented (for a comprehensive overview: [FlyBase Online Resources](#)).

(e) Though one should be careful when extrapolating results from *Drosophila melanogaster* to other species, this model does share many conserved pathways and processes, making it even suitable to study human diseases (Verheyen, 2022).

(f) There are fewer ethical considerations to take into account when using this model, compared to vertebrate models.

(g) Early development of *Drosophila* embryos is fast (~3 hours from egg-laying to gastrulation). This fast pace allows to perform live-imaging, mechanical manipulation and optogenetics to address the underlying mechanisms of embryogenesis and morphogenesis (Saunders, 2021).

Drosophila melanogaster also has its limitations, including anatomical and physiological differences with vertebrates, less complexity in certain shared processes, the existence of *Drosophila*-specific mechanisms, as well as genetic redundancy that can hinder the interpretation of functional genetic studies. Nonetheless, the balance between its advantages and limitations still makes it an attractive model to study developmental biology.

1.2 An introduction to *Drosophila* early development

A common feature of externally-developing eggs is their large size (~100 000 times larger than the average adult somatic cell). Upon fertilization, this large egg will undergo 13 fast-paced cycles of division, generating approximately 6000 nuclei. *Drosophila*, like many insects, undergoes superficial cleavages, where cell division occurs rapidly without the formation of distinct individual cells. As a result, these multiple rounds of division result in a multinucleate mass of cells, termed syncytial blastoderm (even though the correct terminology would be coenocyte). From cycle 10 to 13, nuclei undergo a drastic repositioning and migrate towards the syncytium periphery (Figure 2A). This process was recently shown to rely on cell cycle-dependent cortical contractions that generate a cytoplasmic flow to uniformly spread nuclei (Royou et al., 2002; Deneke et al., 2019). Each nucleus is contained within its own cytoskeleton territory, where the interplay between actin caps and centrosomes drives the regular spacing of nuclei at the periphery (Raff and Glover, 1989; Blake-Hedges and Megraw, 2019). At the end of the 13th cycle, the process of cellularization begins. Cellularization is conserved during the development of animals, plants and eukaryotes (Hamer et al., 1999; Hehenberger et al., 2012; Dudin et al., 2019) and allows each nucleus within the syncytial blastoderm to be enveloped by basolateral membranes growing inwards (Mazumdar and Mazumdar, 2002). This results in a sheet of mononucleate columnar epithelial cells and the formation of the cellular blastoderm (Figure 2B). Before this stage, development relies mostly on maternally deposited mRNAs (Figure 2A), and the molecular machinery driving cellularization is also maternally supplied. However, the timing and function of this machinery

during cellularization are locally orchestrated by a small set of early zygotic genes, including Bnk, Dunk, Nullo, Slam, and Sry-a that are expressed in one pulse at the onset of cellularization and downregulated immediately afterwards (Sokac and Wieschaus, 2008). This transition from maternal to zygotic gene expression, known as the Mid-Blastula Transition, is conserved across species (Schulz and Harrison, 2019). Cellularization takes one hour, resulting in cells that are adherent and polarized along their apicobasal axis. To form new cell sides, the plasma membrane at the cell surface invaginates to create lateral membranes. These invaginations, known as cellularization furrows, are positioned according to the landmarks of the previous metaphase furrows from the 13th division cycle (Schmidt and Grosshans, 2018). During the 14th division cycle, these 'old' furrows, which encapsulated the mother cell and now the two daughter cells, determine the coordinates of the 'new' furrow needed to individualize daughter cells. This positioning is guided by the interface between the microtubule networks radiating from the two daughter cells, each cell being associated with a centrosome pair that nucleates microtubules (MTs) (He et al., 2016).

1.2.1 Cellularization

A molecular machinery involving actin crosslinkers and nucleators, polarity cues, adhesion components and signalling molecules, then compartmentalizes cells and promotes the growth of lateral membranes from these furrows, using the folded surface of the cell as a membrane reservoir (Figure 2B). The cellularization is a two-step process with a first 'slow phase', driven by the exocytosis of RE-derived vesicles to support F-actin assembly and Golgi-derived vesicles to deliver membrane at the cellularization furrows (Cao et al., 2008; Holly et al., 2015). This delivery is guided by the polarized growth of microtubules nucleated from the apical centrosomes towards the basal side of cells and the kinetics of furrow invagination are controlled by fine-tuning endocytosis to regulate the surplus of membrane and proteins within the different cell compartments (Lee and Harris, 2013). The second, or 'fast phase' of cellularization occurs during the final 20 minutes and significantly accelerates membrane growth. This phase uses an additional trafficking route to insert membrane at the subapical compartment, finalizing epithelial polarity and assembling adherens junctions (Müller and Wieschaus, 1996; Harris and Peifer, 2004; Schmidt et al., 2018). Throughout both phases, the bottoms of the furrows are enriched with contractile actomyosin (organized in a ring), which is timely regulated to ensure cell closure only after cellularization is complete, when the cell membrane reaches a depth of ~35 μm (Mavrakakis et al., 2014; Xue and Sokac, 2016). At the end of cellularization, the cellular blastoderm is composed of ~6000 adherent cells organized in a single columnar epithelial sheet (Figure 2C-D) with foundations laid out for the following stage: gastrulation.

If you wish to deepen your knowledge of the fascinating cellularization process and the control of membrane-actin interactions in *Drosophila melanogaster*, I would recommend the excellent review by (Sokac et al., 2023).

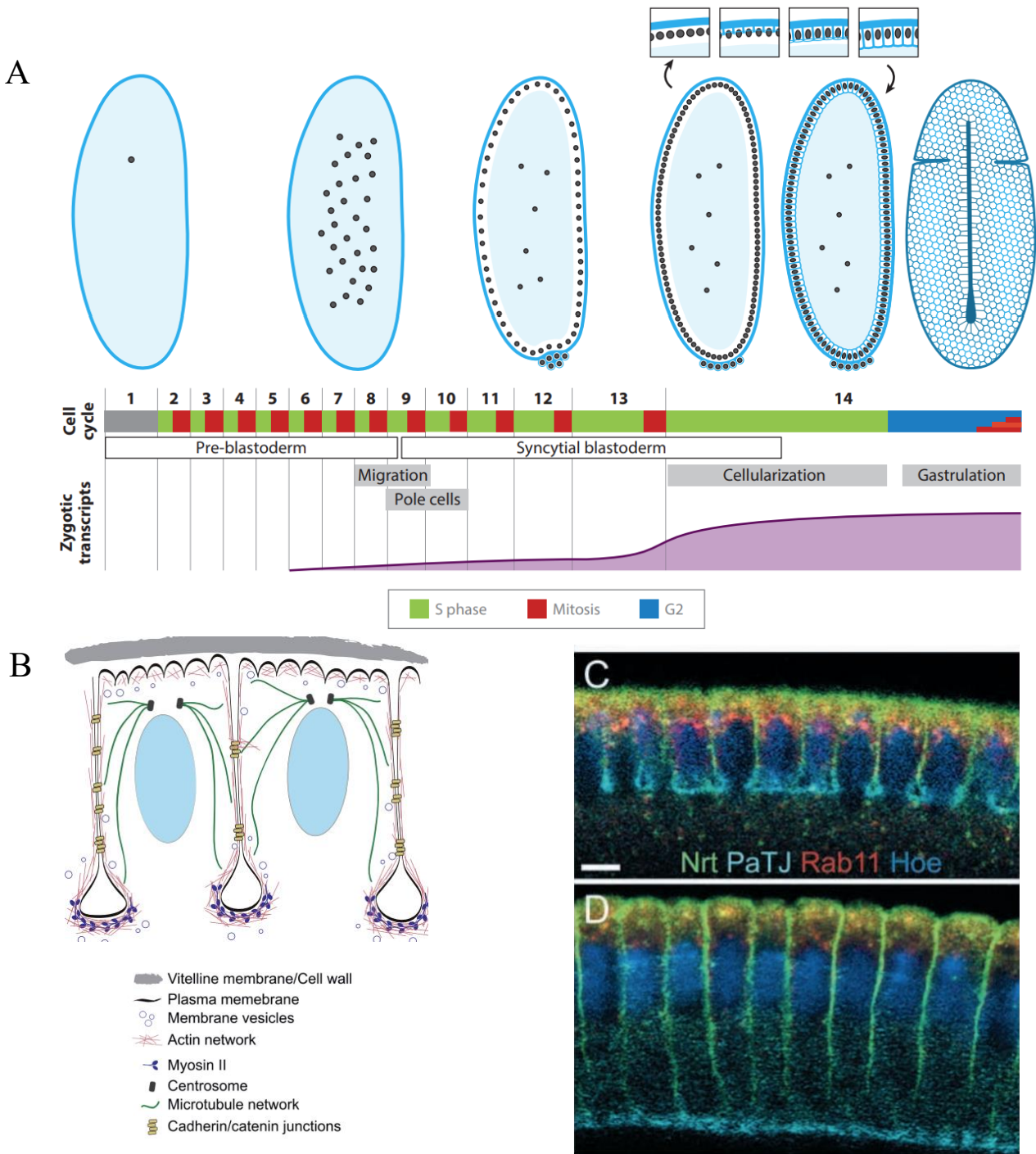


Figure 2. *Drosophila* early division cycles and cellularization

A. Scheme showcasing the 13 successive cycles of division leading to the formation of the syncytial blastoderm, the subsequent repositioning of nuclei to the periphery, followed by the cellularization step to individualize cells (top insets) and early gastrulation. **B.** Detailed scheme of the cellularization process during which basolateral membranes are generated to isolate each of the ~6000 peripheral nuclei. **C-D.** Sagittal sections of a *Drosophila* embryo showing the progression of the cellularization front. Nuclei in dark blue, membranes in green. Images adapted from (Lecuit, 2004; Farrell and O’Farrell, 2014; McCartney and Dudin, 2023).

1.2.2 *Drosophila* axis specification

Following cellularization, the epithelial sheet composing the cellular blastoderm will undergo extensive shape and topology changes to give rise to the final structure of organs and the organism. This reorganization, termed epithelial morphogenesis, is under the strict control of gene regulatory networks directing cell behaviour (Gilmour et al., 2017). Several morphogenetic processes will occur during *Drosophila* gastrulation to segregate the three primary germ layers: mesoderm invagination, anterior and posterior midgut invaginations, germband extension, cephalic furrow formation (a transient fold), germband retraction and dorsal closure (Gheisari et al., 2020). But before morphogenesis begins, one might wonder how the embryo specifies the correct location and timing of these events within the uniform sheet of epithelial cells. To answer this, we need to take a step back and understand how the body axes are established to define anterior-posterior (A-P) and dorsal-ventral (D-V) polarity. The following section will be dedicated to the understanding of axis formation in *Drosophila melanogaster*, that allows subsequent gene patterning to remodel cells at the right time and place during gastrulation.

1.2.2.1 Anterior-Posterior axis formation

The polarization of *Drosophila* actually begins long before gastrulation, during the formation and maturation of the egg, a process termed oogenesis. At this stage, the future embryo is contained within an egg chamber consisting of an oocyte and its 15 sister nurse cells, and surrounded by peripheral somatic follicle cells (Bastock and St Johnston, 2008), forming the protective outer layer of the chamber (Figure 3A). Axis specification starts with the A-P axis, when the oocyte nucleus migrates towards the posterior end of the egg chamber (Godt and Tepass, 1998; Huynh and St Johnston, 2004). The subsequent localization of *gurken* (*grk*) mRNA at the posterior end of the oocyte results in the asymmetric secretion of Gurken protein (González-Reyes et al., 1995), which will signal posteriorly through its interaction with the EGF receptor Torpedo expressed in follicle cells (Roth et al., 1995). This induces these cells to become posterior follicle cells, which will signal back to the oocyte to drive cytoskeletal rearrangement. Notably, Torso feedback through Protein Kinase A (PKA) will result in the polarization of microtubules (Lane and Kalderon, 1995), leading to the asymmetric delivery of mRNAs at the anterior and posterior ends of the oocyte through MT-associated molecular motors (Figure 3A).

One of these mRNA is *bicoid* (*bcd*), which is maternally deposited and becomes localized at the anterior pole of the egg (Frohnhofer and Nüsslein-Volhard, 1986). After fertilization, *bcd* mRNA is translated, and the Bicoid (Bcd) protein diffuses from the anterior, forming a concentration gradient (Driever and Nüsslein-Volhard, 1988a, 1988b). Together with another protein, the morphogen Hunchback (Hb), Bicoid controls gene transcription for anterior specification in *Drosophila* (Simpson-Brose et al., 1994). High levels of Bcd and Hb at the anterior activate anterior-specific genes necessary for head and thorax development. Loss of Bcd results in severe anterior defects, while overexpression leads to ectopic anterior structures (Driever et al.,

1990). Why is it so? There is another protein, called Caudal (Cad) whose mRNA is expressed uniformly throughout the oocyte. Without Bcd, anterior regions would become posterior, but Bicoid represses *cad* mRNA in the anterior region (Rivera-Pomar et al., 1996). As a result, Cad only regulates gene expression posteriorly (Macdonald and Struhl, 1986; Rivera-Pomar et al., 1995). To specify the posterior region, another key factor, Nanos (Nos), is localized and translated at the posterior end (Wang and Lehmann, 1991), forming a gradient that inhibits Hunchback (Hb) translation, restricting this anterior factor to the anterior (Figure 3B). Together, Bcd and Hb specify anterior structures, while Cad and Nos specify posterior structures, establishing a robust A-P pattern. Additionally, *oskar* (*osk*) mRNA, is localized to the posterior end of the oocyte via RNA-binding proteins (such as Staufen, Figure 3B) and the actin and microtubule cytoskeletons (Kim-Ha et al., 1991; Brendza et al., 2000). This localization generates an Oskar protein gradient, which is key to organize the posterior patterning by anchoring other important factors, gathering germ plasm components to drive the formation of germ cells and allow embryonic development (Ephrussi et al., 1991).

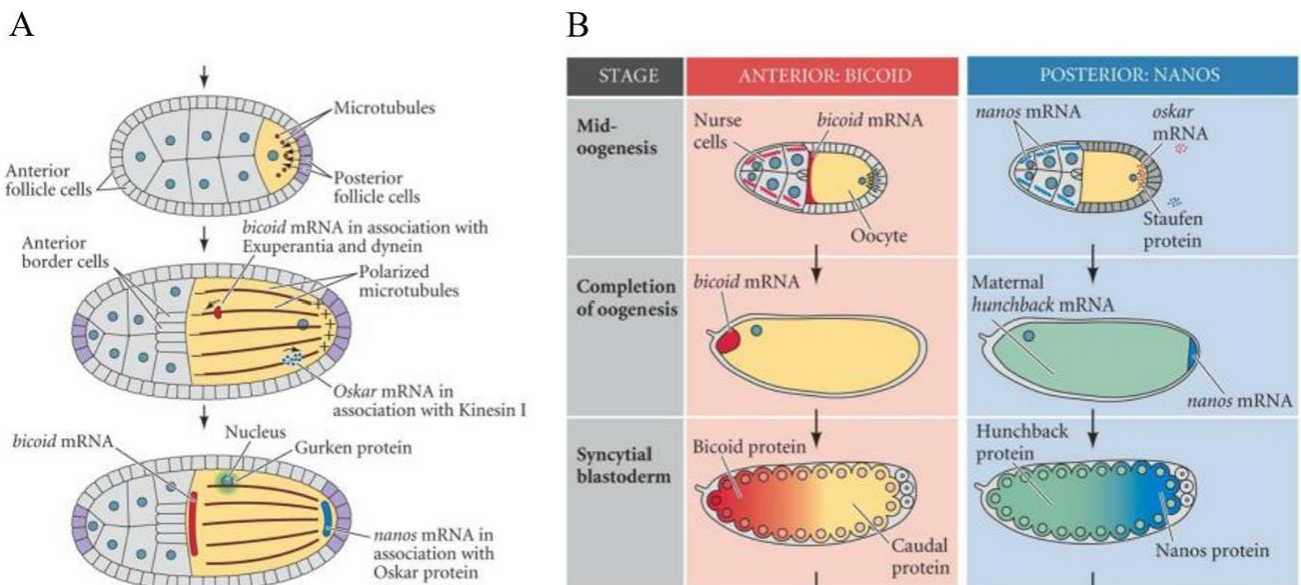


Figure 3. Anterior-Posterior axis specification in *Drosophila melanogaster*

A. Segregation of maternal mRNAs in the oocyte during *Drosophila* oogenesis through Gurken/EGFR-induced microtubule polarization. **B.** Early asymmetric localization of maternal mRNA translates into an embryonic morphogen gradient to specify the anterior-posterior axis. Images adapted from (Gilbert and Barresi, 2016).

The resulting gradient of maternal morphogens will regulate the expression of zygotic gap genes (such as *kruppel*), which in turn use positional information to translate their levels of expression into a pattern of downstream pair-rule genes (such as *even-skipped*), whose products will finally regulate the expression of segment polarity and

homeotic genes (such as *engrailed* or *ultrabithorax*). As a result, this signalling cascade translates early gene patterning into the establishment of an anterior-posterior axis in the embryo (Nasiadka et al., 2002).

1.2.2.2 Dorso-Ventral axis formation

As we saw previously, when the oocyte nucleus reaches the posterior end of the oocyte, the microtubule cytoskeleton is polarized to drive the asymmetric distribution of maternal mRNAs and initiate the anterior-posterior molecular cascade. But this cytoskeletal reorganization also drives the movement of the oocyte nucleus from the posterior end to an anterior-dorsal location through dynein-mediated transport (Koch and Spitzer, 1983; González-Reyes et al., 1995; Januschke et al., 2002) (Figure 4A). The oocyte nucleus is then anchored in the anterior-dorsal position (Guichet et al., 2001) to drive the synthesis of *gurken* mRNA between the nucleus and the neighbouring follicle cells. Gurken protein is locally translated and its short diffusion restricts its interaction to the Torpedo receptors present on the closest follicle cells, leading them to acquire a dorsal fate and morphology (Schüpbach, 1987; Neuman-Silberberg and Schüpbach, 1993). Torpedo signalling results in the local inhibition of the *pipe* gene expression in dorsal follicle cells (Sen et al., 1998). Conversely, Gurken does not diffuse to ventrally-located follicle cells, which can thus express Pipe protein (Figure 4B). Pipe thus allows the activation and the secretion of the Nudel protein at the cell membrane of ventral follicle cells only (Hong and Hashimoto, 1995). Nudel then induces a signalling cascade involving the serine proteases Gastrulation Defective (Gd), Snake (Snk) and Easter (Ea), leading to the cleavage of the Spätzle protein, a ligand of the Toll pathway (Anderson and Nüsslein-Volhard, 1984; Chasan et al., 1992). Even though Toll receptors are maternally deposited and ubiquitously expressed, Spätzle binding only occurs at the ventral oocyte membrane (Anderson et al., 1985; Hashimoto et al., 1988), thus restricting Toll activity to the ventral side (Figure 4C).

Spätzle-Toll signalling finalizes dorso-ventral axis specification by regulating the Dorsal transcription factor, which is ubiquitously expressed and controls key ventral fate determinants (Stathopoulos and Levine, 2004). To prevent the ubiquitous expression of ventral fate genes, Dorsal is bound to the protein Cactus. This binding restricts the nuclear translocation of Dorsal, thereby inhibiting its transcriptional activity (Kidd, 1992; González-Crespo and Levine, 1994). When Spätzle binds to Toll receptors on the ventral side, Toll activation leads to the recruitment of the protein Tube and the activation of the protein kinase Pelle. Pelle phosphorylates Cactus, inducing its degradation and releasing Dorsal (Shelton and Wasserman, 1993; Stathopoulos and Levine, 2002). Consequently, Dorsal translocates into the nucleus, promoting ventral cell fate specification (Figure 4C). Since the serine-protease signalling cascade creates a gradient of Spätzle protein that is highest in the most ventral region (Hashimoto et al., 2003), there is a gradient of Dorsal translocation into the ventral cells of the embryo, with the highest concentrations of Dorsal protein in the most ventral cell nuclei (Reeves and Stathopoulos, 2009). This graded distribution

of Dorsal results in the specification of different fates along the dorso-ventral axis (Stathopoulos et al., 2002), depending on Dorsal nuclear levels (Figure 4C).

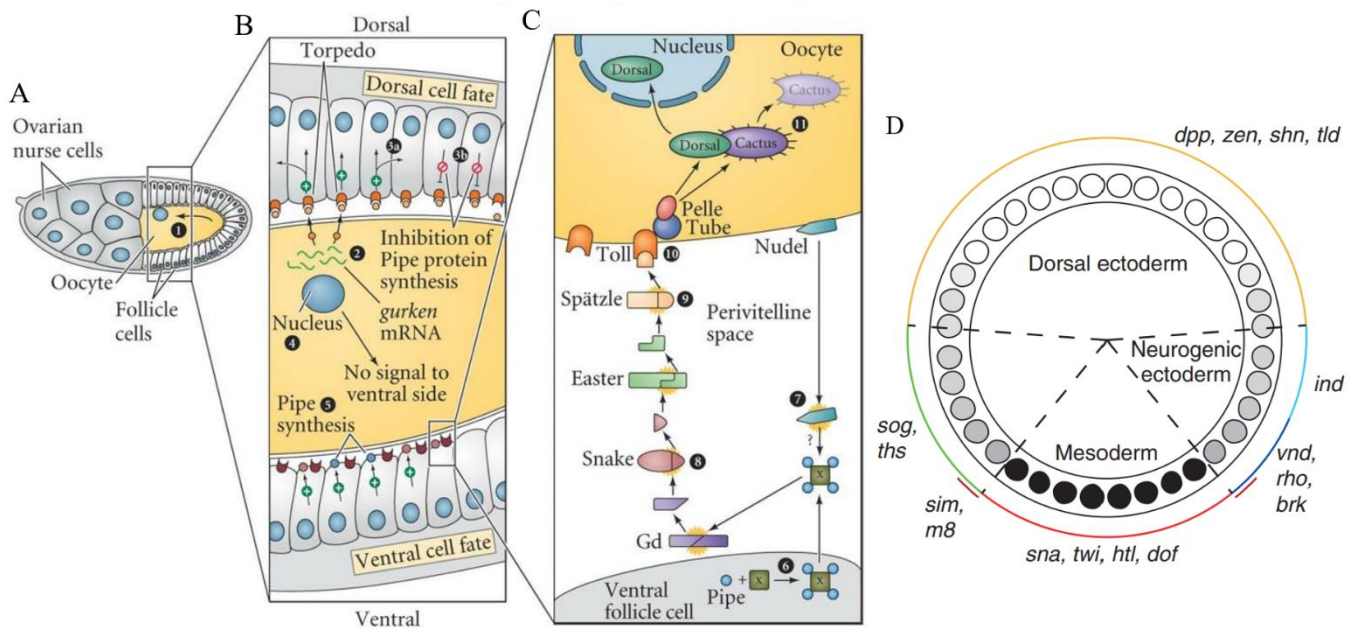


Figure 4. Dorso-Ventral axis specification in *Drosophila melanogaster*

A. Oocyte nucleus migration and anchoring to an anterior-dorsal location. **B.** Gurken signalling leads to the polarization of the oocyte through local inhibition of Pipe synthesis. **C.** Ventral Pipe signalling leads to a serine protease cascade, ultimately enabling Dorsal nuclear translocation and graded activity in ventral cells. **D.** Dorsal graded distribution and its threshold-based transcriptional activity specifies different gene expression and cell fates along the dorso-ventral axis. Images adapted from (Reeves and Stathopoulos, 2009; Gilbert and Barresi, 2016).

1.2.3 Gastrulation

After fertilization, axis specification and cellularization have occurred, the cellular blastoderm composed of an uniform columnar epithelial sheet of ~6000 cells is ready to undergo gastrulation. During this process, morphogenetic events involving changes in shape and topology, as well as fate determination, will organize the primary germ layers and transform the embryo into a multi-layered organism. In the following sections, I will describe three key morphogenetic events occurring during *Drosophila* gastrulation that are relevant to the research project I led, linking the underlying gene patterning of these different tissues to their unique behaviour: mesoderm invagination, germband extension, and posterior midgut invagination.

1.2.3.1 Mesoderm invagination

The Dorsal protein initiates mesodermal cell fate specification by activating the transcription factors Twist (Twi) and Snail (Sna) in ventral cells (Chopra and Levine, 2009). These transcription factors regulate downstream signalling pathways to trigger the first major morphogenetic event of *Drosophila* gastrulation: mesoderm invagination (Figure 5A). During this process, a band of ~1000 cells undergoes invagination, pinching off from the embryonic surface to form a transient ventral tube. This tube then flattens as the cells undergo an epithelial-to-mesenchymal transition (EMT, Figure 5B), migrating beneath the ventral ectoderm (Leptin and Grunewald, 1990). Ultimately, these mesodermal cells will differentiate into muscles, the circulatory system, and other internal tissues during later developmental stages (Frasch and Nguyen, 1999). Mesoderm invagination relies on multiple cell rearrangements: apical constriction, elongation, shortening, and basal expansion of cells, most of which are mediated by actomyosin contractions. Twist and Snail thus essentially regulate the expression of key components modulating actomyosin contractions to drive cell shape and topology changes (Seher et al., 2007).

Twist is a transcriptional activator that promotes the activation of a G-protein-coupled receptor (GPCR) pathway by inducing the expression of the signalling ligand Fog (Parks and Wieschaus, 1991; Costa et al., 1994; Kerridge et al., 2016). Twist also induces the expression of T48, a transmembrane protein that works in parallel with GPCR signalling to promote mesoderm invagination (Kölsch et al., 2007). Additionally, Twist enhances Snail expression, expands its domain, and sustains high Snail levels in the presumptive mesoderm (Stathopoulos et al., 2002). Snail promotes the expression of the GPCR Mist, to which Fog binds to drive cell constriction and tissue invagination (Manning et al., 2013). Twist and Snail coordinate the expression of multiple genes to regulate the cytoskeletal dynamics necessary for mesoderm invagination, with Twist promoting sustained cell apical contractility and Snail fine-tuning gene expression to promote effective cell shape changes and tissue movements (Martin et al., 2009, 2010).

Not only does the spatial distribution of Snail and Twist specify the location of cells that will invaginate, but the timing of their expression in different cells of this band also influences the directionality of folding. Transcriptional pre-patterning of these genes in the most ventral cells compared to ventro-lateral cells leads to a graded distribution of the downstream effectors, imparting directionality to the folding of the presumptive mesoderm along the dorso-ventral axis (Lim et al., 2017).

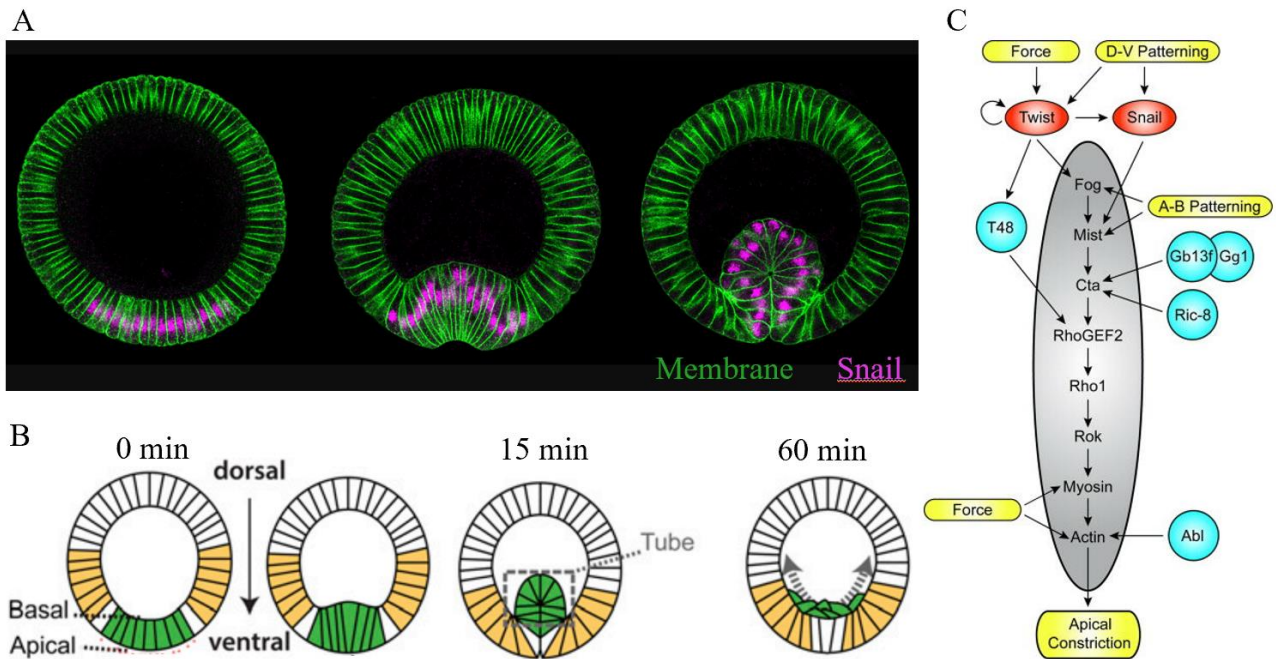


Figure 5. Mesoderm invagination: from morphogens to morphogenesis

A. Cross-section fluorescence images of the embryo showcasing the invagination of the Snail-expressing mesoderm cells at the ventral side. **B.** Schematic representation of mesoderm invagination, ventral tube formation and subsequent EMT and migration of mesoderm cells. **C.** Schematic representation of the Snail and Twist-dependent signalling pathways controlling actomyosin-mediated cell rearrangements during mesoderm invagination. Images adapted from (Manning and Rogers, 2014; Martin, 2020, the He lab).

1.2.3.2 Posterior Midgut Invagination

After the onset of mesoderm invagination, a group of blastoderm cells at the posterior end of the embryo undergo shape changes to generate the posterior midgut (PMG) invagination. These cells move dorsally and anteriorly, forming a pocket that engulfs the primordial germ cells, ensuring the proper positioning of the future gonads and creating the posterior part of the future digestive tract (Figure 6B). The PMG invagination is controlled by the terminal system of AP pattern formation, a signalling pathway responsible for the specification of the anterior and posterior ends. This system is activated by the localized expression of the receptor tyrosine kinase Torso, which is distributed at the anterior and posterior poles of the embryo (Degelmann et al., 1986; Klingler et al., 1988). Upon activation, Torso triggers a signalling cascade that leads to the expression of terminal gap genes such as *huckebein* and *tailless* (Figure 6A). In the posterior endoderm, Fog expression is induced by the transcription factors Huckebein and Tailless, leading to coordinated constriction of endodermal cells (Weigel et al., 1990; Costa et al., 1994). It is interesting to note that the Fog pathway is used iteratively across several morphogenetic processes in *Drosophila*, during mesoderm and PMG invagination at embryonic stages, during salivary gland

internalization at mid-embryogenesis, and during imaginal disc folding at larval stages (Nikolaidou and Barrett, 2004). While Fog is not essential for mesoderm invagination, as *fog* mutant embryos can still fold the presumptive mesoderm, posterior midgut invagination is abolished in *fog* mutants (Costa et al., 1994; Dawes-Hoang et al., 2007). This difference may be due to the existence of redundant mechanisms in the mesoderm, such as the T48 pathway, that compensate for the absence of Fog. Additionally, posterior midgut might rely more than the mesoderm tissue on an intercellular signalling relay involving mechanical coupling between cells (Pouille et al., 2009; Mitrossilis et al., 2017; Bailles et al., 2019). The PMG is also attached to the vitelline membrane via integrin-mediated adhesion, relying on the localized expression of the α PS3 integrin *scab* in the posterior-dorsal region. Interestingly, this attachment is conserved in insect gastrulation and is key for proper embryonic development, as its disruption leads to abnormal gastrulation movements (Bailles et al., 2019; Münster et al., 2019). Finally, recent work has shown that the polarized tissue flow observed during posterior midgut invagination is driven by the interplay between tissue curvature and differential actomyosin contractility at the apical and basal sides of the cells (Gehrels et al., 2023).

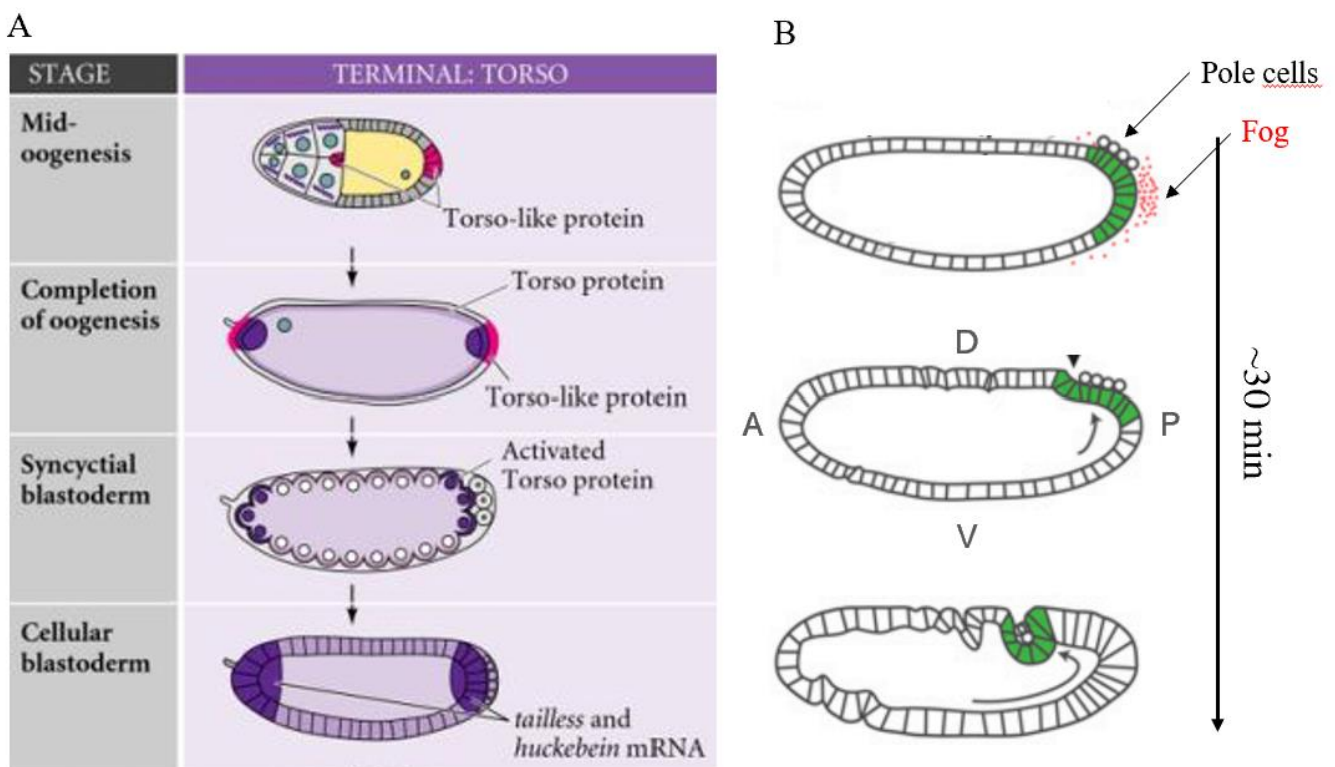


Figure 6. Terminal gene patterning drives posterior midgut invagination through Fog signalling

A. Early terminal patterning and activation of Torso-like leads to the polarized expression of Huckebein and Tailless at the embryo poles. **B.** Schematic representation of Fog signalling driving germ cell internalization and posterior midgut formation. Images adapted from (Gilbert and Barresi, 2016; Martin, 2020).

1.2.3.3 Germband extension

Germ-band extension (GBE) is another key morphogenetic process taking place during *Drosophila* gastrulation, which translates transcriptional patterning into tissue elongation. During this event, the germ band, spanning ventral and lateral ectodermal cells, extends along the A-P axis, doubling its length while narrowing along the D-V axis (Turner and Mahowald, 1977; Hartenstein and Campos-Ortega, 1985)(Figure 7A). GBE begins shortly after mesoderm invagination is initiated and is driven by oriented cell intercalations, where cells exchange their neighbours in a polarized fashion along one axis to drive the extension of the tissue in the orthogonal direction (Irvine and Wieschaus, 1994). Cell intercalations occur through two main rearrangements: T1 transitions and rosette formations (Figure 7B, the different types of cell rearrangements will be detailed in later sections). T1 transitions involve cell neighbour-exchange via actomyosin-mediated junctional shrinkage and expansion (Bertet et al., 2004). Since the actomyosin network is planar polarized in the germband, the junctional remodelling between cells is predominantly oriented along the D-V axis and cell neighbour-exchanges result in the formation of new junctions along the A-P axis throughout the tissue (Figure 7B). The cumulative resolution of these polarized T1 transitions then translates into the global elongation of the germband along the A-P axis. Similarly, rosettes form through the collapse of multiple junctions into a single point (via D-V oriented actomyosin cables), then resolving along the A-P axis (Blankenship et al., 2006).

This fascinating morphogenetic event was shown to be controlled by the A-P patterning system, as mutations in the A-P patterning genes result in reduced or absent GBE (Nüsslein-Volhard and Wieschaus, 1980; Lehmann and Nüsslein-Volhard, 1986; Irvine and Wieschaus, 1994; Zallen and Wieschaus, 2004). Interestingly, mutant embryos for the D-V patterning still manage to undergo GBE (Zallen and Wieschaus, 2004). Lot of efforts have thus been made to uncover how downstream signalling from the A-P patterning system can regulate oriented cell intercalations and tissue elongation. It was first shown that the pair-rule genes *eve* and *runt* control the segmental expression of three Toll family receptors (Toll-2, Toll-6, and Toll-8), which drive the planar polarized distribution of adhesion components (Par3/Bazooka) and actomyosin to extend the germband through polarized cell intercalations (Paré et al., 2014). Later work then revealed that other factors (Tartan, Teneurin-m, and the GPCR Cirl) synergize with the 'Toll code' to specify the correct location of these molecular effectors and impart planar polarity to the tissue, as well as specify compartment boundaries that act as barriers to avoid cell mixing throughout embryonic and larval development (Paré et al., 2019; Lavalou et al., 2021)(Figure 7C-D).

Finally, besides the patterned intrinsic molecular effectors that control cell intercalations, recent studies have highlighted the role of extrinsic factors in the elongation of the ectoderm. Notably, it was shown that the posterior midgut invagination can generate large-scale mechanical deformations and tension that contribute to the extension of the germband (Collinet et al., 2015; Lye et al., 2015; Yu

and Fernandez-Gonzalez, 2016). If you want to deepen your understanding of the conserved processes controlling convergence-extension, please consult the excellent book chapter by (Paré and Zallen, 2020).

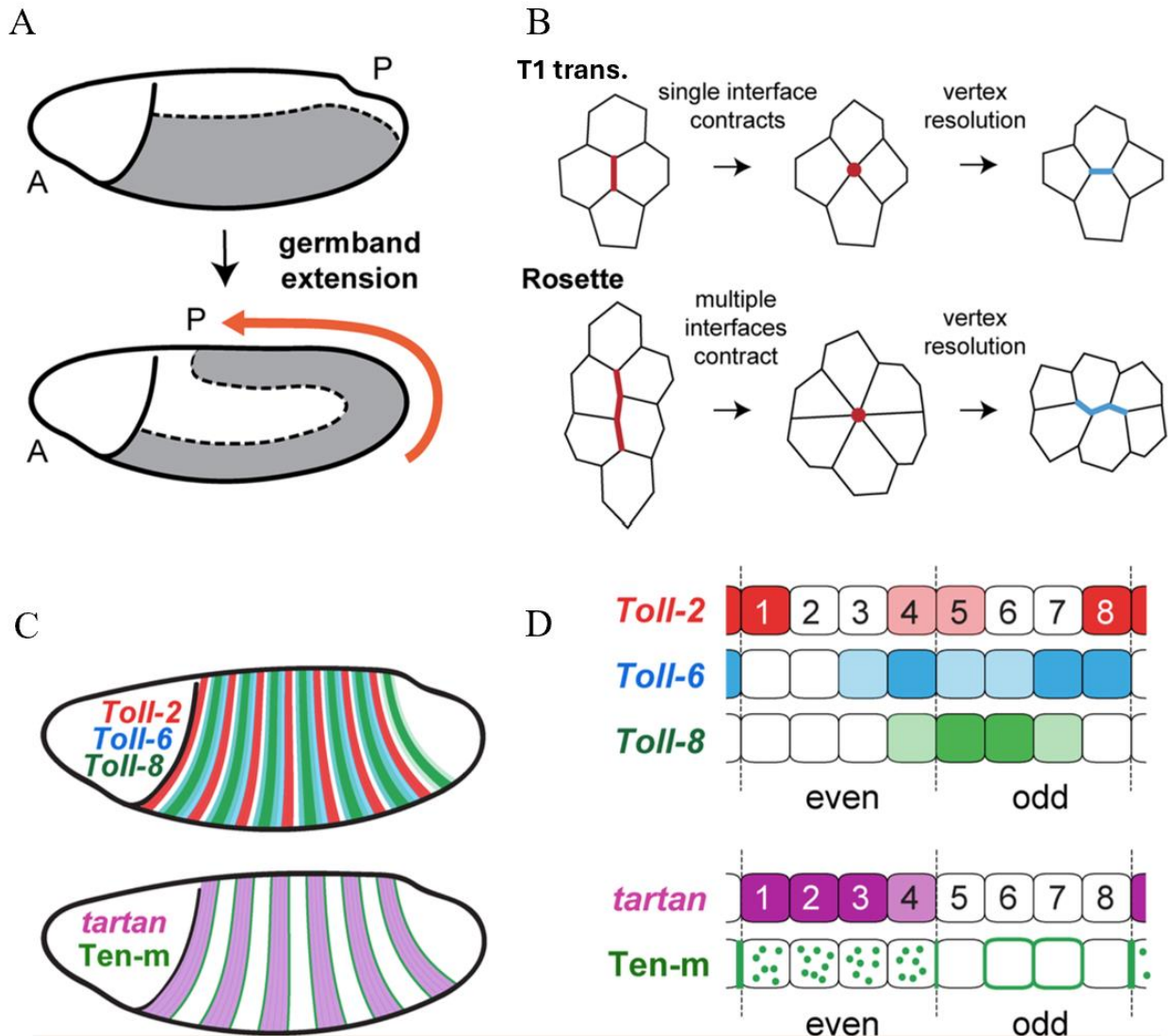


Figure 7. Germband Extension : A-P signalling patterns drive the convergence-extension of the ectoderm

A. The germband drives body axis elongation by doubling its length along the A-P axis. **B.** T1 transitions and rosette drive polarized cell intercalations to extend the tissue. **C-D.** Stripped expression of Toll receptors and Tartan/Teneurin-m drives a positional code to specify planar polarity in the germband. Images adapted from (Paré and Zallen, 2020).

2. Shape and topology changes of epithelia during gastrulation

In the previous section, we discussed the key features of early *Drosophila melanogaster* development, from fertilization and axis specification to the first morphogenetic processes of gastrulation, highlighting how the precise gene patterning of early organisms can spatiotemporally control tissue remodelling. One might wonder how embryos achieve to robustly establish morphogen gradients and self-organize their transcriptional patterning with such precision. Several research projects using both *Drosophila* embryos and mammalian gastruloids have made significant progresses in that regard, establishing mathematical frameworks and genetic studies to show how enhancer-promoter communication and multi-scale feedbacks can fine-tune gene patterning to the single cell resolution. Yet, the mechanisms that allow organisms to suppress noise to robustly develop remain to be discovered (Jaeger et al., 2004; Gregor et al., 2007; Furlong and Levine, 2018; Zoller et al., 2018; Merle et al., 2024).

Since most of the morphogenetic mechanisms are conserved across species, it appears that *Drosophila* gastrulation can be used as a paradigm for epithelial tissue morphogenesis. In the next section, I will now dive into the cellular processes that govern epithelial tissue remodelling. The first part will focus on the conserved nature of epithelial sheets to understand how their structure and specificity prime epithelial cells for shape and topology changes during early development. The second part will describe the cellular behaviours underlying epithelial morphogenesis. To date, many complex shape changes have been observed across species, yet most can be described as a combination of simple transformations. In our lab, we propose that no more than seven categories of events can recapitulate the variety of shapes seen in the animal kingdom: growth, shrinkage, bending (or folding), thinning, thickening, convergence-extension and twisting (John and Rauzi, 2021). For clarity, I will only discuss the cellular behaviours that are relevant to my research project.

2.1 Epithelial sheets: the ideal substrate for tissue morphogenesis

Due to their structural and functional characteristics, epithelial sheets are considered ideal substrates for tissue morphogenesis. Firstly, epithelial cells exhibit a high degree of apical-basal polarity and form cohesive sheets through cell-cell junctions, such as adherens junctions and tight junctions (Figure 8A), which provide mechanical stability during morphogenetic movements (Gumbiner, 1996; Lecuit, 2005). This polarity and connectivity allows coordinated cell behaviours to take place, while maintaining structural integrity (Zallen and Blankenship, 2008). Secondly, epithelial sheets can act as blank canvas on which mechanical forces and transcriptional signalling rearrange cell-cell junctions and cytoskeletal elements to shape the future organism (Lye and Sanson, 2011; Hannezo et al., 2014; Fouchard et al., 2020). Additionally, planar cell polarity pathways in epithelial sheets can instruct the uniform

orientation of cells within the plane of the tissue, which allows the directional tissue movements observed during several developmental processes (Singh and Mlodzik, 2012). Finally, epithelial tissues can interact with underlying mesenchymal layers through basement membranes, and integrate non cell-autonomous chemical and mechanical signals to guide morphogenetic processes (Wang et al., 2021). These properties make epithelial sheets versatile and robust substrates to generate the diverse tissue shapes observed in multicellular organisms. Even though epithelia can have different architectures, such as columnar, cuboidal, and squamous epithelia, as well as simple and stratified forms (Muse et al., 2024), I will mostly discuss the properties of simple columnar epithelial sheets which undergo the major remodelling events observed during early development.

2.1.1 Adhesion and apico-basal polarity in epithelial sheets

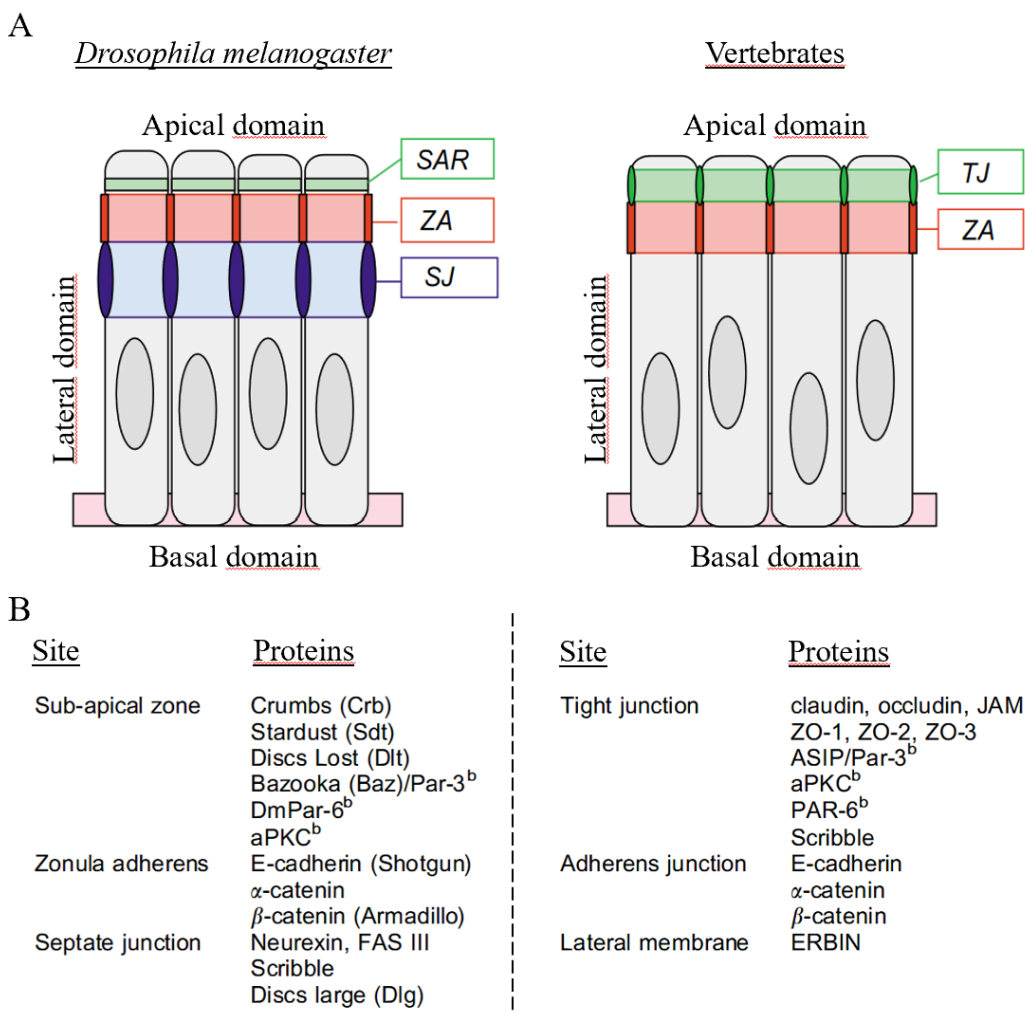


Figure 8. Adhesion proteins and cell domains in columnar epithelial tissues

A. Comparative scheme of the architecture of simple columnar epithelial cells in *Drosophila* and vertebrates. **B.** Conservation and distribution of proteins in the different junctional compartments of columnar epithelial cells in *Drosophila* and vertebrates. Images adapted from (Knust, 2002; Gibson and Perrimon, 2003).

Given the bidirectional relationship between apico-basal polarity and adhesion, I will present how both are co-organized in columnar cells to regulate epithelial functions. Additionally, I will highlight the conservation of their structure and function between *Drosophila* and vertebrates.

In columnar epithelia, cells are more tall than wide, and segregate cellular components into apical and basolateral domains with distinct junctional components to establish an apico-basal polarity (Figure 8A). Cell adhesion in columnar epithelia is mediated primarily through adherens junctions and tight junctions (Knust, 2002). Adherens junctions, located below the apical surface, are composed of cadherin proteins, such as E-cadherin in vertebrates and DE-cadherin in *Drosophila*, which engage in homophilic interactions with cadherins on the neighbouring cells, or are linked intracellularly to the actin cytoskeleton via catenin proteins to control cellular tension and tissue stability (Harris and Tepass, 2010; Harris, 2012). Basal adherens junctions have also been reported in *Drosophila*, transiently during cellularization and more stable in the wing imaginal discs (Hunter and Wieschaus, 2000; Lecuit and Wieschaus, 2000; Kroeger et al., 2024). In imaginal discs, they were described as basal spot junctions, highly sensitive to fluctuations in cytoskeletal tension and coupled to the mechano-sensing Hippo pathway to translate morphogenetic forces into organ size regulation (Kroeger et al., 2024). Tight junctions are another type of junction which create a selective barrier to regulate paracellular transport and maintain cellular polarity in epithelia (Figure 8A). In vertebrates, tight junctions are composed of claudins, occludins, and junctional adhesion molecules (JAMs), which interact with scaffolding proteins like ZO-1, ZO-2, and ZO-3 (Zihni et al., 2016)(Figure 8B). In *Drosophila*, similar functions are performed by septate junctions (SJ), which share molecular components with vertebrate tight junctions (Hall and Ward, 2016). During *Drosophila* early and mid-embryogenesis (stages 4 to 13) adherens junctions prevail, and septate junctions will only be observed long after the onset of gastrulation, during stages 14 to 17 (Tepass and Hartenstein, 1994), in ectodermally-derived epithelia which require SJ to establish a strong paracellular barrier (e.g, in the blood-brain barrier to protect the nervous system from pathogens (Baumgartner et al., 1996)).

The apico-basal organization of epithelial cells is controlled by a network of polarity proteins highly conserved between *Drosophila* and vertebrates, including the Crumbs complex (Crumbs, Stardust, and PATJ), the Par complex (Par-3, Par-6, and aPKC), and the Scribble complex (Scribble, Discs large, and Lethal giant larvae). These complexes are mutually antagonistic to specify the position of apical and basolateral domains of epithelial cells (Figure 9). The Crumbs complex, consisting of Crumbs and PALS1 (Stardust in *Drosophila*), interacts with additional proteins like PATJ and LIN7 to localize to the apical membrane. This complex not only defines the apical identity but also anchors other apical polarity factors (Wodarz et al., 1995). The PAR proteins, including PAR-3 (Bazooka in *Drosophila*), PAR-6, and aPKC, function in a complex to regulate both apical and junctional complexes. PAR-3 (Bazooka) is also key for the organization and positioning of adherens junctions in *Drosophila* and vertebrates (Harris and Peifer, 2004; Thompson, 2022). PAR-6 interacts with aPKC to promote aPKC activation and anchoring at the apical membrane. Scribble complex proteins (Scribble, Dlg, Lgl) in both species establish basolateral identity by

counteracting apical polarity factors and regulate lateral domain architecture through interactions with septate junction and tight junction proteins in *Drosophila* and vertebrates, respectively (Figure 9) (Bilder et al., 2003; Hurd et al., 2003; Tanentzapf and Tepass, 2003; Yamanaka et al., 2003).

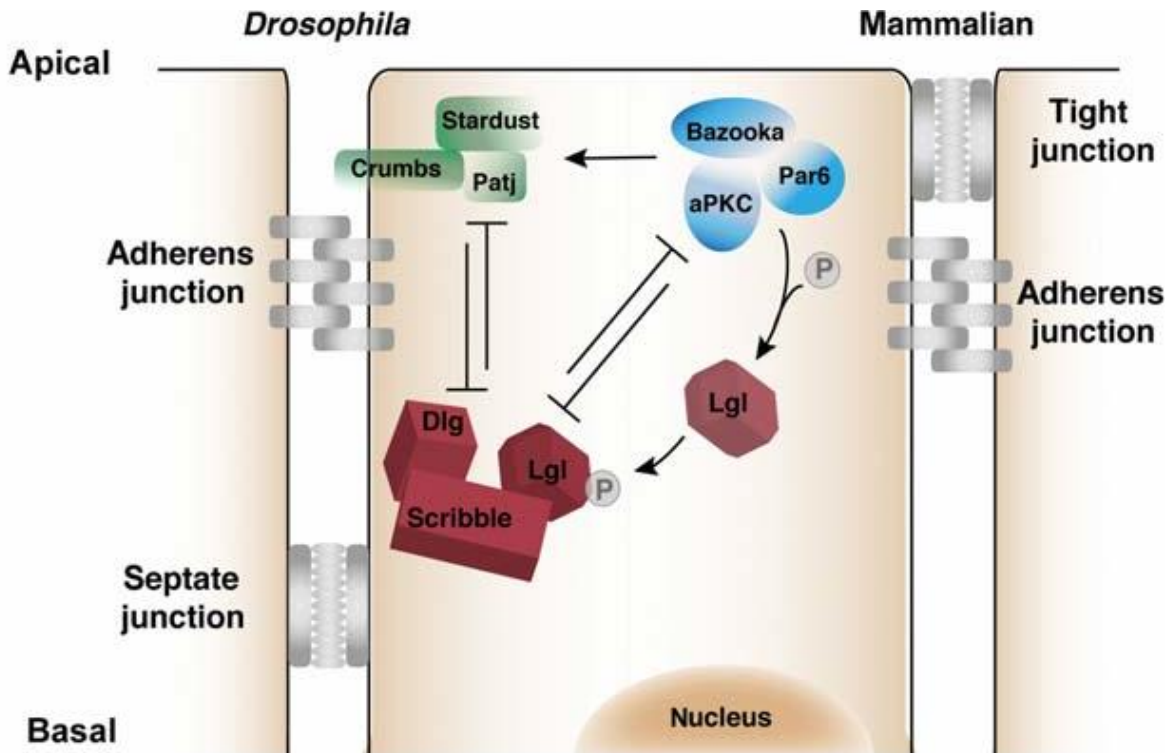


Figure 9. Activity of polarity protein complexes in epithelial polarization in *Drosophila melanogaster* and vertebrates

Image adapted from (Elsum et al., 2012).

The functional conservation of these polarity proteins is striking. For example, in both *Drosophila* and vertebrates, mutations in *crumbs* or *par* genes result in loss of epithelial polarity and adhesion (Tepass, 1996; Hurd et al., 2003; Plant et al., 2003). Additionally, substituting the intracellular domain of *Drosophila* Crb by the intracellular domain of the CeCrb2 ortholog from *C.elegans* did not affect the organization of embryonic epithelial tissues in *Drosophila*, highlighting the evolutionary conserved role of such complexes in epithelial sheets (Shi et al., 2017). Adhesion between epithelial cells, together with the apico-basal organization of epithelia, ensures the proper integrity of the tissue, favours intercellular and paracellular signalling and primes epithelia to sense and transmit forces, making them ideal substrates for morphogenesis (Lecuit and Yap, 2015; Pinheiro and Bellaïche, 2018; Buckley and St Johnston, 2022).

The establishment and maintenance of apico-basal polarity in epithelia is obviously much more complex than what I depicted in this section, I would thus recommend the great review by (Buckley and St Johnston, 2022) for a more complete overview of the subject.

2.1.2 Planar cell polarity in epithelial sheets

The concept of planar cell polarity is fairly old, as the first observations of PCP are thought to date from the 17th century, when Robert Hooke discussed the peculiar orientation of hair bristles in insects (Hooke et al., 1667), which later served as a template for the identification of PCP genes (Gubb and García-Bellido, 1982) that I will discuss in this section.

The core PCP pathway uses a conserved set of PCP components to establish the coordinated cell orientation in epithelia. In *Drosophila*, PCP signalling begins with the asymmetric localization of Frizzled (Fz) and Dishevelled (Dsh), that transmit polarity cues across the cell membrane (Figure 10A). Fz is a seven-pass transmembrane receptor that activate Dsh. Dsh then recruits other core PCP proteins such as Van Gogh (Vang), Prickle (Pk), Diego (Dgo), and Flamingo (Fmi) to the plasma membrane (Figure 10B). Vang interacts with Fz and localizes asymmetrically to opposite sides of cells to maintain the planar polarity (Adler, 2012; Singh and Mlodzik, 2012; Devenport, 2014). Dgo supports the stabilization of the asymmetric complexes by enhancing the interactions between Fz and Dsh, while Fmi is a cadherin-like protein that homodimerizes between adjacent cells to strengthen the planar polarity via cell-cell adhesion (Butler and Wallingford, 2017). In vertebrates, homologs of these core PCP proteins (with additional components such as Vangl1/2) play similar roles in tissues such as the inner ear, where the core PCP pathway ensures the correct orientation of sensory hair cells to allow the development of auditory function, or the proper neural tube closure (Kibar et al., 2001; Murdoch et al., 2001; Seifert and Mlodzik, 2007; Rida and Chen, 2009).

The Fat-Dachsous (Ft-Ds) pathway is a non-core PCP mechanism that complements the core PCP pathway (Figure 10C). Ft and Ds are atypical cadherins that interact hetero-typically across adjacent cells. This interaction leads to the asymmetric distribution of Ft and Ds at the cell membrane, a recurring and necessary step among the PCP pathways to polarize the tissue (Matis and Axelrod, 2013; Sharma and McNeill, 2013). In *Drosophila*, Ft-Ds signalling can synergize with the core PCP proteins by modulating the localization and activity of Dsh and Vang to strengthen the planar polarity across the tissue, as illustrated during the establishment of tissue-wide cell orientation in the wing, eye and abdomen (Bryant et al., 1988; Yang et al., 2002; Mangione and Martín-Blanco, 2018). This pathway is conserved in vertebrates, where Fat4 and Dchs1/2 have been shown to be essential during tissue morphogenesis (Fulford and McNeill, 2020), and mutations in Fat4 can disrupt kidney tubule morphogenesis in mice (Saburi et al., 2008).

One might wonder how the asymmetric distribution of PCP components is achieved? In PCP pathways, interactions between the different components have been described as a ‘feedback amplification of asymmetry’, as asymmetry relies on the antagonist effects of proximal and distal systems to self-organize planar polarity (Tree et al., 2002; Peng and Axelrod, 2012). As a result, disruption of any single core PCP protein is sufficient to disrupt the global asymmetric patterning (Bastock et al., 2003; Strutt

and Strutt, 2007). This amplification actually requires an initial bias, which is thought to rely on the polarized distribution of PCP components by the microtubule (MT) cytoskeleton. Microtubule-based trafficking is used to introduce biases that break symmetry and arrays of planar polarized microtubules have been reported in several PCP-patterned tissues (Hannus et al., 2002; Mathewson et al., 2019). Indeed, these polarized microtubule arrays can bias the transport of vesicles consisting of Dsh, Fz and Fmi towards one side of the cell, to initiate the PCP patterning process (Shimada et al., 2006; Matis et al., 2014). This initial bias can be subtle and with amplification result in the emergence of global asymmetry (Aw et al., 2016). Interestingly, the PCP system might also feedback on cytoskeletal polarization, as it has been shown that intact PCP patterns are necessary for the polarization of microtubule arrays (Olofsson et al., 2014). Finally, one might go one step further and ask how the polarized distribution of microtubules is first established? To answer that, recent work has shown that tissue strain anisotropy can establish the polarity bias of cytoskeletal MTs that will then instruct the PCP (Chien et al., 2015; Singh et al., 2018). Interestingly, MTs appear to be necessary for the establishment but not the maintenance of PCP (Sepich et al., 2011; Shi et al., 2016).

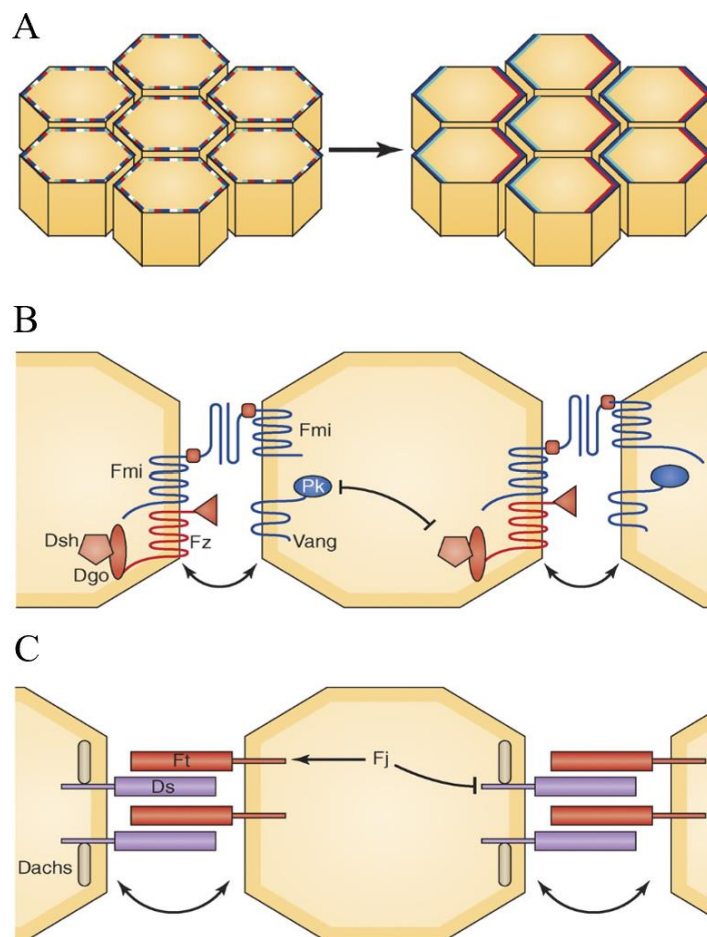


Figure 10. Planar cell polarity pathways drive tissue-wide cell orientation

A. An initial uniform distribution of core PCP proteins progressively becomes asymmetric. Fz, Dsh, and Dgo (red) localize to the distal edge, while Vang and Pk (light blue) localize to the proximal side. Fmi (dark blue) localizes to both sides. **B.** Feedback interactions between core PCP components, where Fz–Fmi complex interacts preferentially with a Vang–Fmi complex between cells, and proximal and distal complexes antagonize each other. **C.** Asymmetric localization of Ft and Ds, which form heterodimers between adjacent cells, and associate with Dachs. Images adapted from (Devenport, 2014).

The interplay between different PCP pathways adds another layer of complexity to the regulation of epithelial polarity: in addition to the core PCP and Ft-Ds pathways, the Hippo pathway and the canonical Wnt/ β -catenin pathway can interact with PCP signalling to coordinate cellular behaviours. For instance, the Hippo pathway regulates tissue growth and cell proliferation by modulating the activity of YAP/TAZ transcription factors, and its activity has been shown to be influenced by the expression of PCP proteins (Bennett and Harvey, 2006; Willecke et al., 2006; Zecca and Struhl, 2010). Conversely, Wnt/ β -catenin signalling can synergize with PCP signalling in vertebrates to ensure the proper directionality of convergent extension movements (Heisenberg et al., 2000; Gao et al., 2011).

Epithelial planar cell polarity can also be controlled by alternate mechanisms, as previously discussed during *Drosophila* GBE, where signalling downstream of AP patterning can regulate the PCP distribution of actomyosin and adhesion molecules to orient cell intercalations and drive directional elongation of the ectoderm tissue (Paré et al., 2014).

2.1.3 Epithelia-Matrix interactions

Another key feature of epithelial sheets is their ability to interact with the underlying extracellular matrix (ECM), mainly through integrin receptors formed by heterodimers of α and β subunits (Ro, 1992). The extracellular domain of integrins binds to ECM proteins, such as laminin and fibronectin, while the intracellular domain associates with cytoskeletal elements, regulating cell adhesion and signal transmission between the ECM and epithelial cells (Katz and Yamada, 1997). This signalling is key during tissue morphogenesis, as it was shown that ECM can guide cell migration and intercalation during *Xenopus* gastrulation (Marsden and DeSimone, 2001) or during *Drosophila* wing disc morphogenesis (Harmansa et al., 2023). Additionally, loss of integrins was shown to impair *Drosophila* wing formation (Brown et al., 2000; Domínguez-Giménez et al., 2007) and cell-ECM interactions were reported to be necessary for kidney development in vertebrates (Kreidberg and Symons, 2000).

2.2 Cell shape and topology changes driving gastrulation movements

Epithelial sheets are thus optimal substrates for morphogenetic processes to take place and shape the organism. In this section, I will now detail the shape and topology

changes occurring in columnar epithelial cells to direct two fundamental morphogenetic processes: tissue bending and tissue elongation.

2.2.1 Cell behaviours driving tissue bending

One of the key features of the epithelial remodelling observed during development is the ability of epithelial sheets to bend into folds, ridges, pits, and tubes. Tissue bending is used iteratively throughout embryogenesis and organogenesis, as illustrated during mesoderm invagination in *Drosophila* embryos (Leptin and Grunewald, 1990; Sweeton et al., 1991), neural tube closure in vertebrates (Haigo et al., 2003), or the formation of the branched architecture of the lung (Kim et al., 2013). Bending can occur via several coordinated cell behaviours that I will describe in this section (Odell et al., 1981; Pearl et al., 2017).

2.2.1.1 Apical constriction

Apical constriction is a shape change that involves the contraction of the apical surface of epithelial cells, leading to a reduction in the cell apical area and the inward bending of the epithelial sheet (Figure 11A). Early physical models demonstrated that differential tension between the apical and basal surfaces, while maintaining cell volume and height, leads to epithelial bending (Lewis, 1947). It was later identified that a contractile network of actomyosin (driven by the association of actin with type II Myosin motors) is recruited at the apical surface of cells to induce apical constriction (Baker and Schroeder, 1967)(Figure 11B).

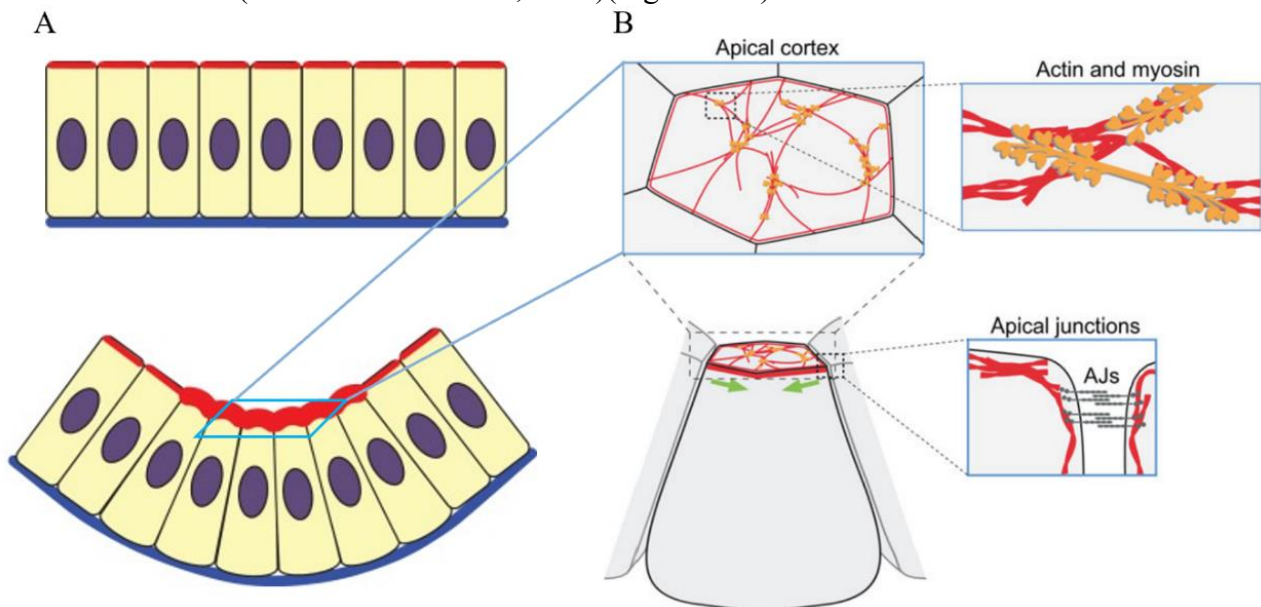


Figure 11. Actomyosin-dependent apical constrictions drive tissue bending

A. Differential apical and basal tension induce bending of the epithelial sheet. **B.** Pulsed apical actomyosin shrinks the apical surface and transmits forces through adherens junctions. Images adapted from (Martin and Goldstein, 2014; Pearl et al., 2017).

Several studies during *Drosophila* mesoderm invagination or vertebrate neural tube closure showed that the localization and activity of this contractile network of actomyosin is under the control of precise gene patterning and downstream signalling involving the Rho pathway and the Shroom family proteins (Haigo et al., 2003; Martin and Goldstein, 2014; Gilmour et al., 2017).

Interestingly, it was shown during *Drosophila* mesoderm invagination that apical cell surface shrinkage occurs through transient pulses of ratchet-like constriction, with individual cells contracting asynchronously and stabilizing in a contracted state between pulses (Figure 11B) (Martin et al., 2009). This pulsatile behaviour of cells and underlying actomyosin flows appear to be conserved across morphogenetic events and species (Munro et al., 2004; Blanchard et al., 2010; Azevedo et al., 2011; Michaux et al., 2018). Finally, it was demonstrated that to translate contractility into cell shape changes, the tension generated by actomyosin contractions must be transmitted through adherens junctions (Roh-Johnson et al., 2012), thus coordinating the contractile behaviour of neighbouring cells and generating the bending of the entire epithelial sheet (Figure 11).

2.2.1.2 Basal relaxation

Theoretical frameworks established that cell volume can only be conserved during apical constriction in folding tissues if it is accompanied by either basal expansion, height increase, or both (Polyakov et al., 2014). Height increase has been observed prior to tracheal and salivary gland placode invagination in *Drosophila* embryos (Kerman et al., 2006), and basal relaxation has been reported during the chick otic placode invagination and shown to be necessary for *Drosophila* ventral mesoderm invagination (Sai and Ladher, 2015; Krueger et al., 2018). Basal relaxation mostly results from the disassembly of actomyosin networks at the basal side of epithelial cells (Figure 12A). The molecular mechanism that spatiotemporally controls such disassembly remains unknown, but it has been postulated that competition between actomyosin networks could be the reason for this local regulation, as appearance of actomyosin in one part of the cell was shown to induce the depletion of other actomyosin pools during cell migration (Lomakin et al., 2015). Interestingly, basal relaxation can also result from the localized reduction of underlying ECM density, as shown during *Drosophila* wing imaginal disc hinge fold formation (Sui et al., 2018).

2.2.1.3 Cable-driven buckling

The folding of epithelial sheets can also result from supracellular structures that coordinate contractions (Röper, 2013), as illustrated during the chicken neural tube closure, where supracellular myosin cables promote cell intercalation and neuroepithelium bending (Nishimura and Takeichi, 2008; Nishimura et al., 2012). Similarly, circumferential actomyosin cables have been reported to drive salivary gland tubulogenesis in *Drosophila* (Figure 12B) (Röper, 2012; Chung et al., 2017).

2.2.1.4 Cell shortening

Another mechanism that complements apical constriction to drive the invagination of epithelial sheets is cell shortening (Figure 12C). Cell shortening has been observed in several developmental processes, such as *Drosophila* leg epithelium joint formation, cephalic furrow formation and mesoderm invagination. During these morphogenetic processes, cell shortening results from the establishment of lateral tension, driven by the recruitment of actomyosin along the apico-basal axis (Monier et al., 2015; Gracia et al., 2019; John and Rauzi, 2021a; Popkova et al., 2024). These observations actually confirm physical models of epithelial folding that postulated that lateral tension was required for epithelial folding, as apical constriction *per se* can only recapitulate the initial furrowing of the tissue but not its internalization (Conte et al., 2012; Fierling et al., 2022). This process appears to be conserved as the sequential recruitment of apical and basolateral actomyosin was reported during ascidian gastrulation, and the resulting apicobasal cell shortening promoted endoderm invagination (Sherrard et al., 2010). Finally, actomyosin-independent shortening of cells was demonstrated during *Drosophila* dorsal formation, where the basal shifting of adherens junctions was shown to induce a mismatch with the apical adherens junctions of neighbouring cells, thus initiating tissue buckling (Wang et al., 2012).

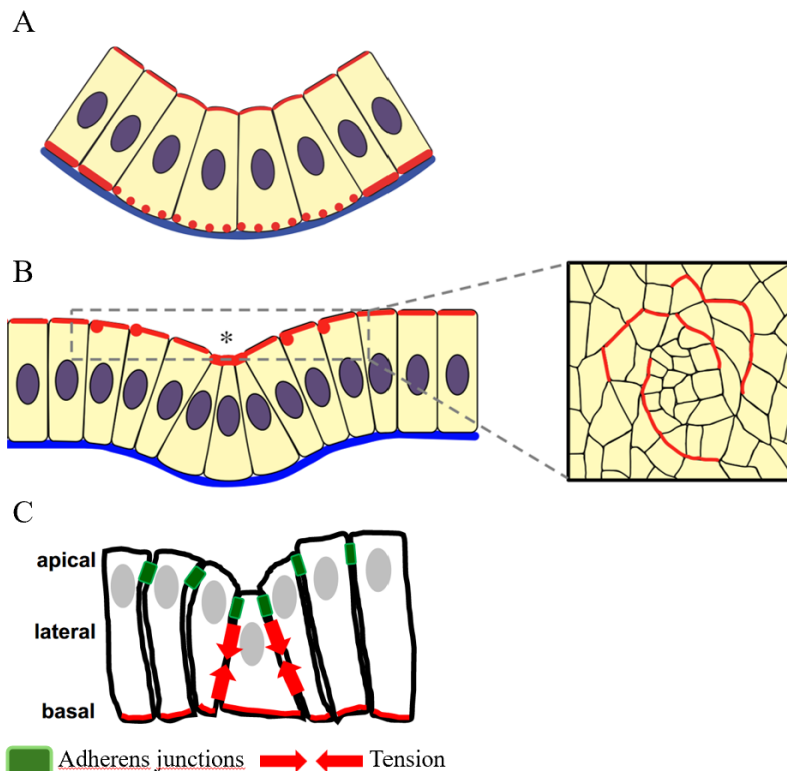


Figure 12. Cellular behaviours promoting epithelial folding

A. Localized actomyosin disassembly leads to basal relaxation and wedge-shaped cells to promote tissue bending. **B.** Supracellular actomyosin cables drive tissue buckling. **C.** Actomyosin-driven lateral tension promotes cell shortening for epithelial folding. Images adapted from (Pearl et al., 2017; Popkova et al., 2024).

2.2.1.5 Programmed cell death

Finally, another cell behaviour that can participate to tissue morphogenesis is cell apoptosis (Toyama et al., 2008; Suzanne and Steller, 2013; Villars et al., 2022). For example, during *Drosophila* organogenesis, gene patterning will induce apoptosis in a subset of cells of the leg epithelium. As a result, cells will extrude and establish an apico-basal MyoII cable that pulls on neighbouring cell surfaces to fold the tissue and promote joint formation. This process appears to be conserved as the same study showed that ectopic induction of apoptosis in the *Drosophila* wing imaginal disc also results in actomyosin-driven tissue folding (Monier et al., 2015).

2.2.2 Cell behaviours driving tissue elongation

Tissue elongation is a fundamental process that extends the body axis during gastrulation, helps body structures reach the correct shape and size during organogenesis, and restores tissue integrity during wound healing throughout the life of an organism. This section will discuss the cellular behaviours that direct tissue elongation.

2.2.2.1 Cell intercalation

Cell intercalation is a conserved topological change that relies on the remodelling of cell-cell contacts to drive neighbour exchange and subsequent tissue shape changes. This process is key during both tissue morphogenesis and homeostasis: during embryonic development, particularly gastrulation, polarized and irreversible cell intercalations drive tissue elongation, while in mature epithelia, intercalation can help release stress from intrinsic and extrinsic forces to maintain tissue structural integrity through non-polarized, reversible rearrangements (Walck-Shannon and Hardin, 2014; Curran et al., 2017; Mongera et al., 2018). Intercalation can be medio-lateral, as illustrated in simple epithelia, or radial as in multi-stratified epithelia, to promote convergence-extension, tissue folding, or rotational movements (Rauzi, 2020). In this section, I will discuss the two main processes driving cell intercalation: T1 transition and rosette formation. T1 transitions involve the remodelling of four neighbouring units, and were first described in foam physics as a way for bubbles to minimize surface area, and balance internal pressures and surface tension (Weaire and Hutzler, 2000). Rosette formation, on the other hand, leads to the intercalation of units that exceed four cells (Blankenship et al., 2006; Zallen and Blankenship, 2008).

Cell intercalation starts with junction shrinkage, leading to cell-cell contact loss. Work in *Drosophila* embryos has shown that tension anisotropy, driven by the polarized distribution of actomyosin (as discussed in earlier sections), initiates junction shrinkage (Bertet et al., 2004; Fernandez-Gonzalez et al., 2009). Additionally, a pool of actomyosin is recruited at the medial-apical cortex of cells, and contracts periodically, or in pulses, to flow from the medial to the junctional regions and induce stepwise shrinkage (Figure 13A) (Rauzi et al., 2010). The pulsatile and anisotropic behaviour of the flow was postulated to depend on the levels of E-cad at the junctions, as actomyosin would preferentially flow to low E-cad junctions in D-V junctions

(Figure 13B). The flow alternates between each D-V junction, depending on the fluctuation of E-cadherin necessary for actomyosin anchorage. E-cad fluctuations at junctions relies on clathrin-mediated endocytosis and is amplified by the actomyosin flow, thus explaining the stepwise shrinkage (Levayer and Lecuit, 2013). Another proposed mechanism to describe the junctional shrinkage step is vertex sliding, where vertices (where three or more cells meet) change position in a stepwise fashion, influenced by fluctuating E-cadherin levels (Vanderleest et al., 2018). Low E-cadherin mobile vertices initiate junction shortening, while high E-cadherin vertices stabilize the junction. Additionally, E-cadherin fluctuations synergize with actomyosin-dependent coordinated contraction/expansion of the cell quartet, generating an asymmetric force that promotes vertex sliding along the junction. (Figure 13C).

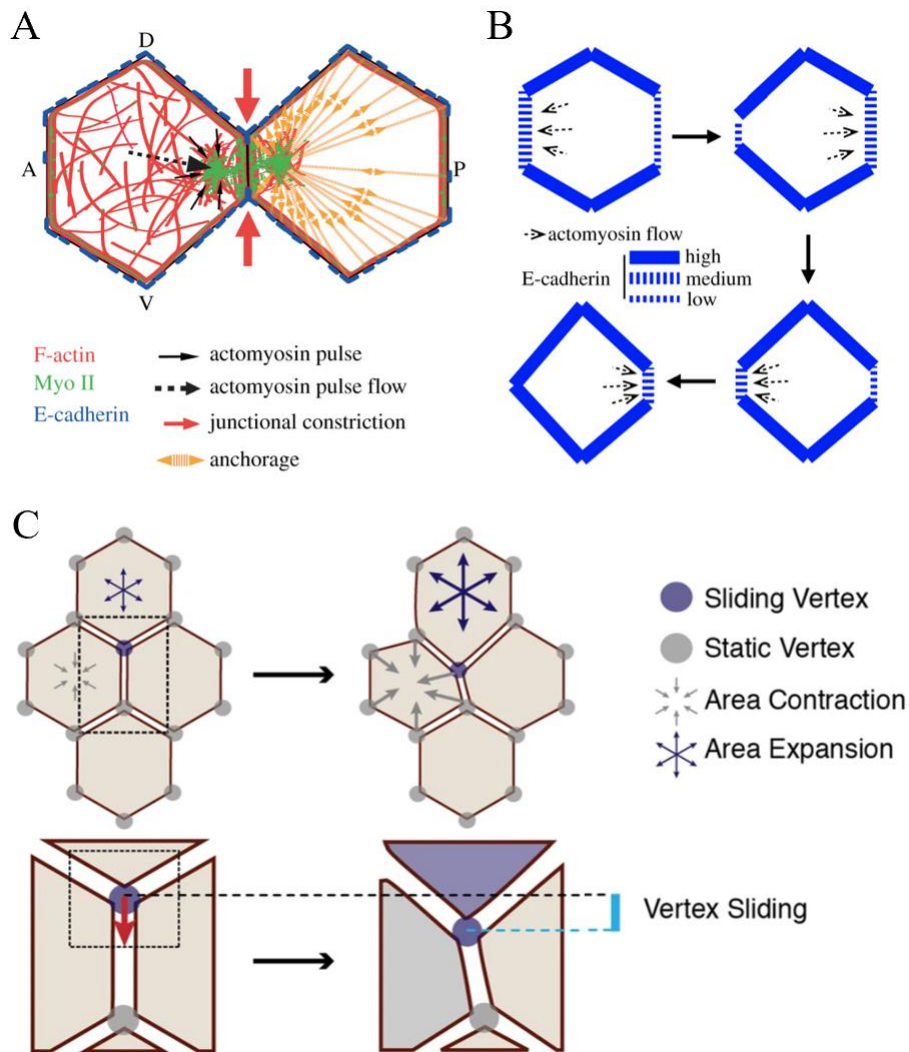


Figure 13. Mechanisms driving junction shrinkage during cell intercalation

A. Anisotropic pulses of actomyosin drive junction remodelling via increased tension. **B.** The anisotropic flow of actomyosin is mediated by junctional E-cad levels to drive stepwise shrinkage. **C.** Vertex sliding model through coordinated contraction and cell area modulation. Images adapted from (Vanderleest et al., 2018; Rauzi, 2020).

After the initial shrinkage step, the four cells share a single junction (theoretically), known as the ‘four-way junction’. Intercalation then proceeds with the establishment of a new cell-cell contact to complete the neighbour exchange. This step relies on the combination of local active processes and extrinsic forces. It was shown during *Drosophila* germband extension, that after the shrinkage of a D-V junction, medial actomyosin contractions in anterior and posterior cells of the intercalating quartet pull on the new junction to lengthen it, as pulses of actomyosin correlated with stepwise lengthening phases (Yu and Fernandez-Gonzalez, 2016). Pharmacological and physical perturbation of the actomyosin network impaired junction lengthening, and an elegant experiment involving laser-induced cavitation bubbles to generate tension resulted in the ectopic lengthening of junctions (Figure 14A). Once the junction starts growing, E-cadherin gradually increases during stalling phases to stabilize the connection between the new neighbouring cells (Collinet et al., 2015). Conversely, it was reported in the *Drosophila* wing epithelium that actomyosin is recruited at newly forming junctions and progressively decreases as the junction grows, and maintaining high levels of MyoII disrupts junction lengthening (Bardet et al., 2013). While junctional E-cadherin polarization directs actomyosin flows during the initial shrinkage phase, the mechanisms that orient actomyosin flows during the lengthening phase remain elusive. A possible mechanism involves the protein Sidekick, which is enriched at tricellular junctions and was shown to be necessary for actomyosin recruitment and E-cad enrichment during junction lengthening (Letizia et al., 2019; Uechi and Kuranaga, 2019). Finally, tissue-scale forces have also been reported to influence the lengthening phase. For example, during *Drosophila* GBE, more intercalation events are reported close to the pulling PMG. Interestingly, reducing tissue strain during germband extension does not reduce the number of intercalation but reduces the length of the newly formed junctions (Butler et al., 2009; Collinet et al., 2015). Similarly, it was shown during *Drosophila* gastrulation that reducing tissue-scale tension anisotropy via laser ablation disrupts junction lengthening in intercalating mesoderm cells (John and Rauzi, 2021), highlighting the role of extrinsic forces to orient and scale the junction lengthening phase.

Medio-lateral cell intercalation in simple epithelia often occurs among four cells but can also involve larger units called rosettes. Rosettes form through the contraction of actomyosin-enriched junctions known as ‘cables’, as observed during *Drosophila*, *Xenopus*, mice and chick morphogenesis (Walck-Shannon and Hardin, 2014; Rozbicki et al., 2015). In a similar fashion to T1 transitions, actomyosin cables increase local tension in given junctions across multiple cells, leading to the shrinking of cell-cell contacts and the formation of a flower-shaped ‘rosette’ of cells, which then resolves by cumulative junction lengthening to converge-extend the tissue (Figure 14B). Additionally, even if most work on cell intercalation has been conducted at the apical side, basal-lateral protrusions have been described during dorsal midline formation in *C. elegans* and notochord primordium formation in the ascidian *Ciona intestinalis*, and bring cells together by directed cell motility to support rosette

formation (Munro and Odell, 2002; Oda-Ishii et al., 2010; Walck-Shannon et al., 2015).

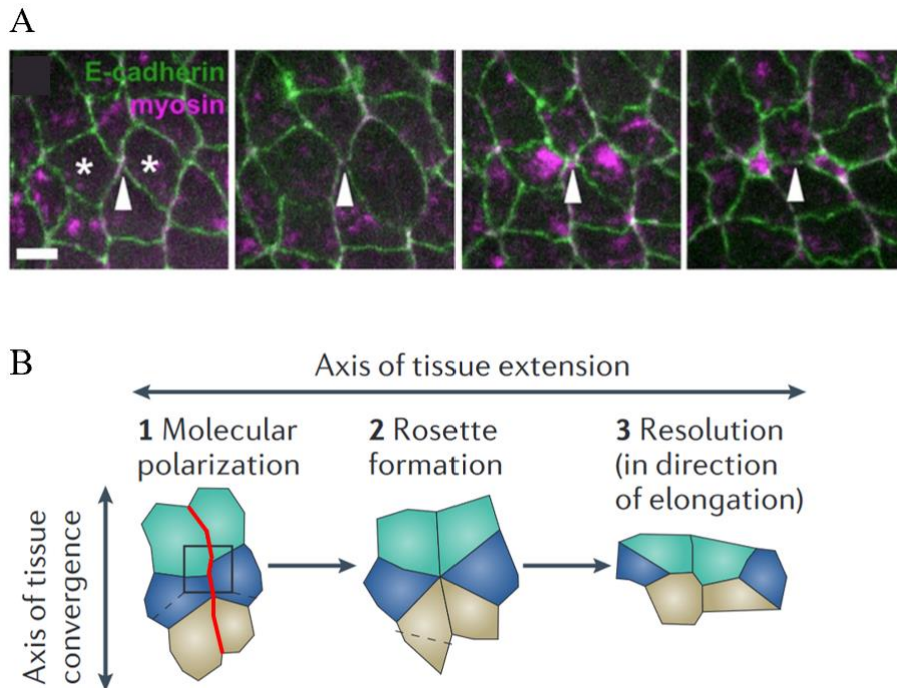


Figure 14. Junction lengthening and rosette formation during cell intercalation

A. Ectopic local tension drives the lengthening of new junctions to resolve intercalation during *Drosophila* T1 transitions. **B.** Schematic representation of actomyosin cable-driven rosette formation during tissue convergence-extension. Images adapted from (Walck-Shannon and Hardin, 2014; Yu and Fernandez-Gonzalez, 2016).

During *Drosophila* germband extension, similar basal protrusions have been shown to exert traction forces and promote polarized cell intercalation (Sun et al., 2017). Recent work by (John and Rauzi, 2021) also identified that mesoderm cells in *Drosophila* embryos do not initiate intercalation apically but rather at $\sim 10\mu\text{m}$ of depth before resolving apically. Intercalation events occurring at different positions of the apicobasal axis were also reported during *Drosophila* anterior pole cellularization, with the exception that they didn't rely on actomyosin contractility but rather geometrical constraints such as cell packing and tissue curvature (Rupprecht et al., 2017). The set of principles governing the apicobasal location of cell intercalation is still unknown, but (Gómez et al., 2021) reported intercalation events spanning the entire apico-basal axis in growing mouse embryonic lung pseudostratified epithelia and postulated that the distribution and movement of nuclei in these cells would generate variability in the cell cross-sectional areas, and that T1 transitions are thus initiated at different depths to minimize lateral cell-cell surface energy accordingly.

2.2.2.2 Collective cell migration

Cell migration is another conserved mechanism employed throughout development and adult life to drive morphogenesis and maintain tissue homeostasis (Friedl and Gilmour, 2009). It has been shown to drive tracheal branching morphogenesis in *Drosophila*, zebrafish lateral line formation, and vertebrate limb formation, during which tightly-regulated migratory behaviours drive tissue elongation and organogenesis (Sutherland et al., 1996; Nechiporuk and Raible, 2008). It is also essential for tissue regeneration, as illustrated during many wound healing processes such as the repair of skin and corneal epithelial layers after injury (Poujade et al., 2007; Zelenka and Arpitha, 2008).

Cell migration usually starts with a polarization step, during which intrinsic and extrinsic cues influence cell fate to initiate directional cell movement. Genetically-determined differentiation leads to the acquisition of ‘leader’ or ‘follower’ identity within the migratory cohort (Cho et al., 2002). As a result, ‘leader’ cells present a polarized morphology and differential gene expression to regulate their contractile behaviour and their ability to detect extracellular cues. Such cues are essential during cell migration, as chemokines and growth factor gradients that are either freely-diffusing (chemotaxis) or tethered to the ECM (haptotaxis) can regulate cell polarization and subsequent directional cell migration through the dynamic reorganization of the cell cytoskeleton (Haas and Gilmour, 2006; Shintani et al., 2008). Indeed, cytoskeletal components can help form protrusions by generating filopodia or lamellipodia to interact with the environment (e.g, integrin signalling with the ECM) and initiate migrations (Nobes and Hall, 1999; Ridley et al., 2003). Using their protrusions, migrating cells form adhesive contacts on their substratum, which function as traction points (Treat et al., 2012). Contraction results in the forward motion of the cell body and releasing contact points at the rear-end as the cell resets the migration loop (Figure 15A). But how can cells move collectively? One possible mechanism is to rely on leader cells to set a path for the followers cells, as illustrated during wound healing: when cells move towards the injury site, they remodel the ECM through localized proteolytic degradation initiated by leader cells using metalloproteinases, and deposit basement membrane components like laminins and collagen IV in a trail to guide the ‘follower’ cells (Wolf et al., 2007). Another key mechanism to coordinate the collective movement of cells is the coupling of cells via adherens, tight or gap junction-mediated cell-cell adhesion. Such adhesion promotes signal transmission and help maintain structural integrity while tissues spread and extend their surface (Figure 15B) (Niessen, 2007; Defranco et al., 2008).

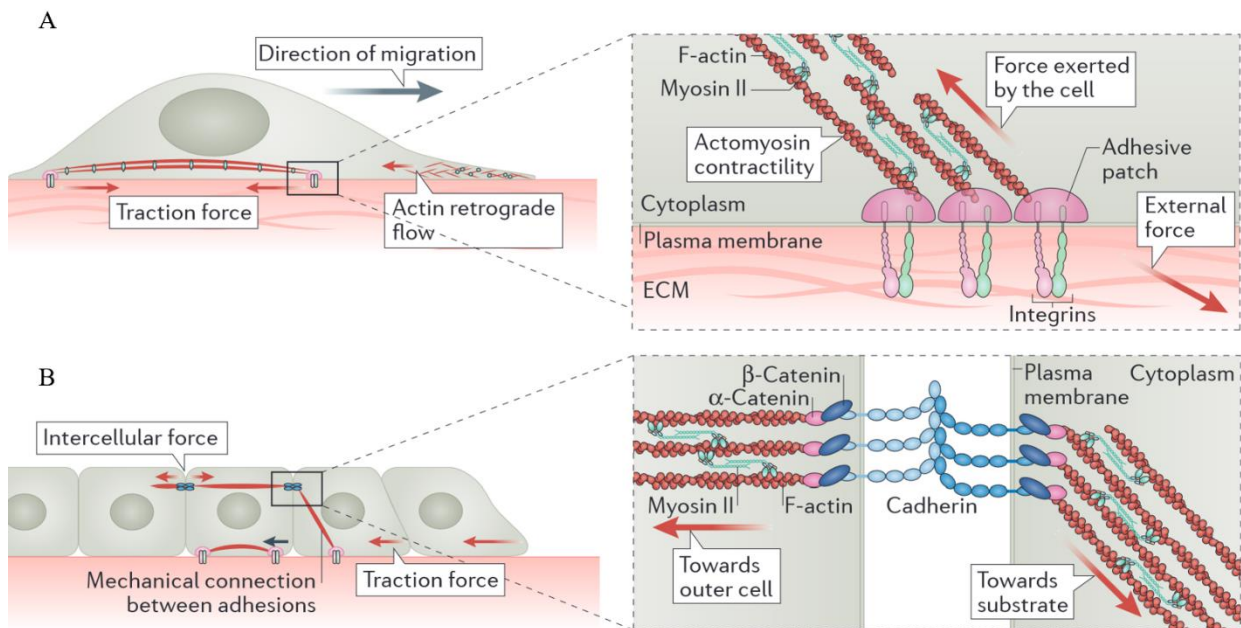


Figure 15. Collective cell migration via cytoskeleton remodelling, cell-cell adhesion and ECM signalling

A. ECM signalling regulates cytoskeletal components to drive protrusion formation and generation traction forces during cell migration. **B.** Collective movement is mediated by cell-cell adhesion. Images adapted from (Ladoux and Mège, 2017).

2.2.2.3 Oriented cell divisions

It has been shown across species that oriented cell divisions can contribute to the directional elongation of tissues (Figure 16)(Li et al., 2014; Tang et al., 2018; Lemke and Nelson, 2021), and specifying correct division axes is also essential for the organization of the organism as early as the first cleavage steps after fertilization (Minc and Piel, 2012). Many efforts have thus been made to understand how cells orient their divisions. Empirical work in frog oocytes first postulated that cells preferably divide along their long axis, a principle known as Hertwig's rule (Hertwig, 1884). Since this first observation, it was shown that several factors can influence cell division orientation, including cell geometry, intrinsic polarity cues, or external PCP patterning (Théry et al., 2007; Gillies and Cabernard, 2011). Seminal work by (Minc et al., 2011) further showed that cells can sense their geometry to orient spindle positioning and specify the division axis. They demonstrated that microtubule-mediated pulling forces elongate the nucleus in an axis which predicted the division plan. They could show that pulling forces scaled with the length of microtubules and established a computational model that recapitulated the orientation of spindle positioning in a variety of cell shapes using this rule. Such mechanism allows cells to

self-organize and escape deterministic gene patterning by sensing their shape and size to robustly orient cell division and subsequent morphogenesis.

Interestingly, recent work has challenged Hertwig's rule, showing that mechanical forces also contribute and can override cell geometry to orient cell division (Scepanovic and Fernandez-Gonzalez, 2018). In *Drosophila* embryos, parasegmental boundaries (PSB) are established to segment the organism from head to tail. The PSB are enriched with actomyosin cables to increase local tension and avoid cell mixing between compartments. Interestingly, in the studied tissue (epidermis), cells are stretched along the D-V axis and thus expected to divide parallel to this axis. Yet, cells that are close to the high-tension PSB divides in the orthogonal A-P axis. The underlying mechanism is not clear but it is hypothesized that higher tension along the PSB could trap the proximal centrosome and limit its repositioning, thus promoting division along the A-P axis. The presence of denser actomyosin cytoskeleton could also affect the local visco-elastic properties of the cell, increasing hydrodynamic drag, thus limiting the mobility of the centrosome and fixing one spindle pole (Scarpa et al., 2018).

Oriented cell divisions can also help maintain tissue integrity during morphogenesis, as illustrated in the spreading of the enveloping cell layer during zebrafish epiboly: it was described that tissue-scale tension anisotropy first instructs the division plane by elongating cells and that the resulting division of cells along the same axis actually resolves the tissue anisotropy, allowing the tissue to spread while keeping its structural integrity (Campinho et al., 2013).

Finally, one should note that the mechanisms described in this section can synergize to drive directional tissue elongation. This is well illustrated in the *Drosophila* wing imaginal disc, where the loss of PCP-driven cell oriented divisions can be compensated by increased cell rearrangements to maintain the proper organ size and shape (Zhou et al., 2019).

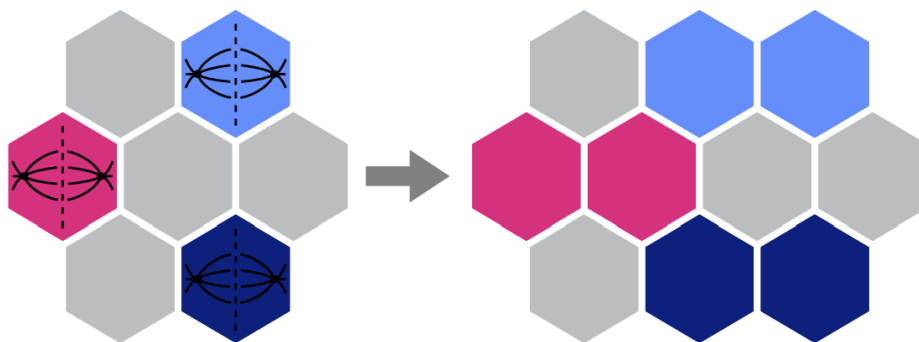


Figure 16. Cell oriented divisions drive tissue elongation

Schematic representation of the alignment of division planes in several cells leading to the directional elongation of the tissue. Image adapted from (Lemke and Nelson, 2021).

2.3 A brief perspective on biophysical approaches of tissue morphogenesis

The cellular behaviours previously described can promote cell shape and topology changes, but would not drive tissue remodelling if they were stochastic and unsynchronized. Understanding the coordination of cell behaviour, as well as the spatiotemporal control of morphogenetic processes is thus necessary. For instance, efforts have been made to understand how embryo-scale forces and non cell-autonomous processes can regulate the orientation, scale and timing of these events (Rauzi et al., 2015). Similarly to the integration of foam physics for the description of intercalations in epithelial cells, new paradigms have also been recently established to map rheological and material properties of tissues and integrate physical approaches in the description of the collective behaviour of epithelial monolayers, such as glass physics, tissue fluidity, rigidity percolation, criticality and tissue phase transitions. These new approaches now allow to address the interplay between the properties of the tissues, the stresses that they experience and the multi-scale multicellular behaviours that drive morphogenesis. Even if I will not cover it in this manuscript, this is an exciting area of research and would definitely recommend the interdisciplinary reports by (Kim et al., 2021; Lenne and Trivedi, 2022; Valet et al., 2022; Mao and Wickström, 2024).

3. Force generation and transmission: cytoskeleton and organelles at play

This approach was actually theorized around the 19th century, when scientists started arguing that the law of physics could not only govern inanimate but also living matter (Fick, 1858). This thought process was later built upon by Sir D'Arcy Thompson, in his famous *On Growth and Forms*, which postulated that shape, growth and pattern formation were directed by physics laws and that simple mathematical transformations mapping the physical forces exerted on tissues could explain the variability of shapes observed in related animals (Thompson, 1945). One might wonder how such forces are generated within cells? In the next section, I will focus on the cytoskeletal components, organelles and molecular machinery that generate and transmit forces, enabling cells to undergo the drastic shape and topology changes observed during tissue morphogenesis.

3.1 The cell cytoskeleton

The cell cytoskeleton is composed of actin filaments, microtubules, intermediate filaments and septins. It is essential to maintain the right cell architecture, and has thus been extensively studied for its contribution to cellular shape changes during tissue morphogenesis. Additionally, cytoskeletal dynamics enable the integration and transmission of biochemical and mechanical signals to coordinate collective cell behaviour.

3.1.1 Microtubules

Microtubules are polymers composed of α - and β -tubulin heterodimers, each ~ 4 - 5 nm in size (Wilson and Friedkin, 1967; Weisenberg et al., 1968). These heterodimers assemble in a head-to-tail fashion to form protofilaments, and 13 parallel protofilaments constitute a hollow microtubule with an outer diameter of ~ 25 nm (Figure 17A). Microtubules are polarized structures, with a plus-end, where β -tubulin is exposed, and a minus-end, where α -tubulin is exposed (Knossow et al., 2020). Growth mostly occurs at the plus-ends and the critical concentration for tubulin has been measured to be ~ 1 - 2 μ M (Johnson and Borisy, 1975; Mirigian et al., 2013; Jonasson et al., 2020). Microtubules have a persistence length of ~ 1 - 2 mm, which is relatively stiff and enables them to withstand significant compressive forces (Hawkins et al., 2010).

Microtubule assembly starts with the nucleation of α/β -tubulin dimers, followed by the elongation and stabilization of the polymer. The assembly relies on the formation of a microtubule-organizing center (MTOC), mainly centrosomes, even though acentrosomal MTOCs can also serve as nucleation sites (Akhmanova and Kapitein, 2022). Gamma-tubulin ring complexes (γ -TuRCs) within the centrosome provide a template for the initial addition of α/β -tubulin dimers and GTP-bound tubulin dimers are progressively added to the growing plus-end (Liu et al., 2020; Wieczorek et al., 2020). This addition creates a cap of GTP-tubulin, which stabilizes the growing end. However, hydrolysis of GTP to GDP occurs shortly after their addition to the microtubule, leading to a GDP-tubulin lattice that is less stable and prone to depolymerization (Carlier, 1989). The interplay between GTP-tubulin addition and GDP-tubulin loss leads to phases of rapid growth (polymerization) and shrinkage (catastrophe), described as the ‘dynamic instability’ of microtubules (Mitchison and Kirschner, 1984). Rescue events, where shrinking microtubules switch back to growth, can also occur to further regulate microtubule dynamicity (Figure 17B). It should be mentioned that recent advances in structural biology have described alternative methods of microtubule assembly, involving the incorporation of sheets of tubulins and the identification of a curved architecture at the end of growing protofilaments, that complement the classical GTP-cap model (Conde and Cáceres, 2009; Gudimchuk and McIntosh, 2021). Many microtubule-associated proteins and post-translational modifications can influence the cycles of assembly/disassembly to modulate the dynamic properties and the architecture of the microtubule cytoskeleton. Based on their functions, the following proteins can be classified: severing proteins, depolymerizing proteins, stabilizing proteins, and motor proteins (Brouhard and Rice, 2018).

3.1.1.1 Partner proteins and post-translational modifications of the microtubule cytoskeleton

Severing proteins, such as katanin or spastin, remodel the cytoskeleton by cutting microtubules into shorter fragments (McNally and Roll-Mecak, 2018).

Depolymerizing proteins, such as the Kinesin-13 family members, bind to the microtubule and induce curvature at specific sites, leading to the rapid disassembly of the polymer (Walczak et al., 2013). Conversely, stabilizing proteins such as MAP2 and tau, bind to microtubules to increase their stability and prevent depolymerization. Motor proteins, such as kinesins and dyneins, are responsible for intracellular transport and force generation. These motor proteins can specify the directional movement of cargos and organelles, as kinesins move towards the plus-end, while dyneins move towards the minus-end (Abraham et al., 2018). In addition to the major categories mentioned previously, other regulatory proteins can influence microtubules. For instance, EB1 (End-Binding protein 1) associates with the growing plus-ends and acts as a platform to recruit other plus-end tracking proteins (+TIPs), as well as adaptor and regulatory proteins to alter microtubule dynamicity, interactions and distribution within cells (Akhmanova and Steinmetz, 2015).

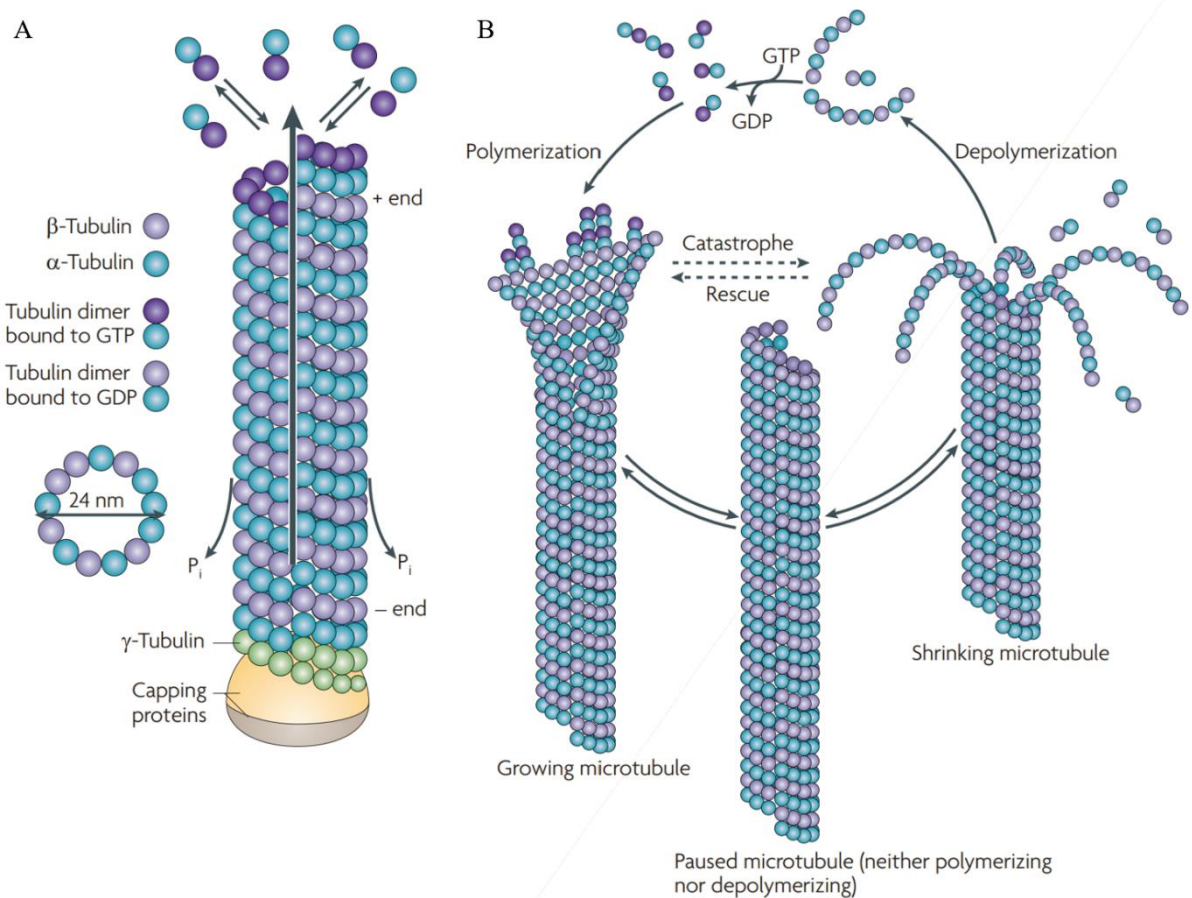


Figure 17. Microtubule assembly and dynamic instability

A. Polarized growth of microtubules by addition of $\alpha\beta$ -tubulin dimers from the γ -TuRC nucleation center. **B.** Dynamic instability of microtubules via phases of growth, shrinkage and rescue. Images adapted from (Conde and Cáceres, 2009).

Microtubule dynamics and interactions can be further regulated by post-translational modifications of tubulin, such as acetylation, detyrosination, or polyglutamylation. Acetylation of α -tubulin has been associated with increased microtubule stability to

sustain mechanical stress, while detyrosination and polyglutamylation can modulate the interaction of microtubules with motor proteins and MAPs (Song and Brady, 2015). Microtubules can also undergo more classical PTMs, such as phosphorylation, ubiquitination or sumoylation, that regulate their turnover rate and dynamic instability. For a complete overview of the ‘tubulin code’, I would suggest great reviews by (Janke and Magiera, 2020; Roll-Mecak, 2020).

3.1.2 Intermediate filaments

Intermediate filaments (IFs) have a diameter of ~10 nm, which is ‘intermediate’ between actin filaments (7 nm) and microtubules (25 nm). IFs are not composed of polymers of a single type, but rather by a variety of more than 50 proteins, classified into six types (Herrmann et al., 2007). Types I and II consist of acidic and basic/neutral keratins and are found in epithelial cells. Type III includes vimentin (present in fibroblasts, smooth muscle cells, and white blood cells), desmin (in muscle cells), GFAP (in glial cells), and peripherin (in neurons). Type IV IFs consist of neurofilaments found in neuron axons, and α -internexin in developing neurons. Type V corresponds to nuclear lamins present at the nuclear envelope in all cell types, and Type VI includes nestin in neural stem cells (Dutour-Provenzano and Etienne-Manneville, 2021). IFs are composed by sheets of tetramers that form protofilaments and organize in a higher order assembly as a rope-like fiber (Eldirany et al., 2021). IFs are not polarized, do not require nucleotide hydrolysis for their assembly, and are mostly involved in the support of cell stiffness, the maintenance of nuclear shape and the regulation of gene expression. Interestingly, cytoplasmic intermediate filaments are not present in *Drosophila* (Cho et al., 2002).

3.1.3 Actin filaments

Actin is a globular protein (G-actin) with a molecular weight of ~43 kDa. In cells, actin exists predominantly in two forms: monomeric G-actin and polymeric filamentous actin called F-actin (Dominguez and Holmes, 2011). G-actin monomers bind to ATP, which is then hydrolysed to ADP upon incorporation into filaments (Kabsch et al., 1990; Murakami et al., 2010). The polymerization of G-actin into F-actin relies on an initial slow nucleation phase, followed by rapid elongation of the filament. F-actin consists of two parallel strands twisted into an helix. Each turn of the helix spans ~37nm and includes ~13.5 actin subunits (the helix has a slight twist in its structure and doesn’t align perfectly each turn to confer higher stability to the filament, hence the non-integer value of actin units per helix turn). The final filament has a diameter of ~7nm (Fujii et al., 2010) and is polarized, with distinct ‘barbed’ (fast-growing) and ‘pointed’ (slow-growing) ends (Figure 18A). These differential growth rates depend on the critical concentration of G-actin for polymerization, which is ~0.1 μ M at the barbed end and ~0.6 μ M at the pointed end (Kuhn and Pollard, 2005; Vavylonis et al., 2005; Fujiwara et al., 2007). Actin filaments have a relatively short persistence length of ~10 μ m, meaning that they can remain straight up to that distance before starting to bend, allowing them to maintain their structural integrity over short distances while the cell undergoes shape changes (Harasim et al., 2013).

3.1.3.1 Actin-binding proteins

There are many actin-binding proteins that can modulate actin dynamic behaviour, as well as its organization in cells (Figure 18B). For instance, nucleation factors, such as formins, are required to initiate filament growth from G-actin monomers (Goode and Eck, 2007; Courtemanche, 2018). Alternatively, the Arp2/3 complex, promotes the nucleation and elongation of new branches on the side of existing filaments within branched networks (Robinson et al., 2001; Rouiller et al., 2008). Capping proteins, such as CapZ $\alpha\beta$ or tropomodulin, can bind to barbed or pointed ends to prevent further polymerization and regulate the length of the filament (Edwards et al., 2014, 2015; Rao et al., 2014). Additionally, severing proteins like ADF/Cofilin or gelsolin can bind to ADP-actin regions and fragment the filament by weakening lateral interactions between adjacent actin subunits within these regions (Bamburg et al., 1980; Nishida, 1985; Cao et al., 2006; Nag et al., 2013). Finally, stabilizing agent such as tropomyosin can protect actin from severing proteins (Burgess et al., 1987; Ishikawa et al., 1989). All these partner proteins modulate the dynamic instability of actin filaments, thus integrating internal and external cues to modulate the structure and behaviour of actin networks to drive key processes such as cytokinesis during cell division, filopodia formation during cell migration, or force generation to initiate cell shape and topology changes during tissue morphogenesis.

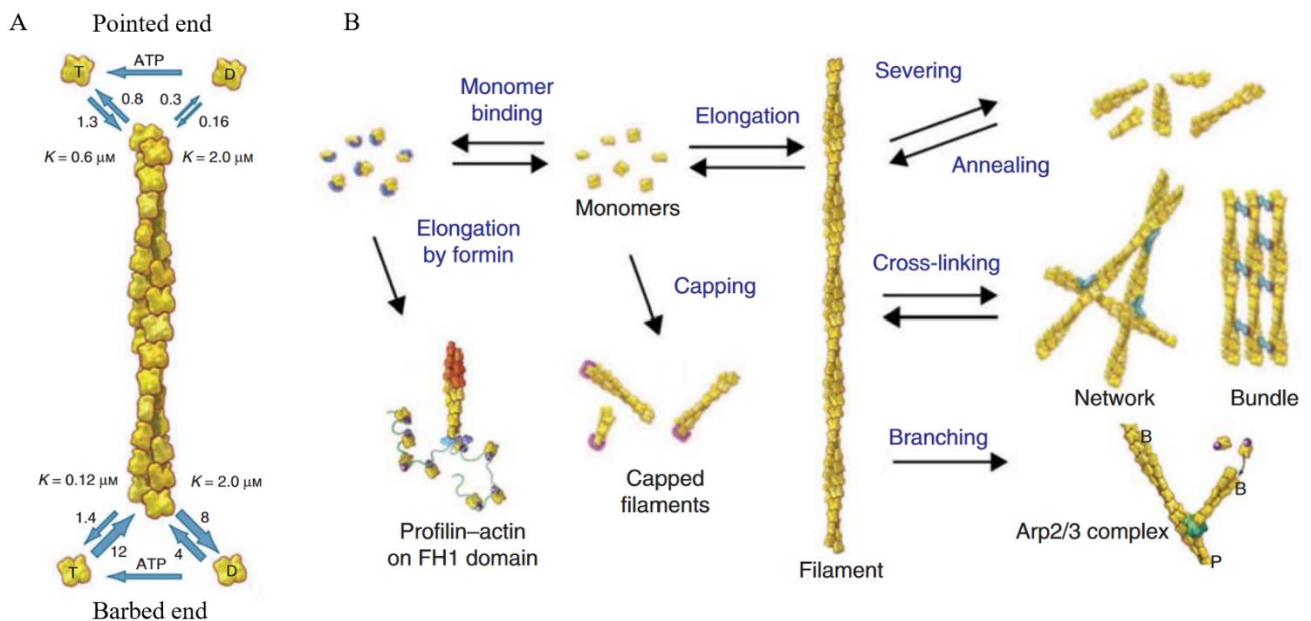


Figure 18. Actin structure, assembly and regulation by partner proteins

A. Schematic representation of F-actin assembly. K indicates the critical concentrations above which G-actin association exceeds its dissociation, thus driving filament polymerization. **B.** Actin-binding proteins that influence actin dynamic instability and network architecture. Images adapted from (Pollard, 2016).

Actin filaments can also be organized into higher-order structures through crosslinking and bundling proteins to enhance the mechanical strength and stability of the network, which is particularly useful given the short persistence length of F-actin (Figure 18B). Crosslinkers such as α -actinin and filamin bind to adjacent filaments, to form elastic and resilient networks (Xu et al., 1998). Bundling proteins like fimbrin and fascin organize filaments into parallel arrays, which are needed to generate stress fibers or filopodia (Matsudaira, 1994). Cross-linking proteins such as filamin and spectrin can also organize filaments into three-dimensional networks: filamin cross-links actin filaments into orthogonal networks to confer elasticity and strength to cells, while spectrin binds actin to generate a scaffold that supports the plasma membrane (Liem, 2016).

Last but not least, actin can also associate with molecular motors, such as MyoII to assemble actomyosin contractile networks. The mechanisms of force generation involving the coupling of motor proteins to cytoskeletal components will be discussed in the following section.

3.2 Force generation by the cell cytoskeleton

Forces can be generated through the coupling of cytoskeletal networks, such as actin and microtubules, with motor proteins. This process converts ATP energy into mechanical stresses that actively drive cell shape and topology changes during tissue morphogenesis. Interestingly, the motor proteins and signalling pathways that control their activity are highly conserved across species (Kull and Endow, 2013; Murrell et al., 2015). Several subcellular mechanisms contribute to force generation, with specialized machineries tailored to different cell types and their specific functions. In the following section, I will only detail the molecular machineries that drive morphogenesis in epithelial tissues.

3.2.1 Actomyosin contractile machinery

It is argued that the F-actin cytoskeleton is the predominant mode of force generation during animal tissue morphogenesis (Quintin et al., 2008; Miao and Blankenship, 2020). F-actin polymerization *per se* can generate pushing forces of 1pN, and has been extensively studied for its role in cell migration (Abraham et al., 1999; Ponti et al., 2004; Koestler et al., 2008). Additionally, F-actin can associate with the non-muscle Myosin II molecular motor (MyoII) to drive the remodelling of epithelial cells, mainly via contractile forces (Clarke and Martin, 2021). In *Drosophila*, a single gene *NMHC2* encodes MyoII, while vertebrates have three paralog genes: *MYH9*, *MYH10* and *MYH14* (Simons et al., 1991; Mansfield et al., 1996; Leal et al., 2003). MyoII is composed of two heavy chains, two essential light chains, and two regulatory light chains (Figure 19A). In *Drosophila*, these subunits are encoded by the genes *zipper* (heavy chain), *spaghetti squash* (regulatory light chain), and *mlc-c* (essential light chain). Vertebrates possess three heavy chain isoforms (NMHC-IIA, NMHC-IIB, NMHC-IIC) and at least one regulatory chain MRLC2 (Conti and Adelstein, 2008). Each MyoII heavy chain possesses an N-terminal globular head with actin and ATP-

binding sites necessary for motor activity, followed by an alpha-helical neck region acting as a pivot point to transmit mechanical forces and a long C-terminal tail that allows dimerization and filament formation (Brito and Sousa, 2020). The essential and regulatory light chains contain two Ca^{2+} -binding domains that interact with the neck regions of the heavy chains to amplify movements from ATP-induced conformational changes (Scholey et al., 1980). MyoII activity is regulated by phosphorylation of a conserved serine residue in the regulatory myosin light chain, which enhances the ATPase activity and stabilizes MyoII filaments (Vicente-Manzanares et al., 2009; Murrell et al., 2015). Conversely, phosphorylation of the heavy chain reduces MyoII filament assembly (Conti et al., 1991; Bresnick, 1999; Dulyaninova et al., 2007). When MyoII is phosphorylated, it oligomerizes into a bipolar mini-filament containing a few dozen heads, able to bind to multiple antiparallel actin filaments and ‘walk’ along them (Figure 19B) (Stricker et al., 2010; Salbreux et al., 2012). The motor activity produces actomyosin contractility: the myosin head domain slides F-actin filaments in opposing directions, thus shortening the actomyosin assembly and generating a contractile force (Figure 19C).

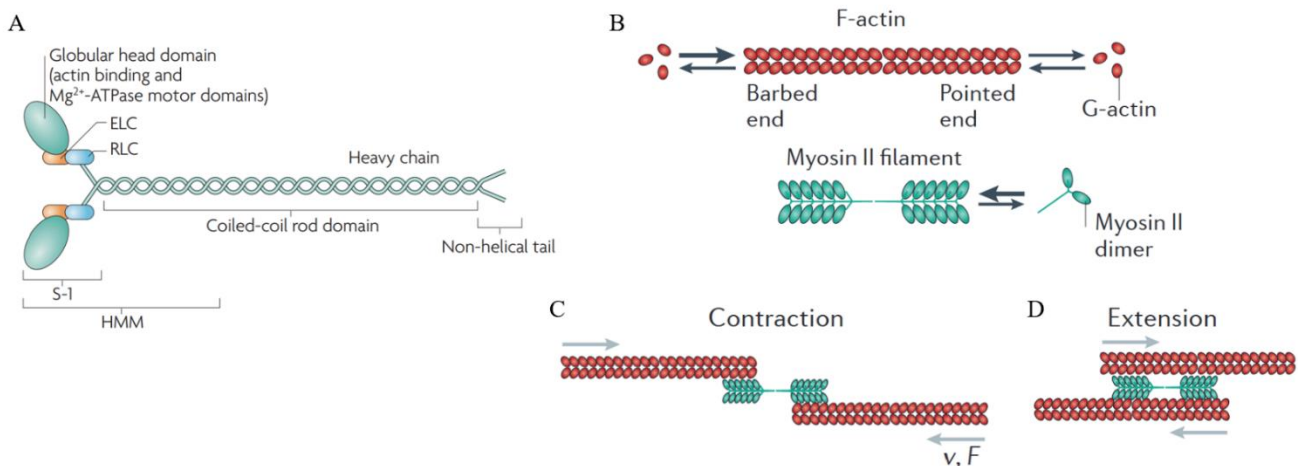


Figure 19. Force generation via the coupling of non-muscle Myosin II and F-actin

A. Structure of the non-muscle MyoII heptameric protein showcasing its head, rod and tail domains, composed of heavy, essential and regulatory light chains. **B.** MyoII assembly into filaments. **C-D.** Coupling of MyoII with F-actin networks drive contraction or extension of the assembly, depending on its proximity with the barbed end on which it pulls. Images adapted from (Vicente-Manzanares et al., 2009; Murrell et al., 2015).

It has been measured that a single MyoII motor with a single actin filament can generate forces of $\sim 3\text{-}5$ pN (Finer et al., 1994; Molloy et al., 1995). Structurally, actomyosin assemblies can be organized in one dimension, such as stress fibers (López-Gay et al., 2020), or in two dimensions as a meshwork that spans the surface of epithelial cells (Mason et al., 2013). Since force generation obeys the law of mass action, an actomyosin network composed of many MyoII mini-filaments can thus

generate stronger forces within the cell, up to ~100-800 pN (Maître et al., 2015; Cartagena-Rivera et al., 2016). Actomyosin can finally organize as a supracellular network which generates tissue-scale tension within the nN range (Campàs et al., 2014). One should mention that extension can also occur when MyoII binds F-actin networks close to their barbed ends (Figure 19D). Nonetheless, in disorganized actin networks, actomyosin will break symmetry and self-organize into contractile networks preferentially. This has been postulated to rely on the intrinsic properties of F-actin filaments, which are able to resist tensile stresses but are much less adept at withstanding compressive or buckling stresses (Lenz et al., 2012; Murrell and Gardel, 2012). As a result, actin filaments will mainly survive within tensile rather than compressive regions, thus self-organizing into contractile networks (Haviv et al., 2008; Wilson et al., 2010; Soares e Silva et al., 2011).

3.2.1.1 Regulation of actomyosin activity

MyoII activity is mainly regulated by the phosphorylation of its regulatory light chains (RLCs), which controls conformational changes in the myosin head and tail domains to form bipolar filaments, bind to F-actin, and promote MyoII ATPase activity (Wendt et al., 2001; Jung et al., 2008). Several kinases are involved in RLC phosphorylation, such as Myosin light chain kinase (MLCK), Rho-associated coiled coil-containing kinase (ROCK), Citron kinase or Myotonic Dystrophy-Related Cdc42-binding Kinase (MRCK), that can directly phosphorylate MyoII RLC. Additionally, ROCK can phosphorylate the myosin binding subunit (MBS) of myosin phosphatases and block their activity, indirectly promoting MyoII activity. Myosin phosphatases are also key for proper force generation, as the balance between MyoII phosphorylation and dephosphorylation was shown to fine-tune MyoII spatiotemporal activity and contribute to tissue morphogenesis during *Drosophila* development (Tan et al., 2003; Valencia-Expósito et al., 2016; Qin et al., 2018). This balance is under the control of several signalling pathways, which involve G protein-coupled receptors (GPCRs), calcium signalling and the apicobasal polarity pathway (Miao and Blankenship, 2020). In *Drosophila* embryos, the GPCRs Smog and Mist, when bound by the ligand Fog (Manning et al., 2013; Kerridge et al., 2016), activate RhoGEF2 through Gα12/13 (Concertina), leading to Rho1 and subsequent Myosin II activation (Figure 20A). In the ectoderm tissue, the Gβ13F/Gγ1 subunits activate p114RhoGEF/Cysts to promote specifically the junctional activity of Rho1/ROCK/Myosin II (Bayonas et al., 2019). This GPCR signalling was shown to be regulated by both ligand availability and the endocytic control of GPCRs (Jha et al., 2018), and even if the receptors and ligand are not conserved, the Gα12/13-dependent control of MyoII RLC phosphorylation is highly conserved in vertebrates (Suzuki et al., 2009; Ito et al., 2022). Additional factors, such as the transmembrane protein T48, can anchor RhoGEF2 at the cortex independently of Fog, thus controlling the subcellular distribution and activity of Rho effectors (Kölsch et al., 2007). Such Rho-GTPases switch between active (GTP-bound) and inactive (GDP-bound) states, in a cycle controlled by guanine nucleotide exchange factors (GEFs) and GTPase activating proteins (GAPs). GEFs catalyze the

exchange of GDP for GTP to activate Rho proteins and promote actin polymerization and MyoII activity (Figure 20B). Conversely, GAPs accelerate GTP hydrolysis to inhibit Rho GTPases (Arnold et al., 2017). The specific localization of GEFs and GAPs within cells then allows to define spatiotemporal patterns of Rho and MyoII activity (Simões et al., 2006; Michaux et al., 2018). For example, the *Drosophila* Cumberland-GAP (C-GAP) has been shown to spatially restrict RhoA pathway activity to the medial portion of the apical cortex of mesoderm cells, and its disruption leads to the loss of actomyosin pulsing (Mason et al., 2016).

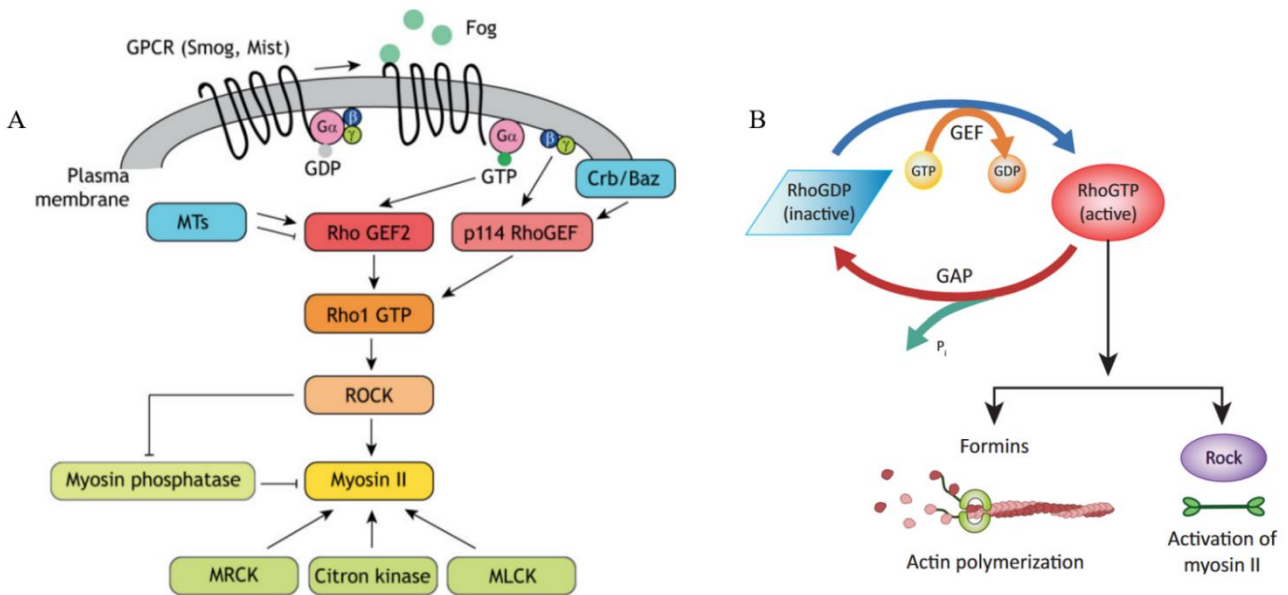


Figure 20. Signalling pathways regulating actomyosin contractility

A. GPCR signalling controlling MyoII activity in *Drosophila* embryos. **B.** RhoGEFs and RhoGAPs control the activity of Rho-GTPases and subsequent actomyosin contractility. Images adapted from (Agarwal and Zaidel-Bar, 2019; Miao and Blankenship, 2020).

Calcium signalling has also been postulated to control actomyosin dynamics, as spontaneous calcium spikes were observed during both *Drosophila* GBE and mesoderm invagination (Markova et al., 2015), and an increase of intracellular free calcium concentration was shown to induce cell shape changes in the amnioserosa cells of *Drosophila* embryos (Hunter et al., 2014). Additionally, pharmacological depletion of Calcium was shown to disrupt convergence-extension movements in both *Xenopus* and zebrafishes (Wallingford et al., 2001; Lam et al., 2009). It was postulated that Ca^{2+} -dependent calmodulin complexes could activate MLCK and subsequent MyoII, but direct evidence of a link between Ca^{2+} dynamics and MyoII-dependent morphogenetic process are still missing (Kitazawa et al., 1991; Kong et al., 2017).

Finally, apical polarity proteins, such as the Par and Crumbs complexes, can also regulate MyoII activity, as illustrated during *Drosophila* oogenesis where the Par complex anchors and accumulates apical myosin, or during *Drosophila* salivary gland formation where Crumbs defines the position of an actomyosin cable to drive tubulogenesis (Wang and Riechmann, 2007; Röper, 2012; Silver et al., 2019).

3.2.2 Microtubules as force generators

Several studies have also proposed that microtubules are not restricted to their primary functions (e.g., intracellular transport and maintenance of cell architecture), but can behave as active force-generating components of the cell cytoskeleton (Matis, 2020). Microtubules can produce forces through polymerization and depolymerization dynamics, as the addition or removal of a GTP-tubulin dimer *per se* can release free energy of ~4 pN that is converted into mechanical work (Hill and Kirschner, 1982; Dogterom and Yurke, 1997). When growing microtubules meet barriers (e.g., the cell cortex), they can exert pushing forces, similarly to protruding actin filaments during filopodia formation, where actin polymerization exerts an axial force that overcomes the bending energy of the lipid bilayer without requiring molecular motors (Hotani, 1990; Peskin et al., 1993). Conversely, depolymerizing microtubules can exert pulling forces, as illustrated during chromosome segregation in cell division (Akiyoshi et al., 2010; Asbury, 2017). Further studies then reported that a single microtubule can actually generate forces up to ~50 pN (Desai and Mitchison, 1997; Dogterom et al., 2005; Molodtsov et al., 2005), and bundling of microtubules linearly increases force generation with the microtubule number (Laan et al., 2008). Finally, microtubule-associated motor proteins, such as kinesins and dyneins, can also generate directional forces when bound to microtubules, and these forces also scale with their concentration (Shimamoto et al., 2015). For instance, kinesins can push away antiparallel microtubules and exert pushing forces in the range of ~1-10 pN (Kapitein et al., 2005; Fink et al., 2009). Dyneins, on the other hand, can be anchored to the cell cortex and pull on microtubules (Laan et al., 2012). Interestingly, pushing forces by microtubules were identified as key drivers of epithelial morphogenesis, as illustrated during *Drosophila* dorsal fold formation, where microtubules first associate with dynein to generate pushing forces (supposedly via sliding) and deform cells, then subsequent remodelling of the network by severing proteins weakens cellular shape and leads to a force imbalance that drives the folding of the tissue (Takeda et al., 2018). Similarly, microtubules can exert pushing forces to elongate cells during *Drosophila* wing formation (Singh et al., 2018, 2024).

3.2.2.1 Interplay between microtubules and actomyosin

Synergy between the cytoskeletal force generators can also occur. Microtubules have been proposed to regulate actomyosin contractility via the transport of Rho effectors responsible for MyoII activity or F-actin turnover, even though this relationship is not fully understood and appears to be context-dependent within epithelial tissues. For instance, negative regulation of actomyosin contractility by microtubules has been reported in *Xenopus* oocytes where microtubule depolymerization via Nocodazole

induces an actomyosin cortical flow (Canman and Bement, 1997). Similarly, depolymerization of microtubules using Colcemid treatment leads to increased medio-apical (but not junctional) recruitment of MyoII during *Drosophila* germband extension (Bayonas et al., 2019). *In vitro* work by (Rogers et al., 2004) identified that RhoGEF2 can bind to the microtubule plus-ends protein EB1 and is released upon activation of the Gα12/13 Concertina in *Drosophila* S2 cells. This study proposed that packets of RhoGEF2 are delivered by microtubules plus-ends close to the cell cortex: if it encounters a region with high concentration of activated Concertina, RhoGEF2 would thus locally activate Rho1/MyoII. It was later shown that microtubules can indeed positively regulate MyoII activity, either through direct transport of F-actin and MyoII (Foe et al., 2000) or via the regulation of actomyosin assembly, as illustrated during *Xenopus* oocyte wound healing where pharmacological depolymerization resulted in the breakage of actomyosin networks (Mandato and Bement, 2003). Additionally, microtubule depolymerization can induce a loss of medio-apical (but not junctional) MyoII during *Drosophila* salivary gland formation, resulting in impaired cell apical constrictions (Booth et al., 2014). Similarly, disrupting microtubules results in compromised actomyosin networks and the abolishment of mesoderm invagination in *Drosophila* embryos (Ko et al., 2019). It is likely that the diversity of interactions between microtubule and actomyosin networks does not rely on a single conserved mechanism but rather a complex synergy between the tissue-specific organization of microtubules within cells and the subcellular distribution of RhoGEF2 cortical partners and anchoring proteins.

Additionally, recent studies showed that microtubule plus-ends (EB1 included) can undergo phase separation and behave as liquid condensates to regulate molecular interactions and valency at the tip, as well as microtubule dynamic instability (Maan et al., 2023; Meier et al., 2023; Song et al., 2023). Addressing if and how this mechanism participates in the spatiotemporal regulation of Rho dynamics *in vivo* could provide new insights on the interplay between microtubule and actomyosin and the generation of forces during tissue morphogenesis.

3.3 Force transmission between epithelial cells

In the previous section, I described the cytoskeletal components, molecular machinery, and signalling pathways that regulate the generation of forces within epithelial cells. This raises the following question: how are intracellular forces transmitted to coordinate cellular behaviours and drive tissue morphogenesis? The following section will detail the cellular components and mechanisms that underly force transmission in cells and within epithelial sheets.

3.3.1 Adhesive contacts

To maintain connectivity, cells are coupled via adhesive contacts to transmit forces between adjacent cytoskeletal networks. The two main adhesive structures involved in force transmission are adherens junctions (AJs) and focal adhesions (FAs), mediating cell–cell adhesion and cell–ECM adhesion, respectively.

3.3.1.1 Adherens junctions

AJs were first identified as electron-dense regions between cells, later described to contain E-cadherin (Farquhar and Palade, 1963; Boller et al., 1985). AJs are formed by the interaction of cadherin single-pass transmembrane receptors and several cytoplasmic binding partners, such as β -catenin, α -catenin, and p120-catenin (Figure 21A). Cadherins engage in homophilic *trans*-ligation with their extracellular domains to form adhesive complexes between adjacent cells and in *cis*-interactions between cadherins within the same membrane to enlarge and strengthen AJs complexes (Shapiro and Weis, 2009), while the cytoplasmic tail of cadherins forms complexes with β -catenin, α -catenin and p120-catenin. As α -Catenin binds to both β -catenin and actin filaments, adhesion can be coupled to the actomyosin cytoskeleton, cell signalling or membrane trafficking (Lecuit and Yap, 2015; Pinheiro and Bellaïche, 2018; Campàs et al., 2024). Additionally, other proteins like vinculin and afadin can be recruited to stabilize the connection between the actin cytoskeleton and the cadherin complexes, and this linkage enables the transmission of mechanical forces across cells, as well as maintains the structural integrity of epithelial layers (Mège and Ishiyama, 2017). These bidirectional connections also allow actin networks to recruit MyoII to regulate the organization of AJs, as well as their mechanical properties, such as rigidity and tension (Lecuit and Lenne, 2007; Charras and Yap, 2018). Conversely, cadherins can couple to cell signalling pathways, such as small GTPases RhoA, Rac1, and Cdc42, to modulate the cytoskeleton (Noren et al., 2001; Ratheesh et al., 2012). Finally, AJs display mechanosensitive properties, as it was shown that cadherins behave as catch-slip bonds that stiffen upon application of an external force (Rakshit et al., 2012; Manibog et al., 2014), and junctional components are remodelled in a tension-dependent manner (Leckband and de Rooij, 2014; Hoffman and Yap, 2015).

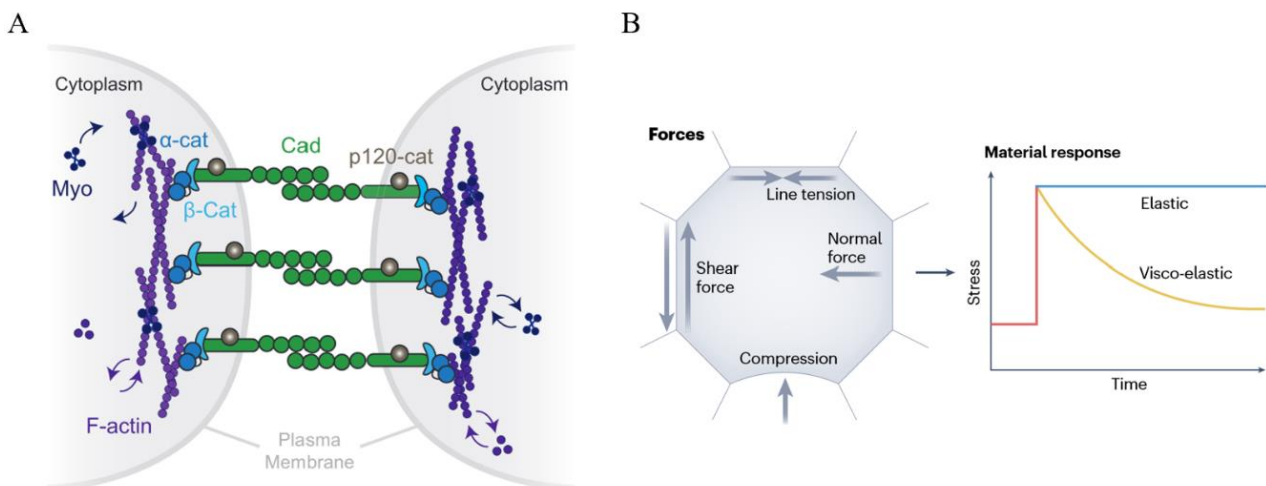


Figure 21. Adherens junction organization and role in force transmission

A. Molecular components driving adhesion between adjacent cells and coupling junctions to intracellular cytoskeletal networks. **B.** Forces experienced by adherens junctions and their material responses. Images adapted from (Pinheiro and Bellaïche, 2018; Campàs et al., 2024).

Adhesion strength and stability can be further modulated by the organization of cell junctions into smaller clusters to increase their force-bearing capacity (Truong Quang et al., 2013; Indra et al., 2018). Super-resolution microscopy has notably revealed a stratified organization of these clusters: an extracellular adhesion layer, a membrane-proximal signalling layer, a force transduction and cytoskeletal adaptor layer, and an F-actin regulatory layer (Bertocchi et al., 2017). Taken together, these features allow adherens junctions to withstand and transmit various forces which are key to remodel epithelial sheets during morphogenesis across species (Halbleib and Nelson, 2006; Maître et al., 2012). Additionally, studies have shown that AJs display viscoelastic properties (Bambardekar et al., 2015). This means that they behave elastically at short timescales but demonstrate fluid-like dynamics that dissipate stresses over longer timescales (Figure 21B). This is particularly relevant as energy dissipation, often mediated by turnover of cadherins or actomyosin molecular components, is postulated to be as important as force generation and force transmission during morphogenesis (McFadden et al., 2017; Mao and Wickström, 2024). For example, endocytic turnover of E-cadherin promotes bond breaking to dissipate stresses and remodel the *Drosophila* wing (Iyer et al., 2019). Additionally, during *Drosophila* germband extension, junctional shrinkage during cell intercalation can be recapitulated by a ‘simple’ viscoelastic model and irreversibility of this shape change depends on the dissipation of stresses by F-actin turnover (Clément et al., 2017).

It is worth mentioning that, while this section focused on the transmission of forces mediated by actomyosin networks, adherens junctions can also interact with and transmit forces from microtubules (Akhmanova et al., 2009). In addition to their role in force transmission, adherens junctions can also alter the mechanical properties of multicellular tissues across scales to assist morphogenetic processes, as nicely reviewed by (Campàs et al., 2024).

3.3.1.2 Focal adhesions

The main components of focal adhesion complexes are integrins, that interact with the extracellular matrix through their α - and β -subunits (Ro, 1992; Hynes, 2002). Integrins display catch-bond behaviour, as it was reported that tension-induced conformational changes in the $\alpha5\beta1$ integrin extracellular domain can enhance its binding to fibronectin to promote long-lasting adhesion under mechanical stresses (Friedland et al., 2009; Kong et al., 2009). While clustering is not required for focal adhesion formation, it participates in the regulation of force transmission, as integrin clusters have been shown to increase receptor density and adhesion strength, with tension threshold ~ 6 times higher than individual integrin heterodimers (Roca-Cusachs et al., 2009). Force transmission by focal adhesions is often described by a ‘molecular clutch’ model, where adaptor proteins at focal adhesions mediate force transmission from F-actin to integrins: as a result, pushing or pulling forces generated by the actin cytoskeleton are physically coupled to cell adhesions, and forces are transmitted to the neighbouring cells (Mitchison and Kirschner, 1988; Elosegui-Artola et al., 2018). Finally, experimental evidence across species showed that disruption of

focal adhesions can impair force transmission and lead to defective morphogenesis (Narasimha and Brown, 2004; Bryan et al., 2020; Molè et al., 2020).

3.3.3 Indirect methods of force transmission through membrane and organelles

While most mechanical forces are transmitted via adhesive contacts within epithelial sheets, recent studies have started investigating the role of membranes and organelles and their molecular components in force transmission at the cell scale (Phuyal et al., 2023). This arises from the observation that cell shape and topology changes can lead to changes in cell behaviour and identity (Iskratsch et al., 2014), which suggests that mechano-sensing structures within cells can convert mechanical forces into biochemical signals (a process termed ‘mechano-transduction’) and implies the existence of intermediates that transmit forces at the scale of organelles or membranes. For instance, membrane deformations can induce changes in its tension and packing of its lipids, thus modulating the distribution and activity of transmembrane proteins (Le Roux et al., 2019). Such changes can activate mechano-sensitive ion channels such as Piezo-1, which has been shown to drive biochemical feedbacks at short timescales on MyoII activity (Ellefsen et al., 2019). Additionally, the behaviour of organelles which are associated to the cell cytoskeleton can be modulated by forces, as illustrated with the Golgi apparatus whose attachment with microtubules can induce cell polarization and subsequent migration (Rivero et al., 2009; Millarte and Farhan, 2012; Tonucci et al., 2015). Understanding how forces are integrated at the subcellular scale and how the resulting physical, biochemical or genetic feedbacks can influence collective cell behaviour is a promising area of research. The most striking examples of such regulation occur at the nucleus, where force-induced deformations can be directly or indirectly transmitted to the cell and its neighbours via several mechanisms.

3.3.3.1 Nuclear linkage to the cell cytoskeleton

To transmit forces, nuclei must first be able to sense them: the main intermediate between the nucleus and force-generating machineries or adhesive complexes is the linker of nucleoskeleton and cytoskeleton complex, or ‘LINC complex’ (Figure 22A). It is composed of nesprins, SUN proteins, and lamin proteins (Wang et al., 2009; Lee and Burke, 2018). Nesprin 1 and Nesprin 2 are rod-like nuclear membrane proteins with an actin-binding domain, a central spectrin-like domain, and a KASH domain that binds to SUN proteins (Crisp et al., 2006; Haque et al., 2006). These nesprins link actin microfilaments to SUN1 and SUN2 on the inner nuclear membrane, which then connect to lamin A on the nuclear envelope (Worman and Gundersen, 2006). Additionally, SUN1 has been proposed to mediate mechanical coupling between the cytoskeleton and nuclear pore complexes, potentially regulating nuclear trafficking (Woodland, 1994). The anchoring function of LINC proteins is conserved across species, as seen with ANC-1 in *C. elegans*, and MSP300 in *Drosophila*, which tether nuclei to the actin cytoskeleton, or ZYG-12 which mediates nuclear attachment to the microtubule cytoskeleton in *C.elegans* (Malone et al., 2003; Yu et al., 2006; Hao et

al., 2021). Disruption of LINC complexes is detrimental to tissue morphogenesis, as illustrated during *Drosophila* salivary gland formation, where KASH-domain proteins have been shown to regulate microtubule organization and integrin localization during collective cell migration, and their disruption strongly impaired epithelial cell rearrangements (Myat et al., 2015). Other recent examples of the indirect transmission of forces by the nucleus stem from studies in amoeboid cells by (Lomakin et al., 2020; Venturini et al., 2020). In these studies, they show that upon a certain threshold of compressive forces, nuclei within cells remodel their nuclear envelope. The envelope normally has a lobulated aspect but under forces starts to unfold and stretch (Figure 22B). As a result, calcium is released from internal membrane stores and activates the calcium-dependent phospholipase cPLA2, which leads to downstream MyoII activation and actomyosin contractility within ~1 min.

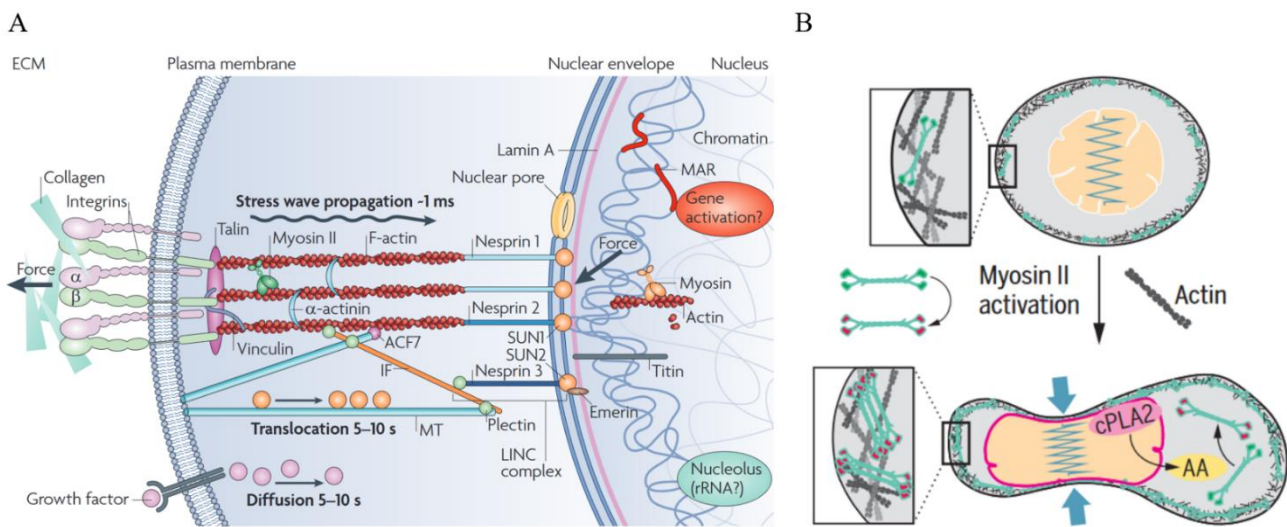


Figure 22. Nuclear envelope and LINC complex as subcellular force transducers

A. Composition of the linker of nucleoskeleton and cytoskeleton complex (LINC).
B. Force-induced nuclear deformations lead to fast MyoII activation in amoeboid cells. Images adapted from (Wang et al., 2009; Venturini et al., 2020).

3.3.3.2 Nuclear repositioning as an integrator of mechanical forces

Cells experience several type of mechanical forces, including stretching (tensile forces), compression, shear stress, hydrostatic pressure, and the stiffness of the surrounding extracellular matrix. These forces often lead to the deformation of cell membranes and organelles, as previously discussed and extensively studied in the literature (Kalukula et al., 2022). Additionally, internal or external mechanical forces can move organelles, such as the nucleus, within cells (Gundersen and Worman, 2013). In this section, I will discuss experimental data demonstrating how nuclear repositioning can contribute to force transmission and drive cellular rearrangements.

The positioning of nuclei can be regulated by a variety of mechanisms, and its central or asymmetric location is key during both developmental processes and diseases (Dupin and Etienne-Manneville, 2011; Gundersen and Worman, 2013; Deshpande and Telley, 2021). First, its ability to bind to cytoskeletal components via the LINC complex allows it to be directly repositioned by forces generated by actomyosin and microtubule networks. This is well illustrated in fibroblasts, where F-actin is coupled to the nucleus and retrograde flows drive the relocation of nuclei to polarize cells and assist their migration (Luxton et al., 2010). Similarly, actin-based filopodia elongation was shown to position the nuclei by interacting with perinuclear crosslinkers in *Drosophila* nurse cells, thus ensuring proper oogenesis (Huelsmann et al., 2013). Additionally, coupling between the LINC complex and microtubules has been shown to regulate nuclear positioning and morphogenesis. For instance, in the vertebrate cerebral cortex, interkinetic nuclear migration, where microtubules drive the bidirectional movement of nuclei, has been shown to regulate neurogenesis (Del Bene et al., 2008; Zhang et al., 2009). Nuclei can also be indirectly moved by forces, as illustrated during early *Drosophila* embryogenesis, where actomyosin-based forces are transmitted via cytoplasmic flows to move nuclei to the periphery (Deneke et al., 2019; Hernández-López et al., 2023; Htet and Lauga, 2023). Interestingly, nuclear positioning is not only dependent on internal or external forces, but is capable of transmitting these forces to impact cell shape and behaviour. For example, research by (Ambrosini et al., 2019) in *Drosophila* has identified that a subset of cells of the leg epithelium possess an actomyosin cable connecting their apical side to their nucleus. As the nucleus is repositioned and anchored basally, the contraction of this cable generates tension, which pulls on the cell surface and folds the epithelial sheet. They further demonstrated that disruption of the basal positioning or anchorage of nuclei reduced apicobasal actomyosin tension, and impaired fold formation.

Other mechanisms involving nucleus-dependent force transmission have been described across cell types. For instance, in migrating fibroblasts, actomyosin contractility can move the nucleus towards the leading edge, via the LINC complex. As a result, the intracellular pressure increases in the front compartment and generates lobopodial protrusions to assist cell migration (Petrie et al., 2014). Similar work showed that such ‘nuclear piston’ can drive protrusion expansion in human migrating mesenchymal stem cells (Lee et al., 2021). This mechanism is particularly relevant as it allows cells to achieve long-range transmission of locally-generated forces. For example, during *Drosophila* mesoderm invagination, it was demonstrated that the apical recruitment of actomyosin can generate a tissue-scale hydrodynamic flow of cytoplasm. This flow is accompanied by the basal movement of nuclei and drags the lateral cell membranes between the apex and the nucleus, resulting in the coordinated elongation of cells (He et al., 2014). It has been proposed that a volume conservation principle governs the nuclear relocation and cell elongation observed during mesoderm invagination. Specifically, the loss of apical area during constriction is compensated by an increase in cell length between the apical side and the nucleus,

thereby conserving the overall cell volume (Gelbart et al., 2012), even though the causal relationship has not been experimentally tested.

4. Composite morphogenesis

In the first chapters of this introduction, I detailed the mechanisms that remodel epithelial tissues across scales to form a functional organism. While most morphogenetic events have been studied individually, it is important to recognize that these processes often occur simultaneously during development, a phenomenon known as ‘composite morphogenesis’ (John and Rauzi, 2021b). One might thus wonder how cells within tissues coordinate multiple, simultaneous changes in shape and topology? In the next section, I will discuss examples of composite morphogenesis during animal development and the potential underlying molecular mechanisms.

4.1 Concomitant morphogenetic processes during development

One of the most commonly conserved processes during embryo gastrulation and neurulation is the simultaneous folding and extension of epithelial sheets. It has recently been proposed that epithelial folding-extension can be classified in two categories :

(a) uniaxial, where folding and extension occur in the same direction, usually driving tissue in-pocketing or budding, as illustrated during *Drosophila* salivary gland, tracheal and intestine development (Limargas and Casanova, 1999; Iwaki et al., 2001; Cheshire et al., 2008), sea urchin archenteron formation (Hardin and Cheng, 1986), or *Xenopus* bottle cell formation (Keller et al., 1985).

(b) orthogonal, where folding and extension occur in orthogonal axes: this is best illustrated during the concomitant tube formation and body extension occurring during neurulation in *Xenopus* (Davidson and Keller, 1999), chick (Catala, 2021), and mouse embryos (Nishimura and Takeichi, 2008; Nishimura et al., 2012). More recently, it was also shown that concomitant folding-extension occurs during *Drosophila* mesoderm invagination (John and Rauzi, 2021a).

Both categories suggest that the cell rearrangements driving simple morphogenetic processes synergize to remodel the epithelial sheets into complex 3D structures. For instance, apical constriction and convergence-extension are both indispensable during *Xenopus* neural tube closure (Haigo et al., 2003; Inoue et al., 2016), and are spatiotemporally coordinated, with convergence-extension movements occurring first in the posterior side of the tissue, then followed by constrictions occurring throughout the neural plate (Christodoulou and Skourides, 2022). Interestingly, there is no clear temporal overlap between these events, indicating that they occur within the same timeframe but not simultaneously within individual cells. Similarly, during mammalian neural tube closure, it was shown that apical constriction and convergence-extension (via polarized intercalations) were spatiotemporally

coordinated via adhesion complexes under the common upstream regulator Scrib (Lesko et al., 2021). These studies show how tissues can be partitioned into regions to sequentially engage in cell constriction or intercalation. If you wish to know more about the conserved gene patterning and signalling pathways that coordinate these distinct events across species, I would recommend great reviews by (John and Rauzi, 2021b; van der Spuy et al., 2023).

Interestingly, recent research in *Drosophila* embryos has revealed that apical constriction and cell intercalation can occur not only concurrently within a tissue but also within the same cell to drive composite morphogenesis.

4.2 *Drosophila* mesoderm invagination as a new paradigm for concomitant folding and extension

During *Drosophila* early gastrulation, extensive research has focused on understanding the mechanisms underlying the invagination of epithelial sheets in the presumptive mesoderm tissue. Over the past few decades, a series of studies have elucidated the gene regulatory networks that organize signalling pathways responsible for force generation (Leptin and Grunewald, 1990; Frasch and Nguyen, 1999). These pathways have been shown to coordinate the behaviour of the contractile machinery along different cellular axes: it is now established that pulsatile apical constrictions driven by actomyosin, coupled with basal relaxation and increased lateral tension, collectively drive the folding of the presumptive mesoderm (Martin et al., 2009; Conte et al., 2012; Krueger et al., 2018; Gracia et al., 2019; Fierling et al., 2022). Yet, it was revealed that the mesoderm tissue not only undergoes folding but is concomitantly extending (John and Rauzi, 2021a). To do so, mesoderm cells establish a two-tier junctional mechanisms with distinct subcellular actomyosin networks: the first tier is located apically and drives apical constriction while the second tier is located laterally (~10 μm from the apical side) and drives polarized cell intercalation (Figure 23). This study also revealed that orthogonal AP and DV gene patterning control the establishment of this two-tier junctional system, but the underlying cytoskeletal rearrangements are yet to be discovered. My research work will thus use *Drosophila* mesoderm tissue as a new paradigm of concomitant folding and extension and try to dissect the molecular mechanisms that allow cells to segregate subcellular actomyosin networks to engage in distinct cell rearrangements.

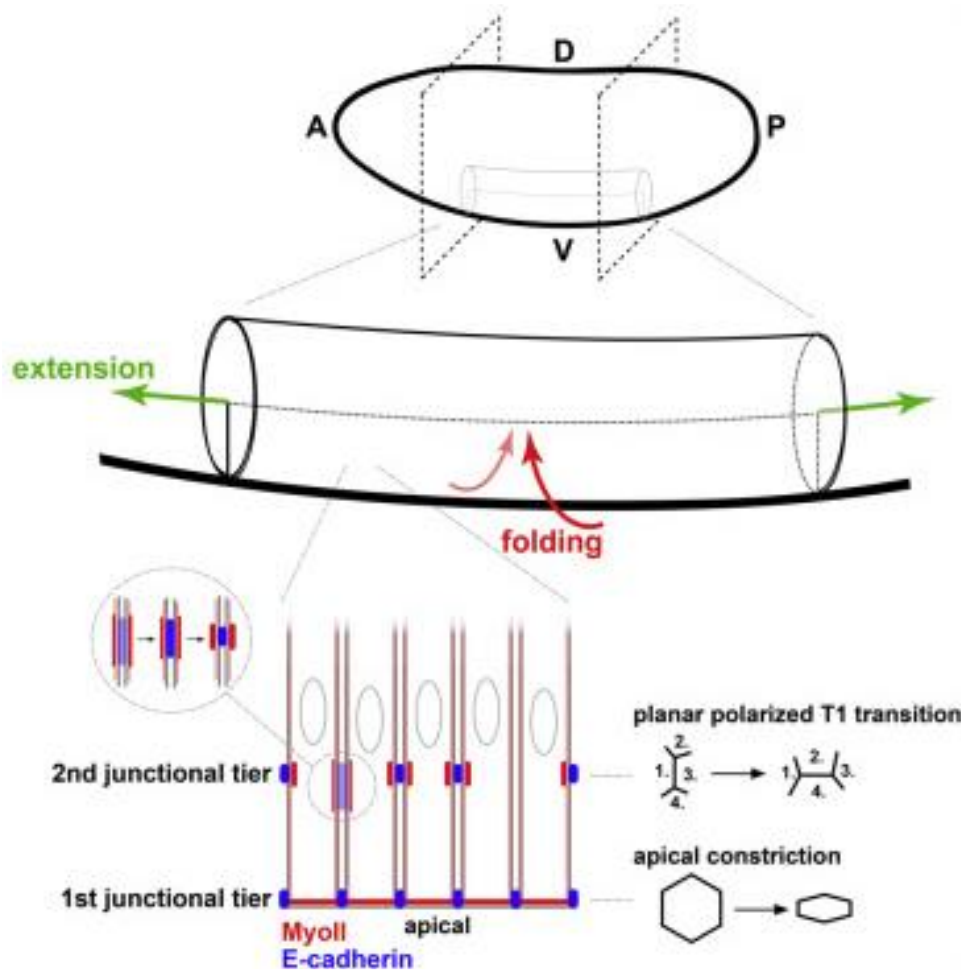


Figure 23. Concomitant folding and extension of the *Drosophila* presumptive mesoderm

Two distinct subcellular actomyosin networks, tethered to adherens junctions, are generated within cells to drive concomitant apical constriction and lateral polarized intercalation, resulting in the folding-extension of the presumptive mesoderm in *Drosophila* embryos. Image adapted from (John and Rauzi, 2021a).

Chapter II-Results

Summary of research findings

The results of my research have now been submitted for peer-review in a scientific journal. You'll find below a summary of the results.

1. Nuclear basal repositioning spatiotemporally correlates with the formation of the lateral actomyosin tier

To study the establishment of the two-tier actomyosin network during early *Drosophila* gastrulation, I used fast, spatially-resolved *in vivo* imaging to map the sequence of events and track nuclear dynamics, MyoII distribution, and cell cortices in the mesoderm tissue. I observed that MyoII enrichment at the cell apex leads to apical constriction and basal nuclear movement. This repositioning is followed by MyoII recruitment at the lateral cortex (forming clusters ~10 μm from the apex). Temporal cross-correlation analysis showed that apical MyoII contractions and nuclear displacement occur simultaneously, while lateral MyoII recruitment is delayed by ~5 minutes, indicating that the second tier of MyoII forms only after nuclear displacement. MyoII lateral clusters (MyoII-LCs) were spatially correlated with nuclear position, with more basally located MyoII-LCs associated with more basally displaced nuclei. Finally, the strong correlation between apical cell surface area and nuclear position supported the idea that apical constriction drives basal nuclear displacement.

2. Constriction-induced nuclear displacement is necessary for the formation of MyoII lateral clusters

I then sought to test the role of apical constriction in driving nuclear basal displacement. Using infrared femtosecond laser dissections to disrupt the apical actomyosin cytoskeleton, I observed that cells failing to constrict retained apically-located nuclei, preventing MyoII-LC formation. Conversely, enhanced constriction in control regions led to more basally located nuclei and increased MyoII-LC recruitment. To ensure these effects were not due to the loss of apical MyoII, I used an optogenetic tool to induce ectopic basal constriction in a subset of mesoderm cells. This kept nuclei apically located and abolished MyoII-LC formation. Injecting fluorescent beads to track cytoplasmic flows, I demonstrated that apical constriction drives a basally-directed flow, and its reversal leads to the loss of previously established MyoII-LCs. These findings confirm that MyoII-mediated apical constriction generates a cytoplasmic flow displacing nuclei necessary for lateral MyoII recruitment, which is a reversible process.

3. Nuclear position defines the location of MyoII lateral clusters

To enable multiple tissue shape changes to occur simultaneously, mesoderm cells establish actomyosin tiers at two distinct apicobasal positions. Given that MyoII-LCs are consistently formed ~10 μm from the apical side and their position appears correlated with the position of the nuclei, I then investigated the mechanisms controlling the apicobasal establishment of MyoII-LCs. By tracking the position of

MyoII-LCs relative to the neighbouring nuclei surrounding the enriched lateral cortex, I identified a predictive model: MyoII-LCs are positioned at half the distance between the apical side of the cell and the average position of the two adjacent nuclei, hereby termed the “halfway rule”. To test this model, I sought to modulate nuclear positioning *in vivo*. First, I developed a novel protocol for embryo centrifugation. This procedure resulted in enhanced nuclear displacement and more basally located MyoII-LCs. Conversely, by using infrared femtosecond laser dissection on a portion of the mesoderm tissue, I induced a sub-tissue delay in constriction, leading to more apically located nuclei. Consequently, MyoII-LCs formed more apically. Strikingly, in both scenarios, the location of MyoII-LCs obeyed the “halfway rule.”

4. Isotropic coalescence of the cortical actomyosin drives the formation of MyoII lateral clusters

Why would MyoII clusters be established ‘halfway’? By monitoring RhoGEF2 distribution in mesoderm cells, I observed that as nuclei displace, RhoGEF2 is recruited to the lateral cortex, as previously reported, spanning the region between the nucleus and the apical side. This recruitment activates the cortical actomyosin network, leading to its coalescence and the formation of MyoII-LCs. Using optogenetic tools to recruit RhoGEF2 to the lateral cortex with varying lengths of activation, I demonstrated that MyoII-LCs consistently coalesce isotropically, forming a cluster at the midpoint of the activated region.

5. Mesoderm cells do not undergo nuclear deformation during early gastrulation

Recent research highlighted the role of nuclear deformations in controlling gene expression, cytoskeletal dynamics, and cell behaviour in various contexts. To determine whether nuclear mechano-transduction plays a role in this process, I monitored nuclear contours throughout early gastrulation in *Drosophila* embryos. I did not observe changes in global eccentricity nor local curvature, ruling out the involvement of nuclear deformation in this process.

6. Nuclear position spatiotemporally controls the distribution of the microtubule network

I explored how the nucleus regulates RhoGEF2 recruitment to the lateral cortex. Initially, I considered the nucleus might physically block cortical access. However, using optogenetics to recruit RhoGEF2 to lateral cortices flanked by nuclei still resulted in MyoII-LC formation, ruling out direct control. Instead, the nucleus may indirectly control RhoGEF2 density. Studies suggested that microtubules deliver RhoGEF2 through +TIP interactions, particularly with EB1. Monitoring EB1 during early gastrulation, I observed that microtubule plus-ends, initially apical, reorganize to the lateral cortex as the nucleus moves basally, mirroring RhoGEF2 redistribution. Infrared femtosecond laser dissection of the apical actomyosin network showed that apical nuclear relocation inhibits EB1 recruitment to the lateral cortex. To further dissect this process, I developed an *in silico* model of a mesoderm cell, using *in vivo* data as boundary conditions and varying parameters such as geometrical constraints

and microtubule properties. I demonstrated that within the columnar shape of mesoderm cells, the nucleus acts as a microtubule compartmentalizer, with most microtubules from the apical MTOCs contained between the nucleus and the apical side. I showed that the apicobasal position of the nucleus regulates the cortical distribution of microtubule plus-ends. Decreasing the nuclear radius inhibited this compartmentalization, while increasing it emphasized the effect, supporting the nucleus as a spatiotemporal organizer of the cytoskeleton.

7. Microtubules can control actomyosin dynamics during early gastrulation

I investigated whether the microtubule network regulates actomyosin activity in mesoderm cells. Observing microtubules radiating from MTOCs towards the lateral cortex, where MyoII-LCs form, I used a pharmacological approach to disrupt microtubules. While MyoII recruitment at the apical tier remained unchanged, defects in the network impaired apical constriction, mimicking ROCK inhibitor effects. In cells with disrupted microtubules, basal nuclei were observed only in those that managed to constrict, supporting constriction-induced nuclear relocation. Additionally, microtubule depolymerization led to the significant loss of the lateral MyoII tier.

8. Microtubules can control the cortical density of RhoGEF2

To achieve spatiotemporal control of microtubule dynamics, I implemented a live-injection protocol to monitor RhoGEF2 cortical distribution at the lateral cortex. I observed that microtubule disruption resulted in the rapid loss of cortical RhoGEF2. A similar outcome was observed using an opto-pharmacological tool to induce spatiotemporal microtubule depolymerization.

9. RhoGEF2 and microtubule plus-ends are planar-cell polarized in the presumptive mesoderm

MyoII-LCs are planar-cell polarized (PCP) in the mesoderm tissue, preferring dorsoventral (D-V) junctions to drive tissue convergence-extension along the anterior-posterior (A-P) axis. To investigate the underlying mechanisms, I imaged RhoGEF2 and could observe its PCP distribution. A similar analysis of the microtubule plus-end protein EB1 initially showed no clear PCP pattern. However, tracking EB1 over time revealed that microtubule plus-ends exhibit temporal PCP, increasingly accumulating at D-V junctions.

10. The RhoGEF2-anchoring protein T48 is necessary for the formation of MyoII lateral clusters and subsequent intercalation

Previous research has shown that the protein T48, usually at the apex of mesoderm cells, anchors RhoGEF2 to initiate apical constrictions. To see if T48 also influences MyoII lateral tier formation, I imaged its subcellular distribution. When overexpressed, T48 was also recruited to lateral cortices. In a T48 mutant line, I could observe a significant loss of MyoII-LCs and aberrant cell intercalations, termed ‘bowtie’ intercalations, and previously described to be defective to extend the tissue.

1 **Nuclear position controls the activity of cortical actomyosin**
2 **networks powering simultaneous morphogenetic events**

3

4 Nicolas Roby, Matteo Rauzi

5 University Côte d'Azur, CNRS, Inserm, iBV, Nice, France

6

7 **ABSTRACT**

8 Tissue morphogenesis shapes epithelial sheets via cell remodeling to form functional living
9 organisms. While the mechanisms underlying single morphogenetic events are well studied,
10 how one tissue can undergo multiple and concomitant shape changes remains largely
11 unexplored. To tackle this question, we study the morphogenetic process of simultaneous
12 mesoderm folding and extension in the early *Drosophila* embryo. This composite tissue
13 transformation relies on a sharply timed reorganization of the cortical actomyosin network in
14 two distinct subcellular tiers to drive concomitant cell apical constriction and lateral
15 intercalation for tissue folding and convergence-extension, respectively. Here we elucidate the
16 spatiotemporal control of the two-tiered actomyosin network. We show that, within the
17 geometric constraints imposed by the columnar shape of mesoderm epithelial cells, the
18 nucleus acts as a barrier shielding the lateral cortex from interactions with the microtubule
19 network, thereby regulating the distribution of the key signaling molecule RhoGEF2. The
20 relocation of the nucleus, driven by the contraction of the first actomyosin tier and the resulting
21 cytoplasmic flow, unshields the lateral cortex for RhoGEF2 delivery to direct the stereotypic
22 formation of the second actomyosin tier. Thus, the nucleus and its position function as a
23 spatiotemporal cytoskeleton compartmentalizer establishing a modular scaffold powering
24 multiple and simultaneous cell transformations for composite morphogenesis.

25

26

27 Introduction

28 The morphogenesis of epithelia displays remarkable plasticity and robustness during embryo
29 development: living tissues actively remodel their shape while maintaining their structural
30 integrity to establish functional organisms. Tissue remodeling relies on the ability of epithelial
31 cells to generate mechanical forces and to acquire new shapes and position while maintaining
32 cell-cell contacts^{1,2}. To achieve this, cells remodel their cytoskeleton in an orchestrated
33 fashion³⁻⁵ under the control of signaling cues established both at the local and organismal
34 levels⁶.

35 An outstanding example of epithelial plasticity and robustness is composite
36 morphogenesis, the process by which an epithelial tissue undergoes multiple and
37 simultaneous shape transformations⁷. For instance, epithelia can simultaneously fold and
38 extend to drive embryo gastrulation, neurulation or tubulogenesis⁸⁻¹⁰. While great advances
39 have been made to unveil the mechanisms underlying single morphogenetic processes, how
40 composite morphogenesis is directed and coordinated is largely unexplored. To tackle this
41 question, we study the concomitant folding and extension of the prospective mesoderm during
42 early *Drosophila* gastrulation. Recent work has shown that mesoderm epithelial cells establish
43 two junctional tiers formed by actomyosin networks tethered to E-cadherin and tailored for
44 distinct functions. The first tier is apically located and mediates cell apical constriction for tissue
45 furrowing (Figure 1a, b and 1b', bottom)¹¹. The second tier is positioned laterally (~10 μm from
46 the apical side) and is planar cell polarized to initiate cell intercalation for tissue convergence-
47 extension (Figure 1a, b and 1b', top)⁸. With this study, we aim to shine new light on the
48 mechanisms that spatiotemporally coordinate the formation of functionally distinct cytoskeletal
49 networks for simultaneous cell shape and topology changes. While the two tiers share the
50 same nature, their origin differs. The first tier is under the control of the cell apical-basal
51 polarity¹² and it is shaped by apical-medial actomyosin contractions¹³. The second tier is
52 formed by the coalescence of the cell lateral actomyosin network, focusing E-cadherin to form
53 a cluster⁸. Overall the formation of the two-tier junctional system is under the control of the

54 synergistic interaction between the embryo anterior-posterior (AP) and dorsal-ventral (DV)
55 gene patterning systems⁸. How the lateral actomyosin network is spatiotemporally controlled
56 is still unknown.

57 In addition to the molecular signaling, the change in position and shape of cellular
58 organelles play a role in cell remodeling^{14,15}. During the phase of apical constriction of
59 mesoderm epithelial cells, the cell nuclei migrate basally^{16,17}. While a great body of work has
60 highlighted the mechanisms controlling nuclear relocation and the role of nuclear
61 mechanotransduction in cell polarity, migration, division, or fate determination¹⁸⁻²⁰, how the
62 position of the nucleus participates in tissue remodeling remains elusive. We now investigate
63 this during mesoderm folding and extension. We provide evidence that the nucleus functions
64 as a cellular compartmentalizer and that its relocation spatiotemporally organizes the cell
65 cytoskeleton and the distribution of the Rho guanine exchange factor RhoGEF2 to establish a
66 second actomyosin tier for cell intercalation.

67 Finally, by implementing advanced live imaging, laser manipulation, optogenetics, and
68 molecular modeling, this study reveals the mechanisms underlying the spatiotemporal control
69 of the cortical actomyosin cytoskeleton to form a modular scaffold for simultaneous
70 morphogenetic events.

71

72 **Results**

73 **MyoII upregulation along the cell lateral cortex follows nuclear migration**

74 During the initial phase of gastrulation, MyoII accumulates both at the apical and lateral side
75 of mesoderm cells to establish a two-tier actomyosin scaffold generating contractile forces for
76 both apical constriction and cell intercalation (Figure 1b, b' bottom and top panel, respectively).
77 To investigate the origin of the lateral tier, we monitored MyoII dynamics and the cellular
78 processes occurring in the mesoderm tissue. Recent work has shown that apical MyoII,
79 mediating constriction of the cell apical surface (Figure 1b and b' bottom panel), precedes
80 lateral MyoII upregulation⁸. Seminal studies have reported that, during apical constriction,

81 mesoderm cell nuclei migrate toward the cell basal side^{16,17}. To time the sequence of events,
82 we performed a cross-correlation analysis between nuclear position and MyoII accumulation
83 at the apical and lateral cortex over time. Our data shows that, while the migration of nuclei is
84 synchronized with the increase of apical MyoII (Supplementary Figure 1b and c), the peak of
85 nuclear displacement rate precedes by about 2 minutes the peak of lateral MyoII accumulation
86 rate (Figure 1c and d, Supplementary Figure 1a and c, Supplementary Movie 1). In addition,
87 the apical-basal location of individual MyoII lateral clusters (MyoII-LCs) appears to correlate
88 with the position of the corresponding nuclei (Supplementary Figure 1d). Altogether, these
89 evidences highlight a possible link between nuclear migration and the formation of the MyoII
90 lateral tier.

91 In 2012, Gelbart and colleagues formulated the volume conservation principles by
92 which apical constriction drives cytoplasm flow pushing the nucleus towards the cell basal
93 side²¹. This model is based on the assumption that the cytoplasm is an incompressible fluid
94 and that the nucleus works as an “impassable piston”. Tissue-scale cytoplasmic flow was then
95 demonstrated by He et al. in 2016²². While Gelbart and colleagues show a strong correlation
96 between apical constriction rate and the rate of nuclear displacement, we now directly tested
97 the relationship between the apical cell surface area and the nuclear position over time. Our
98 analysis shows that the position of the nucleus along the apical-basal axis of the cell is tightly
99 coupled with the apical surface area of the cell (Figure 1e and f).

100 Finally, our analyses further support the idea that MyoII-dependent apical constriction
101 controls nuclear apical-basal position and show that the formation of the MyoII lateral tier
102 follows nuclear migration.

103

104 **Nuclear migration controls lateral MyoII upregulation**

105 Nuclear migration and lateral MyoII upregulation show spatial and temporal correlation. To test
106 if the basal displacement of nuclei is necessary for MyoII-LC formation, we devised a set of
107 experiments to interfere with nuclear migration. As nuclear positioning is strongly correlated
108 with cell surface changes (Figure 1f), we implemented infrared (IR) femtosecond (fs) laser

109 ablation of the apical actomyosin network to abort apical constriction and eventually inhibit
110 nuclear migration while preserving cell membrane integrity (Figure 2a and b, Supplementary
111 Figure 2a and Supplementary Movie 2). It should be noted that IR fs laser ablation is a multi-
112 photonic technique with high spatial specificity²³ (i.e., depth resolution of about 1 μm) that is
113 effective to selectively dissect the actomyosin network located at the apical side of cells
114 (Supplementary Figure 2h, i). Upon ablation, apical constriction is inhibited and nuclei fail to
115 move basally (Figure 2c and d). This evidence directly demonstrates a causal link between
116 nuclear migration and apical constriction, corroborating the idea that nuclei behave as cellular
117 “pistons”²¹. Remarkably, MyoII-LCs are inhibited in the zone where nuclei fail to displace
118 basally (Figure 2c, c' and e). In the zone next to the ablated region (i.e., the control zone),
119 cells rapidly shrink their apical surface area and display enhanced apical constriction as a
120 consequence of released tension in neighboring cells (Supplementary Figure 2a and b, blue).
121 As a result, nuclei in the control zone move significantly more basally compared to nuclei in
122 non-ablated embryos (Figure 2d) preserving or even enhancing the formation of MyoII-LCs
123 (Figure 2c, Supplementary Figure 2g and Supplementary Movie 3). Intriguingly, enhanced
124 formation of MyoII-LCs can similarly appear in non-ablated embryos that overexpress
125 RhoGEF2 (Supplementary Figure 2g and g'). To further test the causal relationship between
126 nuclear migration and lateral MyoII upregulation, we implemented optogenetics to prevent
127 nuclear basal displacement. More specifically, we used two-photon optogenetics to ectopically
128 activate MyoII at the cell basal side, resulting in cell basal constriction (Supplementary Figure
129 3a, b and c)^{24,25}. As a result, nuclei are kept close to the apical cell side (i.e., nuclear migration
130 is impaired) and the formation of lateral MyoII-LCs is inhibited (Supplementary Figure 3d, e
131 and f). Altogether, this shows that nuclear migration is necessary for lateral MyoII upregulation.

132 We then wondered if the formation of MyoII-LCs is a reversible process. To that end,
133 we devised an experimental trial to reverse the cytoplasmic flow and move nuclei back to the
134 apical surface. We injected fluorescent inert beads to monitor cytoplasmic flow
135 (Supplementary Figure 2c) and performed IR fs laser ablation to dilate apically-constricted
136 cells once MyoII-LCs were formed. Ablation results in apical cell surface dilation, leading to a

137 reversal of the cytoplasmic flow (Supplementary Figure 2c'). The cytoplasmic flow scales with
138 the changes in apical cell surface, and the flow directionality can be flipped from centripetal
139 (i.e., from apical to basal) to centrifugal (i.e., from basal to apical) if cells shift from constriction
140 to dilation (Figure 2f). As a consequence, nuclear migration is also reversed in the ablated
141 region (Supplementary Figure 2d and e) and lateral MyoII is downregulated (Supplementary
142 Figure 2f).

143 Overall, our data demonstrate that nuclear basal migration is necessary for the
144 formation of MyoII-LCs, which is a reversible process.

145

146 **Nuclear position defines the actomyosin coalescing zone and the location of MyoII** 147 **lateral clusters**

148 Our previous results show that nuclear migration is necessary for MyoII lateral upregulation
149 and indicate that the location of MyoII-LCs is not stochastic but rather follows the position of
150 nuclei (Supplemental Figure 1d). To better decipher the relationship between nuclear migration
151 and the upregulation of lateral MyoII, we considered four possible working models and
152 performed a thorough quantitative analysis of the relative position between nuclei and MyoII-
153 LCs. In general, a MyoII-LC is surrounded by four cells (i.e., four basal nuclei) and is located
154 at the cortex between two adjacent cells (Figure 3a). Therefore, we hypothesized that the
155 position of the MyoII-LC could be controlled by the most apical (model 1) or the most basal
156 (model 2) nucleus among the four, by the two adjacent nuclei (model 3 - Figure 3a, A and P
157 nuclei) or by the two non-adjacent nuclei (model 4 - Figure 3a, D and V nuclei). To test the
158 predictive capability of the four models, we measured the relative position between the four
159 nuclei and the corresponding MyoII-LC. Our analysis shows that model 3, having the smallest
160 standard deviation, has the greatest predictive power (Figure 3b). Model 3 advances the idea
161 that the MyoII-LC is located at half the distance between the apical side of the cell and the
162 average position of the two adjacent nuclei (i.e., the "halfway rule").

163 To functionally test the "halfway rule", we ectopically modulated the position of nuclei
164 and monitored the location of the MyoII-LCs. First, we aimed to reduce nuclear migration. To

165 that end, we downregulated apical constriction by ablating the apical actomyosin network
166 across a portion of the mesoderm and used the non-ablated portion as an internal control.
167 After ablation, the apical network is progressively restored, resulting in a delayed constriction
168 and a reduced nuclear migration compared to the control region (Figure 3c, Supplementary
169 Figure 4a, b and d, Supplementary Movie 4 and Supplementary Methods). Under these
170 conditions, MyoII-LCs form more apically (Figure 3c and f and Supplementary Figure 4c and
171 e). Next, we enhanced nuclear migration by implementing embryo centrifugation (Figure 3d
172 and Supplementary Methods), a technique previously used in cell culture²⁶. In centrifuged
173 embryos, nuclear migration is eventually enhanced and MyoII-LCs form more basally (Figure
174 3e and f, Supplementary Figure 5a, b and b'). In all conditions, the position of MyoII-LCs obeys
175 the "halfway rule" (Figure 3g). This data corroborates the notion that MyoII-LCs are tightly
176 controlled by nuclear migration and shows that they stereotypically form halfway between the
177 apex of the cell and the average position of the two adjacent A-P nuclei.

178 Which mechanism controls the halfway position of MyoII-LCs? Previous work has
179 shown that MyoII-LCs result from the coalescence of the cell lateral actomyosin network under
180 the control of the activating factor RhoGEF2⁸. Considering that RhoGEF2 is enriched along
181 the lateral cortex between the cell apical side and the nucleus (Supplementary Figure 6a and
182 a' top), we can hypothesize that an isotropic contraction of the lateral actomyosin network
183 would be sufficient to locate MyoII-LCs at the midpoint (Supplementary Figure 6b). To test this,
184 we used optogenetics to ectopically recruit RhoGEF2 along a cell lateral segment²⁴. As a
185 result, MyoII-LCs form in the middle of the activated segment (Supplementary Figure 6c and
186 d and Supplementary Movie 5), comforting the hypothesis that actomyosin isotropic
187 contraction and coalescence determine MyoII-LC position.

188 A growing body of evidence has shown that nuclear deformation can lead to acute
189 changes in genetic expression and cell behavior driven by cytoskeletal remodelling¹⁸. To test
190 if a mechanism involving nuclear deformation is at play during MyoII-LC formation, we imaged
191 and measured nuclear changes in shape in mesoderm cells during this initial phase of
192 gastrulation, starting from late cellularization. Our analyses show that both nuclear local

193 curvature and global eccentricity do not vary during this time period (Supplementary Figure
194 7a, a', b and c).

195 Finally, our data supports a model based on nuclear position, rather than nuclear
196 shape, controlling the size of a contractile zone that is established between the cell apical
197 surface and the nucleus. The position of the MyoII-LCs results from the isotropic contraction
198 and coalescence of the cortical actomyosin network within that space.

199

200 **The nucleus works as a microtubule compartmentalizer regulating the cortical** 201 **distribution of RhoGEF2**

202 We have shown that the apical-basal position of nuclei determines the location of
203 MyoII-LCs. Since ectopic accumulation of RhoGEF2 at the cell lateral cortex leads to local
204 upregulation of MyoII (Supplementary Figure 6a, b, c and d), we wondered if the nucleus per
205 se controls the cortical recruitment of RhoGEF2. Since the cross-sectional area of the nucleus
206 and of the cell are similar (Figure 1e), we can hypothesize that the nucleus can physically limit
207 cortical accessibility to cytosolic RhoGEF2. To test this, we implemented two-photon
208 optogenetics to ectopically increase RhoGEF2 levels specifically along the cell cortex flanked
209 by the nucleus. If the nucleus limits cortical accessibility to RhoGEF2, MyoII-LC formation is
210 expected to be compromised upon activation. After activation, MyoII is upregulated and a
211 cluster forms between nuclei similarly to control conditions (i.e., along the part of the cortex
212 not flanked by nuclei - Supplementary Figure 6e). This evidence speaks against a direct
213 regulation of RhoGEF2 by the nucleus, leaving open the possibility of an indirect nucleus-to-
214 RhoGEF2 regulation.

215 Previous studies have reported an association between RhoGEF2 and microtubule
216 (MT) plus ends, via the end-binding protein EB1^{27,28}. EB1 live imaging in mesoderm cells
217 during furrow formation shows MT plus ends radiating from the MT organizing centers (i.e.,
218 MTOCs, located at the apical side of the nucleus) towards the lateral cortex where MyoII
219 eventually clusters (Supplementary Movie 6). Therefore, we hypothesized that nuclear

220 position can regulate MT distribution. To test this, we measured EB1 density along the cell
221 lateral cortex at the onset and 7 minutes into gastrulation when nuclei migrate basally and
222 RhoGEF2 is laterally enriched. EB1 density increases over time phenocopying RhoGEF2
223 dynamic distribution⁸ (Figure 4a and b and Supplementary Movie 7). To directly test if the
224 nuclear position controls MT plus-end distribution, we inhibited nuclear displacement (using
225 the same experimental design presented in Figure 2b) and measured EB1 cortical distribution.
226 In the region where nuclear migration is impaired, the cortical levels of EB1 significantly drop
227 (Figure 4c and d). This demonstrates that nuclear migration controls the density of MT plus
228 ends along the cell lateral cortex. To explore how the nucleus can dictate MT plus-end
229 distribution, we developed an in silico model using the Cytosim simulator¹⁵ by implementing in
230 vivo measurements of MT properties and cell geometry as boundary conditions
231 (Supplementary Figure 8a, b, c, d and e and Supplementary Movie 8). We measured the
232 density of MT plus ends contacting the lateral cortex at different apical-basal positions and in
233 multiple conditions (e.g., with the nucleus at a more apical or more basal location, see
234 Supplementary Methods). Our analyses show that MT plus ends contact the lateral cortex
235 mostly in the zone between the apical side of the cell and the nucleus and that the plus-end
236 density drops beyond the nucleus position (Figure 4e, f, g and h). We then systematically
237 varied both subcellular geometric features and MT properties to assess their contribution in
238 this process. While the distance between centrosomes plays a mild effect, the only parameter
239 playing a major role is nuclear size: a larger nucleus more effectively limits the number of plus
240 end-to-cortex contacts (Figure 4i and Supplementary Figure 8f, g, h, i, j and k). These
241 evidences outline a model in which the nucleus works as a MT compartmentalizer physically
242 shielding the cortex from MT plus ends.

243 We then functionally tested the role of MT in driving MyoII-LCs. To that end, we used
244 Colcemid to depolymerize MTs while preserving MTOC integrity (Supplementary Figure 9a
245 and b). Colcemid injection during late cellularization leads to a strong downregulation of MyoII-
246 LCs (Supplementary Figure 9f). Previous work has shown that MT disruption does not affect
247 the initial phase of apical constriction that is characterized by cell stochastic ratcheted pulsatile

248 contractions^{11,29}. Nevertheless, while the first phase is indeed preserved, our data show that
249 the following phase, characterized by concerted apical constriction, is strongly compromised
250 (Supplementary Figure 10a and a'). More specifically, a great number of cells fail to apically
251 constrict, phenocopying mesoderm cells from embryos injected with a 5mM ROCK-inhibitor
252 Y-27632, ultimately resulting in furrow formation failure. (Supplementary Figure 10b and
253 Supplementary Movie 9). In Colcemid injected embryos, cells that still apically constrict show
254 a basally located nucleus while un-constricted cells maintain their nucleus to their apical side
255 (Supplementary Figure 10c). These evidences rule out MTs as active contributors to nuclear
256 migration and corroborate the notion that the displacement of nuclei is driven by constriction-
257 dependent cytoplasmic flow. The fact that cells deprived of MTs and with a displaced nucleus
258 show no distinctive MyoII-LC formation (Supplementary Figure 9f), demonstrates that both
259 MTs and nuclear migration are necessary but not sufficient per se to form MyoII-LCs.

260 Mesoderm cell intercalation is initiated by MyoII-LCs that are distributed in a planar cell
261 polarized (PCP) fashion with higher levels along DV junctions⁸. RhoGEF2 and EB1 also show
262 the same PCP distribution (Supplementary Figure 10d, d', e, f, g). In addition, RhoGEF2 show
263 high levels at the two MTOCs (Supplementary Figure 6a', bottom) where EB1 is also highly
264 concentrated (Supplementary Figure 8d). We can thus raise the hypothesis that MT plus ends
265 are prevalently targeting DV junctions for local RhoGEF2 delivery and consequent PCP
266 actomyosin activation. To test this hypothesis, we monitored changes in cortical RhoGEF2
267 density upon MT disruption. To that end, we performed time-controlled injection of Colcemid
268 during lateral MyoII upregulation (i.e., after apical constriction and nuclear migration –
269 Supplementary Figure 9c and Supplementary Methods). After injection, RhoGEF2 is
270 downregulated within 20 seconds (Figure 4j and k). A similar result is obtained when
271 implementing photo-controlled depolymerization of MTs using SbTub4AP¹⁷ (Figure 4k,
272 Supplementary Figure 9d, e and g and Supplementary Movie 10). Overall, this demonstrates
273 that MT plus ends spatiotemporally control RhoGEF2 cortical recruitment.

274 The transmembrane protein Transcript 48 (T48) has been shown to be expressed in
275 mesoderm cells and to act as a cortical anchor to capture RhoGEF2^{14,18}. Live imaging of T48

276 overexpression show that T48 can indeed locate at the cell cortex (Supplementary figure 10h
277 and h'). In T48 mutant embryos, while apical constriction and nuclear migration is overall
278 preserved (showing in most cases only a mild phenotype – Supplementary Movie 11 and 12),
279 MyoII-LCs are inhibited (Figure 4l and m). Moreover, in this mutated background, mesoderm
280 cells exchange neighbours in an aberrant fashion (previously described as bowtie intercalation¹
281 - Supplementary Figure 10i). This shows that T48 is pivotal for the establishment of MyoII-
282 LCs.

283 Finally, our data show that the nucleus functions as a MT compartmentalizer controlling
284 the cell cortex accessibility. Therefore, nuclear migration enables MT to redistribute along the
285 lateral cortex and to deliver RhoGEF2 with spatiotemporal precision with the support of T48
286 to form MyoII-LCs.

287

288 **Discussion**

289 Composite morphogenesis, characterized by multiple and simultaneous tissue shape
290 transformation, is a vital process during embryo development⁷. We investigate the
291 mechanisms underlying the concomitant folding and extension of the prospective mesoderm
292 during *Drosophila* embryo early development. During gastrulation, mesoderm epithelial cells
293 establish a junctional modular system supported by a two-tier actomyosin scaffold at the cell
294 apical and lateral side mediating apical constriction and lateral cell intercalation for
295 concomitant folding and extension, respectively⁸. This study dissects the spatiotemporal
296 coordination of the two-tiered scaffold, shedding new light on the subcellular control of
297 cytoskeletal networks.

298 We show that nucleus relocation within mesoderm epithelial cells is the coordinating and
299 triggering mechanism leading to the stereotypic formation of the lateral actomyosin tier. At the
300 onset of gastrulation, mesoderm cells apically constrict in a concerted fashion driving a basally
301 directed cytoplasmic flow that pushes nuclei towards the cell basal side. This nuclear

302 movement triggers a sudden change in the architecture of the MT network that delivers
303 RhoGEF2 to the lateral cortex. As a result, the cortical actomyosin, activated by RhoGEF2
304 signaling, coalesces isotropically to form the lateral tier. Remarkably, cortical RhoGEF2 levels
305 drop within tens of seconds after MT depolymerizing and lateral MyoII accumulation can be
306 enhanced when ectopically increasing the rate of nuclear relocation. Overall, this supports a
307 model in which RhoGEF2 cortical recruitment is tightly controlled by the time-integrated MT-
308 to-cortex interaction.

309 Nuclear repositioning is pivotal in several processes including body axis
310 determination³⁰, nervous system development³¹, cell proliferation³² and cell death³³. We now
311 show that the relocation of this large organelle plays a paramount role in tissue morphogenesis
312 by regulating cytoskeletal dynamics. Often, nuclear relocation relies on MTs³⁴⁻³⁷. Nevertheless,
313 the actomyosin cytoskeleton can also power the displacement of the nucleus. For instance,
314 actomyosin contraction can drive cytoplasmic advection dragging the nucleus in the center of
315 the mouse oocyte³⁸ and spreading nuclei in the *Drosophila* syncytium³⁹, or it can generate
316 directed traction forces pulling the nucleus during cell apoptosis in pseudo-stratified
317 epithelia³³. We demonstrate that, in epithelial mesoderm cells, the nucleus acts as a piston
318 pushed basally by the cell cytoplasm that behaves as an incompressible fluid, as previously
319 theorized²¹. We further show that basally directed cytoplasmic flow results from actomyosin
320 contraction forces driving the constriction of the apical side²².

321 Columnar cells, characterized by an elongated prism-shape, are common in epithelia
322 and play roles in absorption, secretion, protection, and structural support. This study highlights
323 a novel function for column shaped cells in tissue morphogenesis and embryo development.
324 The elongated geometry of mesoderm cells provides a cellular platform that is functional to
325 establish subcellular niches, with different biochemical and mechanical properties, engaged
326 in distinct morphogenetic transformations. In such a long and narrow cell, the nucleus acts as
327 a cytoskeleton compartmentalizer and its relocation modulates the activity of the actomyosin
328 cortex by controlling the MT-to-cortex interaction. Thus, the nucleus functions as an apicobasal
329 organizer structuring the actomyosin cortex in a multi-tiered scaffold possibly complementing

330 or overcoming the cell apicobasal signaling that is downregulated specifically in the mesoderm
331 during this early gastrulation phase⁴⁰.

332 In the prospective mesoderm, RhoGEF2 is involved in the regulation of the actomyosin
333 cytoskeleton both apically (i.e., the first tier⁴¹⁻⁴⁶) for apical constriction and laterally (i.e., the
334 second tier⁸) for cell intercalation. Intriguingly, in the neighboring ectoderm, cell intercalation
335 is under the control of both RhoGEF2 and DpRhoGEF114²⁸. What is the basis for such
336 difference? The dual control in the ectoderm could rely on a moderate expression of RhoGEF2
337 to avoid strong apical contractile forces and to maintain a more fluid-like medial-apical
338 meshwork facilitating junction remodeling⁴⁷ while preserving the cell apical surface area.
339 Therefore, a second RhoGEF (i.e., DpRhoGEF114), excluded from the cell apical-medial
340 region and specifically recruited at junctions, is necessary to provide the sufficient signaling
341 control for cell intercalation²⁸. Conversely, in the mesoderm, RhoGEF2 may be expressed at
342 higher levels to provide alone a sufficient activating signal for both cell shape and topological
343 changes.

344 We report that RhoGEF2 is planar cell polarized in the mesoderm tissue. How is
345 RhoGEF2 PCP achieved? We show that microtubule plus ends, that tightly regulate the
346 cortical distribution of RhoGEF2, contact the cell lateral cortex more often along cell sides
347 parallel to the DV axis. This supports a model where MTs deliver RhoGEF2 via EB1^{27,28,48}
348 preferentially along DV junctions. How is the MT plus-end PCP established? Plus-end PCP is
349 not the result of mesoderm cell anisotropic shape during tissue furrowing since reducing shape
350 anisotropy by laser ablation does not downregulate but rather enhances MyoII PCP. MT PCP
351 could instead result from a polarized stabilization of the EB1-RhoGEF2-T48 complex at the
352 cortex²⁷. Since the mesoderm share a similar genetic background as the bordering ectoderm,
353 further work is necessary to test if the factors controlling MyoII PCP in the ectoderm^{49,50} are
354 also acting in the mesoderm.

355 A recent study has reported that T48 contributes to regulate cellularization⁵¹. We now
356 show that T48 also plays a specific function in the formation of the two-tier actomyosin scaffold
357 at the onset of gastrulation. While T48 is overall unnecessary for the formation of the apical

358 actomyosin network⁴⁴, it is key for the establishment of the lateral tier. Our data corroborates
359 the notion that T48 is a cortical protein, yet future work is necessary to determine how T48 is
360 specifically distributed along the different cortical sides of mesoderm cells. In T48 mutant
361 embryos, mesoderm cells undergo bowtie intercalations. This aberrant T1 process, also
362 reported in bicoid, nanos and torso triple mutants⁸, is characterized by a stochastic distribution
363 of cell cross-sectional areas probably driven by an unsynchronized nuclear migration.
364 Concertina (the alpha-subunit of the GPCR protein Mist) is another known signaling factor
365 participating in RhoGEF2 localization²⁷ during early mesoderm morphogenesis⁴⁶. A renewed
366 effort is necessary to dissect the role of Concertina in the establishment of the two-tier
367 actomyosin scaffold.

368 Mesoderm morphogenesis, during the early phases of gastrulation, provides a
369 powerful paradigm to study simultaneous tissue folding and extension. Cell columnarisation,
370 apical constriction, nuclear basal migration and microtubule architecture remodeling have
371 been reported also during other vital processes (e.g., during neurulation⁵²) in which tissues
372 concomitantly fold and extend. Now, this study opens a new path to unravel the cellular
373 mechanisms underlying such complex tissue transformation.

374

375 **Acknowledgments**

376 We thank S. De Renzis, E. Wieschaus, S. Streichen, T. Lecuit, and Y. Bellaiche for providing
377 fly stocks; Y. Bellaiche, and all members of the Rauzi lab for critical reading of the manuscript;
378 A. John for initial support, A. B. Tanari for live injection support; B. Delorme for developing
379 ImageJ tools and Python support; S. Dmitrieff and F. Nédelec for support with the Cytosim
380 simulator; O. Thorn-Seshold for sharing the photoactivable drug for microtubule
381 depolymerization and support; S. Noselli, Y. Bellaiche, M. Théry and all members of the Rauzi
382 lab for the fruitful discussions; the PRISM imaging facility for technical support. NR was
383 supported by the scholarship MENRT and is at present supported by the FRM. This work was
384 supported by the French government through the UniCA^{JEDI} Investments for the Future project

385 managed by the National Research Agency (ANR-15-IDEX-01), the ATIP-Avenir program of
386 the CNRS, the Human Frontier Science Program (CDA00027/2017-C), the Region SUD PACA
387 Research and ERC Booster programs, the ANR PRC program (ANR-22-CE13-0024), the ANR
388 PRCI program (ANR-23-CE13-0042); support from the CNRS to the MITI 80 PRIME program
389 and support from Inserm to the Booster Program Mecacell3D.

390

391 **Author Contributions**

392 NR and MR planned the experiments. NR performed the experiments. MR performed initial
393 preliminary experiments. NR performed data processing and quantifications. NR and MR
394 analyzed the data. NR and MR wrote the manuscript.

395

396 **Declaration of Interests**

397 The authors declare no competing interests.

398

References

- 1 Heisenberg, C. P. & Bellaïche, Y. Forces in tissue morphogenesis and patterning. *Cell* 153, 948-962, doi:10.1016/j.cell.2013.05.008 (2013).
- 2 Lecuit, T. & Yap, A. S. E-cadherin junctions as active mechanical integrators in tissue dynamics. *Nat Cell Biol* 17, 533-539, doi:10.1038/ncb3136 (2015).
- 3 Salbreux, G., Charras, G. & Paluch, E. Actin cortex mechanics and cellular morphogenesis. *Trends Cell Biol* 22, 536-545, doi:10.1016/j.tcb.2012.07.001 (2012).
- 4 Roper, K. Microtubules enter centre stage for morphogenesis. *Philos Trans R Soc Lond B Biol Sci* 375, 20190557, doi:10.1098/rstb.2019.0557 (2020).
- 5 Pradeau-Phelut, L. & Etienne-Manneville, S. Cytoskeletal crosstalk: A focus on intermediate filaments. *Curr Opin Cell Biol* 87, 102325, doi:10.1016/j.ceb.2024.102325 (2024).
- 6 Gilmour, D., Rembold, M. & Leptin, M. From morphogen to morphogenesis and back. *Nature* 541, 311-320, doi:10.1038/nature21348 (2017).
- 7 John, A. & Rauzi, M. Composite morphogenesis during embryo development. *Semin Cell Dev Biol* 120, 119-132, doi:10.1016/j.semcdb.2021.06.007 (2021).

- 8 John, A. & Rauzi, M. A two-tier junctional mechanism drives simultaneous tissue folding and extension. *Dev Cell* 56, 1469-1483 e1465, doi:10.1016/j.devcel.2021.04.003 (2021).
- 9 Nishimura, T., Honda, H. & Takeichi, M. Planar cell polarity links axes of spatial dynamics in neural-tube closure. *Cell* 149, 1084-1097, doi:10.1016/j.cell.2012.04.021 (2012).
- 10 Sanchez-Corrales, Y. E., Blanchard, G. B. & Roper, K. Radially patterned cell behaviours during tube budding from an epithelium. *Elife* 7, doi:10.7554/eLife.35717 (2018).
- 11 Martin, A. C., Kaschube, M. & Wieschaus, E. F. Pulsed contractions of an actin-myosin network drive apical constriction. *Nature* 457, 495-499, doi:10.1038/nature07522 (2009).
- 12 Harris, T. J. & Peifer, M. Adherens junction-dependent and -independent steps in the establishment of epithelial cell polarity in *Drosophila*. *J Cell Biol* 167, 135-147, doi:10.1083/jcb.200406024 (2004).
- 13 Weng, M. & Wieschaus, E. Myosin-dependent remodeling of adherens junctions protects junctions from Snail-dependent disassembly. *J Cell Biol* 212, 219-229, doi:10.1083/jcb.201508056 (2016).
- 14 Salle, J. et al. Asymmetric division through a reduction of microtubule centering forces. *J Cell Biol* 218, 771-782, doi:10.1083/jcb.201807102 (2019).
- 15 Petrie, R. J., Koo, H. & Yamada, K. M. Generation of compartmentalized pressure by a nuclear piston governs cell motility in a 3D matrix. *Science* 345, 1062-1065, doi:10.1126/science.1256965 (2014).
- 16 Kam, Z., Minden, J. S., Agard, D. A., Sedat, J. W. & Leptin, M. *Drosophila* gastrulation: analysis of cell shape changes in living embryos by three-dimensional fluorescence microscopy. *Development* 112, 365-370, doi:10.1242/dev.112.2.365 (1991).
- 17 Leptin, M. & Grunewald, B. Cell shape changes during gastrulation in *Drosophila*. *Development* 110, 73-84, doi:10.1242/dev.110.1.73 (1990).
- 18 Kalukula, Y., Stephens, A. D., Lammerding, J. & Gabriele, S. Mechanics and functional consequences of nuclear deformations. *Nat Rev Mol Cell Bio* 23, 583-602, doi:10.1038/s41580-022-00480-z (2022).
- 19 Gundersen, G. G. & Worman, H. J. Nuclear positioning. *Cell* 152, 1376-1389, doi:10.1016/j.cell.2013.02.031 (2013).
- 20 Almonacid, M., Terret, M. E. & Verlhac, M. H. Nuclear positioning as an integrator of cell fate. *Curr Opin Cell Biol* 56, 122-129, doi:10.1016/j.ceb.2018.12.002 (2019).
- 21 Gelbart, M. A. et al. Volume conservation principle involved in cell lengthening and nucleus movement during tissue morphogenesis. *Proc Natl Acad Sci U S A* 109, 19298-19303, doi:10.1073/pnas.1205258109 (2012).
- 22 He, B., Doubrovinski, K., Polyakov, O. & Wieschaus, E. Apical constriction drives tissue-scale hydrodynamic flow to mediate cell elongation. *Nature* 508, 392-396, doi:10.1038/nature13070 (2014).
- 23 Rauzi, M. & Lenne, P. F. Probing cell mechanics with subcellular laser dissection of actomyosin networks in the early developing *Drosophila* embryo. *Methods Mol Biol* 1189, 209-218, doi:10.1007/978-1-4939-1164-6_14 (2015).
- 24 Izquierdo, E., Quinkler, T. & De Renzis, S. Guided morphogenesis through optogenetic activation of Rho signalling during early *Drosophila* embryogenesis. *Nat Commun* 9, 2366, doi:10.1038/s41467-018-04754-z (2018).
- 25 Krueger, D., Tardivo, P., Nguyen, C. & De Renzis, S. Downregulation of basal myosin-II is required for cell shape changes and tissue invagination. *EMBO J* 37, doi:10.15252/embj.2018100170 (2018).
- 26 Zhu, R., Antoku, S. & Gundersen, G. G. Centrifugal Displacement of Nuclei Reveals Multiple LINC Complex Mechanisms for Homeostatic Nuclear Positioning. *Curr Biol* 27, 3097-3110 e3095, doi:10.1016/j.cub.2017.08.073 (2017).

- 27 Rogers, S. L., Wiedemann, U., Hacker, U., Turck, C. & Vale, R. D. Drosophila RhoGEF2 associates with microtubule plus ends in an EB1-dependent manner. *Curr Biol* 14, 1827-1833, doi:10.1016/j.cub.2004.09.078 (2004).
- 28 De Las Bayonas, A. G., Philippe, J. M., Lellouch, A. C. & Lecuit, T. Distinct RhoGEFs Activate Apical and Junctional Contractility under Control of G Proteins during Epithelial Morphogenesis. *Current Biology* 29, 3370+, doi:10.1016/j.cub.2019.08.017 (2019).
- 29 Ko, C. S., Tserunyan, V. & Martin, A. C. Microtubules promote intercellular contractile force transmission during tissue folding. *J Cell Biol* 218, 2726-2742, doi:10.1083/jcb.201902011 (2019).
- 30 Almonacid, M., Terret, M. E. & Verlhac, M. H. Control of nucleus positioning in mouse oocytes. *Semin Cell Dev Biol* 82, 34-40, doi:10.1016/j.semcdb.2017.08.010 (2018).
- 31 Bertipaglia, C., Goncalves, J. C. & Vallee, R. B. Nuclear migration in mammalian brain development. *Semin Cell Dev Biol* 82, 57-66, doi:10.1016/j.semcdb.2017.11.033 (2018).
- 32 Meyer, E. J., Ikmi, A. & Gibson, M. C. Interkinetic nuclear migration is a broadly conserved feature of cell division in pseudostratified epithelia. *Curr Biol* 21, 485-491, doi:10.1016/j.cub.2011.02.002 (2011).
- 33 Ambrosini, A., Rayer, M., Monier, B. & Suzanne, M. Mechanical Function of the Nucleus in Force Generation during Epithelial Morphogenesis. *Dev Cell* 50, 197-211 e195, doi:10.1016/j.devcel.2019.05.027 (2019).
- 34 Miyazaki, A., Kato, K. H. & Nemoto, S. Role of microtubules and centrosomes in the eccentric relocation of the germinal vesicle upon meiosis reinitiation in sea-cucumber oocytes. *Dev Biol* 280, 237-247, doi:10.1016/j.ydbio.2005.01.026 (2005).
- 35 Tissot, N. et al. Distinct molecular cues ensure a robust microtubule-dependent nuclear positioning in the Drosophila oocyte. *Nat Commun* 8, 15168, doi:10.1038/ncomms15168 (2017).
- 36 McNally, K. L., Martin, J. L., Ellefson, M. & McNally, F. J. Kinesin-dependent transport results in polarized migration of the nucleus in oocytes and inward movement of yolk granules in meiotic embryos. *Dev Biol* 339, 126-140, doi:10.1016/j.ydbio.2009.12.021 (2010).
- 37 Tsai, J. W., Chen, Y., Kriegstein, A. R. & Vallee, R. B. LIS1 RNA interference blocks neural stem cell division, morphogenesis, and motility at multiple stages. *J Cell Biol* 170, 935-945, doi:10.1083/jcb.200505166 (2005).
- 38 Almonacid, M. et al. Active diffusion positions the nucleus in mouse oocytes. *Nat Cell Biol* 17, 470-479, doi:10.1038/ncb3131 (2015).
- 39 Deneke, V. E. et al. Self-Organized Nuclear Positioning Synchronizes the Cell Cycle in Drosophila Embryos. *Cell* 177, 925-941 e917, doi:10.1016/j.cell.2019.03.007 (2019).
- 40 Weng, M. & Wieschaus, E. Polarity protein Par3/Bazooka follows myosin-dependent junction repositioning. *Dev Biol* 422, 125-134, doi:10.1016/j.ydbio.2017.01.001 (2017).
- 41 Leptin, M. Twist and Snail as Positive and Negative Regulators during Drosophila Mesoderm Development. *Gene Dev* 5, 1568-1576, doi:DOI 10.1101/gad.5.9.1568 (1991).
- 42 Costa, M., Wilson, E. T. & Wieschaus, E. A putative cell signal encoded by the folded gastrulation gene coordinates cell shape changes during Drosophila gastrulation. *Cell* 76, 1075-1089, doi:10.1016/0092-8674(94)90384-0 (1994).
- 43 Fox, D. T. & Peifer, M. Abelson kinase (Abl) and RhoGEF2 regulate actin organization during cell constriction in Drosophila. *Development* 134, 567-578, doi:10.1242/dev.02748 (2007).
- 44 Kolsch, V., Seher, T., Fernandez-Ballester, G. J., Serrano, L. & Leptin, M. Control of Drosophila gastrulation by apical localization of adherens junctions and RhoGEF2. *Science* 315, 384-386, doi:10.1126/science.1134833 (2007).
- 45 Manning, A. J., Peters, K. A., Peifer, M. & Rogers, S. L. Regulation of Epithelial Morphogenesis by the G Protein-Coupled Receptor Mist and Its Ligand Fog. *Science Signaling* 6, doi:ARTN ra9810.1126/scisignal.2004427 (2013).

- 46 Kerridge, S. et al. Modular activation of Rho1 by GPCR signalling imparts polarized myosin II activation during morphogenesis. *Nature Cell Biology* 18, 261-+, doi:10.1038/ncb3302 (2016).
- 47 Rauzi, M., Lenne, P. F. & Lecuit, T. Planar polarized actomyosin contractile flows control epithelial junction remodelling. *Nature* 468, 1110-1114, doi:10.1038/nature09566 (2010).
- 48 Lin, B., Luo, J. & Lehmann, R. An AMPK phosphoregulated RhoGEF feedback loop tunes cortical flow-driven amoeboid migration in vivo. *Sci Adv* 8, eabo0323, doi:10.1126/sciadv.abo0323 (2022).
- 49 Paré, A. C. et al. A positional Toll receptor code directs convergent extension in (vol 515, pg 523, 2014). *Nature* 527, doi:10.1038/nature15719 (2015).
- 50 Karki, S. et al. Serotonin signaling regulates actomyosin contractility during morphogenesis in evolutionarily divergent lineages. *Nat Commun* 14, 5547, doi:10.1038/s41467-023-41178-w (2023).
- 51 Horo, U., Clarke, D. N. & Martin, A. C. *Drosophila* Fog/Cta and T48 pathways have overlapping and distinct contributions to mesoderm invagination. *Mol Biol Cell* 35, ar69, doi:10.1091/mbc.E24-02-0050 (2024).
- 52 Vijayraghavan, D. S. & Davidson, L. A. Mechanics of Neurulation: From Classical to Current Perspectives on the Physical Mechanics that Shape, Fold, and Form the Neural Tube. *Birth Defects Res* 109, 153-168, doi:10.1002/bdra.23557 (2017).

FIGURE LEGENDS

Figure 1. Nuclear migration precedes MyoII-LC formation. **a**, The prospective mesoderm simultaneously folds and extends at the onset of *Drosophila* gastrulation. Cross-section (left), surface view (top-right) and sagittal section (bottom-right). White arrowhead and dashed line indicate the furrow position. Scale bar, 50 μm . **b**, Sagittal view of mesoderm cells showing a two-tier organization of MyoII. Scale bar, 5 μm . **b'**, Time-lapse showing the lateral and apical pool of MyoII driving cell intercalation (top) and apical constriction (bottom), respectively. Scale bars, 5 μm . **c**, Time-lapse of the mesoderm cross-section during ventral furrowing. Arrowheads indicate MyoII-LCs. Scale bar, 10 μm . **d**, MyoII lateral intensity and nuclear position in function of time. Inset: temporal cross-correlation between the peak of nuclear migration speed and the peak of MyoII lateral recruitment. Apex-to-nucleus distance: distance between the apical side of the cell and the apical side of the nucleus (n=3 embryos, N=45 junctions, N= 30 nuclei). **e**, Mesoderm front view (left) and cross-section (right) time-lapse showing apical constriction and the associated nuclear displacement. Scale bars, 10 μm . **f**, Mean nuclear position in

function of the mean apical cell surface at different phases of mesoderm invagination. Inset: raw values with an exponential fit ($y = 69.212 * e^{-0.096x}$) (n= 5 embryos, N= 925 cells, N= 925 nuclei).

Figure 2. Constriction-induced cytoplasmic flow controls nuclear position and MyoII-LC formation. **a**, Mesoderm tissue upon laser dissection of the apical actomyosin network along two DV segments (dashed lines). Blue and red segments indicate control and cut cells, respectively. Scale bar, 10 μm . **b**, Schematic representation of cell shape, nuclear position and MyoII distribution in the control (blue) and cut (red) region. Cross: dissection of the apical actomyosin network. Arrowheads: apical contraction forces. **c**, Front view at 10 μm from the apical side and sagittal section of the mesoderm at the onset of and 7 minutes into gastrulation. Crosses indicate the sites of ablation. Arrowheads indicate MyoII-LCs. Scale bar, 10 μm . **c'**, Magnified views of MyoII-LC distribution in the control (1) and cut (2) region. Scale bars, 5 μm . **d**, Nuclear position in the control (blue) and cut (red) region and in control embryos (grey) devoid of laser dissection. Apex-to-nucleus distance corresponds to the distance between the apical side of the cell and the apical side of the nucleus (n= 6 embryos, N= 90 nuclei). **e**, MyoII intensity at 10 μm from the apical side at the onset of and 7 minutes into gastrulation in the region where nuclei fail to migrate as a result of apical laser ablation, in the control region and in control embryos (n=6 embryos, N= 88 junctions). **f**, Cytoplasmic flow along the cell apical-basal axis in cut and control cells in function of changes in apical cell surface (n=5 embryos, N= 24 beads, N= 24 cells).

Figure 3. The position of the nucleus dictates MyoII-LC apicobasal location. **a**, Sagittal view of mesoderm cells showing MyoII-LC (white arrowhead) and the two corresponding nuclei. Dashed line highlights the cell outline. Scale bar, 5 μm . **a'**, Top: Schematic representation of two cell sharing a MyoII-LC. Bottom: schematic representation of the initiation of a cell intercalation event (A is anterior, P posterior, D dorsal and V ventral). **b**, Quantification of MyoII-to-nuclei relative position (as described by the inset formula) in different conditions (refer to **a'**). Right axis: associated standard deviation for each condition (n=5

embryos, N=50 clusters, N= 200 nuclei). **c**, Top: time-lapse showing the ablation of the apical actomyosin network over an extended portion of the mesoderm. Bottom: magnified views showing MyoII distribution in the control (left) and cut (right) region. Nuclei, that fail to migrate, are visible in black at 10 μm depth in the cut region. Arrowheads indicate MyoII-LCs. Scale bars, 10 μm . **d**, Schematic representation of the centrifugation protocol employed to drive enhanced nuclear basal migration (see Supplementary Methods). **e**, Mesoderm front view at 15 μm depth and cross-section in centrifuged (top) and control (bottom) embryos. Arrowheads indicate MyoII-LCs. Cross-sections show nuclei in cyan and MyoII in purple. Scale bars, 10 μm . **f**, Apico-basal distribution of MyoII-LCs in embryos undergoing reduced nuclear migration (blue), control embryos (grey) and centrifuged embryos (purple). Inset shows the cumulative density relative to the apico-basal position of MyoII-LCs (n=12 embryos, N= 565 clusters). **g**, MyoII-LC apico-basal position relative to the average AP nuclear position (refer to a'). Apex-to-nucleus distance corresponds to the distance between the apical side of the cell and the apical side of the nucleus. Inset: quantification of MyoII-to-nuclei relative position for each individual cluster-nuclei pair (n=16 embryos, N=140 clusters, N= 280 nuclei).

Figure 4. Nuclear-dependent MT redistribution controls lateral RhoGEF2 recruitment. **a**, Sagittal view of mesoderm cells showing EB1 distribution along the cell lateral cortex at the onset of (top) and 7 min into gastrulation (bottom). Scale bar, 10 μm . **b**, Cortical over cytoplasmic ratio of EB1 at the lateral cortex of mesoderm cells at the onset of and 7 min into gastrulation (n= 3 embryos, N= 29 cortices). **c**, Left: EB1 distribution at 10 μm depth before (top) and after (bottom) apical laser dissection (dashed line) and nuclear displacement. Right: magnified views of the control region (blue) and the region where nuclei relocate apically after ablation (red). Scale bars, 10 μm , 5 μm . **d**, EB1 intensity along the cell lateral cortex at 10 μm depth in the control (blue) and in the apical nuclear relocation (red) region (n= 5 embryos, N= 146 cells). **e**, 3D representation of the MT network by mathematical simulation with the nucleus located apically, basally and with MTOCs separated from the nucleus. **f**, Percentage of MT plus ends along the cell lateral cortex between the apical side and the nucleus (blue) and

between the nucleus and the basal side (red) in different conditions (refer to e). **g,h,i**, MT plus-end distribution along the cell lateral cortex in the three different conditions (refer to e). $n = 100$ simulations per condition. The blue and red areas indicate locations between the apical side of the cell and the nucleus and between the nucleus and the basal side of the cell, respectively (see inset). **j**, RhoGEF2 distribution in mesoderm cells at $10\ \mu\text{m}$ from the apical side upon live-injection of water (top) or Colcemid (bottom). Scale bar, $5\ \mu\text{m}$. **k**, Cortical over cytoplasmic ratios of RhoGEF2 in control embryos (water live-injected or water photo-activated) or upon MT disruption (Colcemid live-injection or SbTub4AP photo-activation with a $405\ \text{nm}$ laser) ($n = 12$ embryos, $N = 145$ cells). **l**, Mesoderm front view time-lapse at $10\ \mu\text{m}$ from the apical side showing MyoII distribution in WT (left) or T48 mutant (right) embryos. Scale bar, $10\ \mu\text{m}$. **m**, Normalized density of MyoII-LCs in WT or T48 mutant embryos ($n = 12$ embryos, $N = 2664$ cells).

Nuclear position controls the activity of cortical actomyosin networks powering simultaneous morphogenetic events

Nicolas Roby, Matteo Rauzi

University Côte d'Azur, CNRS, Inserm, iBV, Nice, France

SUPPLEMENTARY MATERIALS

SUPPLEMENTARY FIGURE LEGENDS

Supplementary Figure 1. MyoII and nucleus dynamics during mesoderm internalization. **a**, Mesoderm front view time-lapse showing MyoII distribution at the cell apical (top row) and lateral (middle row) side and nuclear migration (bottom row). Scale bar, 20 μm . **b**, Apical MyoII intensity and nuclear position in function of time ($n=3$ embryos, $N=45$ junctions, 30 nuclei). $T=0$ min indicates the onset of gastrulation. **c**, MyoII intensity rate at the cell apical (green) and lateral (red) cortex and rate of nuclear basal displacement (blue) in function of time ($n=3$ embryos, $N=45$ junctions, $N=30$ nuclei). $T=0$ min indicates the onset of gastrulation. **d**, Sagittal view of mesoderm cells showing the two-tiered organization of MyoII and the relative position of MyoII-LCs and nuclei. Scale bar, 10 μm .

Supplementary Figure 2. Inversion of nuclear migration disrupts previously established MyoII-LCs. **a**, Mesoderm tissue before and after apical dissection (dashed lines). Red and blue segments indicate cut and control cells, respectively. Scale bar, 10 μm . **b**, Changes in apical cell surface in control (blue) and cut (red) regions ($n=3$ embryos, $N=161$ cells). **c**, Z-projection of mesoderm cells injected with fluorescent beads to map subcellular cytoplasmic flow. Scale bar, 10 μm . **c'**, Sagittal images showing bead position before (green) and after (red) laser dissection in control (top) and cut (bottom) conditions (refer to the schematic representation). Dashed lines indicate the apical side of mesoderm cells. Scale bar, 5 μm . **d**, Mesoderm front view at 10 μm depth and sagittal section (bottom) showing nuclear position and MyoII distribution before and after laser ablation of the apical actomyosin network

(cross). Red and blue segments indicate cut and control cells, respectively. Insets show magnified views of MyoII distribution in the region where nuclei relocate apically after ablation of the apical actomyosin network. Scale bars, 10 μm . **e**, Nuclear position in control (blue) and cut (red) regions. Apex-to-nucleus distance corresponds to the distance between the apical side of the cell and the apical side of the nucleus (n= 3 embryos, n= 60 nuclei). **f**, Lateral MyoII intensity in the region where nuclei relocate apically as a result of apical laser ablation and in the control region (n= 3 embryos, N= 60 junctions). **g**, **g'**, Mesoderm front view showing lateral MyoII distribution upon laser dissection (**g**, dashed lines indicate the ablation regions performed at Z = 0 μm) or RhoGEF2 overexpression (**g'**). Scale bars, 10 μm . **h**, Mesoderm front view just before the onset of gastrulation showing MyoII distribution apically (top) and at 10 μm depth (bottom) before and after apical laser dissection (dashed lines). Red and blue segments indicate cut and control regions, respectively. Scale bar, 15 μm . **i**, Changes in MyoII intensity apically and 10 μm from the apical side upon apical laser dissection in control (blue) and cut (red) regions (n= 3 embryos, N=18 region).

Supplementary Figure 3. Optogenetic inhibition of nuclear migration abolishes MyoII-LCs. **a**, Schematic representation of the CRY2-CIBN optogenetic tool for photo-recruitment of RhoGEF2. **b**, Schematic representation of control (top) and basally-constricted cells upon RhoGEF2 basal photo-recruitment and MyoII basal accumulation (bottom). **c**, Mesoderm front view upon two-photon recruitment of RhoGEF2 (green dashed rectangle) resulting in basal accumulation of MyoII and ectopic constriction. Scale bar, 20 μm . **d**, Mesoderm front view at 10 μm depth and sagittal view upon photo-induced basal constriction. Green dashed rectangle indicates the x-y position of the photo-activated area performed in the basal region at 28 μm depth. Blue and green segments indicate control and activated regions, respectively. Scale bar, 10 μm . **e**, Nuclear position in control (blue) and photo-activated (green) regions. Apex-to-nucleus distance corresponds to the distance between the apical side of the cell and the apical side of the nucleus (n= 5 embryos, N= 200 nuclei). **f**, MyoII intensity at 10 μm from the apical side before and after basal photo-activation in the control and photo-activated region (n=5 embryos, N= 141 junctions).

Supplementary Figure 4. Delayed nuclear migration shifts MyoII-LCs towards the apical region. **a**, Schematic representation of delayed apical-constriction (resulting from laser dissection and repair of the apical actomyosin network) leading to a delay in nuclear basal migration. **b**, Mesoderm front view time-lapse showing control (gray segment) and delayed (blue segment) region. Scale bar, 10 μm . **c**, MyoII distribution in the control (grey) and delayed (blue) region at different apical-basal positions. Arrowheads indicate MyoII-LCs. Scale bar, 5 μm . **d**, Nuclear position in the control (grey) and delayed (blue) region (n= 3 embryos, N= 126 nuclei). **e**, Quantification of MyoII-LC apico-basal position in the control (grey) and delayed (blue) region (n=3 embryos, 52 junctions).

Supplementary Figure 5. Embryo centrifugation enhances nuclear basal migration and leads to a basal shift of MyoII-LCs. **a**, MyoII distribution in control (top) or centrifuged (bottom) embryos at different apicobasal positions. Scale bars, 15 μm . **b**, Mesoderm front view in a centrifuged embryo at the onset of (top) or 7 minutes into (bottom) gastrulation at different depths. **b'**, Magnified views showing nuclear enhanced basal position and subsequent MyoII-LC deep recruitment. Yellow arrowheads indicate MyoII-LCs. Scale bars, 20 and 10 μm .

Supplementary Figure 6. RhoGEF2 opto-recruitment recapitulates MyoII isotropic coalescence. **a**, RhoGEF2 distribution shown over a mesoderm cell sagittal section. Orange arrowheads indicate RhoGEF2 recruitment on the cell lateral cortex and at the MTOCs. Scale bar, 5 μm . **a'**, Top: Schematic representation of RhoGEF2 distribution at centrosome and lateral cortices. Black dotted line indicates the plane of imaging for bottom image. Bottom: Front view view of a mesoderm cell showing RhoGEF2 enrichment at MTOCs Scale bar, 2.5 μm . **b**, Schematic representation of MyoII isotropic coalescence upon RhoGEF2 opto-recruitment (orange dashed rectangle). Black dashed line represents the expected final position of the MyoII focus (i.e., half-way the activated region). **c**, Image sequence of a mesoderm cell sagittal view upon RhoGEF2 opto-recruitment (orange dashed rectangle). This results in MyoII accumulation and isotropic coalescence leading to the formation of a MyoII focus in the mid-position (dashed white line). **d**, MyoII intensity profile along the cell lateral

cortex upon RhoGEF2 opto-recruitment at different post-activation time points. Dashed line indicates the mid-position of the photo-activation region (n=6 embryos). Inset: relative position of the MyoII focus with respect to the activated region (n= 6 embryos). **e**, Optogenetic recruitment of MyoII along the lateral cortex at a depth where nuclei are located. Green dashed rectangle indicates the region of RhoGEF2 opto-recruitment. Scale bar, 5 μ m.

Supplementary Figure 7. Mesoderm cells do not display nuclear deformation during two-tier formation. **a**, Time-lapse showing mesoderm nuclei outlines. Scale bar, 5 μ m. **a'**, 3D segmentation of a representative mesoderm nucleus during the first 10 minutes of gastrulation. Scale bar, 2.5 μ m. **b**, Nucleus local curvature during the first 10 minutes of gastrulation (n= 5 embryos, N= 454 nuclei). Inset shows curvature analysis of a representative nucleus every 3 min. Scale bar, 2.5 μ m. **c**, Nucleus eccentricity measured from 3D segmented nuclei during the first 10 minutes of gastrulation (n= 5 embryos, N= 641 nuclei).

Supplementary Figure 8. *In silico* 3D model to probe the role of cell geometrical constraints on MT plus-end distribution. **a**, Z-projection of mesoderm cell MTOC before (top) and during (bottom) gastrulation. Scale bar, 10 μ m. Right: magnified views before (1) and during (2) gastrulation. Scale bar, 2.5 μ m. **b**, Centrosomal radius in mesoderm cells before and during gastrulation (n= 5 embryos, N= 2684 centrosomes). **c**, Inter-centrosomal distance in mesoderm cells before and during gastrulation (n=5 embryos, N= 390 cells). **d**, Time-lapse of a mesoderm cell sagittal view showing MTOCs and nuclei in constant proximity during nuclear migration. Scale bar, 5 μ m. **e**, Schematic representation of the numerically modelled cell and list of the tuned parameters. **f-k**, Distribution of cortical MT plus-ends upon modulation of geometrical constraints such as nucleus radius (**k**), distance between centrosomes (**l**), distance between nucleus and centrosomes (**m**) or microtubule properties such as growing speed (**n**), shrinking speed (**o**) and total number of polymers (**p**) (n= 25 simulations per condition).

Supplementary Figure 9. Pharmacological approaches to disrupt MT with spatio-temporal precision and inhibit MyoII-LCs. **a**, EB1 z-projection in mesoderm cells for embryos injected with water (top) or Colcemid (bottom). Arrowheads indicate centrosomes enriched with MT plus ends. Scale bars, 10 μm . **b**, Centrosomin distribution in mesoderm cells in water and Colcemid injected embryos. Scale bar, 10 μm . **c**, Time-lapse of the mesoderm tissue z-projection showing MT organization in embryos live injected with Dextran+water (left) or Dextran+Colcemid (right). Yellow dashed line indicates the extent of drug diffusion at a given time and the associated MT disruption. Scale bars, 10 μm . **d**, Time-lapse of mesoderm cells showing progressive MT depolymerization upon photo-activation of the MT disrupting drug SbTub4-AP. Arrowheads indicate MT plus ends (comets). Scale bar: 5 μm . **e**, Quantification of MT plus-end intensity upon photo-activation of SbTub4-AP (n= 4 embryos, N= 11 regions). **f**, Mesoderm tissue at 10 μm depth showing MyoII in water (top) or Colcemid (bottom) injected embryos. Yellow arrows indicate MyoII-LCs. Scale bar, 10 μm . **g**, RhoGEF2 distribution in mesoderm cells at 10 μm from the cell apical surface in water injected embryos (top) or upon photo-activation of the photo-switchable MT depolymerizing drug SbTub4AP. Scale bar, 5 μm .

Supplementary Figure 10. The role of MT and T48 in the formation of the second tier. **a**, Segmentation and quantification of mesoderm cell surface area in embryos injected with water (top) or with the MT-depolymerizing agent Colcemid (bottom) prior to the onset of gastrulation. Scale bar, 10 μm . **a'**, Distribution of mesoderm apical cell surfaces at the onset of gastrulation (T= 0 min) and 7 min into gastrulation in water (top) and Colcemid (bottom) injected embryos (n=13 embryos, N=975 cells). Dashed line indicate mean area. **b**, Apical cell surfaces of mesoderm cells upon different pharmacological treatments at the onset of gastrulation and 7 min into gastrulation (n=29 embryos, N= 2648 cells). **c**, Apical cell surfaces and associated nuclear positioning in water and Colcemid injected embryos at the onset of and 7 min into gastrulation (n=12 embryos, N= 240 cells, N= 240 nuclei). **d**, Mesoderm front view showing RhoGEF2 distribution at 10 μm from the apical surface. Scale bar, 10 μm . **d'**, Orientation with

respect to the AP axis of cells sides that are highly enriched in RhoGEF2 at 10 μm depth (n=3 embryos, N= 30 junctions). **e**, Time-lapse showing EB1 distribution during cell intercalation at 10 μm depth (A is anterior, P posterior, D dorsal and V ventral). Scale bar, 5 μm . **f**, EB1 cumulative intensity rate for different cell sides and intercalation events at 10 μm from the apical surface. AP and DV sides, indicate sides parallel to the anterior-posterior and dorsal-ventral axis, respectively (n=6 embryos, 86 junctions). **g**, Representative EB1 enrichment at cell lateral cortices in function of time for different side types (n=1 embryo, N= 15 junctions). **h**, Mesoderm front view, sagittal and cross-section showing T48 distribution at different apicobasal positions. Scale bar, 20 μm . **h'**, Scheme showing T48-dependent cortical anchoring of RhoGEF2 to induce local actomyosin contractility. **i**, Cell intercalation of mesoderm cells in WT (top) and T48 mutant (bottom) embryos. Yellow dashed lines outline cell contours. Scale bars, 5 μm .

METHODS

Fly stocks and genetics

Drosophila stocks used for live imaging were: Membrane-GFP (Resille::GFP, Spider::GFP), myosin-mCherry (Sqh::mCherry), membrane-mCherry (GAP43::mCherry), centrosome-GFP (cnn::GFP), nuclei-GFP (Ubi::Gfp::nls). UASp EB1::GFP, UASp tubulin::mCherry, UASp T48::GFP were driven maternally by one copy of (67C) *mat α Tub-Gal4VP16* driver. T48 mutant embryos were collected from homozygous T48-, Spider::GFP/T48-, Spider::GFP parents. For optogenetic modulation of basal cell surface, embryos were collected from *ubi:Gap43::mCherry/+; UASp Cry2::RhoGEF2/+; UASp CIBN::pmGFP/osk Gal4* mothers. For photoactivation of MyoII localization, embryos were collected from *Sqh::mCherry/ UASp*

Cry2::RhoGEF2; UASp CIBN::pmGFP/osk Gal4 mothers. The complete list of stocks and genetics is available in Table.1.

***Drosophila* embryo preparation**

Cages containing male and virgin *Drosophilae* of selected genotypes were established one day prior to imaging and were maintained at 18°C. Subsequently, the cages were shifted to 25°C for egg laying. Cages were changed every 3 hours to precisely time embryo development with the onset of *Drosophila* gastrulation. For optogenetic experiments, cages were kept at a temperature of 20°C. Freshly laid embryos were collected on 1% agar plates placed within Petri dishes. To remove the chorion, embryos were briefly exposed to a 50% bleach solution for 30 seconds. Following this treatment, embryos were thoroughly rinsed with distilled water and transferred on agar for mounting.

Sample mounting

For confocal and spinning-disk microscopy, *Drosophila* embryos were collected using a custom-made needle and carefully oriented in water on MatTek dishes with a 0.17mm coverslip bottom. For light-sheet imaging, embryos were mounted within a glass capillary filled with a 0.5% Gelrite solution, ensuring their long axis was parallel to the capillary.

Confocal microscopy

Embryos were imaged using two distinct confocal microscopes. The Zeiss LSM 880 AiryScan was employed to achieve high-resolution imaging for subcellular structures, utilizing a 40X objective with a numerical aperture (NA) of 1.1. For laser dissection, optogenetic experiments, and live injection experiments, the Zeiss LSM 780 was utilized, equipped with a 40X objective (1.2 NA). Appropriate filter sets for fluorescent channels were used for each experiment. When Z-stacks were performed, they were acquired using a Piezo stage with a step size of either 1, 2 or 5 μm , depending on the need for different temporal resolutions. For rapid Z-stack imaging, a Nikon TI2-Eclipse spinning disk microscope with a Nikon 60X objective (1.1 NA) was used.

Light-Sheet microscopy (In Toto 4D Imaging)

In toto 4D imaging of *Drosophila* embryos was conducted using the Luxendo MuviSPIM selective-plane illumination light-sheet microscope. This instrument was equipped with a 20X objective featuring a numerical aperture of 1.0. Additionally, a 1.5X lens was incorporated into the optical path. Z-stacks were acquired with a step size of 1 μm . During each acquisition, embryos were imaged from two opposing orthogonal views, capturing both a 0° dorsal-ventral view and a 90° lateral view. This approach resulted in the acquisition of four 3D stacks for

every individual time point. The fusion of these four stacks was performed using Matlab 4, resulting in a final isotropic pixel resolution of 0.29 μm .

Actomyosin meshwork laser dissection

A femtosecond-pulsed infrared laser (IR fs, MaiTai) integrated with a Zeiss LSM 780 NLO confocal microscope, tuned to a wavelength of 950 nm, was employed for ablating the apical actomyosin meshwork. Experiments were conducted using a 40X objective with 1.2 NA. The Zeiss Zen software was configured with bleach mode (110 mW laser power at the focal plane, single iteration, 2.15 μs pixel dwell time and 1s frame rate). To investigate the modulation of apical cell surface constriction and nuclear positioning, single ablations were exclusively conducted in the dorso-ventral axis of the mesoderm tissue. In cases where ablations were performed prematurely, they were repeated at the appropriate developmental timing to observe the intended effects. For experiments aimed at delaying furrow invagination, a grid pattern of iterative ablations targeting the apical actomyosin network was employed to reduce anisotropic tearing and moderate tear amplitude. Ablations were performed each time the network showed signs of recovery to hinder the restoration of the actomyosin network and further delay constriction in the cut region.

Optogenetic recruitment of RhoGEF2

Cry2 optogenetic experiments were carried out on Zeiss 780 LSM confocal microscope with a 40X 1.2 NA objective, using bleach mode on Zeiss Zen software, with 2-P MaiTai tunable laser. Photo-recruitment of RhoGEF2 was achieved by line or rectangular activation on cortex using 950nm, 18 mW laser power at the focal point, 40 iterations, 3.5 μs pixel dwell.

***Drosophila* micro-injections**

Dechorionated embryos were dried using silica beads for 7-10 minutes, then mounted on heptane glue-coated coverslips in halocarbon oil before microinjection. Microinjection was conducted using micro-needles prepared by a Narishige vertical puller, using borosilicate glass capillaries with filament. Microinjections were executed using an Eppendorf FemtoJet micro-injector. Embryos were injected until they had re-expanded to their original volume from the desiccated state. For the inhibition of MyoII activity, embryos were microinjected laterally with Y-27632, prepared from stock solutions in water with concentrations of 10, 25, or 50 mM. Microtubule depolymerization was achieved by injecting embryos with 2.5 mM Colcemid diluted in water. Control experiments were conducted by injecting water into the embryos. To photo-induce microtubule depolymerization, embryos were injected with 5 mM SBTub-4AP, while being maintained in darkness, then illuminated with a 405 nm laser (3.15 μs pixel dwell time, 10 iterations) at specific time points of interest. For assessment of cytoplasmic flow,

fluorescent beads with a diameter of 1 μm (FluoSphere) were diluted in water at a 1:4 ratio and ventro-laterally injected into embryos. All injections were performed at the late cellularization stage, which was confirmed by monitoring the depth of cellularization front within a range of 25-30 μm .

***Drosophila* embryo centrifugation**

Drosophila embryos were subjected to centrifugation using an Eppendorf Centrifuge 5430R equipped with a swing-bucket rotor to achieve fully-orthogonal force application. Embryos at late cellularization stage were collected, mounted ventral side up on coverslips and loaded onto custom 3D-printed Eppendorf. Centrifugation conditions, such as speed and duration were optimized to achieve nuclear apicobasal displacement while preserving embryo early gastrulation. Final settings used in the study were: 6000 x g/rcf for a duration of 2 min. After centrifugation, embryos were retrieved, mounted in water on MatTek dishes as previously described for microscopy live-imaging.

***In silico* 3D modelling of microtubule architecture**

CytoSIM computational software was employed to simulate microtubule dynamics. Detailed three-dimensional representations of a cell and microtubules took into account parameters described in configuration files (see Supplementary Data). Parameters were estimated using experimental measurements when possible and configured to replicate specific biological contexts. Unknown parameters were varied to assess their weight in the proposed model. A custom-made python script was used to extract and sort cortical MT distribution. You can find more info on CytoSIM official repository <https://gitlab.com/f-nedelec/cytosim>.

2D and 3D segmentation of cells and nuclei

2D segmentations of apical cell surfaces in drug injection and ablation contexts were carried out using respectively ASTEC and IMARIS software by analysing individual optical sections of the acquired membrane images with watershed segmentation. 3D segmentation of nuclei was achieved through volume rendering and initial automated thresholding using nuclear fluorescent signal. Segmentation parameters and thresholds were then optimized to capture cellular and nuclear details. All segmented data were sorted and analysed using a custom-made Python script and R software.

Statistics

Statistical analyses were conducted using GraphPad Prism and R software. Descriptive statistics, which include means and standard deviations, were calculated for all relevant data. The normality of each dataset was tested using the Shapiro-Wilk test. Appropriate statistical

tests were selected and described for each experiment in Supplementary Table 2. A threshold p-value of 0.05 was employed to determine statistical significance. The 95% confidence intervals were visually represented on data plots.

Image analyses and quantifications

Cell area and nuclear positioning measurements

Changes in cell surface and nuclear position were monitored throughout the internalization of the mesoderm by recording time-lapse movies at different intervals, with a depth of 35 μm (Z step = 1 μm). Temporal realignment of embryos was achieved by using the onset of apical constrictions as the reference point, designated as $t = 0$ min. The apex-to-nucleus distance was computed by measuring the Z position of the apical side of the nucleus within each cell and then subtracting the Z position of the apical surface. Manual monitoring was employed to establish the association between each cell surface and its corresponding nucleus.

Nuclear migration and MyoII intensity measurements

To quantify nuclear migration and MyoII lateral intensity, time points were re-stacked to maintain consistency in the invaginating furrow position across all frames. To do so, progression of furrow invagination was monitored over time and black planes were added to the front and back of the image stacks to match the depth of the furrow tip. Apex-to-nucleus distance and lateral MyoII intensity were evaluated in the middle portion of the mesoderm, which exhibited sufficient flatness for analysis. Embryos were temporally aligned by using initial appearance of apical MyoII clusters as the reference point for the onset of gastrulation ($t = 0$ min). Randomly chosen nuclei were tracked throughout gastrulation, spanning 30 time points ($\Delta T = 22$ sec), to establish the migration curve. MyoII lateral intensity was determined by Z-projecting image slices between 8 and 12 μm from the apical side after re-stacking, capturing lateral MyoII signal during mesoderm internalization. Randomly selected junctions were then monitored throughout mesoderm internalization. Apical MyoII intensity was measured using large regions of interest (ROIs) encompassing the mesoderm tissue, from the end of cellularization (identified by the position of the cellularization front) until the furrow reached a depth where tracking became impractical. MyoII accumulation and the rate of nuclear migration were obtained by computing the first derivative of the MyoII intensity and nuclear migration curves, respectively. Further analysis involved cross-correlation between the peak rate of nuclear migration and the peak of lateral MyoII accumulation to estimate the lag time between nuclear migration and the appearance of lateral MyoII clusters.

Nuclear positioning and lateral MyoII intensity measurements in embryos with compromised nuclear migration

Time-lapse movies with a depth of 30 μm (z-step = 2 μm) were examined to track nuclear positioning and MyoII distribution following apical laser dissection and opto-induced inhibition of nuclear migration. Lateral MyoII intensity was assessed in both control and cut/opto regions using the line measurement tool in ImageJ, positioned 10 μm from the apical side. Special care was taken to exclude low nuclear signal to prevent intensity bias in the cut region. The apex-to-nucleus distance was determined by measuring the distance between the apical side of the nucleus and the apical side of the cell. To facilitate comparison between control embryos and ablated embryos (comprising both control and cut regions), gastrulation was timed and Z-stacks in control and ablated embryos were temporally synchronized for analysis specifically 7 minutes after the onset of gastrulation.

Apicobasal flow velocity and apical cell surface ratio measurements

Time-lapse movies with a depth of 35 μm (z-step = 2 μm) were analysed to follow apical cell surface changes and fluorescent bead apicobasal displacement. Prior to and post apical laser dissection, the Z-position of fluorescent beads was measured in both control and ablated regions. Given the tissue invagination during this period, adjustments were made to each bead's Z-position by subtracting the apical surface Z-position at each time point. Bead apicobasal displacement was determined by calculating the difference in Z-position between beads before and after laser dissection. Flow velocity was subsequently obtained by dividing this displacement by the time delay between the two measured time points. Similarly, the apical surfaces of cells containing beads were subjected to 2D segmentation before and after apical laser dissection at corresponding time points. To quantify changes, the apical cell surface ratio was computed by dividing the tracked cell surface after laser dissection by the respective surface before laser dissection.

Apical laser dissection effect on MyoII fluorescence intensity

To mitigate the possibility of signal loss attributed to the application of femtosecond IR laser pulses at the apical region, MyoII fluorescence intensity measurements were taken before and after apical laser dissection in both control and cut regions at different positions: the apical side and at a distance of 10 μm from the apical side. Intensity ratios were then calculated by dividing the fluorescence intensity after laser dissection by the intensity measured before laser dissection.

MyoII apicobasal position measurements

Time points were restacked to account for progressive invagination of the mesoderm tissue. Furrow invagination was monitored over time and black planes were added to the front and back of the stacks accordingly, corresponding to the distance invaginated by the furrow tip. By navigating time-lapse movies of mesoderm invagination, MyoII apicobasal position was determined using time points at which MyoII appeared most coalesced on reconstructed sagittal sections, corresponding to final cluster establishment on the apicobasal axis. Measurements were performed in control, centrifuged and grid-pattern ablated embryos when the furrow reached a depth of 5 μm .

MyoII-to-nuclei relative position measurements

Myosin apicobasal position was determined as it is most focused and initiates cell intercalation processes (four-way junction formation). In control and centrifuged embryos, cell intercalations were identified by screening time-lapse movies during the initial 15 minutes of gastrulation. Reference points for intercalation apicobasal position were established using newly formed four-way junctions enriched in MyoII, which coalesced on the apicobasal axis. In centrifuged embryos, lateral MyoII position analysis focused on nuclei sets with enhanced displacement to account for heterogeneity of nuclear repositioning. In delayed (grid-patterned ablation) embryos, iterative apical laser dissections did not allow for continuous junction monitoring. To standardize measurements, lateral MyoII Z-positions in control, centrifuged, and delayed embryos were realigned relative to the apical Z-position of mesoderm cells. Nuclear positioning was determined by measuring the apex-to-nucleus distance for adjacent nuclei along the anterior-posterior (AP) axis that shared a MyoII-enriched lateral junction. Ratios were calculated by dividing the apicobasal position of lateral MyoII clusters by the average apex-to-nucleus distance of the two adjacent AP nuclei.

Nucleus morphology changes

Nucleus curvature was measured on mesoderm nuclei at different time points of gastrulation using Z-projected mid-sections of nuclear contours, obtained from computed edges from nuclear signal. Semi-automated curvature analysis was performed using ImageJ Kappa plugin and B-spline curve fitting. Nucleus prolate eccentricity was measured by 3D segmentation of mesoderm nuclei using IMARIS software at different time points of gastrulation.

EB1 intensity measurements

EB1 intensity dynamics were tracked throughout gastrulation via sagittal sections of the mesoderm tissue. Embryos were temporally synchronized, and measurements were performed both at the onset (marked by the initial recruitment of apical MyoII) and 7 minutes into gastrulation. Using the line measurement tool in ImageJ, EB1 cortical intensity along the

lateral cortex (2 to 15 μm) was quantified. Concurrently, associated cytoplasmic signal within the same region was measured, excluding nuclear signal from the region of interest (ROI) to prevent intensity bias, particularly in the first time point. Ratios were computed by dividing cortical measurements by corresponding cytoplasmic measurements. In laser-dissected embryos, lateral EB1 intensity was assessed in *en face* sections of the mesoderm tissue at 10 μm from the apical surface. EB1 signal was not normalized to cytoplasmic intensity due to the presence of nuclei occupying that space in the cut regions, which could bias ratios towards higher values. Background subtraction was conducted by utilizing three regions of interest (ROIs) per embryo to determine the average background signal. It was observed that both EB1 density and intensity decreased in the cut region, indicating that the loss of EB1 signal did not arise from a more diffuse signal as cells expanded their perimeter.

EB1 comets density upon photo-induced MT depolymerization

The density of EB1 comets was assessed upon photo-induced MT depolymerization. For every embryo, three random regions of interest were chosen, and comet counts were measured for each region across time points subsequent to MT depolymerization. To establish EB1 comet density, comet counts were standardized based on the area of the analyzed region of interest. Comets that remained partially attached to the centrosomes/MTOC were excluded from the comet count.

EB1 dynamic distribution relative to junction orientation

Mesoderm tissue dynamics during gastrulation were captured from front views with high temporal resolution ($\Delta T = 0.73$ sec). Imaging was conducted on a single stack positioned 12 μm from the apical side, enabling prolonged tracking of the lateral cortex of mesoderm cells as the tissue underwent invagination. Membrane signal served as a reference for identifying intercalation events and guiding the blind measurement of EB1 signal. EB1 fluorescence intensity was quantified at junctions aligned along the anterior-posterior axis, dorsal-ventral (DV) axis, and DV axis during intercalation. Signal integration over time was normalized by the total measurement duration. To address embryo-to-embryo variation, background normalization was executed using the average background signal derived from three distinct regions for each embryo.

RhoGEF2 intensity measurements

RhoGEF2 signal dynamics were examined following microtubule disruption through either the live-injection of the depolymerizing agent Colcemid or timed photo-induced depolymerization using the prodrug SbTub4AP. Front view single optical sections of mesoderm cells were captured at a depth of 12 μm from the apical side and tracked over time ($\Delta T = 3.5$ sec).

Junctional and cytoplasmic levels of RhoGEF2 were quantified using both line and segmented area tools in ImageJ, at the last time point before activation and several frames thereafter ($\Delta T = 14$ sec). Cortical to cytoplasmic ratios were computed by dividing the measurements obtained from these two regions. Cells exhibiting pronounced expansion of cell area and nuclear movement towards the apical side induced by MT depolymerization were excluded from analysis. Upon significant loss of RhoGEF2 junctional signal or an increase in cytoplasmic signal, certain cell boundaries became indistinguishable and analysis relied on the restoration of the region of interest (ROI) selection between the first and second frames analyzed. Control analysis was conducted using the same protocol and similar time points in embryos either live-injected with water or injected with water during late cellularization then subjected to UV photo-activation (settings equivalent to those applied in SbTub4AP embryos).

RhoGEF2 PCP distribution

RhoGEF2 distribution was monitored along front view optical sections of the mesoderm tissue, positioned 12 μm from the apical side, during gastrulation. Upon detecting an elevation in RhoGEF2 cortical signal within mesoderm cells, the orientation of RhoGEF2-enriched junctions was assessed relative to the anterior-posterior (AP) axis, using the membrane reporter as a reference to precisely determine junction orientation.

Apical cell surface modulation upon pharmacological MT depolymerization or ROCK inhibition

To assess apical cell surface modulation following pharmacological treatments, the segmentation of mesoderm cell apical surfaces was performed throughout gastrulation, following previously described segmentation methods. For each embryo, a region of interest encompassing the mesoderm tissue was defined in the frame corresponding to 7 minutes after the initiation of gastrulation. Analysis included only cells whose centroids fell within this defined region and could be consistently tracked in each frame throughout gastrulation. The datasets presented here depict the distribution of apical cell surfaces at two specific time points: at the onset of gastrulation and 7 minutes into gastrulation.

Apical cell surface and associated nuclear positioning upon MT depolymerization

To allow efficient tracking of changes in apical cell surfaces with adequate temporal resolution, only the most apical Z positions of the tissue were captured (with a total depth of 12 μm from the apical surface). Consequently, nuclei that were highly displaced could not be effectively monitored. To address this limitation, three categories of nuclear displacement were established: apical nuclei (0-5 μm), intermediate nuclei (5-10 μm), and displaced nuclei (>10 μm). Nuclear position was quantified as the apex-to-nucleus distance (restacked accordingly)

to the position of the apical cell surface). For each time point in both water and Colcemid-injected embryos, randomly selected nuclei were paired with their respective apical cell surfaces. These surfaces were segmented using the polygon area tool in ImageJ.

Lateral MyoII density in control and T48 mutant backgrounds

MyoII signal dynamics were tracked over front view Z-stacks of the mesoderm tissue (total depth = 35 μm) throughout gastrulation. To maintain consistency with the invaginating furrow, each frame was spatially restacked relative to the apical position of the furrow tip, incorporating black planes either above or below the stack. This ensured the tracking of the same plane relative to the apical surface over time. Following spatial restacking, a region of interest (ROI) was defined within the mesoderm tissue, spanning the cells closest to the ventral midline. Z positions ranging from 8 to 12 μm were subjected to maximum Z-projection, resulting in a movie tracking this portion of the lateral cortex over time. MyoII lateral clusters were then enumerated during the first 10 minutes of gastrulation ($t = 0$ min corresponding to the initial accumulation of apical MyoII). A cluster was characterized as a coalesced high-intensity MyoII signal. Clusters were counted only once, even if the same junction was subsequently enriched again in MyoII at a later time point. The total number of cells within the defined ROI was then quantified for each embryo, and the count of MyoII clusters was normalized by the number of cells to derive the average density of lateral MyoII per embryo.

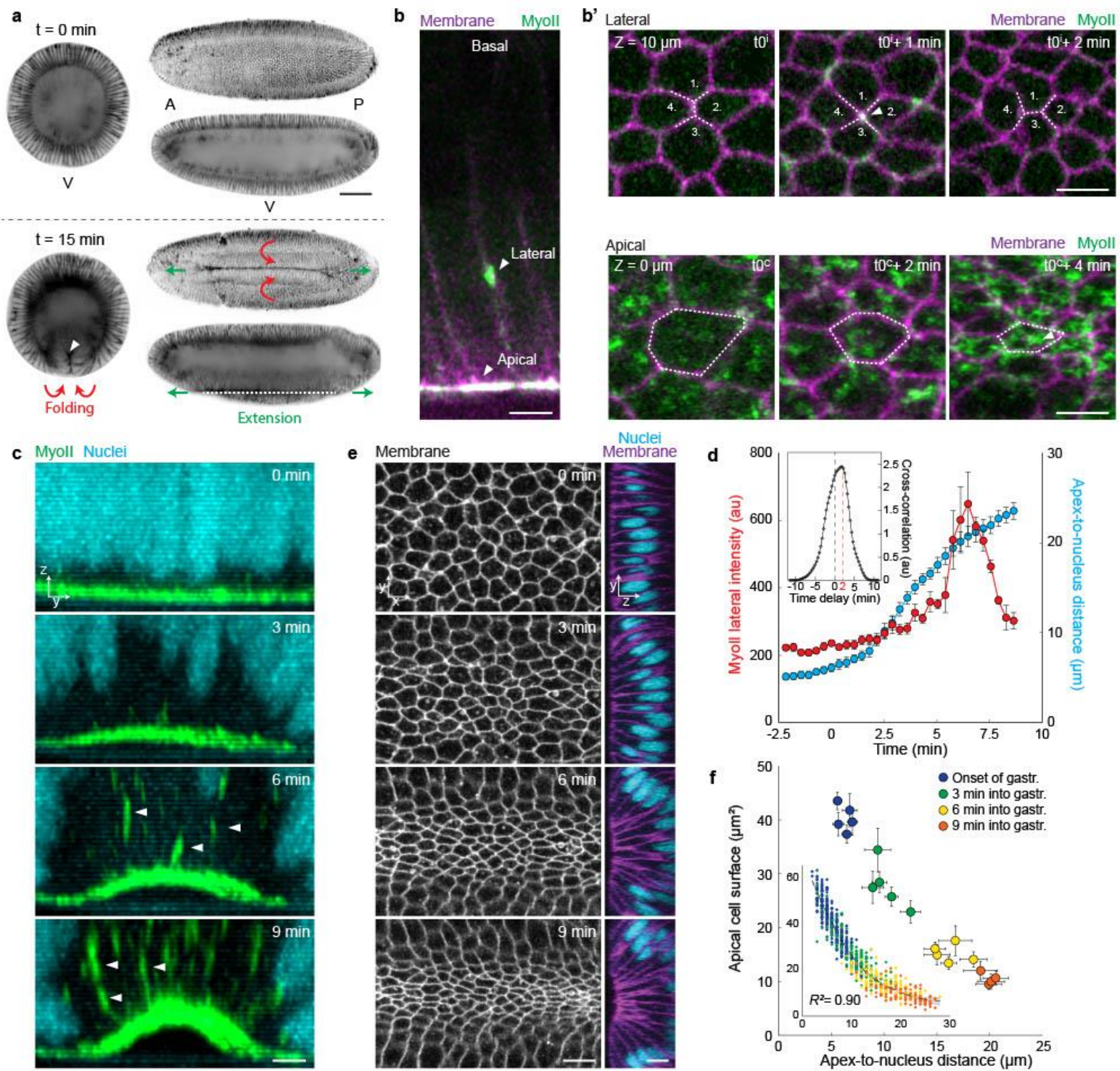
Cortical MT plus-ends apicobasal distribution from 3D in silico CytoSIM model

Boundary conditions, including cell length, cell radius, nucleus radius, nucleus-to-membrane spacing, centrosome radius, and inter-centrosomal distance, were measured *in vivo* to establish a template for the *in silico* model. Simulation of microtubule (MT) dynamics was conducted under various conditions, simulating 10 minutes of developmental time with 10,000 frames and a time step $\Delta T = 0.06$ s. A custom Python script was utilized to extract the positions of cortical MT plus-ends, defined as MT plus-ends within a 0.5 μm range from the cortex. The apicobasal position of each MT plus-end at the cortex was then saved for each frame of the simulation. Subsequently, all apicobasal positions of cortical MT plus-ends were plotted as a function of their respective boundary conditions, such as the position of the nucleus and the distance between the nucleus and centrosomes. 100 simulations were conducted per condition. Each simulation involved randomizing the location of MT nucleation on the centrosomes or the occurrence of catastrophe/rescue events. This approach aimed to capture variability and ensure robustness in the analysis, ultimately obtaining an average trend in cortical MT plus-ends distribution per condition. To evaluate the individual contributions of various parameters in the simulation — such as MT dynamic properties (growth rate, shrinking rates, absolute number of polymers) and cell geometry (nucleus radius, centrosome position)

— simulations were conducted 25 times for each parameter, with variations spanning several orders of magnitude. Employing the same extraction protocol for MT plus ends, subsequent plots of MT distribution were generated.

In silico cortical MT plus-end distribution relative to the nucleus

The mid-position of the nucleus was extracted from the template file used for the *in silico* model in each condition. A custom Python script counted the number of cortical MT plus ends located in two compartments: either “above” the nucleus (defined as the range from the nucleus mid-position to the apical surface) or “below” the nucleus (from the nucleus mid-position to the basal side of the cells). Percentages of MT distribution relative to the nucleus were calculated by dividing the count in each compartment by the total count of cortical MT plus ends in the simulation.



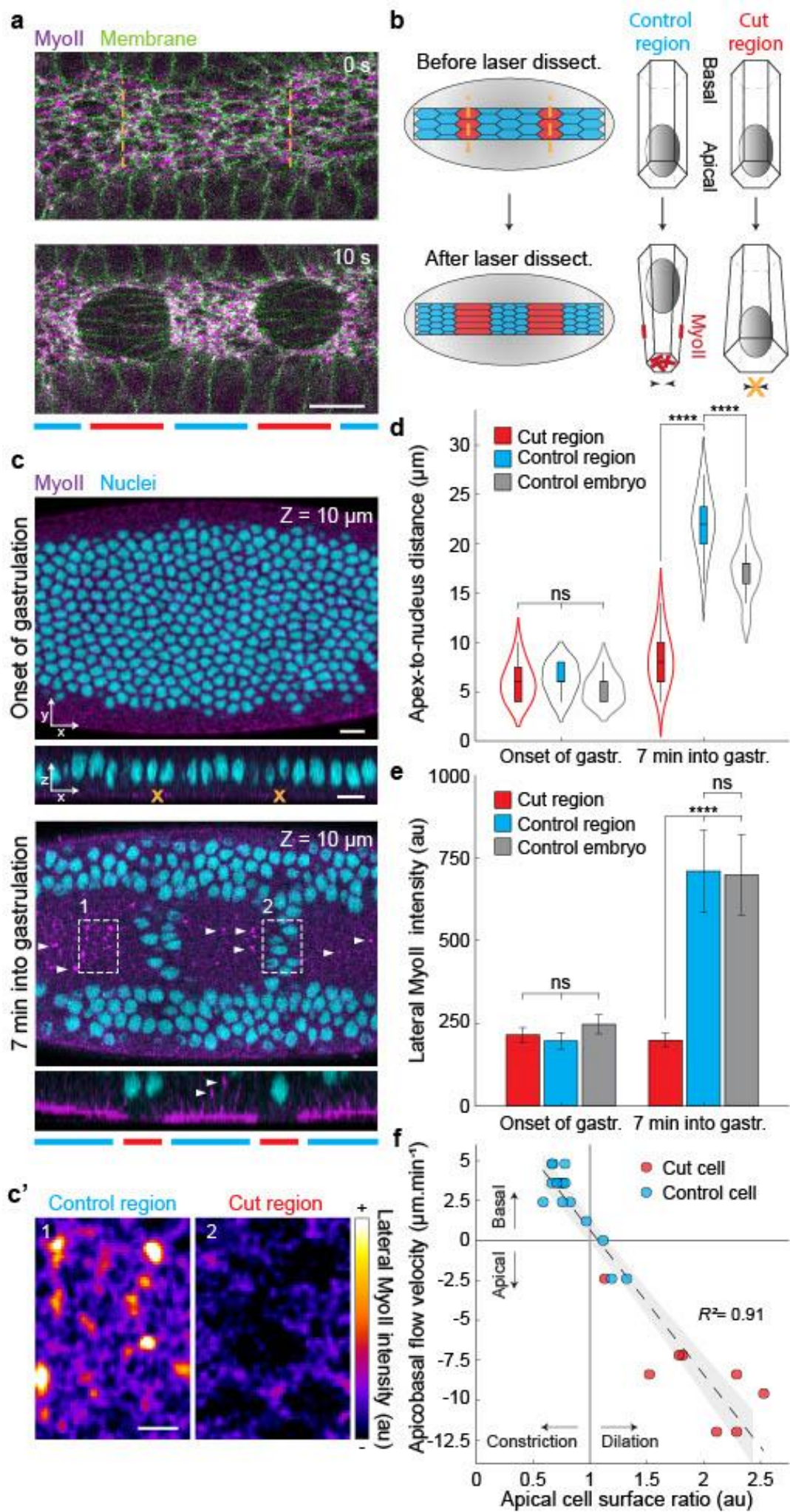


Fig. 2

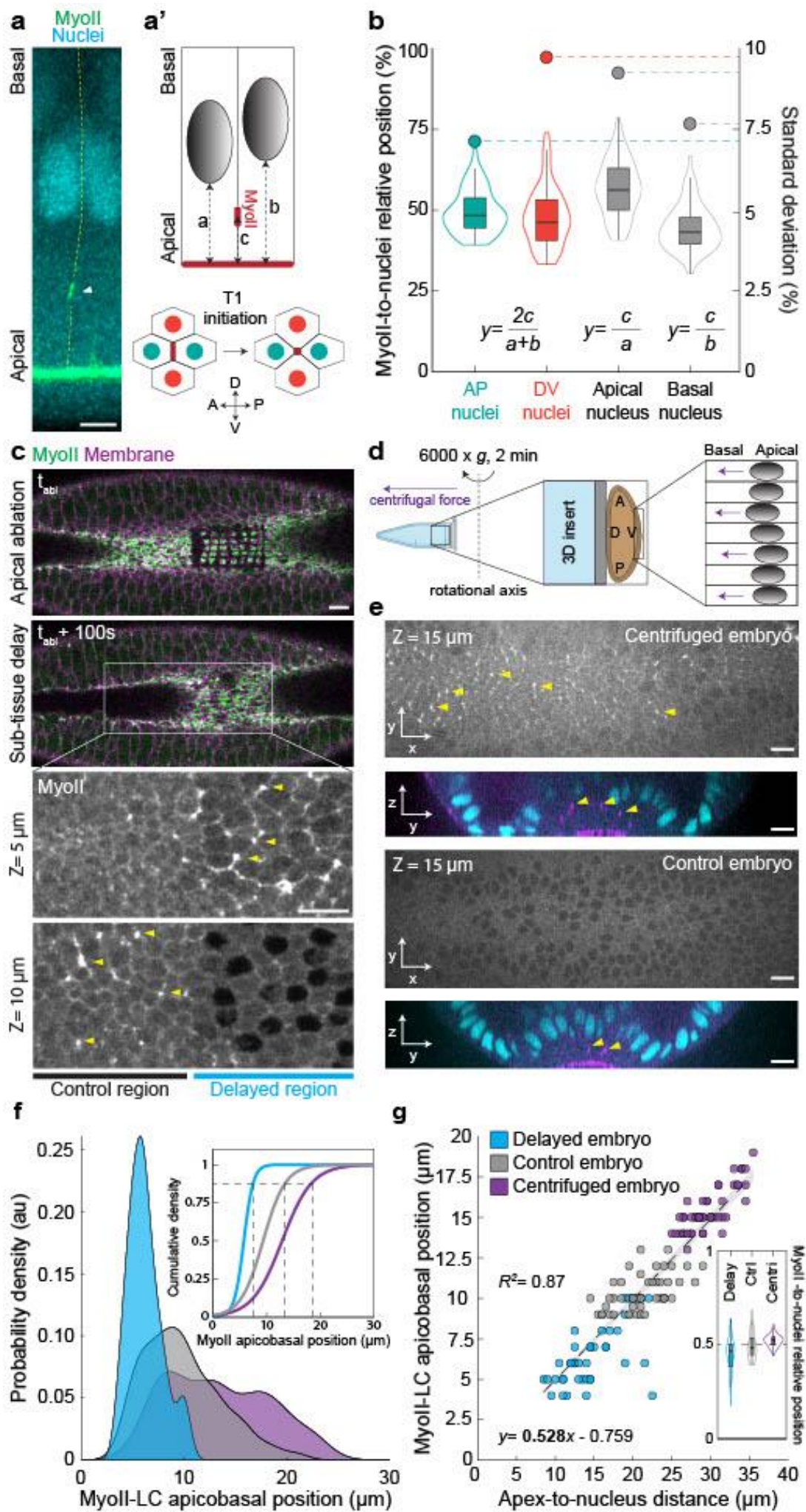


Fig. 3

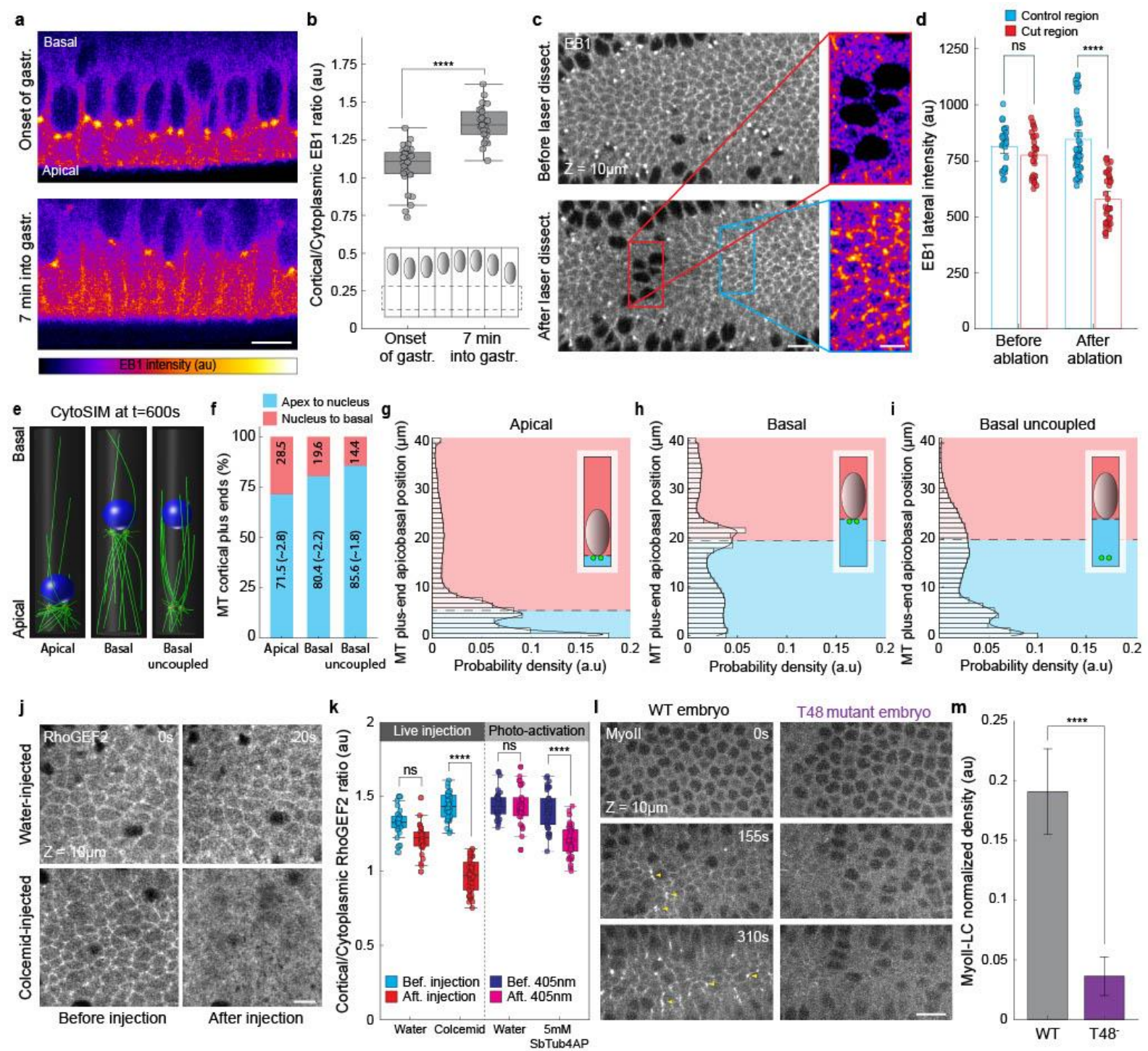
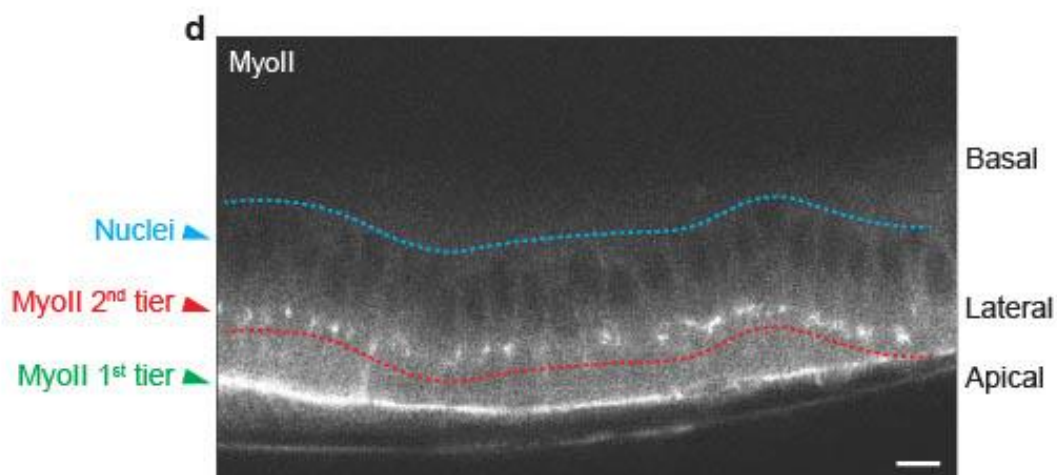
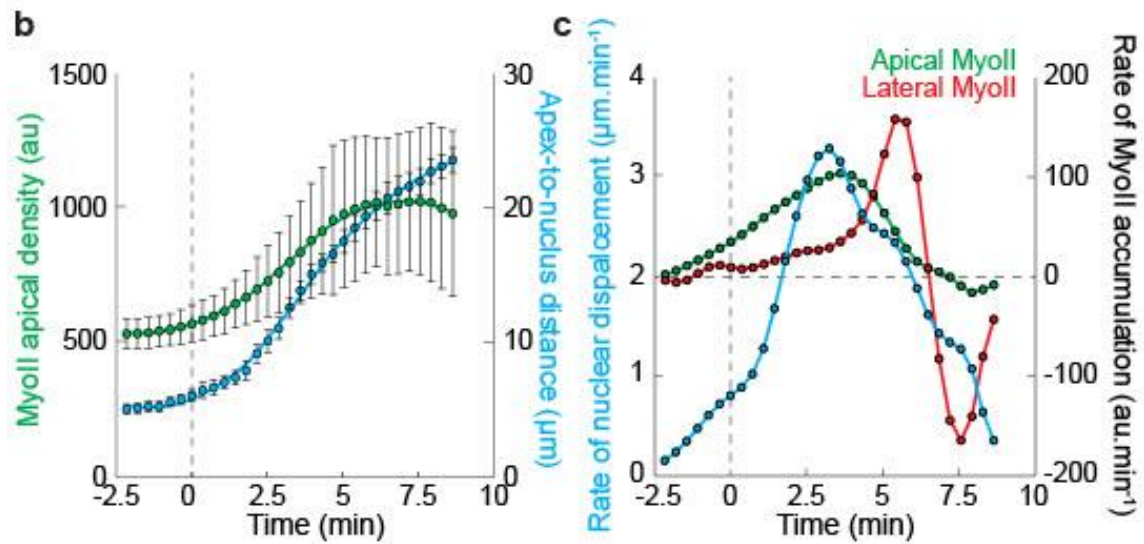
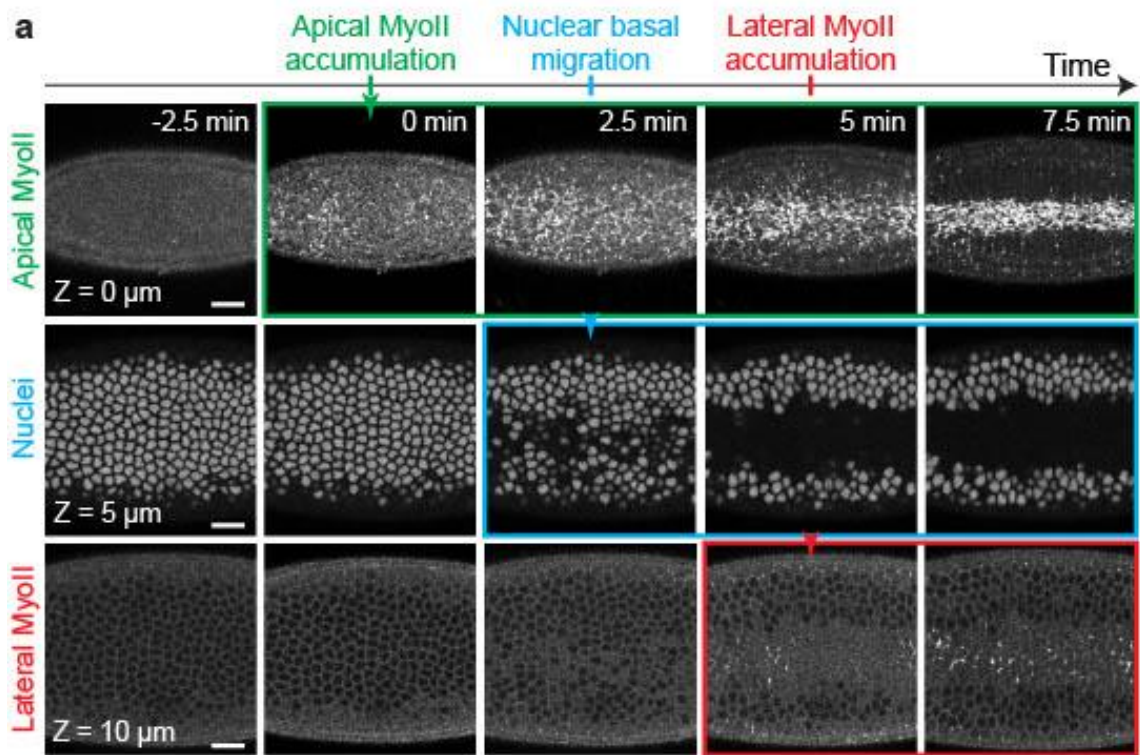
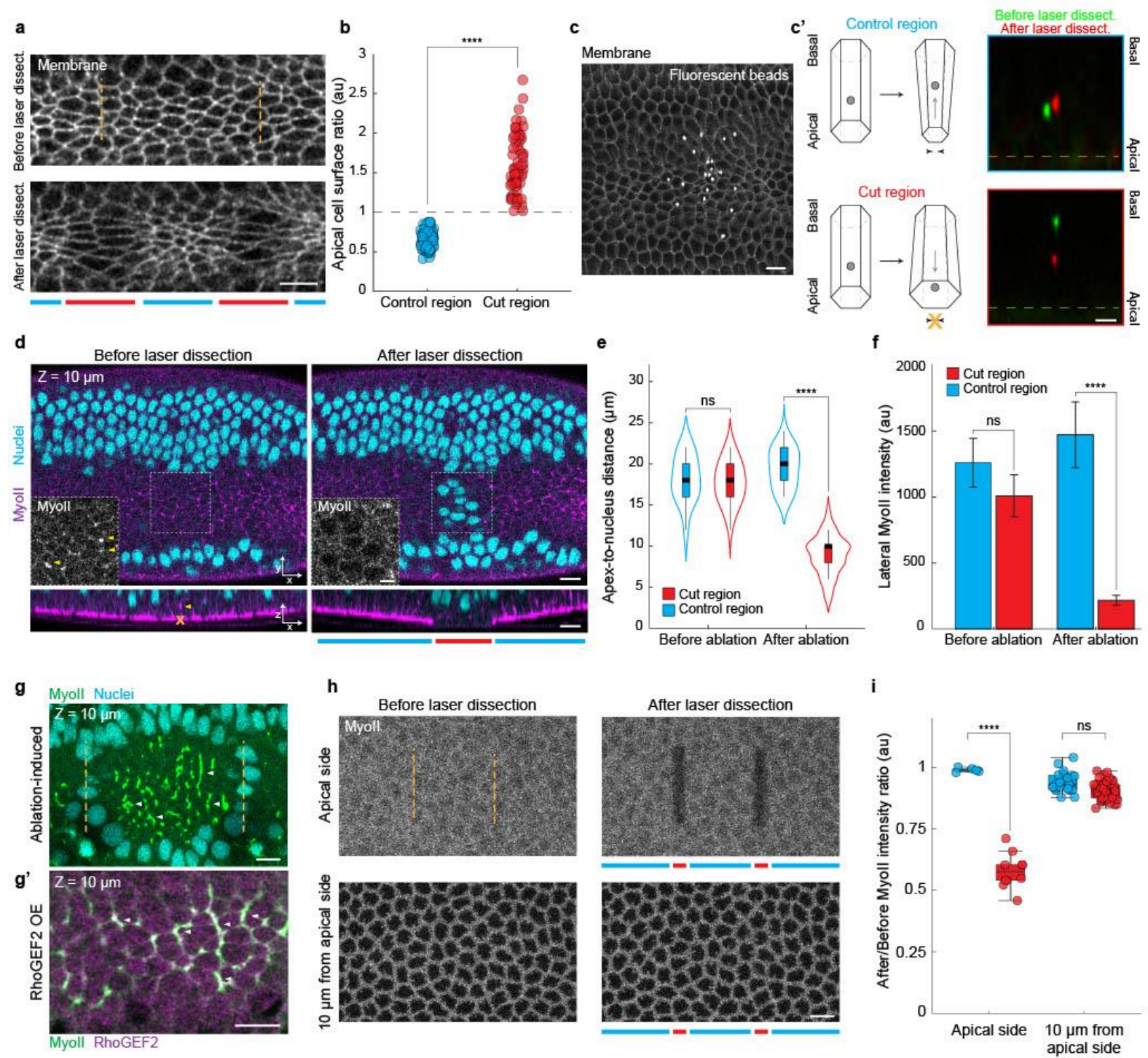


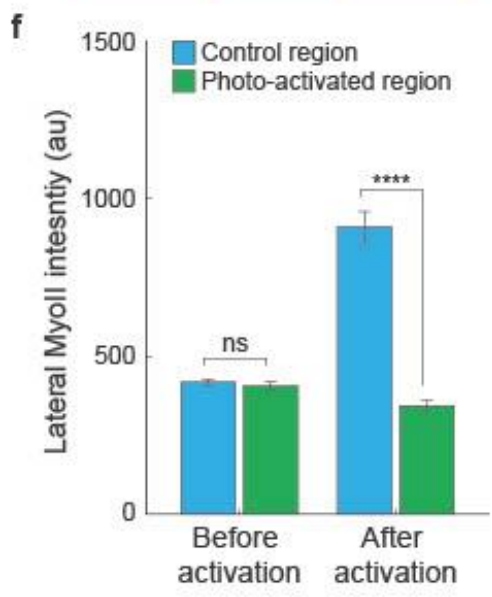
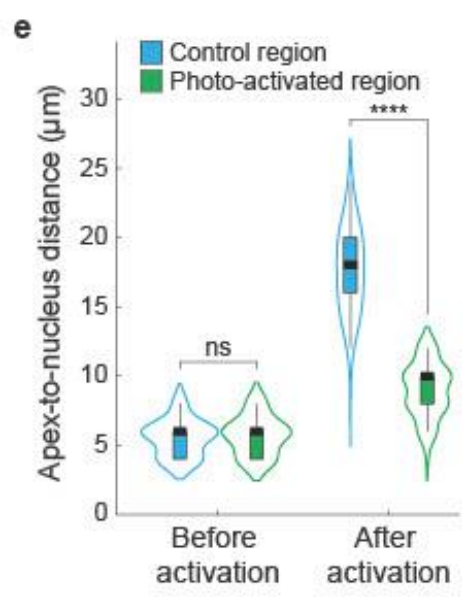
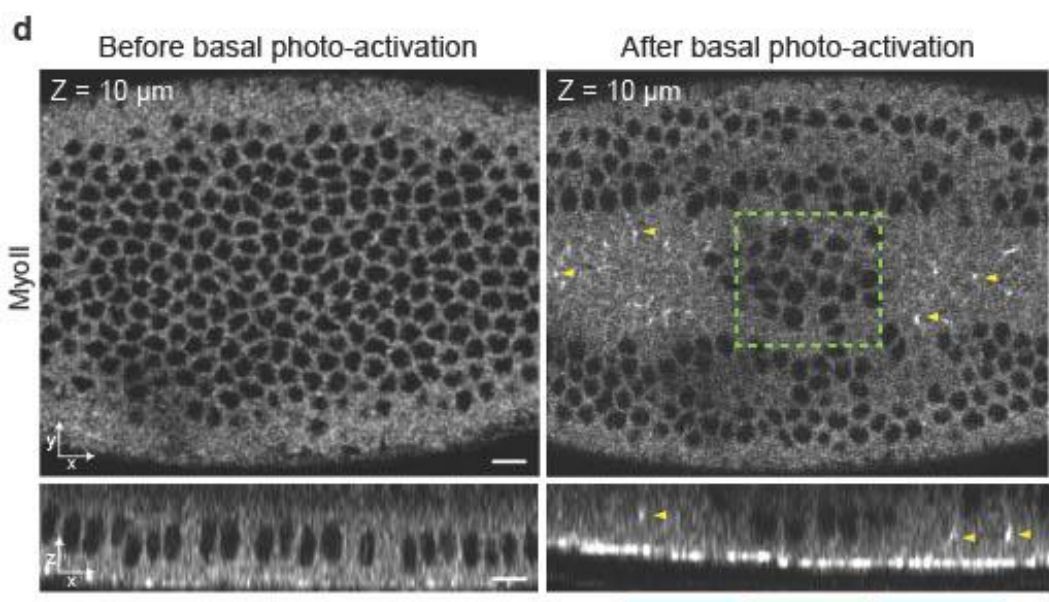
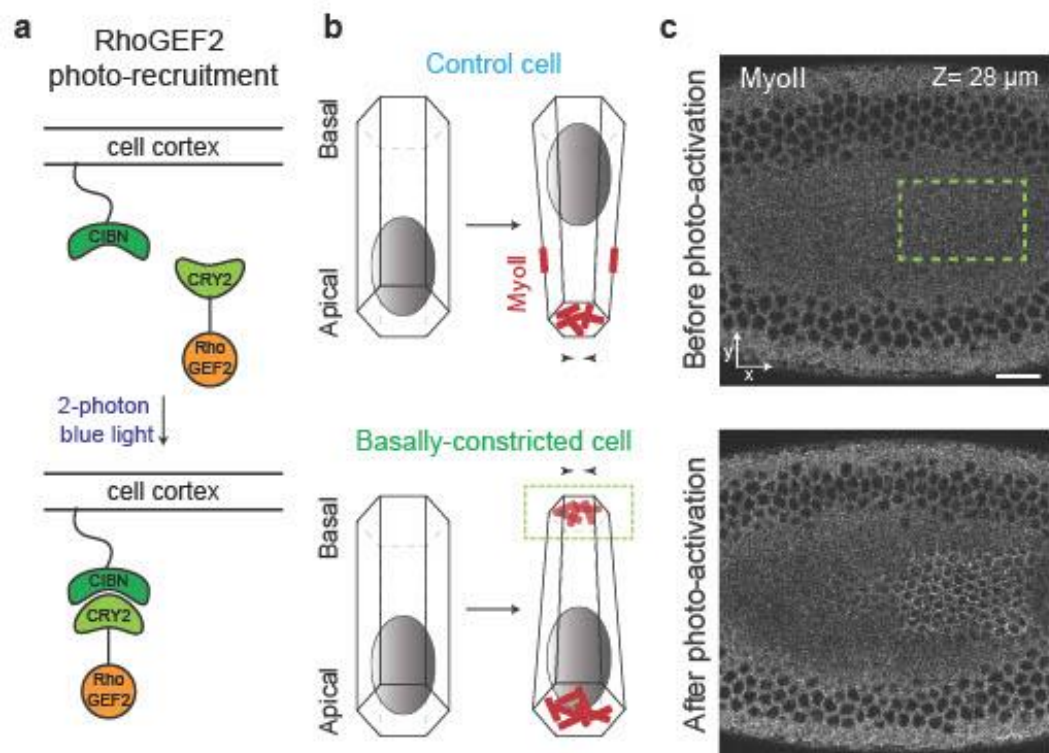
Fig. 4



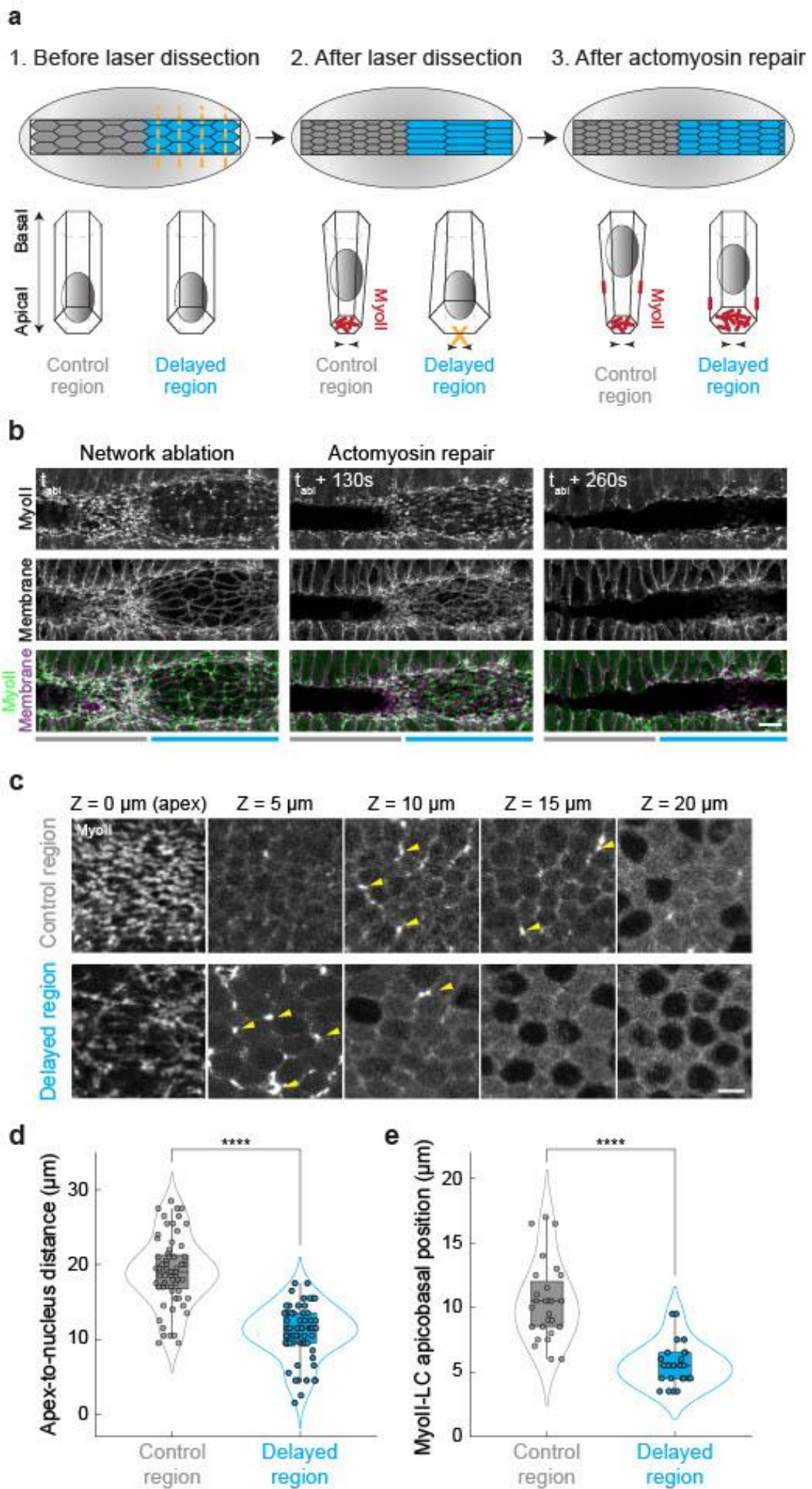
SFig1



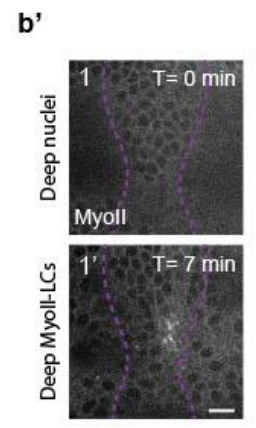
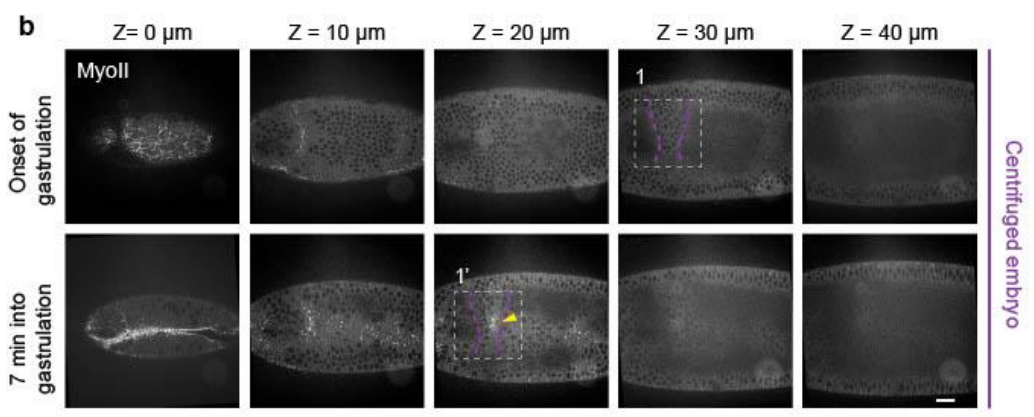
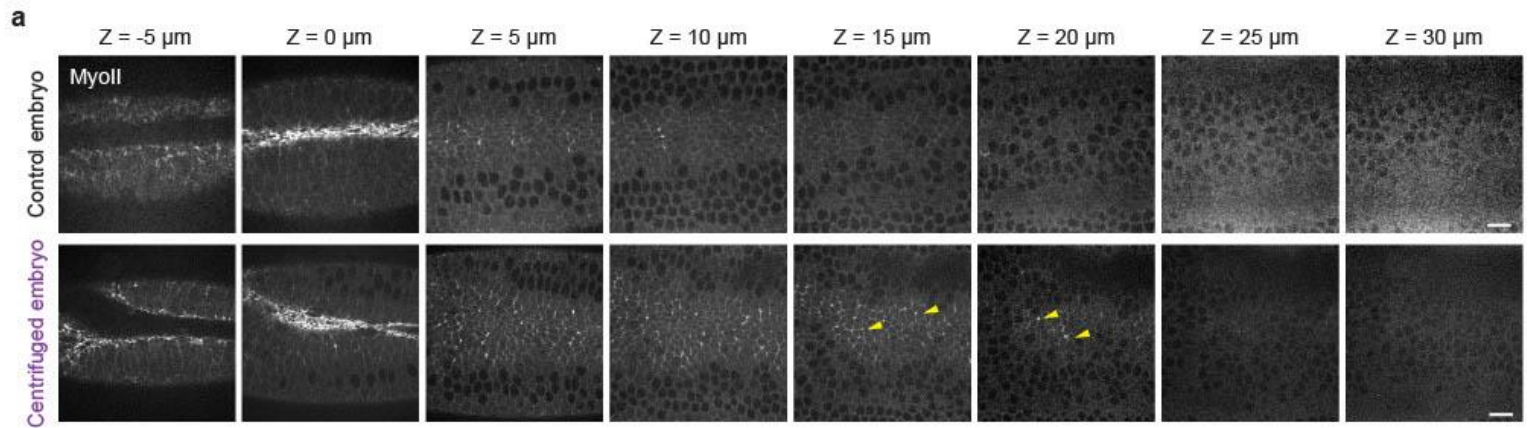
SFig2



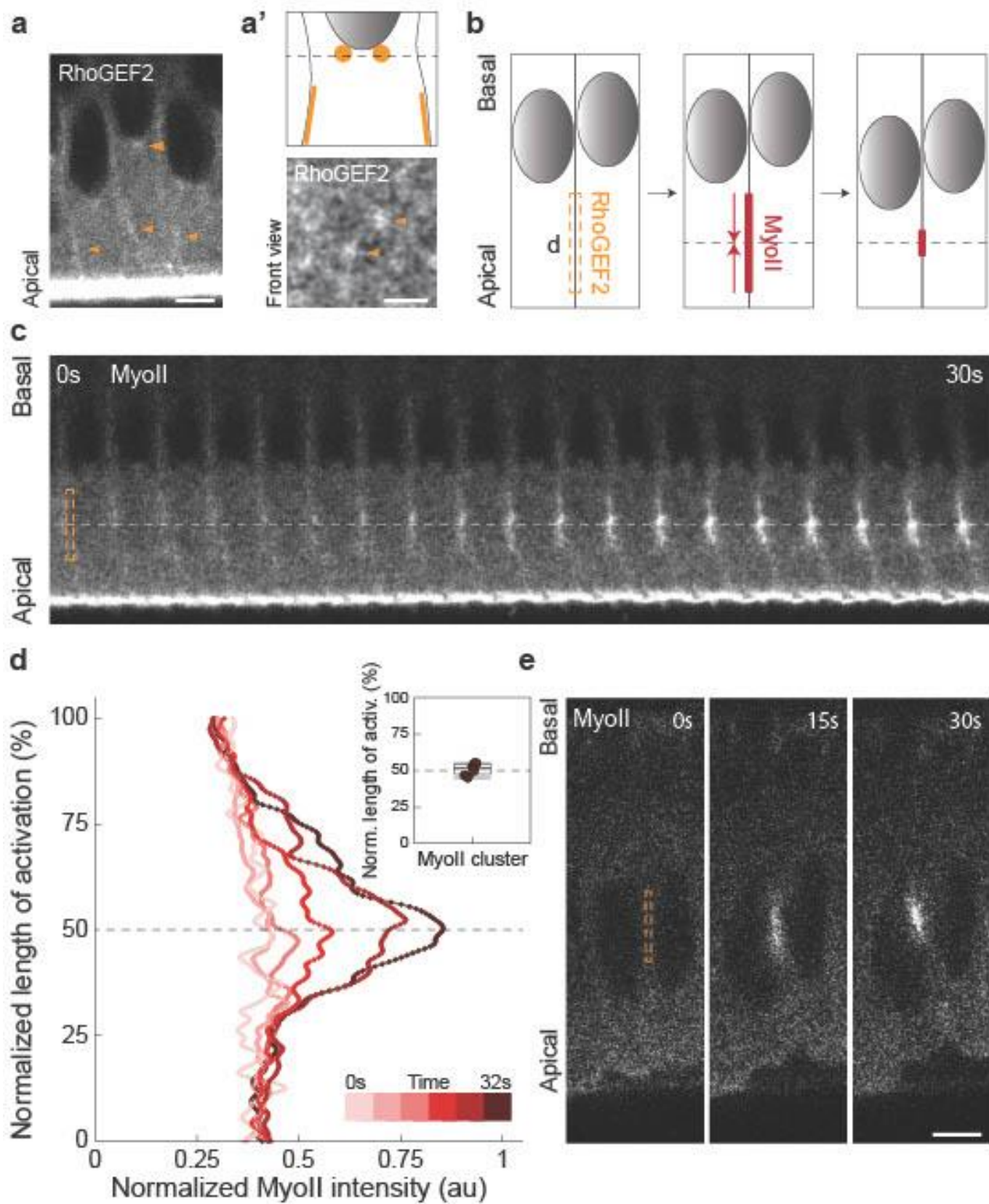
SFig3



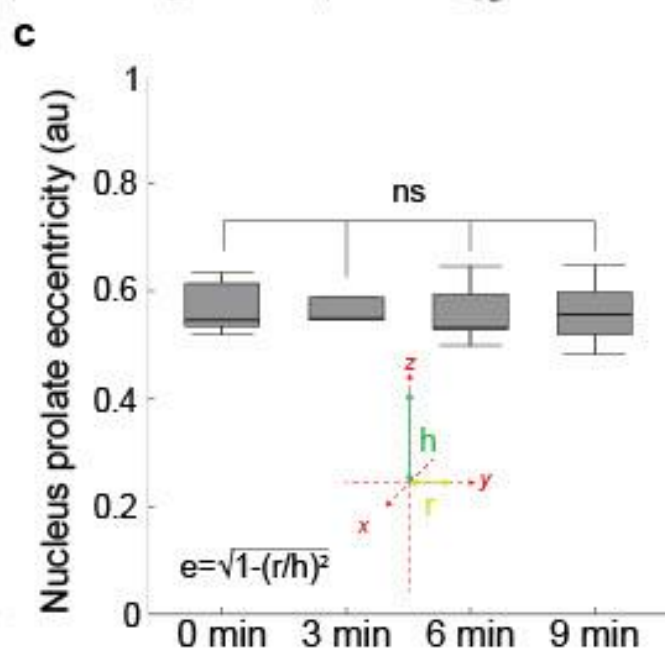
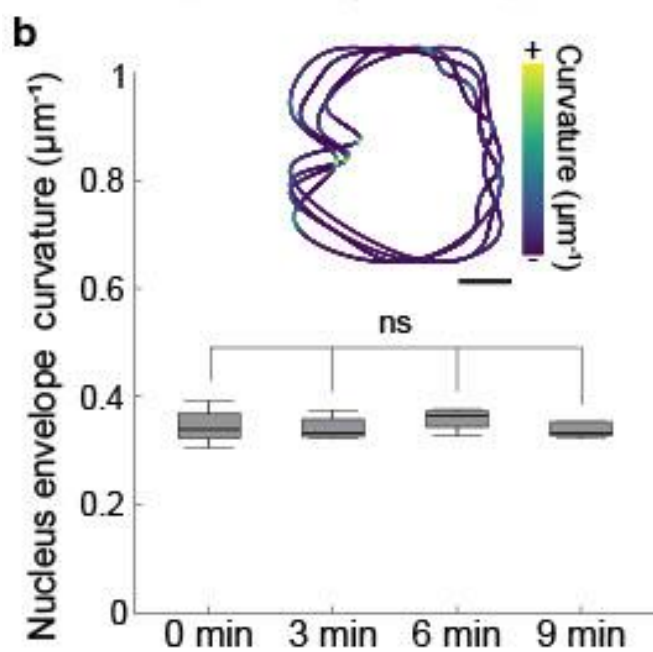
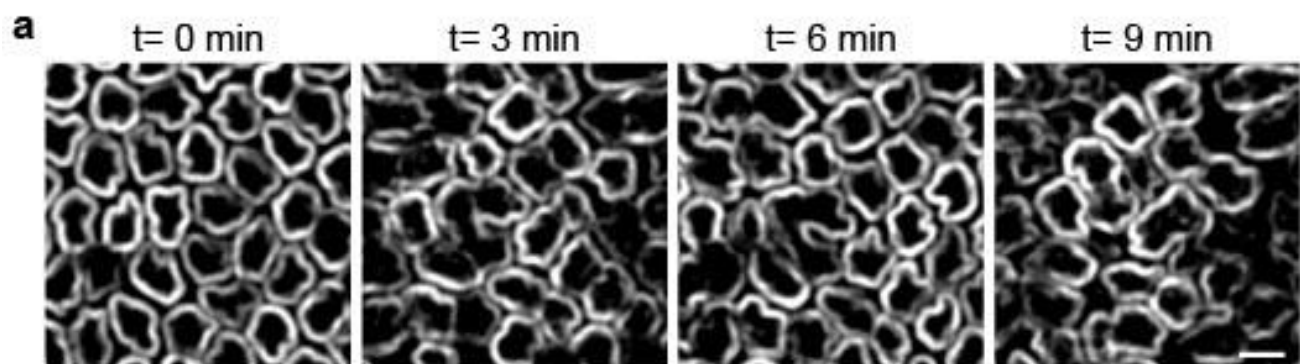
SFig4



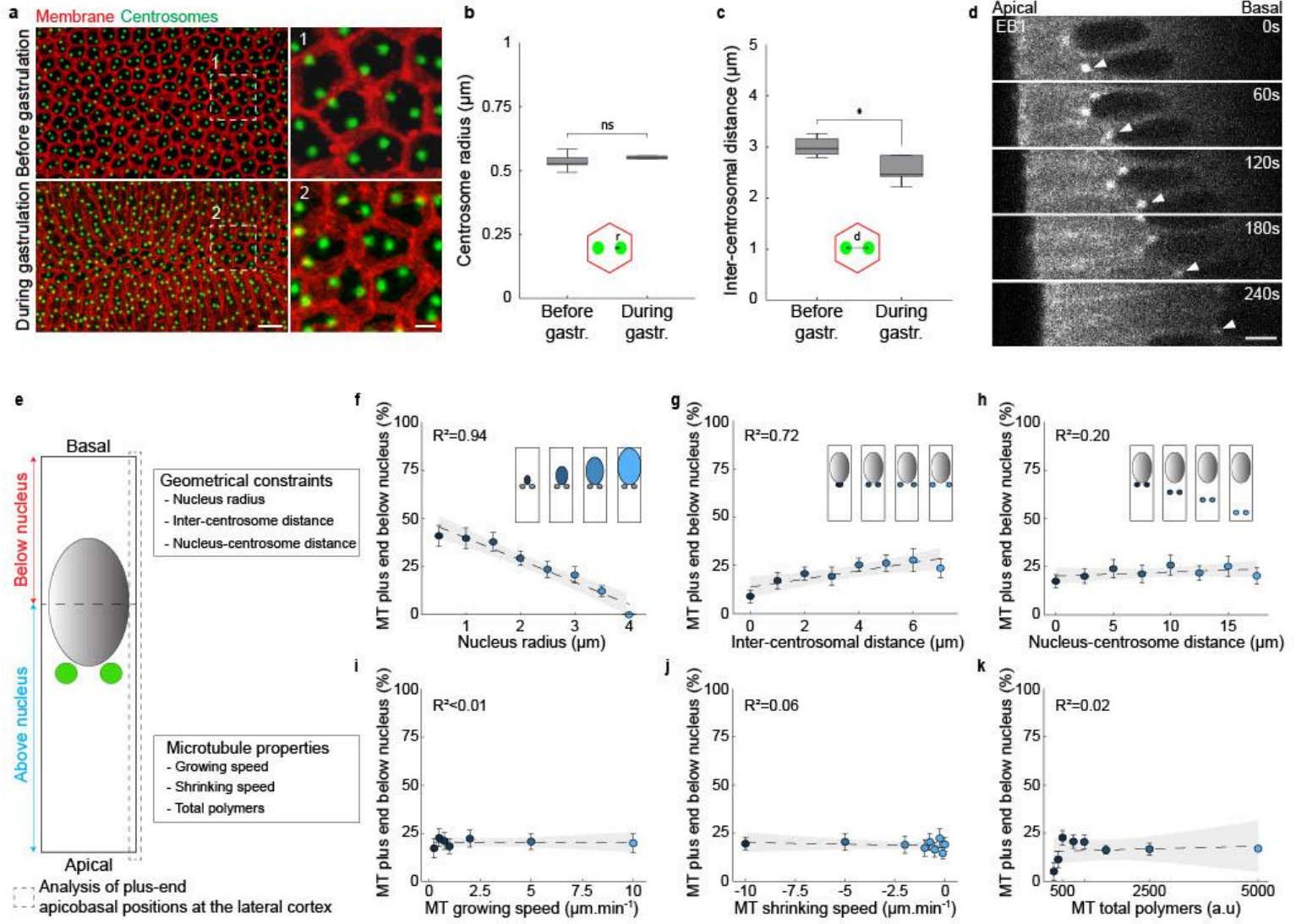
SFig5



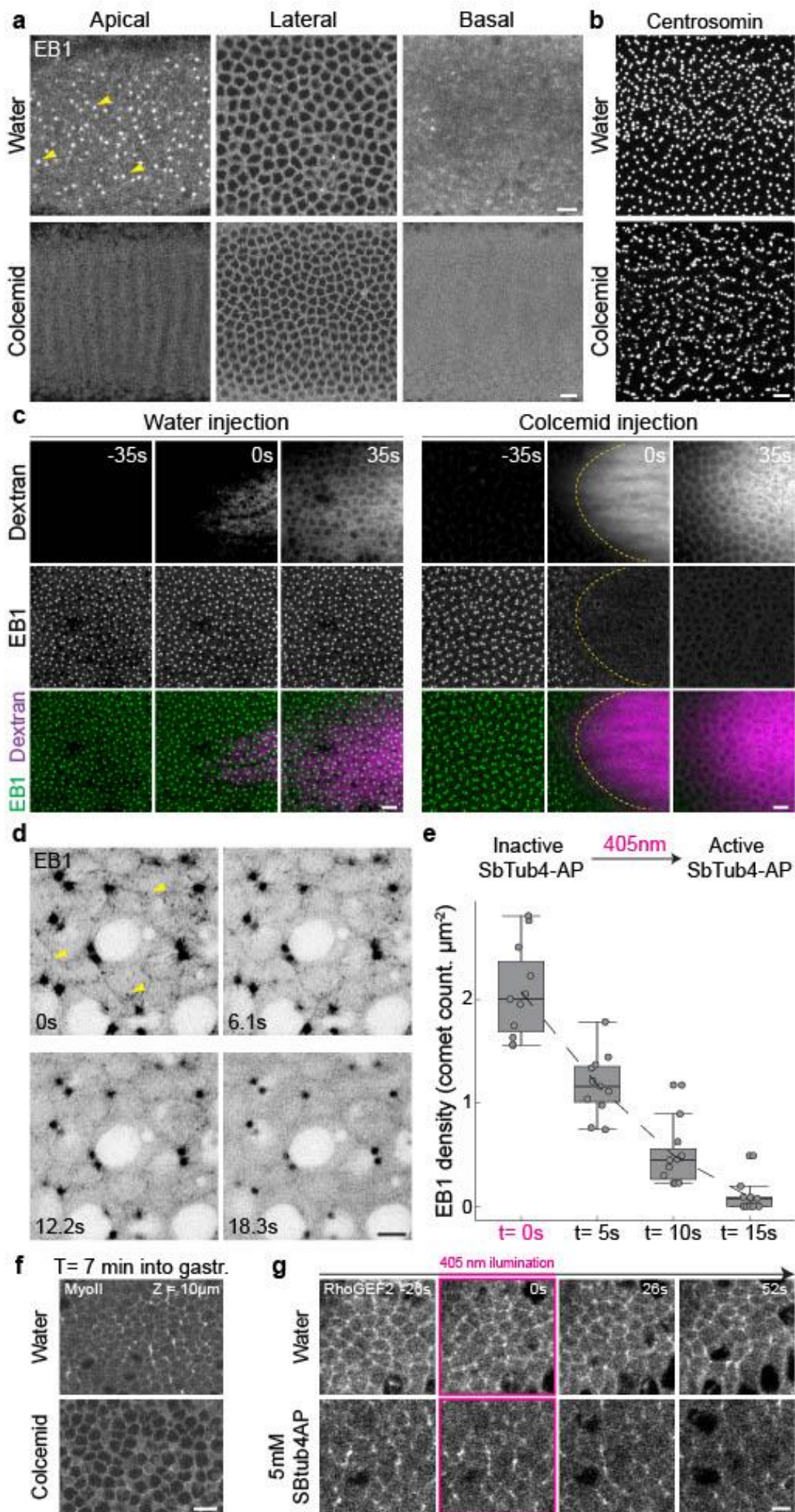
SFig6



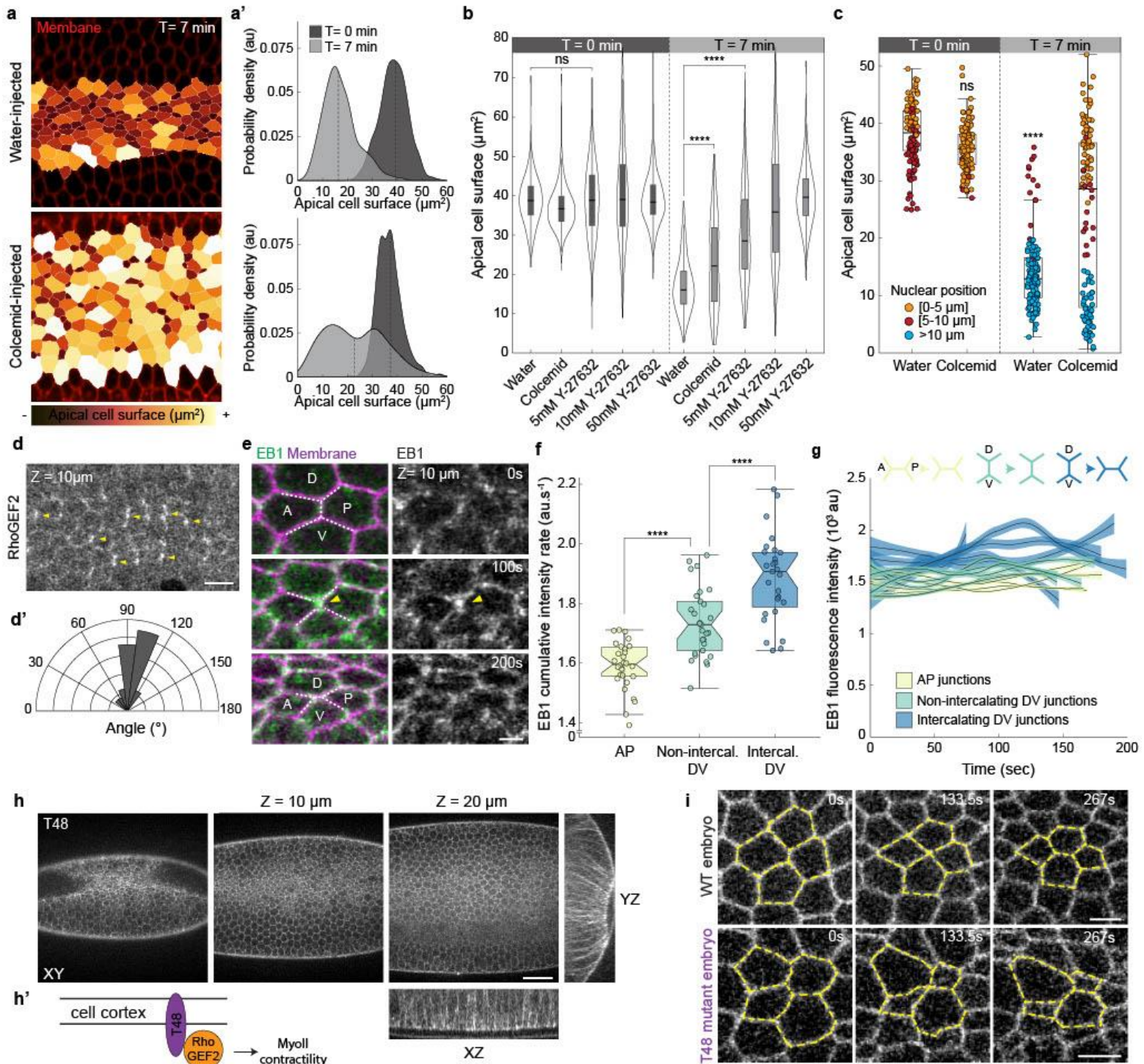
SFig7



SFig8



SFig9



SFig10

Chapter III-Discussion

My thesis project focused on understanding the mechanisms that enable a tissue to undergo simultaneous shape and topology changes, a conserved process during embryogenesis and organogenesis, as illustrated during neurulation, gastrulation, and tubulogenesis. Previous work from my team identified a two-tier mechanism that governs concomitant folding and extension during early *Drosophila* gastrulation. In mesoderm cells, distinct subcellular actomyosin networks, tethered to adherens junctions, drive both constriction and convergence-extension within a 15-minute window. The objective of my research was to elucidate how these cells spatiotemporally control the establishment of distinct subcellular actomyosin networks. I demonstrated that the first tier contracts the apical side of mesoderm cells, creating a basally-directed cytoplasmic flow that displaces the nuclei. As the nuclei move basally, the microtubule network redistributes along the lateral cortices of the mesoderm cells. Consequently, RhoGEF2, which interacts with microtubule +TIP via the EB1 protein, is delivered to the lateral cortex and anchored by T48. This leads to the activation of MyoII along the lateral cortex between the cell apex and the nucleus, resulting in the isotropic coalescence of MyoII to form lateral clusters (MyoII-LCs) at the midpoint of this region that will engage in cell intercalation.

By combining optogenetics, infrared laser dissection, and *in vivo* centrifugation methods to manipulate nuclear positioning in living *Drosophila* embryos, I demonstrated that nuclear positioning regulates the temporal and spatial establishment of MyoII-LCs. MyoII-LCs only form after the nuclei have moved basally. Keeping nuclei apically positioned prevents MyoII-LC formation, and relocating nuclei from the basal to the apical side disrupts previously established MyoII-LCs. MyoII-LCs are typically established approximately 10 μm from the apical side. Their apicobasal position correlates with the nuclei positions along the anteroposterior (A-P) axis. I proposed a model that computes the position of neighboring nuclei to predict the apicobasal positioning of MyoII-LCs. According to this model, MyoII-LCs form midway between the cell apex and the average depth of A-P nuclei that share the enriched junction. Modulating the extent of nuclear basal displacement resulted in more apical or basal MyoII-LCs, and their locations adhered to the predictive "halfway rule" model.

With this work, I propose that the nucleus acts as a cytoskeleton compartmentalizer that controls the spatiotemporal organization of distinct subcellular actomyosin networks, allowing the cell to engage in simultaneous shape and topology changes. These results also raise significant questions that I will try to address in the following section.

1. How is RhoGEF2 planar cell polarity established?

A first intuitive hypothesis would be that T48 is distributed in a PCP-fashion. Addressing the endogenous expression profile of T48 will be needed in the future, as well as understanding how its upstream regulator Twist can promote its PCP distribution, if any.

Previous studies have ruled out the involvement of canonical pathways, such as Frizzled and Fat/Dachsous, in establishing planar cell polarity in early *Drosophila* embryos (Zallen and Wieschaus, 2004). Instead, they demonstrated that the stripe-patterned expression of signaling components, including Toll receptors, Tartan, and Ten-m, drives the polarized distribution of MyoII during ectoderm convergence-extension (Paré et al., 2014, 2019; Lavalou et al., 2021). The anterior-posterior (A-P) gene patterning, involving genes such as *bicoid*, *nanos*, *torso*, and *downstream even-skipped (eve)*, is necessary for the proper expression of these effectors. Previous work in the lab has shown that *bnt* triple mutant embryos exhibit defective MyoII PCP in the mesoderm (John and Rauzi, 2021a). However, none of these studies have investigated the effect on RhoGEFs, RhoGAPs and Rho-GTPases distribution. Future studies analyzing *eve* mutant embryos (*eve* being expressed in the mesoderm) and investigating the role of the Toll code in mesoderm PCP will be needed to elucidate the interplay between tissue-scale transcriptional patterning and the subcellular control of Rho-GTPase dynamics.

Alternatively, the dorsoventral (D-V) patterning system might also be at play. It has been reported that in *twi*- embryos, Snail is expressed in stripes along the A-P axis (Ip et al., 1992; Stathopoulos and Levine, 2002; Stathopoulos et al., 2002). An interesting hypothesis is that the mesoderm tissue could be pre-patterned to recruit Rho effectors in a PCP fashion, potentially through the Snail-dependent expression of the Mist GPCR (Manning et al., 2013). The absence of apical MyoII PCP could be attributed to the presence of Twist, leading to the medio-apical recruitment of MyoII and thus overriding any PCP pattern apically. As a result, MyoII PCP can only be observed laterally. Analysis of both *twi*- mutant embryos and endogenous Mist expression could test this hypothesis.

I showed that the microtubule plus end EB1 protein is PCP-distributed and could thus promote RhoGEF2 PCP delivery. Several studies across species have reported that microtubules can be PCP-distributed and participate in the establishment of planar polarity (Shimada et al., 2006; Bulgakova et al., 2013; Mathewson et al., 2019). However, the mechanism behind this distribution remains unclear. One hypothesis is that tissue-scale tension and the resulting shape anisotropy of mesoderm cells influence microtubule distribution. Evidence from *Drosophila* wing epithelium suggests that a spatial gradient in microtubule growth velocity along perpendicular axes leads to the preferred distribution of microtubules along the long axis of these cells (Singh et al., 2018). If a similar mechanism operates here, it could explain the PCP distribution of EB1 protein. Therefore, I hypothesized that loss of anisotropy would result in the loss of both EB1 PCP and MyoII distribution. However, when

performing apical D-V laser cuts to release the tension, my findings indicate that MyoII PCP recruitment is actually enhanced, thereby ruling out this initial hypothesis. An alternative and more convincing explanation is that the PCP distribution of EB1 actually is the consequence of the interaction between RhoGEF2 and its cortical anchors. As EB1 transports RhoGEF2, stabilization could occur when an EB1-RhoGEF2 assembly interacts with cortical T48, forming a transient complex. Additionally, several studies reported that microtubules can be tethered to adherens junctions via the dynein molecular motor (Ligon et al., 2001; Ligon and Holzbaur, 2007) and reported that E-cadherin adhesive contacts can recruit radially-oriented MT plus-ends (Stehbens et al., 2006). Over time, these interactions could result in the PCP distribution of EB1.

The pioneering research that first described RhoGEF2 localization to microtubule plus ends via the protein EB1 in *Drosophila* S2 cells also demonstrated that the active (GTP-bound) form of the G alpha subunit Concertina (Cta) interacts with RhoGEF2 to induce its release from EB1 (Rogers et al., 2004). This mechanism was further confirmed *in vivo* in *Drosophila* embryos, using RNAi-mediated downregulation and a constitutively active form of Cta while monitoring RhoGEF2 cortical distribution (Kerridge et al., 2016; Bayonas et al., 2019). In contrast, recent research has identified that RhoGEF2 cortical accumulation during the migration of *Drosophila* primordial germ cells does not require Cta. Instead, it requires an unidentified anchor to interact with RhoGEF2 RGS domain (Lin et al., 2022). Nonetheless, assessing the endogenous distribution of Cta in the mesoderm and developing tools to spatiotemporally control its activity could be valuable to understand its role in the PCP distribution of RhoGEF2.

2. What are the molecular requirements to generate MyoII lateral clusters?

I provided evidence that T48 can decorate the lateral cortex of mesoderm cells. As nuclei reposition to enable microtubules to deliver RhoGEF2 to the cortex, I postulate that T48 anchors RhoGEF2 to generate MyoII lateral clusters. Interestingly, in the posterior midgut (PMG), cells also recruit MyoII medio-apically, causing the basal displacement of nuclei similar to the mesoderm (Chanet et al., 2017; Bailles et al., 2019). However, PMG cells do not exhibit any MyoII-LCs, despite nuclear basal displacement. While Cta, RhoGEF2, and microtubules are ubiquitously present in the embryo, T48 is not expressed in the posterior midgut (PMG) (Urbansky et al., 2016, Figure 2A). I hypothesized that the absence of T48 was the reason for the lack of MyoII-LCs in the PMG. To test this, I overexpressed T48 in the PMG. Surprisingly, this did not result in the formation of MyoII-LCs, suggesting that T48 is necessary but not sufficient to drive MyoII-LC formation (Figure 2B). Another possibility is that the GFP-tagged T48 protein may not be fully functional.

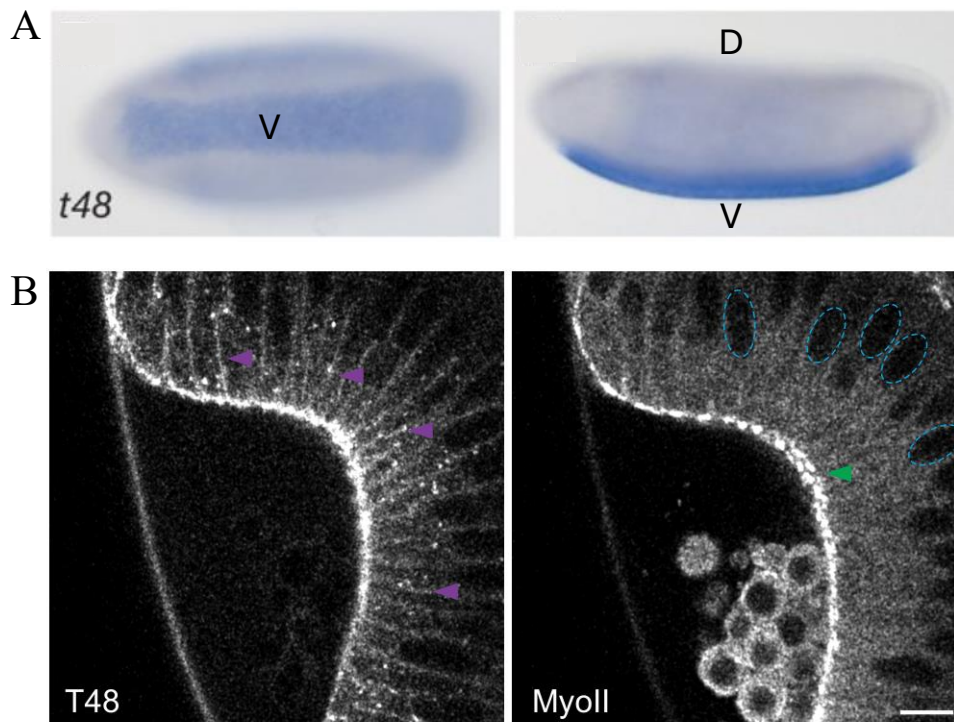


Figure 2. Ectopic T48 expression in the PMG is not sufficient to drive MyoII lateral recruitment. **A**, *t48* mRNA expression in front view (left) and sagittal view (right) stage 6 *Drosophila* embryo (adapted from Urbansky et al., 2016). **B**, T48 ectopic expression (left) and MyoII subcellular distribution (right) in the PMG. Purple arrows indicate lateral T48 expression. Green arrows indicate MyoII apical pool. Cyan circles outline nuclei. Scale bar, 10 μ m.

Previous work has identified several GEFs involved in the intercalation of ectoderm cells. RhoGEF2 directs the medio-apical activity of Rho1, while Dp114RhoGEF directs the polarized junctional recruitment of Rho1 (Bayonas et al., 2019). In the mesoderm, where Dp114RhoGEF is not expressed, RhoGEF2 is used iteratively at both locations. One explanation for this could be that the levels of RhoGEF2 available in the ectoderm are lower than in the mesoderm. The ectoderm requires sufficient RhoGEF2 to generate actomyosin pulses necessary for the polarized flow of MyoII towards junctions while maintaining levels low enough to avoid constricting ectoderm cells (Rauzi et al., 2010). Interestingly, overexpression of Twist and Snail (by downregulation of their upstream repressor *Serpina27A*) in the lateral ectoderm increases RhoGEF2 levels, leading to apical MyoII-dependent constrictions and subsequent nuclear basal displacement. Strikingly, in this context, MyoII lateral recruitment is also observed (John and Rauzi, 2021a). In the future, assessing the

respective contribution of Snail and Twist and their downstream effectors in different tissues will be key to decipher the synergy between RhoGEF2 availability and cortical anchoring to drive the formation of MyoII-LCs.

3. How do microtubules control actomyosin contractility?

The relationship between microtubules and actomyosin regulation remains a topic of debate. Some studies have shown that microtubules positively control actomyosin contractility, as microtubule growth is associated with localized Rho activity (Waterman-Storer et al., 1999; von Dassow et al., 2009; Verma and Maresca, 2019), while others propose that microtubule plus-ends sequester RhoGEFs, leading to increased actomyosin contractility upon microtubule depolymerization (Chang et al., 2008; Hui and Upadhyaya, 2017). However, evidence from several morphogenetic processes in *Drosophila* embryos indicates that microtubule depolymerization disrupts actomyosin networks. For instance, during salivary gland formation, the medio-apical actomyosin pool is lost (Booth et al., 2014), and during mesoderm invagination, actin network repair is impaired, resulting in disrupted apical constriction (Ko et al., 2019, this study). Interestingly, work by (Stehbens et al., 2006) also showed that dynamic microtubules are necessary for local MyoII activation and subsequent E-cadherin accumulation, and that initial recruitment of microtubules relies on interactions with cortical E-cadherin. My work is also surprising as microtubule disruption affects actomyosin in different ways within the same cell. I show that microtubule disruption significantly reduces the formation of the lateral tier of MyoII, while having minimal effect on apical MyoII recruitment. One possible explanation for this dual effect is the existence of redundant pathways in the formation of the apical tier. For instance, the apically-secreted ligand Fog and downstream GPCR signaling could reduce the necessity for localized microtubule delivery of Rho effectors at the apical cortex (Parks and Wieschaus, 1991; Costa et al., 1994). Another explanation could be that cortical partners of EB1-bound RhoGEF2 are preferentially expressed on the lateral cortex rather than the apical side of mesoderm cells.

I also observed a rapid loss of cortical RhoGEF2 at the lateral cortex following microtubule disruption, using both classical and opto-pharmacological tools. This suggests that existing RhoGEF2 clusters at the cortex disappear quickly, likely due to a high turnover rate of RhoGEF2 at the cortex, and could require continuous delivery from microtubules. My attempts to assess RhoGEF2 cortical dynamics using FRAP (Fluorescence Recovery After Photobleaching) were challenging and unsuccessful but several studies tackling the cortical turnover of Rho effectors observed comparable dynamics with turnover rates for RhoA and ROCK within the second-scale (Budnar et al., 2019; Sidor et al., 2020). Alternatively, RhoGEF2-EB1 interaction could be necessary for its binding to cortical partners, and freely diffusing RhoGEF2 might not be primed to drive MyoII-LC formation, thus requiring MT-based delivery.

4. Experimental limitations to address the impact of nucleus positioning on microtubule dynamics

I provided evidence that the nucleus can regulate the cortical distribution of microtubules. I observed that microtubule plus-ends (EB1) are initially located apically then redistribute along the lateral cortex as nuclei move basally. This observation is further supported by *in silico* simulations of microtubule dynamics. Additionally, I showed that apical dissection of the actomyosin network to reposition nuclei apically abolishes the lateral recruitment of EB1. By using a multi-photon laser, we can precisely cut the apical actomyosin network in mesoderm cells without disrupting deeper processes, thereby preserving the microtubule-organizing centers (MTOCs) and the microtubule network. However, this method has limitations. A study has shown that actomyosin contractions in mesoderm cells induce the formation of an apical acentrosomal MTOC under the control of the CAMSAP protein Patronin (Ko et al., 2019), a process also observed during *Drosophila* salivary gland formation (Booth et al., 2014). If this acentrosomal MTOC significantly contributes to the lateral cortex decoration, as indicated by the bidirectional EB1 comets observed along the lateral cortex, then apical laser cuts could disrupt this pool and lead to the observed loss of lateral microtubules, independently of the relocation of the nucleus. Due to the lack of a red fluorophore-tagged EB1 reporter, I could not use optogenetic tools to induce basal contraction of mesoderm cells to inhibit nuclear displacement without disrupting the apical side, as the wavelengths required for opto-activation and imaging of GFP-tagged EB1 would conflict. New methods to modulate nuclear positioning *in vivo* without interfering with other cellular processes will thus be necessary to address this issue, such as acoustic, optical or magnetic tweezers.

5. What is the role of the apicobasal microtubule arrays surrounding the nucleus?

The mechanism I propose relies on the nucleus-dependent control of microtubules. It is worth noting that before gastrulation, at the end of the cellularization process, a microtubule array surrounding the nucleus and aiming towards the basal side, termed "microtubule cage," is observed and remains during early gastrulation (Hampoelz et al., 2011). Why don't these microtubules in contact with the lateral cortex already activate MyoII there? This microtubule cage has been shown to be acetylated (Ko et al., 2019), and acetylation has been associated with increased stability of the microtubule network (Piperno et al., 1987; Webster and Borisy, 1989; Chu et al., 2022). Even though this network still shows some level of dynamicity, I speculate that these acetylated microtubules do not participate in the regulation of contractility. Since microtubule properties and function are strongly influenced by the post-translational (PTM) modifications they carry (Janke and Magiera, 2020), investigating the types of PTM the different microtubule networks undergo could also provide insights into the fine regulation of contractile domains during epithelial morphogenesis.

Interestingly, a recent study suggested that a similar cage, observed in confined melanoma cells, is necessary to protect the nucleus from damage (Ju et al., 2023). In the presumptive mesoderm, acetylated microtubules could thus be dedicated to the formation of a perinuclear cage to buffer mechanical stresses, explaining why I do not observe significant nuclear deformations during early *Drosophila* gastrulation. Recent work also reported that an acetylation gradient is established in cells, with highest acetylation taking place in perinuclear microtubules (Andreu-Carbó et al., 2024), and work by (Li et al., 2023) proposed that MTs could stabilize in response to mechanical stress. Since acetylation is mostly mediated by α TAT1 enzyme (K40 acetylation), one could test this hypothesis and use a knockout *Drosophila* strain for dTAT1 and monitor any nuclear deformations or changes in lateral MyoII recruitment.

6. Why do mesoderm cells rely on nuclear positioning to coordinate morphogenesis?

The essential role of nuclear positioning has been described across various species and contexts. For instance, it was demonstrated that interkinetic nuclear migration controls cell fate in the zebrafish neuroepithelium by exposing the nucleus to a morphogen gradient promoting either proliferation or neurogenesis along the apicobasal axis (Del Bene et al., 2008). Nuclear positioning is also necessary for many different cell behaviours including cell migration (Renkawitz et al., 2019), spindle positioning (Minc et al., 2011), and more recently for gonadogenesis (Agarwal et al., 2024). Efforts have thus been made to understand the mechanisms regulating nuclear positioning.

Here, I report a mechanism where actomyosin contractions generate a cytoplasmic flow, behaving as an incompressible fluid, that pushes the nucleus like a piston. Cytoplasmic streaming has been reported to ensure proper nuclear positioning and synchronize cell division cycles during early *Drosophila* embryogenesis (Deneke et al., 2019; Htet and Lauga, 2023). A piston-like mechanism involving pressure compartmentalization by the nucleus has also been reported to control cell migration and motility (Petrie et al., 2014; Lee et al., 2021). This phenomenon reflects the ability of elongated cells to translate localized cortical actomyosin contractions into long-range forces, as illustrated during the elongation phase of mesoderm cells in *Drosophila* embryo driven by a tissue-scale cytoplasmic flow (He et al., 2014). My findings provide evidence that the compartmentalization of cytoskeletal elements by the nucleus also allows for the spatiotemporal regulation of distinct morphogenetic events within the same cell. This is particularly relevant as this process occurs when the apicobasal polarity pathway is downregulated in the mesoderm tissue (Weng and Wieschaus, 2017), emphasizing the need for other mechanisms to spatially organize cytoskeletal dynamics.

7. Contraction or coalescence: a dive into the differential behaviour of subcellular actomyosin networks

I propose here that isotropic coalescence of the lateral actomyosin network leads to the formation of MyoII lateral clusters (MyoII-LCs) along the apicobasal axis. These MyoII-LCs then drive polarized cell intercalation by contracting cell junctions along the planar axis. This raises an important question: why does the actomyosin network coalesce along the apicobasal axis but contract along the planar axis? It is proposed that the mechanical coupling between the actomyosin network and junctional components, such as E-cadherin, is a necessary step to translate contractile behaviour into cell shape changes (Martin et al., 2009; Roh-Johnson et al., 2012). An interesting hypothesis could be that, in mesoderm cells, adherens junctions are established on the planar axis rather than the apicobasal axis. As MyoII is recruited along the lateral cortices, and no adherens junctions are present there, only coalescence can occur. It has been shown in the lab that the ectopic coalescence of MyoII can cluster scarce E-cad, alpha catenin and Beta-Catenin along the apicobasal axis to generate *ad hoc* spot adherens junctions (John and Rauzi, 2021a), thus serving as anchor points for contractile MyoII network only in the planar axis. It is possible that these newly-formed junctions associate with adhesion components at the tricellular junction, such as the proteins Sidekick or Canoe/Afadin, previously shown to be necessary to form tricellular adhesion junctions and engage with actomyosin networks to drive junctional remodeling (Bonello et al., 2018; Letizia et al., 2019; Uechi and Kuranaga, 2019). Addressing the subcellular distribution and dynamics of these junctional components could provide insights on the selective contractility in different axes here observed.

Interestingly, lateral MyoII accumulation has also been reported to drive lateral tension in mesoderm cells and participate to mesoderm internalization, as laser dissection of the lateral MyoII impedes mesoderm internalization (Gracia et al., 2019; John and Rauzi, 2021a). This suggests that apicobasal MyoII networks can generate contractile forces, probably contributing to the shortening of mesoderm cells during early gastrulation, as proposed by (Conte et al., 2012). However, MyoII-LCs might not be responsible for lateral tension, but rather apico-basal MyoII cables connected to the apical side (Gracia et al., 2019). I propose that these cables form when MyoII remain tethered to the apical adherens junctions, enabling them to pull on the cell cortices and drive contraction along the apicobasal axis. As a result, apicobasal cables responsible for increased lateral tension, and MyoII-LCs responsible for polarized intercalations, would coexist within the tissue to drive the concomitant folding and extension of the presumptive mesoderm. Investigating the factors that determine whether the apical tethering of lateral MyoII is stochastic or controlled would be valuable in understanding how actomyosin contractility is modulated along different axes within the same cell.

References

- Abraham, V. C., Krishnamurthi, V., Taylor, D. L., and Lanni, F. (1999). The Actin-Based Nanomachine at the Leading Edge of Migrating Cells. *Biophys. J.* 77, 1721–1732. doi: 10.1016/S0006-3495(99)77018-9
- Abraham, Z., Hawley, E., Hayosh, D., Webster-Wood, V. A., and Akkus, O. (2018). Kinesin and Dynein Mechanics: Measurement Methods and Research Applications. *J. Biomech. Eng.* 140, 0208051–02080511. doi: 10.1115/1.4037886
- Adler, P. N. (2012). “The *frizzled/stan* Pathway and Planar Cell Polarity in the *Drosophila* Wing,” in *Current Topics in Developmental Biology*, ed. Y. Yang (Academic Press), 1–31. doi: 10.1016/B978-0-12-394592-1.00001-6
- Agarwal, P., Berger, S., Shemesh, T., and Zaidel-Bar, R. (2024). Active nuclear positioning and actomyosin contractility maintain leader cell integrity during gonadogenesis. *Curr. Biol.* 34, 2373–2386.e5. doi: 10.1016/j.cub.2024.03.049
- Agarwal, P., and Zaidel-Bar, R. (2019). Principles of Actomyosin Regulation In Vivo. *Trends Cell Biol.* 29, 150–163. doi: 10.1016/j.tcb.2018.09.006
- Akhmanova, A., and Kapitein, L. C. (2022). Mechanisms of microtubule organization in differentiated animal cells. *Nat. Rev. Mol. Cell Biol.* 23, 541–558. doi: 10.1038/s41580-022-00473-y
- Akhmanova, A., Stehbens, S. J., and Yap, A. S. (2009). Touch, grasp, deliver and control: functional cross-talk between microtubules and cell adhesions. *Traffic Cph. Den.* 10, 268–274. doi: 10.1111/j.1600-0854.2008.00869.x
- Akhmanova, A., and Steinmetz, M. O. (2015). Control of microtubule organization and dynamics: two ends in the limelight. *Nat. Rev. Mol. Cell Biol.* 16, 711–726. doi: 10.1038/nrm4084
- Akiyoshi, B., Sarangapani, K. K., Powers, A. F., Nelson, C. R., Reichow, S. L., Arellano-Santoyo, H., et al. (2010). Tension directly stabilizes reconstituted kinetochore-microtubule attachments. *Nature* 468, 576–579. doi: 10.1038/nature09594
- Ambrosini, A., Rayer, M., Monier, B., and Suzanne, M. (2019). Mechanical Function of the Nucleus in Force Generation during Epithelial Morphogenesis. *Dev. Cell* 50, 197–211.e5. doi: 10.1016/j.devcel.2019.05.027
- Anderson, K. V., Bokla, L., and Nüsslein-Volhard, C. (1985). Establishment of dorsal-ventral polarity in the *Drosophila* embryo: The induction of polarity by the Toll gene product. *Cell* 42, 791–798. doi: 10.1016/0092-8674(85)90275-2
- Anderson, K. V., and Nüsslein-Volhard, C. (1984). Information for the dorsal–ventral pattern of the *Drosophila* embryo is stored as maternal mRNA. *Nature* 311, 223–227. doi: 10.1038/311223a0
- Andreu-Carbó, M., Egoldt, C., Velluz, M.-C., and Aumeier, C. (2024). Microtubule damage shapes the acetylation gradient. *Nat. Commun.* 15, 2029. doi: 10.1038/s41467-024-46379-5

- Arnold, T. R., Stephenson, R. E., and Miller, A. L. (2017). Rho GTPases and actomyosin: Partners in regulating epithelial cell-cell junction structure and function. *Exp. Cell Res.* 358, 20–30. doi: 10.1016/j.yexcr.2017.03.053
- Asbury, C. L. (2017). Anaphase A: Disassembling Microtubules Move Chromosomes toward Spindle Poles. *Biology* 6, 15. doi: 10.3390/biology6010015
- Avagliano, L., Massa, V., George, T. M., Qureshy, S., Bulfamante, G., and Finnell, R. H. (2019). Overview on Neural tube defects: from development to physical characteristics. *Birth Defects Res.* 111, 1455–1467. doi: 10.1002/bdr2.1380
- Aw, W. Y., Heck, B. W., Joyce, B., and Devenport, D. (2016). Transient Tissue-Scale Deformation Coordinates Alignment of Planar Cell Polarity Junctions in the Mammalian Skin. *Curr. Biol.* 26, 2090–2100. doi: 10.1016/j.cub.2016.06.030
- Azevedo, D., Antunes, M., Prag, S., Ma, X., Hacker, U., Brodland, G. W., et al. (2011). DRhoGEF2 Regulates Cellular Tension and Cell Pulsations in the Amnioserosa during *Drosophila* Dorsal Closure. *PLoS ONE* 6. doi: 10.1371/journal.pone.0023964
- Bailles, A., Collinet, C., Philippe, J.-M., Lenne, P.-F., Munro, E., and Lecuit, T. (2019). Genetic induction and mechanochemical propagation of a morphogenetic wave. *Nature* 572, 467–473. doi: 10.1038/s41586-019-1492-9
- Baker, P. C., and Schroeder, T. E. (1967). Cytoplasmic filaments and morphogenetic movement in the amphibian neural tube. *Dev. Biol.* 15, 432–450. doi: 10.1016/0012-1606(67)90036-X
- Bambardekar, K., Clément, R., Blanc, O., Chardès, C., and Lenne, P.-F. (2015). Direct laser manipulation reveals the mechanics of cell contacts in vivo. *Proc. Natl. Acad. Sci. U. S. A.* 112, 1416–1421. doi: 10.1073/pnas.1418732112
- Bamburg, J. R., Harris, H. E., and Weeds, A. G. (1980). Partial purification and characterization of an actin depolymerizing factor from brain. *FEBS Lett.* 121, 178–182. doi: 10.1016/0014-5793(80)81292-0
- Bardet, P.-L., Guirao, B., Paoletti, C., Serman, F., Léopold, V., Bosveld, F., et al. (2013). PTEN Controls Junction Lengthening and Stability during Cell Rearrangement in Epithelial Tissue. *Dev. Cell* 25, 534–546. doi: 10.1016/j.devcel.2013.04.020
- Bastock, R., and St Johnston, D. (2008). *Drosophila* oogenesis. *Curr. Biol. CB* 18, R1082–1087. doi: 10.1016/j.cub.2008.09.011
- Bastock, R., Strutt, H., and Strutt, D. (2003). Strabismus is asymmetrically localised and binds to Prickle and Dishevelled during *Drosophila* planar polarity patterning. *Development* 130, 3007–3014. doi: 10.1242/dev.00526
- Baumgartner, S., Littleton, J. T., Broadie, K., Bhat, M. A., Harbecke, R., Lengyel, J. A., et al. (1996). A *Drosophila* Neurexin Is Required for Septate Junction and Blood-Nerve Barrier Formation and Function. *Cell* 87, 1059–1068. doi: 10.1016/S0092-8674(00)81800-0

- Bayonas, A. G. D. L., Philippe, J.-M., Lellouch, A. C., and Lecuit, T. (2019). Distinct RhoGEFs Activate Apical and Junctional Contractility under Control of G Proteins during Epithelial Morphogenesis. *Curr. Biol.* 29, 3370-3385.e7. doi: 10.1016/j.cub.2019.08.017
- Bennett, F. C., and Harvey, K. F. (2006). Fat Cadherin Modulates Organ Size in *Drosophila* via the Salvador/Warts/Hippo Signaling Pathway. *Curr. Biol.* 16, 2101–2110. doi: 10.1016/j.cub.2006.09.045
- Bertet, C., Sulak, L., and Lecuit, T. (2004). Myosin-dependent junction remodelling controls planar cell intercalation and axis elongation. *Nature* 429, 667–671. doi: 10.1038/nature02590
- Bertocchi, C., Wang, Y., Ravasio, A., Hara, Y., Wu, Y., Sailov, T., et al. (2017). Nanoscale architecture of cadherin-based cell adhesions. *Nat. Cell Biol.* 19, 28–37. doi: 10.1038/ncb3456
- Bilder, D., Schober, M., and Perrimon, N. (2003). Integrated activity of PDZ protein complexes regulates epithelial polarity. *Nat. Cell Biol.* 5, 53–58. doi: 10.1038/ncb897
- Blake-Hedges, C., and Megraw, T. L. (2019). “Coordination of Embryogenesis by the Centrosome in *Drosophila melanogaster*,” in *The Golgi Apparatus and Centriole: Functions, Interactions and Role in Disease*, ed. M. Kloc (Cham: Springer International Publishing), 277–321. doi: 10.1007/978-3-030-23173-6_12
- Blanchard, G. B., Murugesu, S., Adams, R. J., Martinez-Arias, A., and Gorfinkiel, N. (2010). Cytoskeletal dynamics and supracellular organisation of cell shape fluctuations during dorsal closure. *Development* 137, 2743–2752. doi: 10.1242/dev.045872
- Blankenship, J. T., Backovic, S. T., Sanny, J. S. P., Weitz, O., and Zallen, J. A. (2006). Multicellular rosette formation links planar cell polarity to tissue morphogenesis. *Dev. Cell* 11, 459–470. doi: 10.1016/j.devcel.2006.09.007
- Boller, K., Vestweber, D., and Kemler, R. (1985). Cell-adhesion molecule uvomorulin is localized in the intermediate junctions of adult intestinal epithelial cells. *J. Cell Biol.* 100, 327–332. doi: 10.1083/jcb.100.1.327
- Bonello, T. T., Perez-Vale, K. Z., Sumigray, K. D., and Peifer, M. (2018). Rap1 acts via multiple mechanisms to position Canoe and adherens junctions and mediate apical-basal polarity establishment. *Dev. Camb. Engl.* 145, dev157941. doi: 10.1242/dev.157941
- Booth, A. J. R., Blanchard, G. B., Adams, R. J., and Röper, K. (2014). A Dynamic Microtubule Cytoskeleton Directs Medial Actomyosin Function during Tube Formation. *Dev. Cell* 29, 562–576. doi: 10.1016/j.devcel.2014.03.023
- Brendza, R. P., Serbus, L. R., Duffy, J. B., and Saxton, W. M. (2000). A Function for Kinesin I in the Posterior Transport of oskar mRNA and Staufen Protein. *Science* 289, 2120–2122. doi: 10.1126/science.289.5487.2120
- Bresnick, A. R. (1999). Molecular mechanisms of nonmuscle myosin-II regulation. *Curr. Opin. Cell Biol.* 11, 26–33. doi: 10.1016/s0955-0674(99)80004-0

- Brito, C., and Sousa, S. (2020). Non-Muscle Myosin 2A (NM2A): Structure, Regulation and Function. *Cells* 9, 1590. doi: 10.3390/cells9071590
- Brouhard, G. J., and Rice, L. M. (2018). Microtubule dynamics: an interplay of biochemistry and mechanics. *Nat. Rev. Mol. Cell Biol.* 19, 451–463. doi: 10.1038/s41580-018-0009-y
- Brown, N. H., Gregory, S. L., and Martin-Bermudo, M. D. (2000). Integrins as Mediators of Morphogenesis in *Drosophila*. *Dev. Biol.* 223, 1–16. doi: 10.1006/dbio.2000.9711
- Bryan, C. D., Casey, M. A., Pfeiffer, R. L., Jones, B. W., and Kwan, K. M. (2020). Optic cup morphogenesis requires neural crest-mediated basement membrane assembly. *Dev. Camb. Engl.* 147, dev181420. doi: 10.1242/dev.181420
- Bryant, P. J., Huettner, B., Held, L. I., Ryerse, J., and Szidonya, J. (1988). Mutations at the *fat* locus interfere with cell proliferation control and epithelial morphogenesis in *Drosophila*. *Dev. Biol.* 129, 541–554. doi: 10.1016/0012-1606(88)90399-5
- Buckley, C. E., and St Johnston, D. (2022). Apical-basal polarity and the control of epithelial form and function. *Nat. Rev. Mol. Cell Biol.* 23, 559–577. doi: 10.1038/s41580-022-00465-y
- Budnar, S., Husain, K. B., Gomez, G. A., Naghibosadat, M., Varma, A., Verma, S., et al. (2019). Anillin Promotes Cell Contractility by Cyclic Resetting of RhoA Residence Kinetics. *Dev. Cell* 49, 894-906.e12. doi: 10.1016/j.devcel.2019.04.031
- Bulgakova, N. A., Grigoriev, I., Yap, A. S., Akhmanova, A., and Brown, N. H. (2013). Dynamic microtubules produce an asymmetric E-cadherin–Bazooka complex to maintain segment boundaries. *J. Cell Biol.* 201, 887–901. doi: 10.1083/jcb.201211159
- Burgess, D. R., Broschat, K. O., and Hayden, J. M. (1987). Tropomyosin distinguishes between the two actin-binding sites of villin and affects actin-binding properties of other brush border proteins. *J. Cell Biol.* 104, 29–40. doi: 10.1083/jcb.104.1.29
- Butler, L. C., Blanchard, G. B., Kabla, A. J., Lawrence, N. J., Welchman, D. P., Mahadevan, L., et al. (2009). Cell shape changes indicate a role for extrinsic tensile forces in *Drosophila* germ-band extension. *Nat. Cell Biol.* 11, 859–864. doi: 10.1038/ncb1894
- Butler, M. T., and Wallingford, J. B. (2017). Planar cell polarity in development and disease. *Nat. Rev. Mol. Cell Biol.* 18, 375–388. doi: 10.1038/nrm.2017.11
- Campàs, O., Mammoto, T., Hasso, S., Sperling, R. A., O’Connell, D., Bischof, A. G., et al. (2014). Quantifying cell-generated mechanical forces within living embryonic tissues. *Nat. Methods* 11, 183–189. doi: 10.1038/nmeth.2761
- Campàs, O., Noordstra, I., and Yap, A. S. (2024). Adherens junctions as molecular regulators of emergent tissue mechanics. *Nat. Rev. Mol. Cell Biol.* 25, 252–269. doi: 10.1038/s41580-023-00688-7
- Campbell, N. A., Mitchell, L. G., and Reece, J. B. (2000). *Biology: concepts & connections.*, 3rd edition. San Francisco: Benjamin/Cummings.

- Campinho, P., Behrndt, M., Ranft, J., Risler, T., Minc, N., and Heisenberg, C.-P. (2013). Tension-oriented cell divisions limit anisotropic tissue tension in epithelial spreading during zebrafish epiboly. *Nat. Cell Biol.* 15, 1405–1414. doi: 10.1038/ncb2869
- Canman, J. C., and Bement, W. M. (1997). Microtubules suppress actomyosin-based cortical flow in *Xenopus* oocytes. *J. Cell Sci.* 110 (Pt 16), 1907–1917. doi: 10.1242/jcs.110.16.1907
- Cao, J., Albertson, R., Riggs, B., Field, C. M., and Sullivan, W. (2008). Nuf, a Rab11 effector, maintains cytokinetic furrow integrity by promoting local actin polymerization. *J. Cell Biol.* 182, 301–313. doi: 10.1083/jcb.200712036
- Cao, W., Goodarzi, J. P., and De La Cruz, E. M. (2006). Energetics and kinetics of cooperative cofilin-actin filament interactions. *J. Mol. Biol.* 361, 257–267. doi: 10.1016/j.jmb.2006.06.019
- Carlier, M. F. (1989). Role of nucleotide hydrolysis in the dynamics of actin filaments and microtubules. *Int. Rev. Cytol.* 115, 139–170. doi: 10.1016/s0074-7696(08)60629-4
- Cartagena-Rivera, A. X., Logue, J. S., Waterman, C. M., and Chadwick, R. S. (2016). Actomyosin Cortical Mechanical Properties in Nonadherent Cells Determined by Atomic Force Microscopy. *Biophys. J.* 110, 2528–2539. doi: 10.1016/j.bpj.2016.04.034
- Catala, M. (2021). Overview of Secondary Neurulation. *J. Korean Neurosurg. Soc.* 64, 346–358. doi: 10.3340/jkns.2020.0362
- Chanet, S., Miller, C. J., Vaishnav, E. D., Ermentrout, B., Davidson, L. A., and Martin, A. C. (2017). Actomyosin meshwork mechanosensing enables tissue shape to orient cell force. *Nat. Commun.* 8, 15014. doi: 10.1038/ncomms15014
- Chang, Y.-C., Nalbant, P., Birkenfeld, J., Chang, Z.-F., and Bokoch, G. M. (2008). GEF-H1 Couples Nocodazole-induced Microtubule Disassembly to Cell Contractility via RhoA. *Mol. Biol. Cell* 19, 2147–2153. doi: 10.1091/mbc.e07-12-1269
- Charras, G., and Yap, A. S. (2018). Tensile Forces and Mechanotransduction at Cell-Cell Junctions. *Curr. Biol. CB* 28, R445–R457. doi: 10.1016/j.cub.2018.02.003
- Chasan, R., Jin, Y., and Anderson, K. V. (1992). Activation of the easter zymogen is regulated by five other genes to define dorsal-ventral polarity in the *Drosophila* embryo. *Dev. Camb. Engl.* 115, 607–616. doi: 10.1242/dev.115.2.607
- Cheshire, A. M., Kerman, B. E., Zipfel, W. R., Spector, A. A., and Andrew, D. J. (2008). Kinetic and mechanical analysis of live tube morphogenesis. *Dev. Dyn. Off. Publ. Am. Assoc. Anat.* 237, 2874–2888. doi: 10.1002/dvdy.21709
- Chien, Y.-H., Keller, R., Kintner, C., and Shook, D. R. (2015). Mechanical Strain Determines the Axis of Planar Polarity in Ciliated Epithelia. *Curr. Biol.* 25, 2774–2784. doi: 10.1016/j.cub.2015.09.015

- Cho, N. K., Keyes, L., Johnson, E., Heller, J., Ryner, L., Karim, F., et al. (2002). Developmental Control of Blood Cell Migration by the Drosophila VEGF Pathway. *Cell* 108, 865–876. doi: 10.1016/S0092-8674(02)00676-1
- Chopra, V. S., and Levine, M. (2009). Combinatorial patterning mechanisms in the Drosophila embryo. *Brief. Funct. Genomic. Proteomic.* 8, 243–249. doi: 10.1093/bfgp/elp026
- Christodoulou, N., and Skourides, P. A. (2022). Distinct spatiotemporal contribution of morphogenetic events and mechanical tissue coupling during Xenopus neural tube closure. *Dev. Camb. Engl.* 149, dev200358. doi: 10.1242/dev.200358
- Chu, S., Moujaber, O., Lemay, S., and Stochaj, U. (2022). Multiple pathways promote microtubule stabilization in senescent intestinal epithelial cells. *Npj Aging* 8, 1–12. doi: 10.1038/s41514-022-00097-8
- Chung, S., Kim, S., and Andrew, D. J. (2017). Uncoupling apical constriction from tissue invagination. *eLife*. doi: 10.7554/eLife.22235
- Clarke, D. N., and Martin, A. C. (2021). Actin-based force generation and cell adhesion in tissue morphogenesis. *Curr. Biol.* 31, R667–R680. doi: 10.1016/j.cub.2021.03.031
- Clément, R., Dehapiot, B., Collinet, C., Lecuit, T., and Lenne, P.-F. (2017). Viscoelastic Dissipation Stabilizes Cell Shape Changes during Tissue Morphogenesis. *Curr. Biol. CB* 27, 3132–3142.e4. doi: 10.1016/j.cub.2017.09.005
- Collinet, C., Rauzi, M., Lenne, P.-F., and Lecuit, T. (2015). Local and tissue-scale forces drive oriented junction growth during tissue extension. *Nat. Cell Biol.* 17, 1247–1258. doi: 10.1038/ncb3226
- Conde, C., and Cáceres, A. (2009). Microtubule assembly, organization and dynamics in axons and dendrites. *Nat. Rev. Neurosci.* 10, 319–332. doi: 10.1038/nrn2631
- Conte, V., Ulrich, F., Baum, B., Muñoz, J., Veldhuis, J., Brodland, W., et al. (2012). A Biomechanical Analysis of Ventral Furrow Formation in the Drosophila *Melanogaster* Embryo. *PLoS ONE* 7, e34473. doi: 10.1371/journal.pone.0034473
- Conti, M. A., and Adelstein, R. S. (2008). Nonmuscle myosin II moves in new directions. *J. Cell Sci.* 121, 11–18. doi: 10.1242/jcs.007112
- Conti, M. A., Sellers, J. R., Adelstein, R. S., and Elzinga, M. (1991). Identification of the serine residue phosphorylated by protein kinase C in vertebrate nonmuscle myosin heavy chains. *Biochemistry* 30, 966–970. doi: 10.1021/bi00218a012
- Costa, M., Wilson, E. T., and Wieschaus, E. (1994). A putative cell signal encoded by the folded gastrulation gene coordinates cell shape changes during Drosophila gastrulation. *Cell* 76, 1075–1089. doi: 10.1016/0092-8674(94)90384-0
- Courtemanche, N. (2018). Mechanisms of formin-mediated actin assembly and dynamics. *Biophys. Rev.* 10, 1553–1569. doi: 10.1007/s12551-018-0468-6

- Crisp, M., Liu, Q., Roux, K., Rattner, J. B., Shanahan, C., Burke, B., et al. (2006). Coupling of the nucleus and cytoplasm: role of the LINC complex. *J. Cell Biol.* 172, 41–53. doi: 10.1083/jcb.200509124
- Curran, S., Strandkvist, C., Bathmann, J., Gennes, M. de, Kabla, A., Salbreux, G., et al. (2017). Myosin II Controls Junction Fluctuations to Guide Epithelial Tissue Ordering. *Dev. Cell* 43, 480–492.e6. doi: 10.1016/j.devcel.2017.09.018
- Davidson, L. A., and Keller, R. E. (1999). Neural tube closure in *Xenopus laevis* involves medial migration, directed protrusive activity, cell intercalation and convergent extension. *Development* 126, 4547–4556. doi: 10.1242/dev.126.20.4547
- Dawes-Hoang, R. E., Parmar, K. M., Christiansen, A. E., Phelps, C. B., Brand, A. H., and Wieschaus, E. F. (2007). *folded gastrulation*, cell shape change and the control of myosin localization. *Development* 134, 4507–4507. doi: 10.1242/dev.017343
- Defranco, B. H., Nickel, B. M., Baty, C. J., Martinez, J. S., Gay, V. L., Sandulache, V. C., et al. (2008). Migrating Cells Retain Gap Junction Plaque Structure and Function. *Cell Commun. Adhes.* 15, 273–288. doi: 10.1080/15419060802198298
- Degelmann, A., Hardy, P. A., Perrimon, N., and Mahowald, A. P. (1986). Developmental analysis of the torso-like phenotype in *Drosophila* produced by a maternal-effect locus. *Dev. Biol.* 115, 479–489. doi: 10.1016/0012-1606(86)90268-X
- Del Bene, F., Wehman, A. M., Link, B. A., and Baier, H. (2008). Regulation of Neurogenesis by Interkinetic Nuclear Migration through an Apical-Basal Notch Gradient. *Cell* 134, 1055–1065. doi: 10.1016/j.cell.2008.07.017
- del Valle Rodríguez, A., Didiano, D., and Desplan, C. (2012). Power tools for gene expression and clonal analysis in *Drosophila*. *Nat. Methods* 9, 47–55. doi: 10.1038/nmeth.1800
- Deneke, V. E., Puliafito, A., Krueger, D., Narla, A. V., Simone, A. D., Primo, L., et al. (2019). Self-Organized Nuclear Positioning Synchronizes the Cell Cycle in *Drosophila* Embryos. *Cell* 177, 925–941.e17. doi: 10.1016/j.cell.2019.03.007
- Desai, A., and Mitchison, T. J. (1997). Microtubule polymerization dynamics. *Annu. Rev. Cell Dev. Biol.* 13, 83–117. doi: 10.1146/annurev.cellbio.13.1.83
- Deshpande, O., and Telley, I. A. (2021). Nuclear positioning during development: Pushing, pulling and flowing. *Semin. Cell Dev. Biol.* 120, 10–21. doi: 10.1016/j.semcdb.2021.09.020
- Devenport, D. (2014). The cell biology of planar cell polarity. *J. Cell Biol.* 207, 171–179. doi: 10.1083/jcb.201408039
- Dogterom, M., Kerssemakers, J. W. J., Romet-Lemonne, G., and Janson, M. E. (2005). Force generation by dynamic microtubules. *Curr. Opin. Cell Biol.* 17, 67–74. doi: 10.1016/j.ceb.2004.12.011
- Dogterom, M., and Yurke, B. (1997). Measurement of the force-velocity relation for growing microtubules. *Science* 278, 856–860. doi: 10.1126/science.278.5339.856

- Dominguez, R., and Holmes, K. C. (2011). Actin Structure and Function. *Annu. Rev. Biophys.* 40, 169–186. doi: 10.1146/annurev-biophys-042910-155359
- Domínguez-Giménez, P., Brown, N. H., and Martín-Bermudo, M. D. (2007). Integrin-ECM interactions regulate the changes in cell shape driving the morphogenesis of the *Drosophila* wing epithelium. *J. Cell Sci.* 120, 1061–1071. doi: 10.1242/jcs.03404
- Driever, W., and Nüsslein-Volhard, C. (1988a). A gradient of bicoid protein in *Drosophila* embryos. *Cell* 54, 83–93. doi: 10.1016/0092-8674(88)90182-1
- Driever, W., and Nüsslein-Volhard, C. (1988b). The *bicoid* protein determines position in the *Drosophila* embryo in a concentration-dependent manner. *Cell* 54, 95–104. doi: 10.1016/0092-8674(88)90183-3
- Driever, W., Siegel, V., and Nüsslein-Volhard, C. (1990). Autonomous determination of anterior structures in the early *Drosophila* embryo by the bicoid morphogen. *Development* 109, 811–820. doi: 10.1242/dev.109.4.811
- Dudin, O., Ondracka, A., Grau-Bové, X., Haraldsen, A. A., Toyoda, A., Suga, H., et al. (2019). A unicellular relative of animals generates a layer of polarized cells by actomyosin-dependent cellularization. *eLife* 8, e49801. doi: 10.7554/eLife.49801
- Dulyaninova, N. G., House, R. P., Betapudi, V., and Bresnick, A. R. (2007). Myosin-IIA Heavy-Chain Phosphorylation Regulates the Motility of MDA-MB-231 Carcinoma Cells. *Mol. Biol. Cell* 18, 3144–3155. doi: 10.1091/mbc.e06-11-1056
- Dupin, I., and Etienne-Manneville, S. (2011). Nuclear positioning: Mechanisms and functions. *Int. J. Biochem. Cell Biol.* 43, 1698–1707. doi: 10.1016/j.biocel.2011.09.004
- Dutour-Provenzano, G., and Etienne-Manneville, S. (2021). Intermediate filaments. *Curr. Biol.* 31, R522–R529. doi: 10.1016/j.cub.2021.04.011
- Edwards, M., McConnell, P., Schafer, D. A., and Cooper, J. A. (2015). CPI motif interaction is necessary for capping protein function in cells. *Nat. Commun.* 6, 8415. doi: 10.1038/ncomms9415
- Edwards, M., Zwolak, A., Schafer, D. A., Sept, D., Dominguez, R., and Cooper, J. A. (2014). Capping protein regulators fine-tune actin assembly dynamics. *Nat. Rev. Mol. Cell Biol.* 15, 677–689. doi: 10.1038/nrm3869
- Eldirany, S. A., Lomakin, I. B., Ho, M., and Bunick, C. G. (2021). Recent insight into intermediate filament structure. *Curr. Opin. Cell Biol.* 68, 132–143. doi: 10.1016/j.ceb.2020.10.001
- Ellefsen, K. L., Holt, J. R., Chang, A. C., Nourse, J. L., Arulmoli, J., Mekhdjian, A. H., et al. (2019). Myosin-II mediated traction forces evoke localized Piezo1-dependent Ca²⁺ flickers. *Commun. Biol.* 2, 298. doi: 10.1038/s42003-019-0514-3
- Elosegui-Artola, A., Trepap, X., and Roca-Cusachs, P. (2018). Control of Mechanotransduction by Molecular Clutch Dynamics. *Trends Cell Biol.* 28, 356–367. doi: 10.1016/j.tcb.2018.01.008

- Elsum, I., Yates, L., Humbert, P. O., and Richardson, H. E. (2012). The Scribble-Dlg-Lgl polarity module in development and cancer: from flies to man. *Essays Biochem.* 53, 141–168. doi: 10.1042/bse0530141
- Ephrussi, A., Dickinson, L. K., and Lehmann, R. (1991). oskar organizes the germ plasm and directs localization of the posterior determinant nanos. *Cell* 66, 37–50. doi: 10.1016/0092-8674(91)90137-N
- Farquhar, M. G., and Palade, G. E. (1963). Junctional complexes in various epithelia. *J. Cell Biol.* 17, 375–412. doi: 10.1083/jcb.17.2.375
- Farrell, J., and O'Farrell, P. (2014). From Egg to Gastrula: How the Cell Cycle Is Remodeled During the Drosophila Mid-Blastula Transition. *Annu. Rev. Genet.* 48. doi: 10.1146/annurev-genet-111212-133531
- Fernandez-Gonzalez, R., Simoes, S. de M., Röper, J.-C., Eaton, S., and Zallen, J. A. (2009). Myosin II Dynamics Are Regulated by Tension in Intercalating Cells. *Dev. Cell* 17, 736–743. doi: 10.1016/j.devcel.2009.09.003
- Fick, A. (1858). *Die medizinische Physik*. Vieweg.
- Fierling, J., John, A., Delorme, B., Torzynski, A., Blanchard, G. B., Lye, C. M., et al. (2022). Embryo-scale epithelial buckling forms a propagating furrow that initiates gastrulation. *Nat. Commun.* 13, 3348. doi: 10.1038/s41467-022-30493-3
- Finer, J. T., Simmons, R. M., and Spudich, J. A. (1994). Single myosin molecule mechanics: piconewton forces and nanometre steps. *Nature* 368, 113–119. doi: 10.1038/368113a0
- Fink, G., Hajdo, L., Skowronek, K. J., Reuther, C., Kasprzak, A. A., and Diez, S. (2009). The mitotic kinesin-14 Ncd drives directional microtubule-microtubule sliding. *Nat. Cell Biol.* 11, 717–723. doi: 10.1038/ncb1877
- Foe, V. E., Field, C. M., and Odell, G. M. (2000). Microtubules and mitotic cycle phase modulate spatiotemporal distributions of F-actin and myosin II in Drosophila syncytial blastoderm embryos. *Dev. Camb. Engl.* 127, 1767–1787. doi: 10.1242/dev.127.9.1767
- Fouchard, J., Wyatt, T. P. J., Proag, A., Lisica, A., Khalilgharibi, N., Recho, P., et al. (2020). Curling of epithelial monolayers reveals coupling between active bending and tissue tension. *Proc. Natl. Acad. Sci.* 117, 9377–9383. doi: 10.1073/pnas.1917838117
- Frasch, M., and Nguyen, H. T. (1999). “Genetic Control of Mesoderm Patterning and Differentiation During *Drosophila* Embryogenesis,” in *Advances in Developmental Biochemistry*, ed. P. M. Wassarman (Academic Press), 1–47. doi: 10.1016/S1064-2722(08)60015-8
- Friedl, P., and Gilmour, D. (2009). Collective cell migration in morphogenesis, regeneration and cancer. *Nat. Rev. Mol. Cell Biol.* 10, 445–457. doi: 10.1038/nrm2720

- Friedland, J. C., Lee, M. H., and Boettiger, D. (2009). Mechanically activated integrin switch controls alpha5beta1 function. *Science* 323, 642–644. doi: 10.1126/science.1168441
- Frohnhofer, H. G., and Nüsslein-Volhard, C. (1986). Organization of anterior pattern in the *Drosophila* embryo by the maternal gene bicoid. *Nature* 324, 120–125. doi: 10.1038/324120a0
- Fujii, T., Iwane, A. H., Yanagida, T., and Namba, K. (2010). Direct visualization of secondary structures of F-actin by electron cryomicroscopy. *Nature* 467, 724–728. doi: 10.1038/nature09372
- Fujiwara, I., Vavylonis, D., and Pollard, T. D. (2007). Polymerization kinetics of ADP- and ADP-Pi-actin determined by fluorescence microscopy. *Proc. Natl. Acad. Sci. U. S. A.* 104, 8827–8832. doi: 10.1073/pnas.0702510104
- Fulford, A. D., and McNeill, H. (2020). Fat/Dachsous family cadherins in cell and tissue organisation. *Curr. Opin. Cell Biol.* 62, 96–103. doi: 10.1016/j.ceb.2019.10.006
- Furlong, E. E. M., and Levine, M. (2018). Developmental enhancers and chromosome topology. *Science* 361, 1341–1345. doi: 10.1126/science.aau0320
- Gao, B., Song, H., Bishop, K., Elliot, G., Garrett, L., English, M. A., et al. (2011). Wnt Signaling Gradients Establish Planar Cell Polarity by Inducing Vangl2 Phosphorylation through Ror2. *Dev. Cell* 20, 163–176. doi: 10.1016/j.devcel.2011.01.001
- Gasser, E. (1878). *Der Primitivstreifen bei Vogelembryonen (Huhn und Gans)*. Marburg. Available at: <http://archive.org/details/primitivstreife00gass> (Accessed June 11, 2024).
- Gehrels, E. W., Chakraborty, B., Perrin, M.-E., Merkel, M., and Lecuit, T. (2023). Curvature gradient drives polarized tissue flow in the *Drosophila* embryo. *Proc. Natl. Acad. Sci.* 120, e2214205120. doi: 10.1073/pnas.2214205120
- Gelbart, M. A., He, B., Martin, A. C., Thiberge, S. Y., Wieschaus, E. F., and Kaschube, M. (2012). Volume conservation principle involved in cell lengthening and nucleus movement during tissue morphogenesis. *Proc. Natl. Acad. Sci.* 109, 19298–19303. doi: 10.1073/pnas.1205258109
- Gerri, C., Menchero, S., Mahadevaiah, S. K., Turner, J. M. A., and Niakan, K. K. (2020). Human Embryogenesis: A Comparative Perspective. *Annu. Rev. Cell Dev. Biol.* 36, 411–440. doi: 10.1146/annurev-cellbio-022020-024900
- Gheisari, E., Aakhte, M., and Müller, H.-A. J. (2020). Gastrulation in *Drosophila melanogaster*: Genetic control, cellular basis and biomechanics. *Mech. Dev.* 163, 103629. doi: 10.1016/j.mod.2020.103629
- Gibson, M. C., and Perrimon, N. (2003). Apicobasal polarization: epithelial form and function. *Curr. Opin. Cell Biol.* 15, 747–752. doi: 10.1016/j.ceb.2003.10.008
- Gilbert, S. F., and Barresi, M. J. F. (2016). *Developmental Biology*. Sinauer Associates, Incorporated.

- Gillies, T. E., and Cabernard, C. (2011). Cell Division Orientation in Animals. *Curr. Biol.* 21, R599–R609. doi: 10.1016/j.cub.2011.06.055
- Gilmour, D., Rembold, M., and Leptin, M. (2017). From morphogen to morphogenesis and back. *Nature* 541, 311–320. doi: 10.1038/nature21348
- Godt, D., and Tepass, U. (1998). Drosophila oocyte localization is mediated by differential cadherin-based adhesion. *Nature* 395, 387–391. doi: 10.1038/26493
- Gómez, H. F., Dumond, M. S., Hodel, L., Vetter, R., and Iber, D. (2021). 3D cell neighbour dynamics in growing pseudostratified epithelia. *eLife* 10, e68135. doi: 10.7554/eLife.68135
- González-Crespo, S., and Levine, M. (1994). Related target enhancers for dorsal and NF-kappa B signaling pathways. *Science* 264, 255–258. doi: 10.1126/science.8146656
- González-Reyes, A., Elliott, H., and St Johnston, D. (1995). Polarization of both major body axes in Drosophila by gurken-torpedo signalling. *Nature* 375, 654–658. doi: 10.1038/375654a0
- Goode, B. L., and Eck, M. J. (2007). Mechanism and Function of Formins in the Control of Actin Assembly. *Annu. Rev. Biochem.* 76, 593–627. doi: 10.1146/annurev.biochem.75.103004.142647
- Gracia, M., Theis, S., Proag, A., Gay, G., Benassayag, C., and Suzanne, M. (2019). Mechanical impact of epithelial–mesenchymal transition on epithelial morphogenesis in Drosophila. *Nat. Commun.* 10, 2951. doi: 10.1038/s41467-019-10720-0
- Gregor, T., Tank, D. W., Wieschaus, E. F., and Bialek, W. (2007). Probing the limits to positional information. *Cell* 130, 153–164. doi: 10.1016/j.cell.2007.05.025
- Gubb, D., and García-Bellido, A. (1982). A genetic analysis of the determination of cuticular polarity during development in Drosophila melanogaster. *Development* 68, 37–57. doi: 10.1242/dev.68.1.37
- Gudimchuk, N. B., and McIntosh, J. R. (2021). Regulation of microtubule dynamics, mechanics and function through the growing tip. *Nat. Rev. Mol. Cell Biol.* 22, 777–795. doi: 10.1038/s41580-021-00399-x
- Guichet, A., Peri, F., and Roth, S. (2001). Stable Anterior Anchoring of the Oocyte Nucleus Is Required to Establish Dorsoventral Polarity of the *Drosophila* Egg. *Dev. Biol.* 237, 93–106. doi: 10.1006/dbio.2001.0354
- Gumbiner, B. M. (1996). Cell adhesion: the molecular basis of tissue architecture and morphogenesis. *Cell* 84, 345–357. doi: 10.1016/s0092-8674(00)81279-9
- Gundersen, G. G., and Worman, H. J. (2013). Nuclear Positioning. *Cell* 152, 1376–1389. doi: 10.1016/j.cell.2013.02.031
- Haas, P., and Gilmour, D. (2006). Chemokine Signaling Mediates Self-Organizing Tissue Migration in the Zebrafish Lateral Line. *Dev. Cell* 10, 673–680. doi: 10.1016/j.devcel.2006.02.019

- Haigo, S. L., Hildebrand, J. D., Harland, R. M., and Wallingford, J. B. (2003). Shroom Induces Apical Constriction and Is Required for Hinge-point Formation during Neural Tube Closure. *Curr. Biol.* 13, 2125–2137. doi: 10.1016/j.cub.2003.11.054
- Halbleib, J. M., and Nelson, W. J. (2006). Cadherins in development: cell adhesion, sorting, and tissue morphogenesis. *Genes Dev.* 20, 3199–3214. doi: 10.1101/gad.1486806
- Hall, S., and Ward, R. E. (2016). Septate Junction Proteins Play Essential Roles in Morphogenesis Throughout Embryonic Development in *Drosophila*. *G3 Bethesda Md* 6, 2375–2384. doi: 10.1534/g3.116.031427
- Hamer, J. E., Morrell, J. A., Hamer, L., Wolkow, T., and Momany, M. (1999). “Cellularization in *Aspergillus nidulans*,” in *The Fungal Colony*, eds. G. D. Robson, G. M. Gadd, and N. A. R. Gow (Cambridge: Cambridge University Press), 201–228. doi: 10.1017/CBO9780511549694.010
- Hampoelz, B., Azou-Gros, Y., Fabre, R., Markova, O., Puech, P.-H., and Lecuit, T. (2011). Microtubule-induced nuclear envelope fluctuations control chromatin dynamics in *Drosophila* embryos. *Development* 138, 3377–3386. doi: 10.1242/dev.065706
- Hannezo, E., Prost, J., and Joanny, J.-F. (2014). Theory of epithelial sheet morphology in three dimensions. *Proc. Natl. Acad. Sci.* 111, 27–32. doi: 10.1073/pnas.1312076111
- Hannus, M., Feiguin, F., Heisenberg, C.-P., and Eaton, S. (2002). Planar cell polarization requires *Widerborst*, a B' regulatory subunit of protein phosphatase 2A. *Development* 129, 3493–3503. doi: 10.1242/dev.129.14.3493
- Hao, H., Kalra, S., Jameson, L. E., Guerrero, L. A., Cain, N. E., Bolivar, J., et al. (2021). The Nesprin-1/-2 ortholog ANC-1 regulates organelle positioning in *C. elegans* independently from its KASH or actin-binding domains. *eLife* 10, e61069. doi: 10.7554/eLife.61069
- Haque, F., Lloyd, D. J., Smallwood, D. T., Dent, C. L., Shanahan, C. M., Fry, A. M., et al. (2006). SUN1 interacts with nuclear lamin A and cytoplasmic nesprins to provide a physical connection between the nuclear lamina and the cytoskeleton. *Mol. Cell. Biol.* 26, 3738–3751. doi: 10.1128/MCB.26.10.3738-3751.2006
- Harasim, M., Wunderlich, B., Peleg, O., Kröger, M., and Bausch, A. R. (2013). Direct Observation of the Dynamics of Semiflexible Polymers in Shear Flow. *Phys. Rev. Lett.* 110, 108302. doi: 10.1103/PhysRevLett.110.108302
- Hardin, J. D., and Cheng, L. Y. (1986). The mechanisms and mechanics of archenteron elongation during sea urchin gastrulation. *Dev. Biol.* 115, 490–501. doi: 10.1016/0012-1606(86)90269-1
- Harmansa, S., Erlich, A., Eloy, C., Zurlo, G., and Lecuit, T. (2023). Growth anisotropy of the extracellular matrix shapes a developing organ. *Nat. Commun.* 14, 1220. doi: 10.1038/s41467-023-36739-y
- Harris, T. J. C. (2012). Adherens junction assembly and function in the *Drosophila* embryo. *Int. Rev. Cell Mol. Biol.* 293, 45–83. doi: 10.1016/B978-0-12-394304-0.00007-5

- Harris, T. J. C., and Peifer, M. (2004). Adherens junction-dependent and -independent steps in the establishment of epithelial cell polarity in *Drosophila*. *J. Cell Biol.* 167, 135–147. doi: 10.1083/jcb.200406024
- Harris, T. J. C., and Tepass, U. (2010). Adherens junctions: from molecules to morphogenesis. *Nat. Rev. Mol. Cell Biol.* 11, 502–514. doi: 10.1038/nrm2927
- Hartenstein, V., and Campos-Ortega, J. A. (1985). Fate-mapping in wild-type *Drosophila melanogaster*. *Wilhelm Roux Arch. Dev. Biol.* 194, 181–195. doi: 10.1007/BF00848246
- Hashimoto, C., Hudson, K. L., and Anderson, K. V. (1988). The Toll gene of *Drosophila*, required for dorsal-ventral embryonic polarity, appears to encode a transmembrane protein. *Cell* 52, 269–279. doi: 10.1016/0092-8674(88)90516-8
- Hashimoto, C., Kim, D. R., Weiss, L. A., Miller, J. W., and Morisato, D. (2003). Spatial regulation of developmental signaling by a serpin. *Dev. Cell* 5, 945–950. doi: 10.1016/s1534-5807(03)00338-1
- Haviv, L., Gillo, D., Backouche, F., and Bernheim-Groswasser, A. (2008). A Cytoskeletal Demolition Worker: Myosin II Acts as an Actin Depolymerization Agent. *J. Mol. Biol.* 375, 325–330. doi: 10.1016/j.jmb.2007.09.066
- Hawkins, T., Mirigian, M., Selcuk Yasar, M., and Ross, J. L. (2010). Mechanics of microtubules. *J. Biomech.* 43, 23–30. doi: 10.1016/j.jbiomech.2009.09.005
- He, B., Doubrovinski, K., Polyakov, O., and Wieschaus, E. (2014). Apical constriction drives tissue-scale hydrodynamic flow to mediate cell elongation. *Nature* 508, 392–396. doi: 10.1038/nature13070
- He, B., Martin, A., and Wieschaus, E. (2016). Flow-dependent myosin recruitment during *Drosophila* cellularization requires zygotic *dunk* activity. *Dev. Camb. Engl.* 143, 2417–2430. doi: 10.1242/dev.131334
- Hehenberger, E., Kradolfer, D., and Köhler, C. (2012). Endosperm cellularization defines an important developmental transition for embryo development. *Development* 139, 2031–2039. doi: 10.1242/dev.077057
- Heisenberg, C.-P., Tada, M., Rauch, G.-J., Saúde, L., Concha, M. L., Geisler, R., et al. (2000). Silberblick/Wnt11 mediates convergent extension movements during zebrafish gastrulation. *Nature* 405, 76–81. doi: 10.1038/35011068
- Hernández-López, C., Puliafito, A., Xu, Y., Lu, Z., Di Talia, S., and Vergassola, M. (2023). Two-fluid dynamics and micron-thin boundary layers shape cytoplasmic flows in early *Drosophila* embryos. *Proc. Natl. Acad. Sci.* 120, e2302879120. doi: 10.1073/pnas.2302879120
- Herrmann, H., Bär, H., Kreplak, L., Strelkov, S. V., and Aebi, U. (2007). Intermediate filaments: from cell architecture to nanomechanics. *Nat. Rev. Mol. Cell Biol.* 8, 562–573. doi: 10.1038/nrm2197
- Hertwig, O. (1875). *Beiträge zur Kenntniss der Bildung, Befruchtung und Theilung des thierischen Eies* ... W. Engelmann.

- Hertwig, O. (1884). *Das Problem der Befruchtung und der Isotropie des Eies: eine Theorie der Vererbung*. Verlag von Gustav Fischer.
- Hill, T. L., and Kirschner, M. W. (1982). Bioenergetics and kinetics of microtubule and actin filament assembly-disassembly. *Int. Rev. Cytol.* 78, 1–125.
- Hoffman, B. D., and Yap, A. S. (2015). Towards a Dynamic Understanding of Cadherin-Based Mechanobiology. *Trends Cell Biol.* 25, 803–814. doi: 10.1016/j.tcb.2015.09.008
- Holly, R. M., Mavor, L. M., Zuo, Z., and Blankenship, J. T. (2015). A rapid, membrane-dependent pathway directs furrow formation through RalA in the early *Drosophila* embryo. *Dev. Camb. Engl.* 142, 2316–2328. doi: 10.1242/dev.120998
- Hong, C. C., and Hashimoto, C. (1995). An unusual mosaic protein with a protease domain, encoded by the nudel gene, is involved in defining embryonic dorsoventral polarity in *Drosophila*. *Cell* 82, 785–794. doi: 10.1016/0092-8674(95)90475-1
- Hooke, R., Allestry, J., Allestry, J., and Royal Society (Great Britain) (1667). *Micrographia, or, Some physiological descriptions of minute bodies made by magnifying glasses : with observations and inquiries thereupon /.*, (London : Printed for James Allestry, printer to the Royal Society, and to be sold at his shop, at the Rose and Crown in Duck-Lane,). doi: 10.5962/bhl.title.113984
- Hotani, H. (1990). Dynamic features of microtubules as visualized by dark-field microscopy. *Adv. Biophys.* 26, 135–156. doi: 10.1016/0065-227X(90)90010-Q
- Htet, P. H., and Lauga, E. (2023). Cortex-driven cytoplasmic flows in elongated cells: fluid mechanics and application to nuclear transport in *Drosophila* embryos. *J. R. Soc. Interface* 20, 20230428. doi: 10.1098/rsif.2023.0428
- Huelsmann, S., Ylännä, J., and Brown, N. H. (2013). Filopodia-like actin cables position nuclei in association with perinuclear actin in *Drosophila* nurse cells. *Dev. Cell* 26, 604–615. doi: 10.1016/j.devcel.2013.08.014
- Hui, K. L., and Upadhyaya, A. (2017). Dynamic microtubules regulate cellular contractility during T-cell activation. *Proc. Natl. Acad. Sci.* 114, E4175–E4183. doi: 10.1073/pnas.1614291114
- Hunter, C., and Wieschaus, E. (2000). Regulated Expression of nullo Is Required for the Formation of Distinct Apical and Basal Adherens Junctions in the *Drosophila* Blastoderm. *J. Cell Biol.* 150, 391–402.
- Hunter, G. L., Crawford, J. M., Jenkins, J. Z., and Kiehart, D. P. (2014). Ion channels contribute to the regulation of cell sheet forces during *Drosophila* dorsal closure. *Development* 141, 325–334. doi: 10.1242/dev.097097
- Hurd, T. W., Gao, L., Roh, M. H., Macara, I. G., and Margolis, B. (2003). Direct interaction of two polarity complexes implicated in epithelial tight junction assembly. *Nat. Cell Biol.* 5, 137–142. doi: 10.1038/ncb923

- Huynh, J.-R., and St Johnston, D. (2004). The origin of asymmetry: early polarisation of the *Drosophila* germline cyst and oocyte. *Curr. Biol. CB* 14, R438-449. doi: 10.1016/j.cub.2004.05.040
- Hynes, R. O. (2002). Integrins: bidirectional, allosteric signaling machines. *Cell* 110, 673–687. doi: 10.1016/s0092-8674(02)00971-6
- Indra, I., Choi, J., Chen, C.-S., Troyanovsky, R. B., Shapiro, L., Honig, B., et al. (2018). Spatial and temporal organization of cadherin in punctate adherens junctions. *Proc. Natl. Acad. Sci. U. S. A.* 115, E4406–E4415. doi: 10.1073/pnas.1720826115
- Inoue, Y., Suzuki, M., Watanabe, T., Yasue, N., Tateo, I., Adachi, T., et al. (2016). Mechanical roles of apical constriction, cell elongation, and cell migration during neural tube formation in *Xenopus*. *Biomech. Model. Mechanobiol.* 15, 1733–1746. doi: 10.1007/s10237-016-0794-1
- Ip, Y. T., Park, R. E., Kosman, D., Yazdanbakhsh, K., and Levine, M. (1992). dorsal-twist interactions establish snail expression in the presumptive mesoderm of the *Drosophila* embryo. *Genes Dev.* 6, 1518–1530. doi: 10.1101/gad.6.8.1518
- Irvine, K. D., and Wieschaus, E. (1994). Cell intercalation during *Drosophila* germband extension and its regulation by pair-rule segmentation genes. *Development* 120, 827–841. doi: 10.1242/dev.120.4.827
- Ishikawa, R., Yamashiro, S., and Matsumura, F. (1989). Differential modulation of actin-severing activity of gelsolin by multiple isoforms of cultured rat cell tropomyosin. Potentiation of protective ability of tropomyosins by 83-kDa nonmuscle caldesmon. *J. Biol. Chem.* 264, 7490–7497.
- Iskratsch, T., Wolfenson, H., and Sheetz, M. P. (2014). Appreciating force and shape — the rise of mechanotransduction in cell biology. *Nat. Rev. Mol. Cell Biol.* 15, 825–833. doi: 10.1038/nrm3903
- Ito, M., Okamoto, R., Ito, H., Zhe, Y., and Dohi, K. (2022). Regulation of myosin light-chain phosphorylation and its roles in cardiovascular physiology and pathophysiology. *Hypertens. Res.* 45, 40–52. doi: 10.1038/s41440-021-00733-y
- Iwaki, D. D., Johansen, K. A., Singer, J. B., and Lengyel, J. A. (2001). drumstick, bowl, and lines are required for patterning and cell rearrangement in the *Drosophila* embryonic hindgut. *Dev. Biol.* 240, 611–626. doi: 10.1006/dbio.2001.0483
- Iyer, K. V., Piscitello-Gómez, R., Pajmans, J., Jülicher, F., and Eaton, S. (2019). Epithelial Viscoelasticity Is Regulated by Mechanosensitive E-cadherin Turnover. *Curr. Biol.* 29, 578-591.e5. doi: 10.1016/j.cub.2019.01.021
- Jaeger, J., Surkova, S., Blagov, M., Janssens, H., Kosman, D., Kozlov, K. N., et al. (2004). Dynamic control of positional information in the early *Drosophila* embryo. *Nature* 430, 368–371. doi: 10.1038/nature02678
- Janke, C., and Magiera, M. M. (2020). The tubulin code and its role in controlling microtubule properties and functions. *Nat. Rev. Mol. Cell Biol.* 21, 307–326. doi: 10.1038/s41580-020-0214-3

- Januschke, J., Gervais, L., Dass, S., Kaltschmidt, J. A., Lopez-Schier, H., Johnston, D. S., et al. (2002). Polar Transport in the *Drosophila* Oocyte Requires Dynein and Kinesin I Cooperation. *Curr. Biol.* 12, 1971–1981. doi: 10.1016/S0960-9822(02)01302-7
- Jha, A., van Zanten, T. S., Philippe, J.-M., Mayor, S., and Lecuit, T. (2018). Quantitative Control of GPCR Organization and Signaling by Endocytosis in Epithelial Morphogenesis. *Curr. Biol. CB* 28, 1570-1584.e6. doi: 10.1016/j.cub.2018.03.068
- John, A., and Rauzi, M. (2021a). A two-tier junctional mechanism drives simultaneous tissue folding and extension. *Dev. Cell* 56, 1469-1483.e5. doi: 10.1016/j.devcel.2021.04.003
- John, A., and Rauzi, M. (2021b). Composite morphogenesis during embryo development. *Semin. Cell Dev. Biol.* 120, 119–132. doi: 10.1016/j.semcdb.2021.06.007
- Johnson, K. A., and Borisy, G. G. (1975). The equilibrium assembly of microtubules in vitro. *Soc. Gen. Physiol. Ser.* 30, 119–141.
- Jonasson, E. M., Mauro, A. J., Li, C., Labuz, E. C., Mahserejian, S. M., Scripture, J. P., et al. (2020). Behaviors of individual microtubules and microtubule populations relative to critical concentrations: dynamic instability occurs when critical concentrations are driven apart by nucleotide hydrolysis. *Mol. Biol. Cell* 31, 589–618. doi: 10.1091/mbc.E19-02-0101
- Ju, R. J., Falconer, A. D., Dean, K. M., Fiolka, R. P., Sester, D. P., Nobis, M., et al. (2023). Compression-dependent microtubule reinforcement comprises a mechanostat which enables cells to navigate confined environments. 2022.02.08.479516. doi: 10.1101/2022.02.08.479516
- Jung, H. S., Komatsu, S., Ikebe, M., and Craig, R. (2008). Head–Head and Head–Tail Interaction: A General Mechanism for Switching Off Myosin II Activity in Cells. *Mol. Biol. Cell* 19, 3234–3242. doi: 10.1091/mbc.e08-02-0206
- Kabsch, W., Mannherz, H. G., Suck, D., Pai, E. F., and Holmes, K. C. (1990). Atomic structure of the actin:DNase I complex. *Nature* 347, 37–44. doi: 10.1038/347037a0
- Kalinka, A. T., and Tomancak, P. (2012). The evolution of early animal embryos: conservation or divergence? *Trends Ecol. Evol.* 27, 385–393. doi: 10.1016/j.tree.2012.03.007
- Kalukula, Y., Stephens, A. D., Lammerding, J., and Gabriele, S. (2022). Mechanics and functional consequences of nuclear deformations. *Nat. Rev. Mol. Cell Biol.* 23, 583–602. doi: 10.1038/s41580-022-00480-z
- Kapitein, L. C., Peterman, E. J. G., Kwok, B. H., Kim, J. H., Kapoor, T. M., and Schmidt, C. F. (2005). The bipolar mitotic kinesin Eg5 moves on both microtubules that it crosslinks. *Nature* 435, 114–118. doi: 10.1038/nature03503
- Katz, B. Z., and Yamada, K. M. (1997). Integrins in morphogenesis and signaling. *Biochimie* 79, 467–476. doi: 10.1016/S0300-9084(97)82738-1

- Keller, R. E., Danilchik, M., Gimlich, R., and Shih, J. (1985). The function and mechanism of convergent extension during gastrulation of *Xenopus laevis*. *J. Embryol. Exp. Morphol.* 89 Suppl, 185–209.
- Kerman, B. E., Cheshire, A. M., and Andrew, D. J. (2006). From fate to function: the *Drosophila trachea* and salivary gland as models for tubulogenesis. *Differ. Res. Biol. Divers.* 74, 326–348. doi: 10.1111/j.1432-0436.2006.00095.x
- Kerridge, S., Munjal, A., Philippe, J.-M., Jha, A., de las Bayonas, A. G., Saurin, A. J., et al. (2016). Modular activation of Rho1 by GPCR signalling imparts polarized myosin II activation during morphogenesis. *Nat. Cell Biol.* 18, 261–270. doi: 10.1038/ncb3302
- Kibar, Z., Vogan, K. J., Groulx, N., Justice, M. J., Underhill, D. A., and Gros, P. (2001). Ltap, a mammalian homolog of *Drosophila Strabismus/Van Gogh*, is altered in the mouse neural tube mutant Loop-tail. *Nat. Genet.* 28, 251–255. doi: 10.1038/90081
- Kidd, S. (1992). Characterization of the *Drosophila cactus* locus and analysis of interactions between cactus and dorsal proteins. *Cell* 71, 623–635. doi: 10.1016/0092-8674(92)90596-5
- Kiecker, C., Bates, T., and Bell, E. (2015). Molecular specification of germ layers in vertebrate embryos. *Cell. Mol. Life Sci. CMLS* 73, 923–947. doi: 10.1007/s00018-015-2092-y
- Kim, H. Y., Varner, V. D., and Nelson, C. M. (2013). Apical constriction initiates new bud formation during monopodial branching of the embryonic chicken lung. *Dev. Camb. Engl.* 140, 3146–3155. doi: 10.1242/dev.093682
- Kim, S., Pochitaloff, M., Stooke-Vaughan, G. A., and Campàs, O. (2021). Embryonic tissues as active foams. *Nat. Phys.* 17, 859–866. doi: 10.1038/s41567-021-01215-1
- Kim-Ha, J., Smith, J. L., and Macdonald, P. M. (1991). oskar mRNA is localized to the posterior pole of the *Drosophila* oocyte. *Cell* 66, 23–35. doi: 10.1016/0092-8674(91)90136-M
- Kitazawa, T., Gaylinn, B. D., Denney, G. H., and Somlyo, A. P. (1991). G-protein-mediated Ca²⁺ sensitization of smooth muscle contraction through myosin light chain phosphorylation. *J. Biol. Chem.* 266, 1708–1715. doi: 10.1016/S0021-9258(18)52353-X
- Klingler, M., Erdélyi, M., Szabad, J., and Nüsslein-Volhard, C. (1988). Function of torso in determining the terminal Anlagen of the *Drosophila* embryo. *Nature* 335, 275–277. doi: 10.1038/335275a0
- Knossow, M., Campanacci, V., Khodja, L. A., and Gigant, B. (2020). The Mechanism of Tubulin Assembly into Microtubules: Insights from Structural Studies. *iScience* 23. doi: 10.1016/j.isci.2020.101511
- Knust, E. (2002). Regulation of epithelial cell shape and polarity by cell - cell adhesion (Review). *Mol. Membr. Biol.* 19, 113–120. doi: 10.1080/09687680210137219

- Ko, C. S., Tserunyan, V., and Martin, A. C. (2019). Microtubules promote intercellular contractile force transmission during tissue folding. *J. Cell Biol.* 218, 2726–2742. doi: 10.1083/jcb.201902011
- Koch, E. A., and Spitzer, R. H. (1983). Multiple effects of colchicine on oogenesis in *Drosophila*: Induced sterility and switch of potential oocyte to nurse-cell developmental pathway. *Cell Tissue Res.* 228, 21–32. doi: 10.1007/BF00206261
- Koestler, S. A., Auinger, S., Vinzenz, M., Rottner, K., and Small, J. V. (2008). Differentially oriented populations of actin filaments generated in lamellipodia collaborate in pushing and pausing at the cell front. *Nat. Cell Biol.* 10, 306–313. doi: 10.1038/ncb1692
- Kölsch, V., Seher, T., Fernandez-Ballester, G. J., Serrano, L., and Leptin, M. (2007). Control of *Drosophila* Gastrulation by Apical Localization of Adherens Junctions and RhoGEF2. *Science* 315, 384–386. doi: 10.1126/science.1134833
- Kong, D., Wolf, F., and Großhans, J. (2017). Forces directing germ-band extension in *Drosophila* embryos. *Mech. Dev.* 144, 11–22. doi: 10.1016/j.mod.2016.12.001
- Kong, F., García, A. J., Mould, A. P., Humphries, M. J., and Zhu, C. (2009). Demonstration of catch bonds between an integrin and its ligand. *J. Cell Biol.* 185, 1275–1284. doi: 10.1083/jcb.200810002
- Kreidberg, J. A., and Symons, J. M. (2000). Integrins in kidney development, function, and disease. *Am. J. Physiol.-Ren. Physiol.* 279, F233–F242. doi: 10.1152/ajprenal.2000.279.2.F233
- Kroeger, B., Manning, S. A., Fonseka, Y., Oorschot, V., Crawford, S. A., Ramm, G., et al. (2024). Basal spot junctions of *Drosophila* epithelial tissues respond to morphogenetic forces and regulate Hippo signaling. *Dev. Cell* 59, 262–279.e6. doi: 10.1016/j.devcel.2023.11.024
- Krueger, D., Tardivo, P., Nguyen, C., and De Renzis, S. (2018). Downregulation of basal myosin-II is required for cell shape changes and tissue invagination. *EMBO J.* 37, e100170. doi: 10.15252/embj.2018100170
- Kuhn, J. R., and Pollard, T. D. (2005). Real-time measurements of actin filament polymerization by total internal reflection fluorescence microscopy. *Biophys. J.* 88, 1387–1402. doi: 10.1529/biophysj.104.047399
- Kull, F. J., and Endow, S. A. (2013). Force generation by kinesin and myosin cytoskeletal motor proteins. *J. Cell Sci.* 126, 9–19. doi: 10.1242/jcs.103911
- Laan, L., Husson, J., Munteanu, E. L., Kerssemakers, J. W. J., and Dogterom, M. (2008). Force-generation and dynamic instability of microtubule bundles. *Proc. Natl. Acad. Sci. U. S. A.* 105, 8920–8925. doi: 10.1073/pnas.0710311105
- Laan, L., Pavin, N., Husson, J., Romet-Lemonne, G., van Duijn, M., López, M. P., et al. (2012). Cortical dynein controls microtubule dynamics to generate pulling forces that position microtubule asters. *Cell* 148, 502–514. doi: 10.1016/j.cell.2012.01.007

- Ladoux, B., and Mège, R.-M. (2017). Mechanobiology of collective cell behaviours. *Nat. Rev. Mol. Cell Biol.* 18, 743–757. doi: 10.1038/nrm.2017.98
- Lam, P. Y., Webb, S. E., Leclerc, C., Moreau, M., and Miller, A. L. (2009). Inhibition of stored Ca²⁺ release disrupts convergence-related cell movements in the lateral intermediate mesoderm resulting in abnormal positioning and morphology of the pronephric anlagen in intact zebrafish embryos. *Dev. Growth Differ.* 51, 429–442. doi: 10.1111/j.1440-169X.2009.01106.x
- Lane, M. E., and Kalderon, D. (1995). Localization and functions of Protein Kinase A during *Drosophila* oogenesis. *Mech. Dev.* 49, 191–200. doi: 10.1016/0925-4773(94)00317-G
- Lavalou, J., Mao, Q., Harmansa, S., Kerridge, S., Lellouch, A. C., Philippe, J.-M., et al. (2021). Formation of polarized contractile interfaces by self-organized Toll-8/Cirl GPCR asymmetry. *Dev. Cell* 56, 1574-1588.e7. doi: 10.1016/j.devcel.2021.03.030
- Le Roux, A.-L., Quiroga, X., Walani, N., Arroyo, M., and Roca-Cusachs, P. (2019). The plasma membrane as a mechanochemical transducer. *Philos. Trans. R. Soc. B Biol. Sci.* 374, 20180221. doi: 10.1098/rstb.2018.0221
- Leal, A., Endele, S., Stengel, C., Huehne, K., Loetterle, J., Barrantes, R., et al. (2003). A novel myosin heavy chain gene in human chromosome 19q13.3. *Gene* 312, 165–171. doi: 10.1016/S0378-1119(03)00613-9
- Leckband, D. E., and de Rooij, J. (2014). Cadherin adhesion and mechanotransduction. *Annu. Rev. Cell Dev. Biol.* 30, 291–315. doi: 10.1146/annurev-cellbio-100913-013212
- Lecuit, T. (2004). Junctions and vesicular trafficking during *Drosophila* cellularization. *J. Cell Sci.* 117, 3427–3433. doi: 10.1242/jcs.01312
- Lecuit, T. (2005). Adhesion remodeling underlying tissue morphogenesis. *Trends Cell Biol.* 15, 34–42. doi: 10.1016/j.tcb.2004.11.007
- Lecuit, T., and Lenne, P.-F. (2007). Cell surface mechanics and the control of cell shape, tissue patterns and morphogenesis. *Nat. Rev. Mol. Cell Biol.* 8, 633–644. doi: 10.1038/nrm2222
- Lecuit, T., and Wieschaus, E. (2000). Polarized insertion of new membrane from a cytoplasmic reservoir during cleavage of the *Drosophila* embryo. *J. Cell Biol.* 150, 849–860. doi: 10.1083/jcb.150.4.849
- Lecuit, T., and Yap, A. S. (2015). E-cadherin junctions as active mechanical integrators in tissue dynamics. *Nat. Cell Biol.* 17, 533–539. doi: 10.1038/ncb3136
- Lee, D. M., and Harris, T. J. C. (2013). An Arf-GEF regulates antagonism between endocytosis and the cytoskeleton for *Drosophila* blastoderm development. *Curr. Biol. CB* 23, 2110–2120. doi: 10.1016/j.cub.2013.08.058
- Lee, H., Alisafaei, F., Adebawale, K., Chang, J., Shenoy, V. B., and Chaudhuri, O. (2021). The nuclear piston activates mechanosensitive ion channels to generate cell migration

- paths in confining microenvironments. *Sci. Adv.* 7, eabd4058. doi: 10.1126/sciadv.abd4058
- Lee, Y. L., and Burke, B. (2018). LINC complexes and nuclear positioning. *Semin. Cell Dev. Biol.* 82, 67–76. doi: 10.1016/j.semcdb.2017.11.008
- Lehmann, R., and Nüsslein-Volhard, C. (1986). Abdominal segmentation, pole cell formation, and embryonic polarity require the localized activity of *oskar*, a maternal gene in drosophila. *Cell* 47, 141–152. doi: 10.1016/0092-8674(86)90375-2
- Lemke, S. B., and Nelson, C. M. (2021). Dynamic changes in epithelial cell packing during tissue morphogenesis. *Curr. Biol.* 31, R1098–R1110. doi: 10.1016/j.cub.2021.07.078
- Lenne, P.-F., and Trivedi, V. (2022). Sculpting tissues by phase transitions. *Nat. Commun.* 13, 664. doi: 10.1038/s41467-022-28151-9
- Lenz, M., Thoresen, T., Gardel, M. L., and Dinner, A. R. (2012). Contractile units in disordered actomyosin bundles arise from F-actin buckling. *Phys. Rev. Lett.* 108, 238107. doi: 10.1103/PhysRevLett.108.238107
- Leptin, M., and Grunewald, B. (1990). Cell shape changes during gastrulation in Drosophila. *Dev. Camb. Engl.* 110, 73–84. doi: 10.1242/dev.110.1.73
- Lesko, A. C., Keller, R., Chen, P., and Sutherland, A. (2021). *Scribble* mutation disrupts convergent extension and apical constriction during mammalian neural tube closure. *Dev. Biol.* 478, 59–75. doi: 10.1016/j.ydbio.2021.05.013
- Letizia, A., He, D., Astigarraga, S., Colombelli, J., Hatini, V., Llimargas, M., et al. (2019). Sidekick Is a Key Component of Tricellular Adherens Junctions that Acts to Resolve Cell Rearrangements. *Dev. Cell* 50, 313–326.e5. doi: 10.1016/j.devcel.2019.07.007
- Levayer, R., and Lecuit, T. (2013). Oscillation and Polarity of E-Cadherin Asymmetries Control Actomyosin Flow Patterns during Morphogenesis. *Dev. Cell* 26, 162–175. doi: 10.1016/j.devcel.2013.06.020
- Lewis, W. H. (1947). Mechanics of invagination. *Anat. Rec.* 97, 139–156. doi: 10.1002/ar.1090970203
- Li, Y., Kučera, O., Cuvelier, D., Rutkowski, D. M., Deygas, M., Rai, D., et al. (2023). Compressive forces stabilize microtubules in living cells. *Nat. Mater.* 22, 913–924. doi: 10.1038/s41563-023-01578-1
- Li, Y., Naveed, H., Kachalo, S., Xu, L. X., and Liang, J. (2014). Mechanisms of Regulating Tissue Elongation in Drosophila Wing: Impact of Oriented Cell Divisions, Oriented Mechanical Forces, and Reduced Cell Size. *PLOS ONE* 9, e86725. doi: 10.1371/journal.pone.0086725
- Liem, R. K. H. (2016). Cytoskeletal Integrators: The Spectrin Superfamily. *Cold Spring Harb. Perspect. Biol.* 8, a018259. doi: 10.1101/cshperspect.a018259

- Ligon, L. A., and Holzbaaur, E. L. F. (2007). Microtubules tethered at epithelial cell junctions by dynein facilitate efficient junction assembly. *Traffic Cph. Den.* 8, 808–819. doi: 10.1111/j.1600-0854.2007.00574.x
- Ligon, L. A., Karki, S., Tokito, M., and Holzbaaur, E. L. (2001). Dynein binds to beta-catenin and may tether microtubules at adherens junctions. *Nat. Cell Biol.* 3, 913–917. doi: 10.1038/ncb1001-913
- Lim, B., Levine, M., and Yamazaki, Y. (2017). Transcriptional Pre-patterning of Drosophila Gastrulation. *Curr. Biol.* 27, 286–290. doi: 10.1016/j.cub.2016.11.047
- Lin, B., Luo, J., and Lehmann, R. (2022). An AMPK phosphoregulated RhoGEF feedback loop tunes cortical flow-driven amoeboid migration in vivo. *Sci. Adv.* 8, eabo0323. doi: 10.1126/sciadv.abo0323
- Lipinski, R. J., and Krauss, R. S. (2023). Gene-environment interactions in birth defect etiology: Challenges and opportunities. *Curr. Top. Dev. Biol.* 152, 1–30. doi: 10.1016/bs.ctdb.2022.10.001
- Liu, P., Zupa, E., Neuner, A., Böhler, A., Loerke, J., Flemming, D., et al. (2020). Insights into the assembly and activation of the microtubule nucleator γ -TuRC. *Nature* 578, 467–471. doi: 10.1038/s41586-019-1896-6
- Llimargas, M., and Casanova, J. (1999). EGF signalling regulates cell invagination as well as cell migration during formation of tracheal system in Drosophila. *Dev. Genes Evol.* 209, 174–179. doi: 10.1007/s004270050241
- Lomakin, A. J., Cattin, C. J., Cuvelier, D., Alraies, Z., Molina, M., Nader, G. P. F., et al. (2020). The nucleus acts as a ruler tailoring cell responses to spatial constraints. *Science* 370, eaba2894. doi: 10.1126/science.aba2894
- Lomakin, A. J., Lee, K.-C., Han, S. J., Bui, D. A., Davidson, M., Mogilner, A., et al. (2015). Competition for actin between two distinct F-actin networks defines a bistable switch for cell polarization. *Nat. Cell Biol.* 17, 1435–1445. doi: 10.1038/ncb3246
- López-Gay, J. M., Nunley, H., Spencer, M., di Pietro, F., Guirao, B., Bosveld, F., et al. (2020). Apical stress fibers enable a scaling between cell mechanical response and area in epithelial tissue. *Science* 370, eabb2169. doi: 10.1126/science.abb2169
- Luxton, G. W. G., Gomes, E. R., Folker, E. S., Vintinner, E., and Gundersen, G. G. (2010). Linear arrays of nuclear envelope proteins harness retrograde actin flow for nuclear movement. *Science* 329, 956–959. doi: 10.1126/science.1189072
- Lye, C. M., Blanchard, G. B., Naylor, H. W., Muresan, L., Huisken, J., Adams, R. J., et al. (2015). Mechanical Coupling between Endoderm Invagination and Axis Extension in Drosophila. *PLOS Biol.* 13, e1002292. doi: 10.1371/journal.pbio.1002292
- Lye, C. M., and Sanson, B. (2011). Tension and epithelial morphogenesis in Drosophila early embryos. *Curr. Top. Dev. Biol.* 95, 145–187. doi: 10.1016/B978-0-12-385065-2.00005-0
- Maan, R., Reese, L., Volkov, V. A., King, M. R., van der Sluis, E. O., Andrea, N., et al. (2023). Multivalent interactions facilitate motor-dependent protein accumulation at

growing microtubule plus-ends. *Nat. Cell Biol.* 25, 68–78. doi: 10.1038/s41556-022-01037-0

Macdonald, P. M., and Struhl, G. (1986). A molecular gradient in early *Drosophila* embryos and its role in specifying the body pattern. *Nature* 324, 537–545. doi: 10.1038/324537a0

Maître, J.-L., Berthoumieux, H., Krens, S. F. G., Salbreux, G., Jülicher, F., Paluch, E., et al. (2012). Adhesion functions in cell sorting by mechanically coupling the cortices of adhering cells. *Science* 338, 253–256. doi: 10.1126/science.1225399

Maître, J.-L., Niwayama, R., Turlier, H., Nédélec, F., and Hiiragi, T. (2015). Pulsatile cell-autonomous contractility drives compaction in the mouse embryo. *Nat. Cell Biol.* 17, 849–855. doi: 10.1038/ncb3185

Malone, C. J., Misner, L., Le Bot, N., Tsai, M.-C., Campbell, J. M., Ahringer, J., et al. (2003). The *C. elegans* hook protein, ZYG-12, mediates the essential attachment between the centrosome and nucleus. *Cell* 115, 825–836. doi: 10.1016/s0092-8674(03)00985-1

Mandato, C. A., and Bement, W. M. (2003). Actomyosin transports microtubules and microtubules control actomyosin recruitment during *Xenopus* oocyte wound healing. *Curr. Biol. CB* 13, 1096–1105. doi: 10.1016/s0960-9822(03)00420-2

Mangione, F., and Martín-Blanco, E. (2018). The Dachsous/Fat/Four-Jointed Pathway Directs the Uniform Axial Orientation of Epithelial Cells in the *Drosophila* Abdomen. *Cell Rep.* 25, 2836–2850.e4. doi: 10.1016/j.celrep.2018.11.036

Manibog, K., Li, H., Rakshit, S., and Sivasankar, S. (2014). Resolving the molecular mechanism of cadherin catch bond formation. *Nat. Commun.* 5, 3941. doi: 10.1038/ncomms4941

Manning, A. J., Peters, K. A., Peifer, M., and Rogers, S. L. (2013). Regulation of Epithelial Morphogenesis by the G Protein–Coupled Receptor Mist and Its Ligand Fog. *Sci. Signal.* 6, ra98–ra98. doi: 10.1126/scisignal.2004427

Manning, A., and Rogers, S. (2014). The Fog signaling pathway: Insights into signaling in morphogenesis. *Dev. Biol.* 394. doi: 10.1016/j.ydbio.2014.08.003

Mansfield, G. S., Al-Shirawi, D. Y., Ketchum, A. S., Newbern, C. E., and Kiehart, D. P. (1996). Molecular Organization and Alternative Splicing in zipper, the Gene that Encodes the *Drosophila* Non-muscle Myosin II Heavy Chain. *J. Mol. Biol.* 255, 98–109. doi: 10.1006/jmbi.1996.0009

Mao, Y., and Wickström, S. A. (2024). Mechanical state transitions in the regulation of tissue form and function. *Nat. Rev. Mol. Cell Biol.*, 1–17. doi: 10.1038/s41580-024-00719-x

Markova, O., Sénatore, S., Chardès, C., and Lenne, P.-F. (2015). Calcium Spikes in Epithelium: study on *Drosophila* early embryos. *Sci. Rep.* 5, 11379. doi: 10.1038/srep11379

- Marsden, M., and DeSimone, D. W. (2001). Regulation of cell polarity, radial intercalation and epiboly in *Xenopus*: novel roles for integrin and fibronectin. *Development* 128, 3635–3647. doi: 10.1242/dev.128.18.3635
- Martin, A. C. (2020). The Physical Mechanisms of *Drosophila* Gastrulation: Mesoderm and Endoderm Invagination. *Genetics* 214, 543–560. doi: 10.1534/genetics.119.301292
- Martin, A. C., Gelbart, M., Fernandez-Gonzalez, R., Kaschube, M., and Wieschaus, E. F. (2010). Integration of contractile forces during tissue invagination. *J. Cell Biol.* 188, 735–749. doi: 10.1083/jcb.200910099
- Martin, A. C., and Goldstein, B. (2014). Apical constriction: themes and variations on a cellular mechanism driving morphogenesis. *Development* 141, 1987–1998. doi: 10.1242/dev.102228
- Martin, A. C., Kaschube, M., and Wieschaus, E. F. (2009). Pulsed contractions of an actin–myosin network drive apical constriction. *Nature* 457, 495–499. doi: 10.1038/nature07522
- Mason, F. M., Tworoger, M., and Martin, A. C. (2013). Apical domain polarization localizes actin-myosin activity to drive ratchet-like apical constriction. *Nat. Cell Biol.* 15, 926–936. doi: 10.1038/ncb2796
- Mason, F. M., Xie, S., Vasquez, C. G., Tworoger, M., and Martin, A. C. (2016). RhoA GTPase inhibition organizes contraction during epithelial morphogenesis. *J. Cell Biol.* 214, 603–617. doi: 10.1083/jcb.201603077
- Mathewson, A. W., Berman, D. G., and Moens, C. B. (2019). Microtubules are required for the maintenance of planar cell polarity in monociliated floorplate cells. *Dev. Biol.* 452, 21–33. doi: 10.1016/j.ydbio.2019.04.007
- Matis, M. (2020). The Mechanical Role of Microtubules in Tissue Remodeling. *BioEssays* 42, 1900244. doi: 10.1002/bies.201900244
- Matis, M., and Axelrod, J. D. (2013). Regulation of PCP by the Fat signaling pathway. *Genes Dev.* 27, 2207–2220. doi: 10.1101/gad.228098.113
- Matis, M., Russler-Germain, D. A., Hu, Q., Tomlin, C. J., and Axelrod, J. D. (2014). Microtubules provide directional information for core PCP function. *eLife* 3. doi: 10.7554/eLife.02893
- Matsudaira, P. (1994). Actin crosslinking proteins at the leading edge. *Semin. Cell Biol.* 5, 165–174. doi: 10.1006/scel.1994.1021
- Mavrikakis, M., Azou-Gros, Y., Tsai, F.-C., Alvarado, J., Bertin, A., Iv, F., et al. (2014). Septins promote F-actin ring formation by crosslinking actin filaments into curved bundles. *Nat. Cell Biol.* 16, 322–334. doi: 10.1038/ncb2921
- Mazumdar, A., and Mazumdar, M. (2002). How one becomes many: blastoderm cellularization in *Drosophila melanogaster*. *BioEssays News Rev. Mol. Cell. Dev. Biol.* 24, 1012–1022. doi: 10.1002/bies.10184

- McCartney, B., and Dudin, O. (2023). Cellularization across eukaryotes: Conserved mechanisms and novel strategies. *Curr. Opin. Cell Biol.* 80, 102157. doi: 10.1016/j.ceb.2023.102157
- McFadden, W. M., McCall, P. M., Gardel, M. L., and Munro, E. M. (2017). Filament turnover tunes both force generation and dissipation to control long-range flows in a model actomyosin cortex. *PLoS Comput. Biol.* 13, e1005811. doi: 10.1371/journal.pcbi.1005811
- McKellar, C. E., and Wyttenbach, R. A. (2017). A Protocol Demonstrating 60 Different Drosophila Behaviors in One Assay. *J. Undergrad. Neurosci. Educ.* 15, A110–A116.
- McNally, F. J., and Roll-Mecak, A. (2018). Microtubule-severing enzymes: From cellular functions to molecular mechanism. *J. Cell Biol.* 217, 4057–4069. doi: 10.1083/jcb.201612104
- Mège, R. M., and Ishiyama, N. (2017). Integration of Cadherin Adhesion and Cytoskeleton at Adherens Junctions. *Cold Spring Harb. Perspect. Biol.* 9, a028738. doi: 10.1101/cshperspect.a028738
- Meier, S. M., Farcas, A.-M., Kumar, A., Ijavi, M., Bill, R. T., Stelling, J., et al. (2023). Multivalency ensures persistence of a +TIP body at specialized microtubule ends. *Nat. Cell Biol.* 25, 56–67. doi: 10.1038/s41556-022-01035-2
- Merle, M., Friedman, L., Chureau, C., Shoushtarizadeh, A., and Gregor, T. (2024). Precise and scalable self-organization in mammalian pseudo-embryos. *Nat. Struct. Mol. Biol.*, 1–7. doi: 10.1038/s41594-024-01251-4
- Miao, H., and Blankenship, J. T. (2020). The pulse of morphogenesis: actomyosin dynamics and regulation in epithelia. *Dev. Camb. Engl.* 147, dev186502. doi: 10.1242/dev.186502
- Michaux, J. B., Robin, F. B., McFadden, W. M., and Munro, E. M. (2018). Excitable RhoA dynamics drive pulsed contractions in the early *C. elegans* embryo. *J. Cell Biol.* 217, 4230–4252. doi: 10.1083/jcb.201806161
- Millarte, V., and Farhan, H. (2012). The Golgi in cell migration: regulation by signal transduction and its implications for cancer cell metastasis. *ScientificWorldJournal* 2012, 498278. doi: 10.1100/2012/498278
- Miller, D. E., Cook, K. R., and Hawley, R. S. (2019). The joy of balancers. *PLoS Genet.* 15, e1008421. doi: 10.1371/journal.pgen.1008421
- Minc, N., Burgess, D., and Chang, F. (2011). Influence of cell geometry on division-plane positioning. *Cell* 144, 414–426. doi: 10.1016/j.cell.2011.01.016
- Minc, N., and Piel, M. (2012). Predicting division plane position and orientation. *Trends Cell Biol.* 22, 193–200. doi: 10.1016/j.tcb.2012.01.003
- Mirigian, M., Mukherjee, K., Bane, S. L., and Sackett, D. L. (2013). Measurement of in vitro microtubule polymerization by turbidity and fluorescence. *Methods Cell Biol.* 115, 215–229. doi: 10.1016/B978-0-12-407757-7.00014-1

- Mitchison, T., and Kirschner, M. (1984). Dynamic instability of microtubule growth. *Nature* 312, 237–242. doi: 10.1038/312237a0
- Mitchison, T., and Kirschner, M. (1988). Cytoskeletal dynamics and nerve growth. *Neuron* 1, 761–772. doi: 10.1016/0896-6273(88)90124-9
- Mitrossilis, D., Röper, J.-C., Le Roy, D., Driquez, B., Michel, A., Ménager, C., et al. (2017). Mechanotransductive cascade of Myo-II-dependent mesoderm and endoderm invaginations in embryo gastrulation. *Nat. Commun.* 8, 13883. doi: 10.1038/ncomms13883
- Molè, M. A., Galea, G. L., Rolo, A., Weberling, A., Nychyk, O., Castro, S. C. D., et al. (2020). Integrin-Mediated Focal Anchorage Drives Epithelial Zippering during Mouse Neural Tube Closure. *Dev. Cell* 52, 321–334.e6. doi: 10.1016/j.devcel.2020.01.012
- Molloy, J. E., Burns, J. E., Kendrick-Jones, J., Tregear, R. T., and White, D. C. S. (1995). Movement and force produced by a single myosin head. *Nature* 378, 209–212. doi: 10.1038/378209a0
- Molodtsov, M. I., Grishchuk, E. L., Efremov, A. K., McIntosh, J. R., and Ataullakhanov, F. I. (2005). Force production by depolymerizing microtubules: a theoretical study. *Proc. Natl. Acad. Sci. U. S. A.* 102, 4353–4358. doi: 10.1073/pnas.0501142102
- Mongera, A., Rowghanian, P., Gustafson, H. J., Shelton, E., Kealhofer, D. A., Carn, E. K., et al. (2018). A fluid-to-solid jamming transition underlies vertebrate body axis elongation. *Nature* 561, 401–405. doi: 10.1038/s41586-018-0479-2
- Monier, B., Gettings, M., Gay, G., Mangeat, T., Schott, S., Guarner, A., et al. (2015). Apico-basal forces exerted by apoptotic cells drive epithelium folding. *Nature* 518, 245–248. doi: 10.1038/nature14152
- Morgan, T. H. (1910). Sex Limited Inheritance in *Drosophila*. *Science* 32, 120–122. doi: 10.1126/science.32.812.120
- Müller, H. A., and Wieschaus, E. (1996). armadillo, bazooka, and stardust are critical for early stages in formation of the zonula adherens and maintenance of the polarized blastoderm epithelium in *Drosophila*. *J. Cell Biol.* 134, 149–163. doi: 10.1083/jcb.134.1.149
- Munro, E. M., and Odell, G. M. (2002). Polarized basolateral cell motility underlies invagination and convergent extension of the ascidian notochord. *Dev. Camb. Engl.* 129, 13–24. doi: 10.1242/dev.129.1.13
- Munro, E., Nance, J., and Priess, J. R. (2004). Cortical Flows Powered by Asymmetrical Contraction Transport PAR Proteins to Establish and Maintain Anterior-Posterior Polarity in the Early *C. elegans* Embryo. *Dev. Cell* 7, 413–424. doi: 10.1016/j.devcel.2004.08.001
- Münster, S., Jain, A., Mietke, A., Pavlopoulos, A., Grill, S. W., and Tomancak, P. (2019). Attachment of the blastoderm to the vitelline envelope affects gastrulation of insects. *Nature* 568, 395–399. doi: 10.1038/s41586-019-1044-3

- Murakami, K., Yasunaga, T., Noguchi, T. Q. P., Gomibuchi, Y., Ngo, K. X., Uyeda, T. Q. P., et al. (2010). Structural Basis for Actin Assembly, Activation of ATP Hydrolysis, and Delayed Phosphate Release. *Cell* 143, 275–287. doi: 10.1016/j.cell.2010.09.034
- Murdoch, J. N., Doudney, K., Paternotte, C., Copp, A. J., and Stanier, P. (2001). Severe neural tube defects in the loop-tail mouse result from mutation of *Lpp1*, a novel gene involved in floor plate specification. *Hum. Mol. Genet.* 10, 2593–2601. doi: 10.1093/hmg/10.22.2593
- Murrell, M., Oakes, P. W., Lenz, M., and Gardel, M. L. (2015). Forcing cells into shape: the mechanics of actomyosin contractility. *Nat. Rev. Mol. Cell Biol.* 16, 486–498. doi: 10.1038/nrm4012
- Murrell, M. P., and Gardel, M. L. (2012). F-actin buckling coordinates contractility and severing in a biomimetic actomyosin cortex. *Proc. Natl. Acad. Sci. U. S. A.* 109, 20820–20825. doi: 10.1073/pnas.1214753109
- Muse, M. E., Shumway, K. R., and Crane, J. S. (2024). “Physiology, Epithelialization,” in *StatPearls*, (Treasure Island (FL): StatPearls Publishing). Available at: <http://www.ncbi.nlm.nih.gov/books/NBK532977/> (Accessed June 18, 2024).
- Myat, M. M., Rashmi, R., Manna, D., Xu, N., Patel, U., Galiano, M., et al. (2015). Drosophila KASH-domain protein Klarsicht regulates microtubule stability and integrin receptor localization during collective cell migration. *Dev. Biol.* 407, 103–114. doi: 10.1016/j.ydbio.2015.08.003
- Nag, S., Larsson, M., Robinson, R. C., and Burtnick, L. D. (2013). Gelsolin: The tail of a molecular gymnast. *Cytoskeleton* 70, 360–384. doi: 10.1002/cm.21117
- Narasimha, M., and Brown, N. H. (2004). Novel Functions for Integrins in Epithelial Morphogenesis. *Curr. Biol.* 14, 381–385. doi: 10.1016/j.cub.2004.02.033
- Nasiadka, A., Dietrich, B. H., and Krause, H. M. (2002). “Anterior-posterior patterning in the *Drosophila* embryo,” in *Advances in Developmental Biology and Biochemistry*, (Elsevier), 155–204. doi: 10.1016/S1569-1799(02)12027-2
- Nechiporuk, A., and Raible, D. W. (2008). FGF-Dependent Mechanosensory Organ Patterning in Zebrafish. *Science* 320, 1774–1777. doi: 10.1126/science.1156547
- Neuman-Silberberg, F. S., and Schüpbach, T. (1993). The *Drosophila* dorsoventral patterning gene *gurken* produces a dorsally localized RNA and encodes a TGF alpha-like protein. *Cell* 75, 165–174.
- Niessen, C. M. (2007). Tight Junctions/Adherens Junctions: Basic Structure and Function. *J. Invest. Dermatol.* 127, 2525–2532. doi: 10.1038/sj.jid.5700865
- Nikolaidou, K. K., and Barrett, K. (2004). A Rho GTPase signaling pathway is used reiteratively in epithelial folding and potentially selects the outcome of Rho activation. *Curr. Biol. CB* 14, 1822–1826. doi: 10.1016/j.cub.2004.09.080
- Nishida, E. (1985). Opposite effects of cofilin and profilin from porcine brain on rate of exchange of actin-bound adenosine 5'-triphosphate. *Biochemistry* 24, 1160–1164. doi: 10.1021/bi00326a015

- Nishimura, T., Honda, H., and Takeichi, M. (2012). Planar Cell Polarity Links Axes of Spatial Dynamics in Neural-Tube Closure. *Cell* 149, 1084–1097. doi: 10.1016/j.cell.2012.04.021
- Nishimura, T., and Takeichi, M. (2008). Shroom3-mediated recruitment of Rho kinases to the apical cell junctions regulates epithelial and neuroepithelial planar remodeling. *Dev. Camb. Engl.* 135, 1493–1502. doi: 10.1242/dev.019646
- Nobes, C. D., and Hall, A. (1999). Rho GTPases Control Polarity, Protrusion, and Adhesion during Cell Movement. *J. Cell Biol.* 144, 1235–1244. doi: 10.1083/jcb.144.6.1235
- Noren, N. K., Niessen, C. M., Gumbiner, B. M., and Burridge, K. (2001). Cadherin engagement regulates Rho family GTPases. *J. Biol. Chem.* 276, 33305–33308. doi: 10.1074/jbc.C100306200
- Nüsslein-Volhard, C., and Wieschaus, E. (1980). Mutations affecting segment number and polarity in *Drosophila*. *Nature* 287, 795–801. doi: 10.1038/287795a0
- Oda-Ishii, I., Ishii, Y., and Mikawa, T. (2010). Eph Regulates Dorsoventral Asymmetry of the Notochord Plate and Convergent Extension-Mediated Notochord Formation. *PLOS ONE* 5, e13689. doi: 10.1371/journal.pone.0013689
- Odell, G. M., Oster, G., Alberch, P., and Burnside, B. (1981). The mechanical basis of morphogenesis: I. Epithelial folding and invagination. *Dev. Biol.* 85, 446–462. doi: 10.1016/0012-1606(81)90276-1
- Olofsson, J., Sharp, K. A., Matis, M., Cho, B., and Axelrod, J. D. (2014). Prickle/spiny-legs isoforms control the polarity of the apical microtubule network in planar cell polarity. *Development* 141, 2866–2874. doi: 10.1242/dev.105932
- Paré, A. C., Naik, P., Shi, J., Mirman, Z., Palmquist, K. H., and Zallen, J. A. (2019). An LRR Receptor-Teneurin System Directs Planar Polarity at Compartment Boundaries. *Dev. Cell* 51, 208–221.e6. doi: 10.1016/j.devcel.2019.08.003
- Paré, A. C., Vichas, A., Fincher, C. T., Mirman, Z., Farrell, D. L., Mainieri, A., et al. (2014). A positional Toll receptor code directs convergent extension in *Drosophila*. *Nature* 515, 523–527. doi: 10.1038/nature13953
- Paré, A. C., and Zallen, J. A. (2020). Cellular, molecular, and biophysical control of epithelial cell intercalation. *Curr. Top. Dev. Biol.* 136, 167–193. doi: 10.1016/bs.ctdb.2019.11.014
- Parks, S., and Wieschaus, E. (1991). The *Drosophila* gastrulation gene *concertina* encodes a G alpha-like protein. *Cell* 64, 447–458. doi: 10.1016/0092-8674(91)90652-f
- Pearl, E. J., Li, J., and Green, J. B. A. (2017). Cellular systems for epithelial invagination. *Philos. Trans. R. Soc. B Biol. Sci.* 372, 20150526. doi: 10.1098/rstb.2015.0526
- Peng, Y., and Axelrod, J. D. (2012). “Chapter Two - Asymmetric Protein Localization in Planar Cell Polarity: Mechanisms, Puzzles, and Challenges,” in *Current Topics in Developmental Biology*, ed. Y. Yang (Academic Press), 33–53. doi: 10.1016/B978-0-12-394592-1.00002-8

- Peskin, C. S., Odell, G. M., and Oster, G. F. (1993). Cellular motions and thermal fluctuations: the Brownian ratchet. *Biophys. J.* 65, 316–324. doi: 10.1016/S0006-3495(93)81035-X
- Petrie, R. J., Koo, H., and Yamada, K. M. (2014). Generation of compartmentalized pressure by a nuclear piston governs cell motility in a 3D matrix. *Science* 345, 1062–1065. doi: 10.1126/science.1256965
- Phuyal, S., Romani, P., Dupont, S., and Farhan, H. (2023). Mechanobiology of organelles: illuminating their roles in mechanosensing and mechanotransduction. *Trends Cell Biol.* 33, 1049–1061. doi: 10.1016/j.tcb.2023.05.001
- Pinheiro, D., and Bellaïche, Y. (2018). Mechanical Force-Driven Adherens Junction Remodeling and Epithelial Dynamics. *Dev. Cell* 47, 3–19. doi: 10.1016/j.devcel.2018.09.014
- Piperno, G., LeDizet, M., and Chang, X. J. (1987). Microtubules containing acetylated alpha-tubulin in mammalian cells in culture. *J. Cell Biol.* 104, 289–302. doi: 10.1083/jcb.104.2.289
- Plant, P. J., Fawcett, J. P., Lin, D. C. C., Holdorf, A. D., Binns, K., Kulkarni, S., et al. (2003). A polarity complex of mPar-6 and atypical PKC binds, phosphorylates and regulates mammalian Lgl. *Nat. Cell Biol.* 5, 301–308. doi: 10.1038/ncb948
- Pollard, T. D. (2016). Actin and Actin-Binding Proteins. *Cold Spring Harb. Perspect. Biol.* 8, a018226. doi: 10.1101/cshperspect.a018226
- Polyakov, O., He, B., Swan, M., Shaevitz, J. W., Kaschube, M., and Wieschaus, E. (2014). Passive Mechanical Forces Control Cell-Shape Change during Drosophila Ventral Furrow Formation. *Biophys. J.* 107, 998–1010. doi: 10.1016/j.bpj.2014.07.013
- Ponti, A., Machacek, M., Gupton, S. L., Waterman-Storer, C. M., and Danuser, G. (2004). Two distinct actin networks drive the protrusion of migrating cells. *Science* 305, 1782–1786. doi: 10.1126/science.1100533
- Popkova, A., Andrenšek, U., Pagnotta, S., Zihlerl, P., Krajnc, M., and Rauzi, M. (2024). A mechanical wave travels along a genetic guide to drive the formation of an epithelial furrow during Drosophila gastrulation. *Dev. Cell* 59, 400–414.e5. doi: 10.1016/j.devcel.2023.12.016
- Pouille, P.-A., Ahmadi, P., Brunet, A.-C., and Farge, E. (2009). Mechanical Signals Trigger Myosin II Redistribution and Mesoderm Invagination in Drosophila Embryos. *Sci. Signal.* 2, ra16–ra16. doi: 10.1126/scisignal.2000098
- Poujade, M., Grasland-Mongrain, E., Hertzog, A., Jouanneau, J., Chavrier, P., Ladoux, B., et al. (2007). Collective migration of an epithelial monolayer in response to a model wound. *Proc. Natl. Acad. Sci.* 104, 15988–15993. doi: 10.1073/pnas.0705062104
- Qin, X., Hannezo, E., Mangeat, T., Liu, C., Majumder, P., Liu, J., et al. (2018). A biochemical network controlling basal myosin oscillation. *Nat. Commun.* 9, 1210. doi: 10.1038/s41467-018-03574-5

- Quintin, S., Gally, C., and Labouesse, M. (2008). Epithelial morphogenesis in embryos: asymmetries, motors and brakes. *Trends Genet.* 24, 221–230. doi: 10.1016/j.tig.2008.02.005
- Raff, J. W., and Glover, D. M. (1989). Centrosomes, and not nuclei, initiate pole cell formation in *Drosophila* embryos. *Cell* 57, 611–619. doi: 10.1016/0092-8674(89)90130-X
- Rakshit, S., Zhang, Y., Manibog, K., Shafraz, O., and Sivasankar, S. (2012). Ideal, catch, and slip bonds in cadherin adhesion. *Proc. Natl. Acad. Sci.* 109, 18815–18820. doi: 10.1073/pnas.1208349109
- Rao, J. N., Madasu, Y., and Dominguez, R. (2014). Mechanism of actin filament pointed-end capping by tropomodulin. *Science* 345, 463–467. doi: 10.1126/science.1256159
- Ratheesh, A., Gomez, G. A., Priya, R., Verma, S., Kovacs, E. M., Jiang, K., et al. (2012). Centralspindlin and α -catenin regulate Rho signalling at the epithelial zonula adherens. *Nat. Cell Biol.* 14, 818–828. doi: 10.1038/ncb2532
- Rauzi, M. (2020). Cell intercalation in a simple epithelium. *Philos. Trans. R. Soc. B Biol. Sci.* 375, 20190552. doi: 10.1098/rstb.2019.0552
- Rauzi, M., Krzic, U., Saunders, T. E., Krajnc, M., Zihlerl, P., Hufnagel, L., et al. (2015). Embryo-scale tissue mechanics during *Drosophila* gastrulation movements. *Nat. Commun.* 6, 8677. doi: 10.1038/ncomms9677
- Rauzi, M., Lenne, P.-F., and Lecuit, T. (2010). Planar polarized actomyosin contractile flows control epithelial junction remodelling. *Nature* 468, 1110–1114. doi: 10.1038/nature09566
- Reeves, G. T., and Stathopoulos, A. (2009). Graded Dorsal and Differential Gene Regulation in the *Drosophila* Embryo. *Cold Spring Harb. Perspect. Biol.* 1, a000836. doi: 10.1101/cshperspect.a000836
- Renkawitz, J., Kopf, A., Stopp, J., de Vries, I., Driscoll, M. K., Merrin, J., et al. (2019). Nuclear positioning facilitates amoeboid migration along the path of least resistance. *Nature* 568, 546–550. doi: 10.1038/s41586-019-1087-5
- Rida, P. C. G., and Chen, P. (2009). Line up and listen: Planar cell polarity regulation in the mammalian inner ear. *Semin. Cell Dev. Biol.* 20, 978–985. doi: 10.1016/j.semcdb.2009.02.007
- Ridley, A. J., Schwartz, M. A., Burridge, K., Firtel, R. A., Ginsberg, M. H., Borisy, G., et al. (2003). Cell Migration: Integrating Signals from Front to Back. *Science* 302, 1704–1709. doi: 10.1126/science.1092053
- Rivera-Pomar, R., Lu, X., Perrimon, N., Taubert, H., and Jäckle, H. (1995). Activation of posterior gap gene expression in the *Drosophila* blastoderm. *Nature* 376, 253–256. doi: 10.1038/376253a0

- Rivera-Pomar, R., Niessing, D., Schmidt-Ott, U., Gehring, W. J., and Jackl , H. (1996). RNA binding and translational suppression by bicoid. *Nature* 379, 746–749. doi: 10.1038/379746a0
- Rivero, S., Cardenas, J., Bornens, M., and Rios, R. M. (2009). Microtubule nucleation at the cis-side of the Golgi apparatus requires AKAP450 and GM130. *EMBO J.* 28, 1016–1028. doi: 10.1038/emboj.2009.47
- Ro, H. (1992). Integrins: versatility, modulation, and signaling in cell adhesion. *Cell* 69. doi: 10.1016/0092-8674(92)90115-s
- Robinson, R. C., Turbedsky, K., Kaiser, D. A., Marchand, J.-B., Higgs, H. N., Choe, S., et al. (2001). Crystal Structure of Arp2/3 Complex. *Science* 294, 1679–1684. doi: 10.1126/science.1066333
- Roca-Cusachs, P., Gauthier, N. C., Del Rio, A., and Sheetz, M. P. (2009). Clustering of alpha(5)beta(1) integrins determines adhesion strength whereas alpha(v)beta(3) and talin enable mechanotransduction. *Proc. Natl. Acad. Sci. U. S. A.* 106, 16245–16250. doi: 10.1073/pnas.0902818106
- Rogers, S. L., Wiedemann, U., H cker, U., Turck, C., and Vale, R. D. (2004). *Drosophila* RhoGEF2 Associates with Microtubule Plus Ends in an EB1-Dependent Manner. *Curr. Biol.* 14, 1827–1833. doi: 10.1016/j.cub.2004.09.078
- Roh-Johnson, M., Shemer, G., Higgins, C. D., McClellan, J. H., Werts, A. D., Tulu, U. S., et al. (2012). Triggering a Cell Shape Change by Exploiting Preexisting Actomyosin Contractions. *Science* 335, 1232–1235. doi: 10.1126/science.1217869
- Roll-Mecak, A. (2020). The Tubulin Code in Microtubule Dynamics and Information Encoding. *Dev. Cell* 54, 7–20. doi: 10.1016/j.devcel.2020.06.008
- R per, K. (2012). Anisotropy of Crumbs and aPKC Drives Myosin Cable Assembly during Tube Formation. *Dev. Cell* 23, 939–953. doi: 10.1016/j.devcel.2012.09.013
- R per, K. (2013). Supracellular actomyosin assemblies during development. *BioArchitecture* 3, 45–49. doi: 10.4161/bioa.25339
- Rossant, J., and Tam, P. P. L. (2022). Early human embryonic development: Blastocyst formation to gastrulation. *Dev. Cell* 57, 152–165. doi: 10.1016/j.devcel.2021.12.022
- Roth, S., Neuman-Silberberg, F. S., Barcelo, G., and Sch pbach, T. (1995). cornichon and the EGF receptor signaling process are necessary for both anterior-posterior and dorsal-ventral pattern formation in *Drosophila*. *Cell* 81, 967–978. doi: 10.1016/0092-8674(95)90016-0
- Rouiller, I., Xu, X.-P., Amann, K. J., Egile, C., Nickell, S., Nicastro, D., et al. (2008). The structural basis of actin filament branching by the Arp2/3 complex. *J. Cell Biol.* 180, 887–895. doi: 10.1083/jcb.200709092
- Royou, A., Sullivan, W., and Karess, R. (2002). Cortical recruitment of nonmuscle myosin II in early syncytial *Drosophila* embryos : its role in nuclear axial expansion and its regulation by Cdc2 activity. *J. Cell Biol.* 158, 127–137. doi: 10.1083/jcb.200203148

- Rozbicki, E., Chuai, M., Karjalainen, A. I., Song, F., Sang, H. M., Martin, R., et al. (2015). Myosin-II-mediated cell shape changes and cell intercalation contribute to primitive streak formation. *Nat. Cell Biol.* 17, 397–408. doi: 10.1038/ncb3138
- Rupprecht, J.-F., Ong, K. H., Yin, J., Huang, A., Dinh, H.-H.-Q., Singh, A. P., et al. (2017). Geometric constraints alter cell arrangements within curved epithelial tissues. *Mol. Biol. Cell* 28, 3582–3594. doi: 10.1091/mbc.e17-01-0060
- Saburi, S., Hester, I., Fischer, E., Pontoglio, M., Eremina, V., Gessler, M., et al. (2008). Loss of Fat4 disrupts PCP signaling and oriented cell division and leads to cystic kidney disease. *Nat. Genet.* 40, 1010–1015. doi: 10.1038/ng.179
- Sai, X., and Ladher, R. K. (2015). Early steps in inner ear development: induction and morphogenesis of the otic placode. *Front. Pharmacol.* 6. doi: 10.3389/fphar.2015.00019
- Salbreux, G., Charras, G., and Paluch, E. (2012). Actin cortex mechanics and cellular morphogenesis. *Trends Cell Biol.* 22, 536–545. doi: 10.1016/j.tcb.2012.07.001
- Saunders, T. E. (2021). The early *Drosophila* embryo as a model system for quantitative biology. *Cells Dev.* 168, 203722. doi: 10.1016/j.cdev.2021.203722
- Scarpa, E., Finet, C., Blanchard, G. B., and Sanson, B. (2018). Actomyosin-Driven Tension at Compartmental Boundaries Orients Cell Division Independently of Cell Geometry *In Vivo*. *Dev. Cell* 47, 727-740.e6. doi: 10.1016/j.devcel.2018.10.029
- Scepanovic, G., and Fernandez-Gonzalez, R. (2018). Oriented Cell Division: The Pull of the Pole. *Dev. Cell* 47, 686–687. doi: 10.1016/j.devcel.2018.11.040
- Schmidt, A., and Grosshans, J. (2018). Dynamics of cortical domains in early *Drosophila* development. *J. Cell Sci.* 131, jcs212795. doi: 10.1242/jcs.212795
- Schmidt, A., Lv, Z., and Großhans, J. (2018). ELMO and Sponge specify subapical restriction of Canoe and formation of the subapical domain in early *Drosophila* embryos. *Dev. Camb. Engl.* 145, dev157909. doi: 10.1242/dev.157909
- Scholey, J. M., Taylor, K. A., and Kendrick-Jones, J. (1980). Regulation of non-muscle myosin assembly by calmodulin-dependent light chain kinase. *Nature* 287, 233–235. doi: 10.1038/287233a0
- Schulz, K. N., and Harrison, M. M. (2019). Mechanisms regulating zygotic genome activation. *Nat. Rev. Genet.* 20, 221–234. doi: 10.1038/s41576-018-0087-x
- Schüpbach, T. (1987). Germ line and soma cooperate during oogenesis to establish the dorsoventral pattern of egg shell and embryo in *Drosophila melanogaster*. *Cell* 49, 699–707. doi: 10.1016/0092-8674(87)90546-0
- Seher, T. C., Narasimha, M., Vogelsang, E., and Leptin, M. (2007). Analysis and reconstitution of the genetic cascade controlling early mesoderm morphogenesis in the *Drosophila* embryo. *Mech. Dev.* 124, 167–179. doi: 10.1016/j.mod.2006.12.004

- Seifert, J. R. K., and Mlodzik, M. (2007). Frizzled/PCP signalling: a conserved mechanism regulating cell polarity and directed motility. *Nat. Rev. Genet.* 8, 126–138. doi: 10.1038/nrg2042
- Sen, J., Goltz, J. S., Stevens, L., and Stein, D. (1998). Spatially restricted expression of pipe in the *Drosophila* egg chamber defines embryonic dorsal-ventral polarity. *Cell* 95, 471–481. doi: 10.1016/s0092-8674(00)81615-3
- Sepich, D. S., Usmani, M., Pawlicki, S., and Solnica-Krezel, L. (2011). Wnt/PCP signaling controls intracellular position of MTOCs during gastrulation convergence and extension movements. *Development* 138, 543–552. doi: 10.1242/dev.053959
- Shapiro, L., and Weis, W. I. (2009). Structure and biochemistry of cadherins and catenins. *Cold Spring Harb. Perspect. Biol.* 1, a003053. doi: 10.1101/cshperspect.a003053
- Sharma, P., and McNeill, H. (2013). Fat and Dachshous cadherins. *Prog. Mol. Biol. Transl. Sci.* 116, 215–235. doi: 10.1016/B978-0-12-394311-8.00010-8
- Shelton, C. A., and Wasserman, S. A. (1993). pelle encodes a protein kinase required to establish dorsoventral polarity in the *Drosophila* embryo. *Cell* 72, 515–525. doi: 10.1016/0092-8674(93)90071-w
- Sherrard, K., Robin, F., Lemaire, P., and Munro, E. (2010). Sequential Activation of Apical and Basolateral Contractility Drives Ascidian Endoderm Invagination. *Curr. Biol.* 20, 1499–1510. doi: 10.1016/j.cub.2010.06.075
- Shi, D., Usami, F., Komatsu, K., Oka, S., Abe, T., Uemura, T., et al. (2016). Dynamics of planar cell polarity protein Vangl2 in the mouse oviduct epithelium. *Mech. Dev.* 141, 78–89. doi: 10.1016/j.mod.2016.05.002
- Shi, Q., Cao, H., Xu, R., Zhang, D., and Huang, J. (2017). Functional conservation study of polarity protein Crumbs intracellular domain. *Yi Chuan Hered.* 39, 32–40. doi: 10.16288/j.ycz.16-377
- Shimada, Y., Yonemura, S., Ohkura, H., Strutt, D., and Uemura, T. (2006). Polarized Transport of Frizzled along the Planar Microtubule Arrays in *Drosophila* Wing Epithelium. *Dev. Cell* 10, 209–222. doi: 10.1016/j.devcel.2005.11.016
- Shimamoto, Y., Forth, S., and Kapoor, T. M. (2015). Measuring Pushing and Braking Forces Generated by Ensembles of Kinesin-5 Crosslinking Two Microtubules. *Dev. Cell* 34, 669–681. doi: 10.1016/j.devcel.2015.08.017
- Shintani, Y., Fukumoto, Y., Chaika, N., Svoboda, R., Wheelock, M. J., and Johnson, K. R. (2008). Collagen I-mediated up-regulation of N-cadherin requires cooperative signals from integrins and discoidin domain receptor 1. *J. Cell Biol.* 180, 1277–1289. doi: 10.1083/jcb.200708137
- Sidor, C., Stevens, T. J., Jin, L., Boulanger, J., and Röper, K. (2020). Rho-Kinase Planar Polarization at Tissue Boundaries Depends on Phospho-regulation of Membrane Residence Time. *Dev. Cell* 52, 364-378.e7. doi: 10.1016/j.devcel.2019.12.003

- Silver, J. T., Wirtz-Peitz, F., Simões, S., Pellikka, M., Yan, D., Binari, R., et al. (2019). Apical polarity proteins recruit the RhoGEF Cysts to promote junctional myosin assembly. *J. Cell Biol.* 218, 3397–3414. doi: 10.1083/jcb.201807106
- Simões, S., Denholm, B., Azevedo, D., Sotillos, S., Martin, P., Skaer, H., et al. (2006). Compartmentalisation of Rho regulators directs cell invagination during tissue morphogenesis. *Dev. Camb.* 133 (21), 4257–4267. doi: 10.1242/dev.02588
- Simons, M., Wang, M., McBride, O. W., Kawamoto, S., Yamakawa, K., Gdula, D., et al. (1991). Human nonmuscle myosin heavy chains are encoded by two genes located on different chromosomes. *Circ. Res.* 69, 530–539. doi: 10.1161/01.RES.69.2.530
- Simpson-Brose, M., Treisman, J., and Desplan, C. (1994). Synergy between the hunchback and bicoid morphogens is required for anterior patterning in *Drosophila*. *Cell* 78, 855–865. doi: 10.1016/S0092-8674(94)90622-X
- Singh, A., Saha, T., Begemann, I., Ricker, A., Nüsse, H., Thorn-Seshold, O., et al. (2018). Polarized microtubule dynamics directs cell mechanics and coordinates forces during epithelial morphogenesis. *Nat. Cell Biol.* 20, 1126–1133. doi: 10.1038/s41556-018-0193-1
- Singh, A., Thale, S., Leibner, T., Lamparter, L., Ricker, A., Nüsse, H., et al. (2024). Dynamic interplay of microtubule and actomyosin forces drive tissue extension. *Nat. Commun.* 15, 3198. doi: 10.1038/s41467-024-47596-8
- Singh, J., and Mlodzik, M. (2012). Planar cell polarity signaling: coordination of cellular orientation across tissues. *Wiley Interdiscip. Rev. Dev. Biol.* 1, 479–499. doi: 10.1002/wdev.32
- Soares e Silva, M., Depken, M., Stuhmann, B., Korsten, M., MacKintosh, F. C., and Koenderink, G. H. (2011). Active multistage coarsening of actin networks driven by myosin motors. *Proc. Natl. Acad. Sci.* 108, 9408–9413. doi: 10.1073/pnas.1016616108
- Sokac, A. M., Biel, N., and De Renzis, S. (2023). Membrane-actin interactions in morphogenesis: Lessons learned from *Drosophila* cellularization. *Semin. Cell Dev. Biol.* 133, 107–122. doi: 10.1016/j.semcd.2022.03.028
- Sokac, A. M., and Wieschaus, E. (2008). Zygotically controlled F-actin establishes cortical compartments to stabilize furrows during *Drosophila* cellularization. *J. Cell Sci.* 121, 1815–1824. doi: 10.1242/jcs.025171
- Song, X., Yang, F., Yang, T., Wang, Y., Ding, M., Li, L., et al. (2023). Phase separation of EB1 guides microtubule plus-end dynamics. *Nat. Cell Biol.* 25, 79–91. doi: 10.1038/s41556-022-01033-4
- Song, Y., and Brady, S. T. (2015). Post-translational modifications of tubulin: pathways to functional diversity of microtubules. *Trends Cell Biol.* 25, 125–136. doi: 10.1016/j.tcb.2014.10.004

- Stathopoulos, A., Drenth, M. V., Erives, A., Markstein, M., and Levine, M. (2002). Whole-Genome Analysis of Dorsal-Ventral Patterning in the *Drosophila* Embryo. *Cell* 111, 687–701. doi: 10.1016/S0092-8674(02)01087-5
- Stathopoulos, A., and Levine, M. (2002). Linear signaling in the Toll-Dorsal pathway of *Drosophila*: activated Pelle kinase specifies all threshold outputs of gene expression while the bHLH protein Twist specifies a subset. *Development* 129, 3411–3419. doi: 10.1242/dev.129.14.3411
- Stathopoulos, A., and Levine, M. (2004). Whole-genome analysis of *Drosophila* gastrulation. *Curr. Opin. Genet. Dev.* 14, 477–484. doi: 10.1016/j.gde.2004.07.004
- Stehbens, S. J., Paterson, A. D., Crampton, M. S., Shewan, A. M., Ferguson, C., Akhmanova, A., et al. (2006). Dynamic microtubules regulate the local concentration of E-cadherin at cell-cell contacts. *J. Cell Sci.* 119, 1801–1811. doi: 10.1242/jcs.02903
- Stricker, J., Falzone, T., and Gardel, M. L. (2010). Mechanics of the F-actin cytoskeleton. *J. Biomech.* 43, 9–14. doi: 10.1016/j.jbiomech.2009.09.003
- Strutt, D., and Strutt, H. (2007). Differential activities of the core planar polarity proteins during *Drosophila* wing patterning. *Dev. Biol.* 302, 181–194. doi: 10.1016/j.ydbio.2006.09.026
- Sui, L., Alt, S., Weigert, M., Dye, N., Eaton, S., Jug, F., et al. (2018). Differential lateral and basal tension drive folding of *Drosophila* wing discs through two distinct mechanisms. *Nat. Commun.* 9, 4620. doi: 10.1038/s41467-018-06497-3
- Sun, Z., Amourda, C., Shagirov, M., Hara, Y., Saunders, T. E., and Toyama, Y. (2017). Basolateral protrusion and apical contraction cooperatively drive *Drosophila* germ-band extension. *Nat. Cell Biol.* 19, 375–383. doi: 10.1038/ncb3497
- Sutherland, D., Samakovlis, C., and Krasnow, M. A. (1996). *branchless* Encodes a *Drosophila* FGF Homolog That Controls Tracheal Cell Migration and the Pattern of Branching. *Cell* 87, 1091–1101. doi: 10.1016/S0092-8674(00)81803-6
- Suzanne, M., and Steller, H. (2013). Shaping organisms with apoptosis. *Cell Death Differ.* 20, 669–675. doi: 10.1038/cdd.2013.11
- Suzuki, N., Hajicek, N., and Kozasa, T. (2009). Regulation and physiological functions of G12/13-mediated signaling pathways. *Neurosignals* 17, 55–70. doi: 10.1159/000186690
- Sweeton, D., Parks, S., Costa, M., and Wieschaus, E. (1991). Gastrulation in *Drosophila*: the formation of the ventral furrow and posterior midgut invaginations. *Development* 112, 775–789. doi: 10.1242/dev.112.3.775
- Takeda, M., Sami, M. M., and Wang, Y.-C. (2018). A homeostatic apical microtubule network shortens cells for epithelial folding via a basal polarity shift. *Nat. Cell Biol.* 20, 36–45. doi: 10.1038/s41556-017-0001-3
- Tan, C., Stronach, B., and Perrimon, N. (2003). Roles of myosin phosphatase during *Drosophila* development. *Dev. Camb. Engl.* 130, 671–681.

- Tanentzapf, G., and Tepass, U. (2003). Interactions between the crumbs, lethal giant larvae and bazooka pathways in epithelial polarization. *Nat. Cell Biol.* 5, 46–52. doi: 10.1038/ncb896
- Tang, Z., Hu, Y., Wang, Z., Jiang, K., Zhan, C., Marshall, W. F., et al. (2018). Mechanical Forces Program the Orientation of Cell Division during Airway Tube Morphogenesis. *Dev. Cell* 44, 313–325.e5. doi: 10.1016/j.devcel.2017.12.013
- Tepass, U. (1996). Crumbs, a Component of the Apical Membrane, Is Required for Zonula Adherens Formation in Primary Epithelia of *Drosophila*. *Dev. Biol.* 177, 217–225. doi: 10.1006/dbio.1996.0157
- Tepass, U., and Hartenstein, V. (1994). The development of cellular junctions in the *Drosophila* embryo. *Dev. Biol.* 161, 563–596. doi: 10.1006/dbio.1994.1054
- Théry, M., Jiménez-Dalmaroni, A., Racine, V., Bornens, M., and Jülicher, F. (2007). Experimental and theoretical study of mitotic spindle orientation. *Nature* 447, 493–496. doi: 10.1038/nature05786
- Thompson, B. J. (2022). Par-3 family proteins in cell polarity & adhesion. *Febs J.* 289, 596. doi: 10.1111/febs.15754
- Thompson, D. W. (1945). *On growth and form*. Cambridge : University Press ; New York : Macmillan. Available at: <http://archive.org/details/ongrowthform00thom> (Accessed June 25, 2024).
- Tolwinski, N. S. (2017). Introduction: *Drosophila*—A Model System for Developmental Biology. *J. Dev. Biol.* 5, 9. doi: 10.3390/jdb5030009
- Tonucci, F. M., Hidalgo, F., Ferretti, A., Almada, E., Favre, C., Goldenring, J. R., et al. (2015). Centrosomal AKAP350 and CIP4 act in concert to define the polarized localization of the centrosome and Golgi in migratory cells. *J. Cell Sci.* 128, 3277–3289. doi: 10.1242/jcs.170878
- Toyama, Y., Peralta, X. G., Wells, A. R., Kiehart, D. P., and Edwards, G. S. (2008). Apoptotic Force and Tissue Dynamics During *Drosophila* Embryogenesis. *Science* 321, 1683–1686. doi: 10.1126/science.1157052
- Tree, D. R. P., Shulman, J. M., Rousset, R., Scott, M. P., Gubb, D., and Axelrod, J. D. (2002). Prickle Mediates Feedback Amplification to Generate Asymmetric Planar Cell Polarity Signaling. *Cell* 109, 371–381. doi: 10.1016/S0092-8674(02)00715-8
- Treat, X., Chen, Z., and Jacobson, K. (2012). Cell migration. *Compr. Physiol.* 2, 2369–2392. doi: 10.1002/cphy.c110012
- Truong Quang, B.-A., Mani, M., Markova, O., Lecuit, T., and Lenne, P.-F. (2013). Principles of E-cadherin supramolecular organization in vivo. *Curr. Biol. CB* 23, 2197–2207. doi: 10.1016/j.cub.2013.09.015
- Turner, F. R., and Mahowald, A. P. (1977). Scanning electron microscopy of *Drosophila melanogaster* embryogenesis. *Dev. Biol.* 57, 403–416. doi: 10.1016/0012-1606(77)90225-1

- Uechi, H., and Kuranaga, E. (2019). The Tricellular Junction Protein Sidekick Regulates Vertex Dynamics to Promote Bicellular Junction Extension. *Dev. Cell* 50, 327–338.e5. doi: 10.1016/j.devcel.2019.06.017
- Urbansky, S., González Avalos, P., Wosch, M., and Lemke, S. (2016). Folded gastrulation and T48 drive the evolution of coordinated mesoderm internalization in flies. *eLife* 5, e18318. doi: 10.7554/eLife.18318
- Valencia-Expósito, A., Grosheva, I., Míguez, D. G., González-Reyes, A., and Martín-Bermudo, M. D. (2016). Myosin light-chain phosphatase regulates basal actomyosin oscillations during morphogenesis. *Nat. Commun.* 7, 10746. doi: 10.1038/ncomms10746
- Valet, M., Siggia, E. D., and Brivanlou, A. H. (2022). Mechanical regulation of early vertebrate embryogenesis. *Nat. Rev. Mol. Cell Biol.* 23, 169–184. doi: 10.1038/s41580-021-00424-z
- van der Spuy, M., Wang, J. X., Kociszewska, D., and White, M. D. (2023). The cellular dynamics of neural tube formation. *Biochem. Soc. Trans.* 51, 343–352. doi: 10.1042/BST20220871
- Vanderleest, T. E., Smits, C. M., Xie, Y., Jewett, C. E., Blankenship, J. T., and Loerke, D. (2018). Vertex sliding drives intercalation by radial coupling of adhesion and actomyosin networks during *Drosophila* germband extension. *eLife* 7, e34586. doi: 10.7554/eLife.34586
- Vavylonis, D., Yang, Q., and O’Shaughnessy, B. (2005). Actin polymerization kinetics, cap structure, and fluctuations. *Proc. Natl. Acad. Sci. U. S. A.* 102, 8543–8548. doi: 10.1073/pnas.0501435102
- Venturini, V., Pezzano, F., Català Castro, F., Häkkinen, H.-M., Jiménez-Delgado, S., Colomer-Rosell, M., et al. (2020). The nucleus measures shape changes for cellular proprioception to control dynamic cell behavior. *Science* 370, eaba2644. doi: 10.1126/science.aba2644
- Verheyen, E. M. (2022). The power of *Drosophila* in modeling human disease mechanisms. *Dis. Model. Mech.* 15, dmm049549. doi: 10.1242/dmm.049549
- Verma, V., and Maresca, T. J. (2019). Microtubule plus-ends act as physical signaling hubs to activate RhoA during cytokinesis. *eLife* 8, e38968. doi: 10.7554/eLife.38968
- Vicente-Manzanares, M., Ma, X., Adelstein, R. S., and Horwitz, A. R. (2009). Non-muscle myosin II takes centre stage in cell adhesion and migration. *Nat. Rev. Mol. Cell Biol.* 10, 778–790. doi: 10.1038/nrm2786
- Villars, A., Matamoro-Vidal, A., Levillayer, F., and Levayer, R. (2022). Microtubule disassembly by caspases is an important rate-limiting step of cell extrusion. *Nat. Commun.* 13, 3632. doi: 10.1038/s41467-022-31266-8
- von Dassow, G., Verbrugghe, K. J. C., Miller, A. L., Sider, J. R., and Bement, W. M. (2009). Action at a distance during cytokinesis. *J. Cell Biol.* 187, 831–845. doi: 10.1083/jcb.200907090

- Walck-Shannon, E., and Hardin, J. (2014). Cell intercalation from top to bottom. *Nat. Rev. Mol. Cell Biol.* 15, 34–48. doi: 10.1038/nrm3723
- Walck-Shannon, E., Reiner, D., and Hardin, J. (2015). Polarized Rac-dependent protrusions drive epithelial intercalation in the embryonic epidermis of *C. elegans*. *Development* 142, 3549–3560. doi: 10.1242/dev.127597
- Walczak, C. E., Gayek, S., and Ohi, R. (2013). Microtubule-depolymerizing kinesins. *Annu. Rev. Cell Dev. Biol.* 29, 417–441. doi: 10.1146/annurev-cellbio-101512-122345
- Wallingford, J. B., Ewald, A. J., Harland, R. M., and Fraser, S. E. (2001). Calcium signaling during convergent extension in *Xenopus*. *Curr. Biol.* 11, 652–661. doi: 10.1016/S0960-9822(01)00201-9
- Wang, C., and Lehmann, R. (1991). Nanos is the localized posterior determinant in *Drosophila*. *Cell* 66, 637–647. doi: 10.1016/0092-8674(91)90110-K
- Wang, N., Tytell, J. D., and Ingber, D. E. (2009). Mechanotransduction at a distance: mechanically coupling the extracellular matrix with the nucleus. *Nat. Rev. Mol. Cell Biol.* 10, 75–82. doi: 10.1038/nrm2594
- Wang, S., Matsumoto, K., Lish, S. R., Cartagena-Rivera, A. X., and Yamada, K. M. (2021). Budding epithelial morphogenesis driven by cell-matrix versus cell-cell adhesion. *Cell* 184, 3702–3716.e30. doi: 10.1016/j.cell.2021.05.015
- Wang, Y., and Riechmann, V. (2007). The role of the actomyosin cytoskeleton in coordination of tissue growth during *Drosophila* oogenesis. *Curr. Biol. CB* 17, 1349–1355. doi: 10.1016/j.cub.2007.06.067
- Wang, Y.-C., Khan, Z., Kaschube, M., and Wieschaus, E. F. (2012). Differential positioning of adherens junctions is associated with initiation of epithelial folding. *Nature* 484, 390–393. doi: 10.1038/nature10938
- Waterman-Storer, C. M., Worthylake, R. A., Liu, B. P., Burrridge, K., and Salmon, E. D. (1999). Microtubule growth activates Rac1 to promote lamellipodial protrusion in fibroblasts. *Nat. Cell Biol.* 1, 45–50. doi: 10.1038/9018
- Weaire, D., and Hutzler, S. (2000). *The Physics of Foams*. Oxford University Press. doi: 10.1093/oso/9780198505518.001.0001
- Webster, D. R., and Borisy, G. G. (1989). Microtubules are acetylated in domains that turn over slowly. *J. Cell Sci.* 92, 57–65. doi: 10.1242/jcs.92.1.57
- Weigel, D., Jürgens, G., Klingler, M., and Jäckle, H. (1990). Two Gap Genes Mediate Maternal Terminal Pattern Information in *Drosophila*. *Science* 248, 495–498. doi: 10.1126/science.2158673
- Weisenberg, R. C., Borisy, G. G., and Taylor, E. W. (1968). The colchicine-binding protein of mammalian brain and its relation to microtubules. *Biochemistry* 7, 4466–4479. doi: 10.1021/bi00852a043
- Wendt, T., Taylor, D., Trybus, K. M., and Taylor, K. (2001). Three-dimensional image reconstruction of dephosphorylated smooth muscle heavy meromyosin reveals

- asymmetry in the interaction between myosin heads and placement of subfragment 2. *Proc. Natl. Acad. Sci. U. S. A.* 98, 4361–4366. doi: 10.1073/pnas.071051098
- Weng, M., and Wieschaus, E. (2017). Polarity protein Par3/Bazooka follows myosin-dependent junction repositioning. *Dev. Biol.* 422, 125–134. doi: 10.1016/j.ydbio.2017.01.001
- Wieczorek, M., Urnavicius, L., Ti, S.-C., Molloy, K. R., Chait, B. T., and Kapoor, T. M. (2020). Asymmetric Molecular Architecture of the Human γ -Tubulin Ring Complex. *Cell* 180, 165–175.e16. doi: 10.1016/j.cell.2019.12.007
- Willecke, M., Hamaratoglu, F., Kango-Singh, M., Udan, R., Chen, C., Tao, C., et al. (2006). The Fat Cadherin Acts through the Hippo Tumor-Suppressor Pathway to Regulate Tissue Size. *Curr. Biol.* 16, 2090–2100. doi: 10.1016/j.cub.2006.09.005
- Wilson, C. A., Tsuchida, M. A., Allen, G. M., Barnhart, E. L., Applegate, K. T., Yam, P. T., et al. (2010). Myosin II contributes to cell-scale actin network treadmilling through network disassembly. *Nature* 465, 373–377. doi: 10.1038/nature08994
- Wilson, L., and Friedkin, M. (1967). The biochemical events of mitosis. II. The in vivo and in vitro binding of colchicine in grasshopper embryos and its possible relation to inhibition of mitosis. *Biochemistry* 6, 3126–3135. doi: 10.1021/bi00862a021
- Wodarz, A., Hinz, U., Engelbert, M., and Knust, E. (1995). Expression of crumbs confers apical character on plasma membrane domains of ectodermal epithelia of drosophila. *Cell* 82, 67–76. doi: 10.1016/0092-8674(95)90053-5
- Wolf, K., Wu, Y. I., Liu, Y., Geiger, J., Tam, E., Overall, C., et al. (2007). Multi-step pericellular proteolysis controls the transition from individual to collective cancer cell invasion. *Nat. Cell Biol.* 9, 893–904. doi: 10.1038/ncb1616
- Woodland, H. r. (1994). Nuclear trafficking. *FEBS Lett.* 337, 309–310. doi: 10.1016/0014-5793(94)80218-1
- Worman, H. J., and Gundersen, G. G. (2006). Here come the SUNs: a nucleocytoskeletal missing link. *Trends Cell Biol.* 16, 67–69. doi: 10.1016/j.tcb.2005.12.006
- Xu, J., Wirtz, D., and Pollard, T. D. (1998). Dynamic cross-linking by alpha-actinin determines the mechanical properties of actin filament networks. *J. Biol. Chem.* 273, 9570–9576. doi: 10.1074/jbc.273.16.9570
- Xue, Z., and Sokac, A. M. (2016). -Back-to-back mechanisms drive actomyosin ring closure during Drosophila embryo cleavage. *J. Cell Biol.* 215, 335–344. doi: 10.1083/jcb.201608025
- Yamanaka, T., Horikoshi, Y., Sugiyama, Y., Ishiyama, C., Suzuki, A., Hirose, T., et al. (2003). Mammalian Lgl Forms a Protein Complex with PAR-6 and aPKC Independently of PAR-3 to Regulate Epithelial Cell Polarity. *Curr. Biol.* 13, 734–743. doi: 10.1016/S0960-9822(03)00244-6

- Yang, C., Axelrod, J. D., and Simon, M. A. (2002). Regulation of Frizzled by Fat-like Cadherins during Planar Polarity Signaling in the Drosophila Compound Eye. *Cell* 108, 675–688. doi: 10.1016/S0092-8674(02)00658-X
- Yu, J. C., and Fernandez-Gonzalez, R. (2016). Local mechanical forces promote polarized junctional assembly and axis elongation in Drosophila. *eLife* 5, e10757. doi: 10.7554/eLife.10757
- Yu, J., Starr, D. A., Wu, X., Parkhurst, S. M., Zhuang, Y., Xu, T., et al. (2006). The KASH domain protein MSP-300 plays an essential role in nuclear anchoring during Drosophila oogenesis. *Dev. Biol.* 289, 336–345. doi: 10.1016/j.ydbio.2005.10.027
- Zallen, J. A., and Blankenship, J. T. (2008). Multicellular dynamics during epithelial elongation. *Semin. Cell Dev. Biol.* 19, 263–270. doi: 10.1016/j.semcdb.2008.01.005
- Zallen, J. A., and Wieschaus, E. (2004). Patterned Gene Expression Directs Bipolar Planar Polarity in Drosophila. *Dev. Cell* 6, 343–355. doi: 10.1016/S1534-5807(04)00060-7
- Zecca, M., and Struhl, G. (2010). A Feed-Forward Circuit Linking Wingless, Fat-Dachsous Signaling, and the Warts-Hippo Pathway to Drosophila Wing Growth. *PLOS Biol.* 8, e1000386. doi: 10.1371/journal.pbio.1000386
- Zehring, W. A., Wheeler, D. A., Reddy, P., Konopka, R. J., Kyriacou, C. P., Rosbash, M., et al. (1984). P-element transformation with period locus DNA restores rhythmicity to mutant, arrhythmic Drosophila melanogaster. *Cell* 39, 369–376. doi: 10.1016/0092-8674(84)90015-1
- Zelenka, P. S., and Arpitha, P. (2008). Coordinating cell proliferation and migration in the lens and cornea. *Semin. Cell Dev. Biol.* 19, 113–124. doi: 10.1016/j.semcdb.2007.10.001
- Zhang, X., Lei, K., Yuan, X., Wu, X., Zhuang, Y., Xu, T., et al. (2009). SUN1/2 and Syne/Nesprin-1/2 complexes connect centrosome to the nucleus during neurogenesis and neuronal migration in mice. *Neuron* 64, 173–187. doi: 10.1016/j.neuron.2009.08.018
- Zhou, Z., Alégot, H., and Irvine, K. D. (2019). Oriented Cell Divisions Are Not Required for Drosophila Wing Shape. *Curr. Biol.* 29, 856–864.e3. doi: 10.1016/j.cub.2019.01.044
- Zhu, M., and Zernicka-Goetz, M. (2020). Principles of Self-Organization of the Mammalian Embryo. *Cell* 183, 1467–1478. doi: 10.1016/j.cell.2020.11.003
- Zihni, C., Mills, C., Matter, K., and Balda, M. S. (2016). Tight junctions: from simple barriers to multifunctional molecular gates. *Nat. Rev. Mol. Cell Biol.* 17, 564–580. doi: 10.1038/nrm.2016.80
- Zoller, B., Little, S. C., and Gregor, T. (2018). Diverse Spatial Expression Patterns Emerge from Unified Kinetics of Transcriptional Bursting. *Cell* 175, 835–847.e25. doi: 10.1016/j.cell.2018.09.056

